A novel thermoplastic/clay/thermoset hybrid system for toughening of unsaturated polyesters

Sina Chaeichian

A Thesis

In the Department

of

Mechanical and Industrial Engineering

Presented in Partial Fulfillment of the Requirements

For the Degree of Doctor of Philosophy at

Concordia University

Montreal, Quebec, Canada

August 2013

CONCORDIA UNIVERSITY
SCHOOL OF GRADUATE STUDIES

This is to certify that the thesis prepared

By: **Sina Chaeichian**

Entitled: A novel thermoplastic/clay/thermoset hybrid system for toughening of unsaturated polyesters

and submitted in partial fulfillment of the requirements for the degree of

Doctor of Philosophy (Mechanical Engineering)

Complies with the regulations of the University and meets the accepted standards with respect to originality and quality.

Signed by final examining committee

_____ Chair
Dr. M. Reza Soleymani

_____ External Examiner
Dr. Musa Kamal

_____ External to Program
Dr. Charles Dubois

_____ Examiner
Dr. Martin D. Pugh

_____ Examiner
Dr. Lyes Kadem

_____ Thesis Supervisor
Dr. Paula Wood-Adams

_____ Thesis Supervisor
Dr. Suong Van Hoa

Approved by

_____
Chair of Department or Graduate Program Director

_____ 2013

_____
Dean of Faculty

ABSTRACT

A novel thermoplastic/clay/thermoset hybrid system for toughening of unsaturated polyesters

Sina Chaeichian, Ph.D.
Concordia University, 2013

Nanoclay and a thermoplastic were incorporated into general purpose unsaturated polyesters in order to provide for toughening. The effect of each additive on physical and mechanical properties of the composite was explored to understand the advantages and drawbacks. Since, the morphology of multiphase systems plays a key role in determining the final properties, the micro- and nano-structures of the various binary and ternary systems, were evaluated by electron, optical, and atomic force microscopy.

Different mixing methods for preparing clay/polyester nanocomposites were used to explore the effect of nanostructure on characteristics such as glass transition temperature, flexural properties, and fracture toughness. The results indicated that the incorporation of nanoclay causes a slight improvement in fracture toughness and that the degree of intercalation/exfoliation did not significantly affect the properties.

Polystyrene and poly(styrene/methyl methacrylate) were synthesized by in situ free radical polymerization in the presence of Cloisite 20A to provide a toughening agent. This approach enabled the pursuit of two aims: (i) improving the degree of dispersion and the distribution of clay silicate layers, and (ii) preparing the thermoplastic additive. A second curing agent, methyl methacrylate, was included to promote the conversion of styrene inside the clay galleries as well as in the thermoplastic-rich phase. The morphological study showed that the thermoplastic additive forms a second phase, dispersed throughout the continuous thermoset-rich phase. In the ternary systems, X-ray diffraction and transmission electron microscopy (TEM) revealed a fine intercalated/exfoliated structure, where the majority of clay silicate layers were located inside the thermoplastic-rich phase. Experimental results indicated that the incorporation

of the thermoplastic caused a slight improvement in fracture toughness. In contrast, a combination of the thermoplastic and the nanoclay caused a significant improvement in fracture toughness, without any reduction in glass transition temperature and elastic modulus.

The effect of the characteristics of the two phases and the microstructure on fracture toughness was explored. Results revealed that the microstructure (the size and distribution of thermoplastic-rich particles) had the greatest effect on fracture toughness. An interesting correlation between fracture toughness and the microstructure was found indicating the best particle size and spacing.

Dedicated to

My Mom Zohreh and My Dad Mehdi

ACKNOWLEDGEMENT

I would like to express my deep gratitude to Dr. Paula Wood-Adams and Dr. Suong Van Hoa, my supervisors, for their patient guidance, enthusiastic encouragement and useful critiques of this research work. I am sincerely grateful to them for giving me this opportunity to get precious experiences during my program.

I am particularly grateful to Dr. Rolf Schmidt for his kindly assistance with laboratory procedures and his valuable recommendations.

Assistance provided by Dr. Daneil Rosca, Dr. Ming Xie for their technical support and valuable guidance is greatly appreciated. Also, I wish to acknowledge the help provided by Mr. Heng Wang.

My special thanks are extended to Ali Alem and Ehsan Rezabeigi for their friendship, help and time during my research work. I would like to thank my other friends and colleagues for providing a nice and friendly environment to work with.

Contributions of Authors

This thesis contains chapters that present results that have been published in the form of an unaltered original journal article as well as materials which are in preparation for submission. The complete citation for the published paper is provided below:

Chapter 4: Sina Chaeichian, Paula Wood-Adams, Suong Van Hoa "In situ polymerization of polyester-based hybrid systems for the preparation of clay nanocomposites." Published in: *Polymer; Vol. 54, No. 5, pp. 1512-1523 (2012)*

Other chapters are in preparation for submission. All the papers presented in this thesis were co-authored and reviewed prior to submission to publication by Dr. Paula Wood-Adams and Dr. Suong Van Hoa, my supervisors. All of the remaining work and manuscript preparation were performed by the author of this thesis.

TABLE OF CONTENTS

LIST OF FIGURES

LIST OF TABLES

NOMENCLATURES

M_n	Number average molecular weight(g/mol)
σ_{ii}	Normal stress component (MPa)
τ_{ij}	Shear Stress component (MPa)
e_{ii}	Normal strain
e_{ij}	Shear strain
ε_{ij}	Strain tensor component
w_{ij}	Rotation tensor component
Δ	Volume strain
ε'_{ij}	Strain deviator component
σ'_{ij}	Deviator Stress component
J_i	Invariant of deviator stress tensor (MPa)
σ_y	Tensile Yield strength (MPa)
U_E	Elastic strain energy per thickness (J/m)
E	Elastic modulus (GPa)
a	Half of the length of the internal crack (m)
U_S	Surface energy (J)
γ_s	Specific surface energy (J/m^2)
ΔU	Potential energy (J)
ϑ	Poisson's ratio
γ_p	Specific plastic deformation energy (J/m^2)

K	Stress intensity factor (MPa.m$^{1/2}$)
K_c	Critical stress intensity factor (MPa.m$^{1/2}$)
σ_c	Critical stress (MPa)
r_y	radius of a circular plastic zone at the tip of a crack (μm)
K_{Ici}	critical stress intensity factor for initiation (MPa.m$^{1/2}$)
K_{Ica}	critical stress intensity factor for arrest (MPa.m$^{1/2}$)
T_β	β transition temperature
T_g	Glass transition temperature
T_α	α transition temperature
H_β	β activation energy (KJ/mol)
σ^{rr}	Radial stress (MPa)
$\sigma^{\theta\theta}$	Hoop stress (MPa)
$\tau^{r\theta}$	Shear stress (MPa)
T	Applied tensile stress (MPa)
τ_{oct}	Octahedral shear stress component (MPa)
Vp	Volume fraction of the particles
χ_{ij}	Flory-Huggins interaction parameter
V_r	Reference molar volume (m^3)
δ_i	Solubility parameter(Cal/cm^3)$^{1/2}$
R	Gas constant (J/K.mol)
ρ	Density (g/cm^3)
M	Molecular weight of the repeat unit
G	group molar attraction coefficient
r_{ij}	reactivity ratio

K_{ij}	kinetic constant
Q	Quality factor, representing viscous damping
$\Delta\varphi$	Phase shift (°)
E^*	Effective modulus (GPa)
r	Radius of thermoplastic-rich domains (μm)
c	Interparticle distance (μm)
σ_i	Inelastic strength (MPa)
σ_y	Yield strength (MPa)
K^P_c	Fracture toughness of the particles (MPa.m$^{1/2}$)
K^m_c	Fracture toughness of the matrix (MPa.m$^{1/2}$)
E_p	Particle modulus (GPa)
E_m	Matrix modulus (GPa)

ABBREVIATIONS

AFM	Atomic force microscopy
BPO	Benzoyl peroxide
CEC	Cation Exchange Capacity
CSR	Core shell rubber
CTBN	Carboxyl-terminated butadiene-acrylonitrile copolymers
DCDP	Dicyclopentadiene
DM	Direct mixing method
DMA	Dynamic mechanical analysis
DSC	Differential scanning calorimetry
DVB	Divinylbenzene
FTIR	Fourier transform infrared
GP	General purpose
GPC	Gel permeation chromatography
HN	Hybrid nanocomposite
^{1}H NMR	Proton nuclear magnetic resonance
HP	Hybrid polyester
HPMM	High-pressure mixing method
LPA	Low profile additive
MA	Maleic anhydride
MEKP	Methyl ethyl ketone peroxide
MMA	Methyl methacrylate

MMA/St_{CA}	Molar ratio of methyl methacrylate to styrene (as curing agents)
MMT	Montmorillonite
PA	Phthalic anhydride
P(MMA/S)	Poly(methyl methacrylate-co-stryene)
PS	Polystyrene
PVAc	Poly(vinyl acetate)
RI	Refractive index
SEM	Scanning electron microscopy
SHM	Solvent-aided mixing method
SN	Simple nanocomposite
SP	Simple polyester
St	Styrene
TEM	Transmission electron microscopy
THF	Tetrahydrofuran
TM-AFM	Tapping mode atomic force microscopy
TP	Thermoplastic component
TS	Tensile strength (MPa)
UP	Unsaturated polyester
UPR	Unsaturated polyester resin
XRD	X-ray diffraction

Chapter 1

1.1. Introduction

Polymer composites have been widely used in numerous fields, including the aerospace, automobile, and marine industries. The variety of applications of this group of materials is expanding due to their outstanding characteristics and properties, such as low weight, high specific stiffness and strength, good fatigue and corrosion resistance, and low cost. In general, polymer materials can be classified into two main categories based on their response to temperature, namely thermoplastics and thermosets. Highly crosslinked thermosets have been widely used as the matrix for manufacturing polymer composites, since their high crosslink density contributes to superior properties. One group of these thermosetting resins is unsaturated polyester resins.

Unsaturated polyesters (UPs) are usually synthesized by the reaction of an unsaturated dibasic acid with a polyhydric alcohol. Their resins (UPRs) are prepared by diluting them with a vinylene monomer. UPRs have outstanding advantages such as low cost, versatility, excellent wetting, ease of curing, and a wide temperature range of processability for forming. On the other hand, the highly crosslink density of these polymers, as with other thermosets, results in brittleness, calling for the use of toughening agents in a wide range of their applications.

Incorporation of a second phase in thermosets is a common technique for toughening, where the most frequently used additives are mineral fillers, nano-reinforcements, and rubbery and thermoplastic particles. However, each technique has its own drawbacks. For instance, the addition of rubber significantly improves fracture toughness at the expense of other properties, such as thermal stability and Young's modulus. Therefore, the biggest challenge is how to increase toughness without sacrificing these other properties.

Recently, a combination of different additives has been used not only to compensate for and modify the drawbacks of each additive, but also to employ their likely synergistic effect. Therefore, ternary systems, which typically consist of an organic additive, such as thermoplastic or rubber, nano-reinforcements as well as thermosetting resins, have attracted a lot of interest. Since, in commercial UPRs, thermoplastics are used as low

profile additives to control volume shrinkage of these resins, typically without the cost of stiffness and glass transition temperature, they have the potential to be applied as toughening agents. In addition, layered silicates have been widely used as nano-reinforcements to improve different properties of polymers, such as stiffness and fracture toughness. Therefore, in this work, we studied a thermoplastic/clay/thermoset ternary system.

1.2. Objectives

The main objective of this work is to improve fracture toughness of unsaturated polyester resins without sacrificing elastic modulus and glass transition temperature. For this purpose, we synthesized ternary hybrid nanocomposite systems by incorporating a combination of clay and thermoplastic. Firstly, the effect of each toughening agent on different properties of UP must be evaluated to find and understand the advantages and drawbacks of each additive, as well as the mechanisms controlling fracture toughness in each technique. Understanding the behavior of each simpler system is also helpful to understanding and explaining behaviors of the final complex ternary systems. Since within systems composed of different phases, the morphology plays a key role in controlling different properties, especially fracture toughness, the microstructure of each system must be also explored. In addition, the morphology of ternary systems has not been well understood in the literature, which emphasizes the need for these morphological studies.

To achieve the main goal, the following scientific and technical challenges must be addressed as secondary objectives:

- In systems composed of two or more components with different molecular sizes like unsaturated polyester resins, the order of mixing can be an important factor in clay dispersion and delamination. Different mixing techniques must be applied to further explore the formation mechanism of clay nanocomposites based on unsaturated polyesters.
- In clay nanocomposites based on UPs, clay galleries can reduce the homogeneity and degree of dispersion of raw reactants (unsaturated polyester and curing agent)

by trapping small molecules of curing agent. This may cause a reduction in crosslink density of the cured network, resulting in a reduction of some properties, such as tensile strength and T_g. Therefore, the effect of clay on chemical reactions during curing of the system must be further understood to deal with this issue.

- Nanostructure of the nanocomposites must be studied to find the effect of clay on fracture toughness and to understand the controlling mechanisms.
- The thermoplastic component can be prepared by in situ polymerization (in the presence of clay silicate layers). This approach is useful to improve dispersion and distribution of silicate layers throughout the system. A suitable mixing procedure to prepare a mixture of clay and raw reactants must be developed. Appropriate conditions of in situ copolymerization must be determined to synthesize a thermoplastic with suitable characteristics.
- The effect of the thermoplastic component on fracture toughness of the system and controlling mechanisms must be explored. In addition, a suitable thermoplastic must be selected based on the fracture toughness property.
- Variables and parameters affecting material characteristics, including the characteristics of the continuous phase and dispersed phase, must be found.
- The effect of material characteristics, affected by synthesis process variables, on fracture toughness must be understood.
- The nano- and microstructures of the hybrid nanocomposite systems must be studied to understand mechanisms controlling fracture toughness. In addition, the effect of different variables on microstructure must be explored.
- A correlation between microstructure and fracture toughness must be explored.

1.3. Thesis organization

This thesis consists of seven chapters. Chapter 1 gives a general introduction to the topic and explains the objectives of the project. Chapter 2 is a literature review giving information about unsaturated polyester resins, fracture mechanics, and mechanisms controlling fracture toughness in thermosets, as well as a summary of different toughening techniques for thermosets. In Chapter 3, the synthesis of clay nanocomposites based on unsaturated polyesters is evaluated. The effect of clay on curing and properties

of the thermoset is explored. Effective mechanisms controlling fracture toughness in this system are discussed. Finally drawbacks of the incorporation of clay into unsaturated polyester are pointed out. In Chapter 4, new ternary hybrid nanocomposites, in situ copolymerization, and the preparation procedure for the system are introduced. Experiments are conducted to choose a suitable thermoplastic component. The effect of the clay and thermoplastic on different properties is evaluated. Preliminary investigation into the morphology of the system and mechanisms controlling fracture toughness is performed. In Chapter 5, more investigation into the morphology of the system is done and section analysis of phase images, which gives valuable information about local mechanical properties of each phase and also interface, is done. In Chapter 6, different synthesis process variables affecting the characteristics of the matrix and dispersed phase are explored. The effect of these variables and material characteristics on different properties and the morphology of the system are evaluated. The relationship between the microstructure and toughness is explored. Likely mechanisms controlling fracture toughness are compared. In Chapter 7, a general conclusion and contributions are summarized, as well as recommendations for future work are proposed.

Chapter 2

Literature review

2.1.Unsaturated polyester resins

2.1.1.Chemical structure and classification

Unsaturated polyester resins (UPRs) are thermosetting polymers whose commercial applications began in the late 1940s. UPRs have two main components, unsaturated polyester (UP) and a reactive diluent. Most commercial resins contain styrene (St) monomer as the diluent, but other vinyl monomers such as methyl styrene and alkyl methacrylate monomers can be used. These diluents play two roles in the system: they reduce viscosity to facilitate processing of the resins and they cause chemical bonds (crosslinks) to form connection between polyester molecules.

Unsaturated polyesters (UPs) are low molecular weight fumarate esters[1]. The chemical structure of UP can be tailored according to the final application. The most important characteristic of UPs is the fumarate, which provides the active sites for radical crosslinking with the diluent monomers. Thus, for the preparation of the polyester, the following considerations are important:

- The fumarate ratio must be precisely selected to provide enough reactivity and crosslink density.
- The rest of the polyester molecule must be designed in such a way as to provide good solubility in styrene, as well as desirable properties for the cured material.

A classical esterification process is used to synthesize unsaturated polyester: a single hydroxyl compound (glycol) or a mixture reacts with maleic anhydride and/or together with other dicarboxylic acids, either aromatic or aliphatic. The maleate structure has two unsaturated isomers, cis and fumarate (Figure 2.1), where the latter is favorable due to its high reactivity. Since the esterification process is done at an elevated temperature, the conditions are suitable for the generation of fumarates through an isomerization step. The isomerization of maleate to fumarate occurs at a reaction temperature around 200°C, with a minimum of 80% conversion in most cases. To achieve a higher degree of

isomerization (over 90%), careful selection of raw reactants and good control of the heating period are required. After polyester preparation, the product is dissolved in a diluent. Stabilizers such as hydroquinone and t-butyl hydroquinone may be added to prevent premature reactions[1].

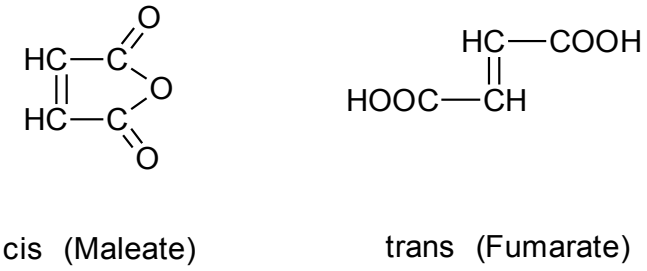

Fig. 2.1. Cis maleate and trans fumarate isomer.

The simplest unsaturated polyester resin is the product of condensation polymerization between maleic anhydride and propylene glycol, which is dissolved in styrene. The portion of maleic anhydride containing the reactive double bonds in the chemical structure of this polyester leads to an extremely brittle solid after the curing process. Without any modification, this solid material would have high tensile modulus, but low tensile elongation. Thus, such a brittle material has very limited applications. For most general purpose applications, a softer material with suitable crosslink density is required. For this purpose, there are three options to modify the properties of the polymer[1]:

- Incorporating other components (glycols or acids) to change the chemical structure
- Changing functional groups in the polymer
- Altering the molecular weight of the polymer

With such an approach, many combinations and variations for the preparation of these resins can be obtained. In the UPR industry, there is hardly any standard type of product and it is unlikely to find identical products from two different producers. Despite this fact, UPRs could be classified into four main groups based on chemical structure[1]:

- General purpose orthophthalic resins or GP resins, composed of phthalic anhydride, maleic anhydride, and glycol. The presence of phthalic anhydride in

the formulation reduces the active double bond sites (maleic anhydride portion), resulting in less brittleness in the final cured material. In addition, the aromatic structure can increase the strength of the material. Since these resins have adequate properties for most applications, they are called general purpose resins.

- Isophthalic resins, which are the condensation product of isophthalic acid, maleic anhydride, and glycol. Since GP resins do not have good resistance to wet environments, especially under elevated temperatures, isophthalic resins were introduced to the industry. Isophthalic acid has a very high melting point and low solubility in organic systems. These two factors cause difficult conditions for chemical reactions of the acid with maleic anhydride and glycol. This leads to an inhomogeneous distribution of active double bonds in the backbone of the polymer, leading to a loss of physical properties. To avoid this problem, a two-step synthesis process must be used. Firstly, isophthalic acid is reacted with an excess amount of glycol to produce a diol intermediate. This diol is then reacted with maleic anhydride to form reactive sites in the polymer. The higher cost of isophthalic acid and the complex polymerization procedure make these resins more expensive.
- Dicyclopentadiene (DCDP)-capped resins, which have end group modification. Unsaturated polyesters typically have a low molecular weight, with M_n (number average molecular weight) in the range of 1500-3000. If large groups are placed at the chain ends, different properties and performance can be achieved. A common group is DCPD. These large groups cause spatial restrictions, resulting in a reduction in volume shrinkage during curing. These resins are very brittle.
- Vinyl ester resins, which are produced from the esterification reaction of low molecular weight epoxy resin with an unsaturated carboxylic acid, such as methacrylic acid. These resins can be considered as modified epoxy resins. They have a combination of the mechanical properties of epoxy resins and the ease of processing of polyester resins. Thus, their final properties fall between those of epoxy resins and UPRs.

2.1.2.Curing and solidification

Solidification of UPR is done via a curing process that consists of free radical chain growth copolymerization between C=C bonds of styrene monomers and those of unsaturated polyester molecules. However, other reactions can happen during curing. In general, all reactions can be classified into four types[2]: (I) intermolecular crosslinking, when two adjacent polyester molecules are chemically connected with or without styrene linking bridges; (II) intramolecular crosslinking, when two unsaturated sites of one polyester molecule are connected with or without styrene linking bridges; (III) free styrene homopolymerization; (IV) styrene oligomers making branches in polyester molecules. Reaction I results in macroscopic network formation. Reaction II causes an increase in crosslink density. Reaction III leads to an increase in the length of linking bridges and/or forms styrene homopolymer or oligomer. Thus it does not contribute to the macroscopic network formation. Reaction IV consumes the curing agent monomers and has a slight effect on network formation.

Reaction conditions as well as the types of reactants and additives have different effects on this free radical polymerization. In the case of UPR, many studies have been done on the effects of temperature [3-5], resin chemistry [6], initiators and promoters [6-7], vinyl monomers [8-10], inhibitors [11-12], and retarders [13] on the curing reaction parameters: rate, degree of cure, released heat, induction time, and gel time. In general, an increase in temperature, promoter content, or initiator quantity increases the curing rate, whereas an increase in the content of inhibitors, vinyl monomers, or retarders results in a curing rate reduction. The effects of these factors on the final degree of cure and crosslink density have also been studied extensively due to the important effect of these characteristics on final properties, such as glass transition temperature [14-15], tensile strength [16-17], creep [16], and fracture toughness [16].

2.1.3.Polymerization mechanism and final morphology

During the curing process, decomposition of the initiators starts free radical polymerization to make long-chain molecules. Indeed, these molecules are composed of some styrene and polyester molecules, which are chemically connected by intra- and intermolecular reactions [2]. They form a spherical type structure, called microgel particles, dispersed in monomers and oligomers [18-20]. In the early stage of curing, the

concentration of microgels is low and they are locally distributed. As a result, intramicrogel crosslinking is dominant [18]. As the curing proceeds, the number of these microgel particles increases leading to dense distribution of the microgels. In this state, the particles can be connected to each other by interparticle crosslinking, wherein curing agent monomers (e.g., styrene monomers) serve as chain extenders or linking bridges. The progress of interparticle crosslinking eventually leads to a marked increase in viscosity. In this state, the curing reactions become diffusion-limited. This step of curing is called gelation, when the macrogel structure has formed. As the reaction proceeds, the glass transition temperature of the system increases until it reaches the cure temperature. Under this condition, the system transitions to the glassy state or undergoes vitrification. The mobility of the reacting groups is restricted due to the reduction of free volume. Consequently, the reactions become extremely slow [21].

The concentrations of curing agent monomers and microgel particles determine the morphology of the final cured material [2]. There are two extreme cases. At high styrene concentration and low microgel content, individual microgel particles can be observed, connected by styrene chains. The overall network shape is a tree-like structure with some dumbbell shapes connected to each other as shown in Figure 2.2a.

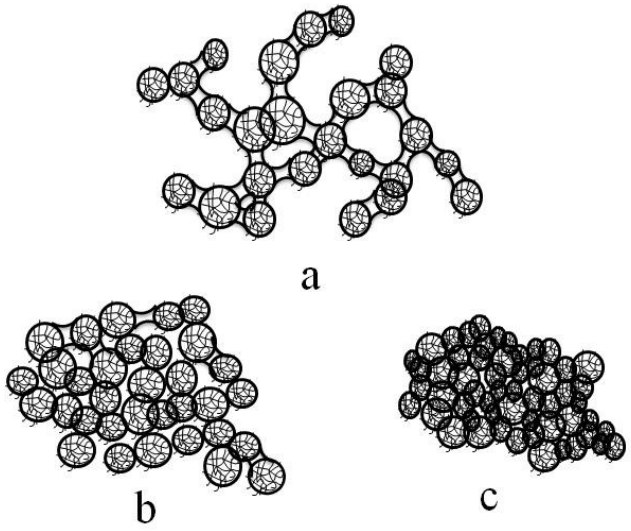

Fig. 2.2. Schematic diagrams of UPR structures based on microgels: a) tree-like structure with dumbbell shape, b) flake-and-pore structure, c) flake-type structure (adapted from Ref. 2).

In the case of low styrene concentration or high microgel content, closely packed microgels can be observed in which the particles overlap with each other (Figure 2.2c). In this case, at a fracture surface, a flake-like structure can be seen. In the third morphology, where the concentration of microgels is moderate, the structure type falls between these two extreme cases (Figure 2.2b). Since the number of microgel particles is insufficient to fill the entire space, some pores are observed in the flake-like structure. In this case, the size of flakes is smaller and the structure can be considered flake-and-pore type. In general, a higher concentration of curing agent results in an increase in the size of microgel particles, due to the swelling effect of the curing agent's small molecules.

2.1.4.Properties of unsaturated polyester resins

The properties of unsaturated polyester resins change as functions of the molecular weight, chemical structure (determined by raw materials used), and crosslink density. Despite these variables, all UPRs have some general properties in common. They can reach high crosslink density, leading to high modulus, specific strength, and creep resistance, as well as good solvent resistance and dimensional stability at elevated temperatures [22]. In addition, they have outstanding advantages such as the possibility of very low viscosity, ease of curing over a wide temperature range, low cost, excellent wetting, ease of structural modification, and a wide temperature range of processability for forming [23]. Due to these superior properties, they have attracted a lot of interest in different fields, such as the automobile industry, agriculture, transport, and construction. However, they have some drawbacks, like poor chemical and flame resistance, and moderate to high volume shrinkage [23]. Although high crosslink density gives UPRs superior properties, it makes them brittle with poor resistance to crack initiation and propagation.

Brittleness is a drawback that is common in all highly crosslinked thermosets. Since thermosets exhibit similar fracture behavior, the following discussion will generally concern fracture mechanics/mechanisms and toughening techniques for thermosets. However, most of the reported investigations into fracture behavior of thermosets are of epoxy resins, which are the strongest type of thermosets.

2.2.Fracture behavior of highly crosslinked thermosets

2.2.1.Stress and strain definition

2.2.1.1. Stress

Stress is simply defined as force per unit area, but it is necessary to resolve the stresses on a body into components to describe the stress state in terms of a stress tensor:

$$\sigma_{ij} = \begin{pmatrix} \sigma_x & \tau_{xy} & \tau_{xz} \\ \tau_{yx} & \sigma_y & \tau_{yz} \\ \tau_{zx} & \tau_{zy} & \sigma_z \end{pmatrix} \quad (2.1)$$

The components $\sigma_x, \sigma_y,$ and σ_z are normal stresses while the other components are known as shear stresses. If the body is not rotated (equilibrium state), the stress tensor will be symmetric, where the shear stresses are related by:

$$\tau_{xy} = \tau_{yx}, \tau_{xz} = \tau_{zx}, \tau_{yz} = \tau_{zy} \quad (2.2)$$

For any state of stress, a new coordinate system can be defined that has axes perpendicular to the planes on which the maximum normal stresses act, where shear stresses are zero. These planes are called principal planes and the stresses normal to these planes are the principal stresses, which are termed $\sigma_1, \sigma_2,$ and σ_3. Algebraically, σ_1 is the greatest principal normal stress and σ_3 is the smallest stress. If the three principal stresses are unequal, the general three-dimensional state is called a triaxial state of stress. If two of the three principal stresses are equal, the stress state is called cylindrical, while in the case of three equal principal stresses, the stress state is known as hydrostatic, or spherical [24].

Since plastic flow involves shear stresses, it is also important to identify the planes on which the maximum or principal shear stresses act. Principal shear stresses are termed $\tau_1, \tau_2,$ and τ_3, which are:

$$\tau_1 = \frac{\sigma_2 - \sigma_3}{2} \quad (2.3)$$

$$\tau_2 = \frac{\sigma_1 - \sigma_3}{2} \quad (2.4)$$

$$\tau_3 = \frac{\sigma_1 - \sigma_2}{2} \tag{2.5}$$

The maximum shear stress is important in theories of yielding. τ_2 has the maximum value, since σ_1 and σ_3 are the largest and smallest normal stresses.

2.2.1.2. Strain

The displacement of points in a static solid results from deformation, which may be made up of dilatation (change in volume) or distortion (change in shape). In a Cartesian coordinate system, consider the components of the displacement of a point in the directions of the three axes *x*, *y*, and *z* as *u*, *v*, and *w* respectively (Figure 2.3). The displacement tensor is [24]:

$$e_{ij} = \begin{pmatrix} e_{xx} & e_{xy} & e_{xz} \\ e_{yx} & e_{yy} & e_{yz} \\ e_{zx} & e_{zy} & e_{zz} \end{pmatrix} = \begin{pmatrix} \frac{\partial u}{\partial x} & \frac{\partial u}{\partial y} & \frac{\partial u}{\partial z} \\ \frac{\partial v}{\partial x} & \frac{\partial v}{\partial y} & \frac{\partial v}{\partial z} \\ \frac{\partial w}{\partial x} & \frac{\partial w}{\partial y} & \frac{\partial w}{\partial z} \end{pmatrix} \tag{2.6}$$

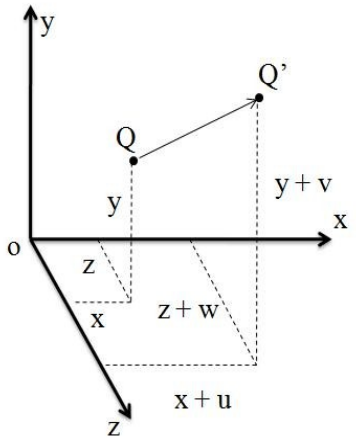

Fig. 2.3. Displacement of point Q.

In general, the displacement components produce normal and shear strains as well as rigid-body rotation. The displacement tensor can be decomposed into a symmetric tensor, called the strain tensor, and an antisymmetric tensor, called the rotation tensor.

$$e_{ij} = \frac{1}{2}\left(e_{ij} + e_{ji}\right) + \frac{1}{2}\left(e_{ij} - e_{ji}\right) \tag{2.7}$$

$$e_{ij} = \varepsilon_{ij} + w_{ij} \tag{2.8}$$

$$\varepsilon_{ij} = \frac{1}{2}\left(\frac{\partial u_i}{\partial x_j} + \frac{\partial u_j}{\partial x_i}\right) \qquad \text{(Strain tensor)} \quad (2.9)$$

$$w_{ij} = \frac{1}{2}\left(\frac{\partial u_i}{\partial x_j} - \frac{\partial u_j}{\partial x_i}\right) \qquad \text{(Rotation tensor)} \quad (2.10)$$

The strain tensor is symmetric, since $\varepsilon_{ij} = \varepsilon_{ji}$, whereas the rotation tensor is antisymmetric, since $w_{ij} = -w_{ji}$. If $w_{ij} = 0$, the deformation is called irrotational.

2.2.1.3. Hydrostatic and deviator components of stress and strain

As mentioned, the deformation of a solid involves dilation and distortion. It is useful to determine the contribution of each component to the whole deformation. The volume strain (cubical dilatation) is the change in volume per unit volume, Δ. Since only normal strains result in volume change, the volume strain is [24]:

$$\Delta = \varepsilon_x + \varepsilon_y + \varepsilon_z \qquad (2.11)$$

We can define $(\varepsilon_x + \varepsilon_y + \varepsilon_z)/3$ as the mean strain or the hydrostatic component of strain.

$$\varepsilon_m = (\varepsilon_x + \varepsilon_y + \varepsilon_z)/3 = \frac{\varepsilon_{kk}}{3} = \frac{\Delta}{3} \qquad (2.12)$$

The other part of the strain tensor involves in shape change, called the strain deviator ε'_{ij}. The deviatoric strain can be simply obtained by subtracting ε_m from each of the normal strain components. Therefore:

$$\varepsilon'_{ij} = \begin{pmatrix} \varepsilon_x - \varepsilon_m & \varepsilon_{xy} & \varepsilon_{xz} \\ \varepsilon_{yx} & \varepsilon_y - \varepsilon_m & \varepsilon_{yz} \\ \varepsilon_{zx} & \varepsilon_{zy} & \varepsilon_z - \varepsilon_m \end{pmatrix} \qquad (2.13)$$

Similar to the strain tensor, the total stress tensor can be divided into a hydrostatic tensor (σ_m) and a deviator stress tensor (σ'_{ij}). The hydrostatic tensor only involves tension and compression, while the deviator stress tensor involves the shear stresses in the total state of the stress. The hydrostatic stress is given by [24]:

$$\sigma_m = \frac{\sigma_{kk}}{3} = \frac{\sigma_x + \sigma_y + \sigma_z}{3} \qquad (2.14)$$

The deviator stress is:

$$\sigma'_{ij} = \begin{pmatrix} \frac{2\sigma_x - \sigma_y - \sigma_z}{3} & \tau_{xy} & \tau_{xz} \\ \tau_{yx} & \frac{2\sigma_y - \sigma_z - \sigma_x}{3} & \tau_{yz} \\ \tau_{zx} & \tau_{zy} & \frac{2\sigma_z - \sigma_x - \sigma_y}{3} \end{pmatrix} \quad (2.15)$$

We can consider principle axes for σ'_{ij} since it is a second-rank tensor. The principal values of the stress deviator are the roots of the following equation[24]:

$$(\sigma')^3 - J_1(\sigma')^2 - J_2\sigma' - J_3 = 0 \quad (2.16)$$

where J_1, J_2, and $J_3$are the invariants of the deviator stress tensor, which are independent of rotations of the coordinate system. J_1 is the sum of the main diagonal terms:

$$J_1 = (\sigma_x - \sigma_m) + (\sigma_y - \sigma_m) + (\sigma_z - \sigma_m) = 0 \quad (2.17)$$

J_2 is the sum of the principal minors of σ'_{ij}:

$$J_2 = \frac{1}{6}\begin{bmatrix} (\sigma_x - \sigma_y)^2 + (\sigma_y - \sigma_z)^2 + (\sigma_z - \sigma_x)^2 \\ +6(\tau_{xy}^2 + \tau_{yz}^2 + \tau_{xz}^2) \end{bmatrix} \quad (2.18)$$

J_2 is used in a yielding criterion (the Von Mises yield criterion), which will be discussed in the following section. The third invariant is the determinant of Eq. (2.15).

2.2.1.4. Yield criteria

Based on the Von Mises yield criterion, the yielding of materials occurs when the second deviatoric stress invariant (J_2) reaches a critical value described by the following equation [25]:

$$J_2 = \frac{\sigma_y^2}{3} \quad (2.16)$$

where σ_y is the tensile yield strength of the material. Substituting J_2 in terms of stress tensor components:

$$\sigma_y^2 = \frac{1}{2}\begin{bmatrix} (\sigma_x - \sigma_y)^2 + (\sigma_y - \sigma_z)^2 + (\sigma_z - \sigma_x)^2 \\ +6(\tau_{xy}^2 + \tau_{yz}^2 + \tau_{xz}^2) \end{bmatrix} \quad (2.17)$$

In terms of principal stresses, this becomes:

$$2\sigma_y^2 = [(\sigma_1 - \sigma_2)^2 + (\sigma_2 - \sigma_3)^2 + (\sigma_3 - \sigma_1)^2] \qquad (2.18)$$

There is another yield criterion, suggested by Tresca, which expresses that yielding occurs when the maximum shear stresses reaches a critical value [25]:

$$(\sigma_1 - \sigma_3) = \pm\sigma_y; (\sigma_1 - \sigma_2) = \pm\sigma_y; (\sigma_2 - \sigma_3) = \pm\sigma_y \qquad (2.19)$$

2.2.1.Stress/strain behavior

Thermosets belong to a class of glassy polymers with a reputation for being very brittle, which is reflected in their stress/strain behavior. Figure 2.4 shows typical stress/strain behaviors with different states of stress for epoxy as seen in the work of Kinloch et al.[26]. Under uniaxial tension at low temperature (lower than T_g of the resin), the thermoset is brittle and a linear relationship between stress and strain is observed. The fracture stress is reduced by increasing temperature. Approaching T_g, the curves become non-linear and limited ductile behavior may be observed, but there is no cold drawing or necking, as is seen with some thermoplastic polymers approaching T_g.

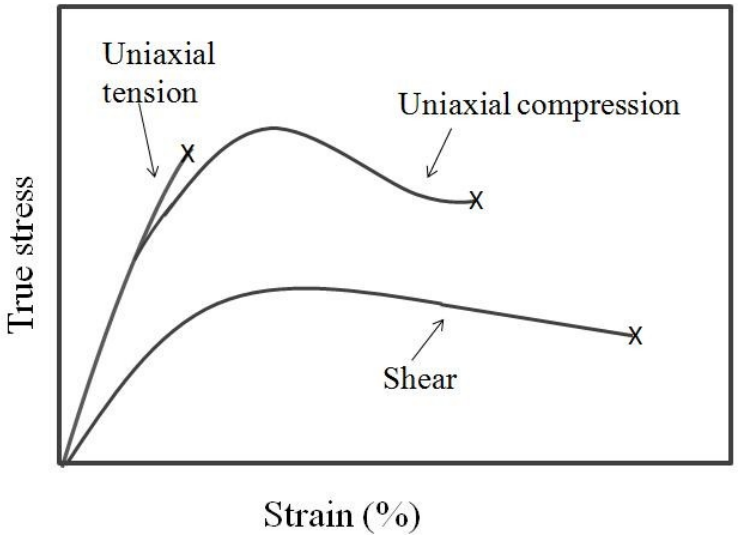

Fig. 2.4. General true stress/strain behavior of epoxy, deformed at room temperature under different stress states (adapted from Ref 26).

In contrast, under compression or shear stress, thermosets yield and undergo plastic deformation, although the amount of plastic deformation after yielding is less than that in thermoplastics.

2.2.2.Fracture mechanics

To study fracture behavior, the best approach is to control the defect size and geometry, as well as to consider the corresponding stress-field inhomogeneity [27]. Since all specimens have defects producing stress concentrations, a sharp crack (radius of the order of 10μm) is made in the test specimen. This crack induces a stress concentration effect much stronger than that produced by other defects, and hence governs the fracture initiation. Three different modes were defined for crack propagation: mode I, the crack opening or tensile mode, where a tensile stress is applied in a direction normal to the faces of the crack; mode II, sliding or shearing mode, where shear stress is applied in the plane of the crack; and mode III, tearing or parallel shear mode, where shear stress is applied parallel to the leading edge of the crack. Figure 2.5 shows all modes of crack deformation. Of these three modes, mode I is used for isotropic materials, which have the lowest toughness value. In the case of adhesives and laminates, other modes must be applied.

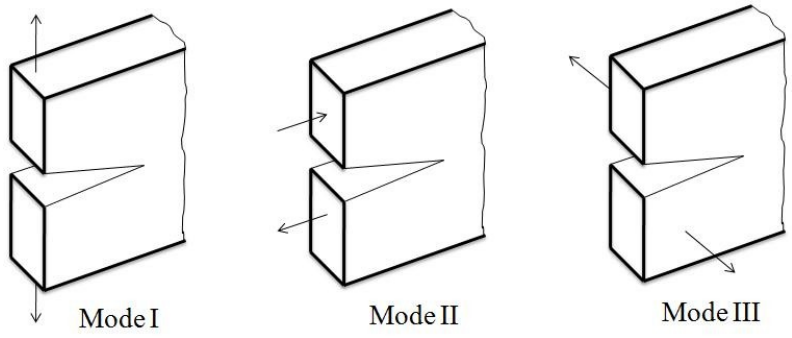

Fig. 2.5. Different modes of loading.

Griffith [28] proposed a criterion to predict the crack propagation conditions based on an energy balance approach. During crack propagation, elastic strain energy (i.e., energy stored in the material during elastic deformation) is released. In addition, the crack extension process causes an increase in the surface energy of the system due to the

formation of new surfaces at the faces of a crack. Griffith considered that for crack propagation, the decrease in elastic strain energy is at least equal to the required energy for the formation of new crack surfaces. He introduced the crack model shown in Figure 2.6. The stress state is considered plane stress, since the thickness of the plate is small enough which depends on the sample geometry and material properties.

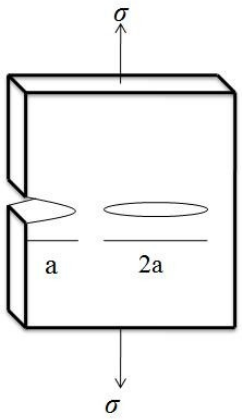

Fig. 2.6. Griffith crack model.

The shape of the cracks is assumed to be elliptical, where both interior and edge cracks have the same effect on fracture behavior. The elastic strain energy per unit of plate thickness is equal to [24]:

$$U_E = -\frac{\pi a^2 \sigma^2}{E} \tag{2.20}$$

where E and a are the modulus of elasticity and one half the length of an internal crack, respectively. σ is tensile stress acting normal to the crack. Since crack growth releases elastic strain energy, the negative sign must be used. During crack propagation, new crack surfaces are formed, where the surface energy is [24]:

$$U_s = 4a\gamma_s \tag{2.21}$$

where γ_s is specific surface energy. The crack growth results in a total change in potential energy:

$$\Delta U = U_s + U_E \tag{2.22}$$

According to Griffith's criterion, an increase in surface energy must be compensated by a decrease in elastic strain energy. Therefore [24]:

$$\frac{d\Delta U}{da} = 0 = \frac{d}{da}\left(4a\gamma_s - \frac{\pi a^2\sigma^2}{E}\right)$$

$$4\gamma_S - \frac{2\pi a\sigma^2}{E} = 0$$

$$\sigma = \left(\frac{2E\gamma_S}{\pi a}\right)^{1/2} \qquad (2.23)$$

Equation 2.23 gives the required energy for crack propagation in a brittle material as a function of the microcrack size. For a plate that is thick compared to the length of the crack (plane strain state), the Griffith equation is given by [24]:

$$\sigma = \left[\frac{2E\gamma_S}{(1-\vartheta^2)\pi a}\right]^{1/2} \qquad (2.24)$$

where ϑ is Poisson's ratio.

These equations apply for brittle materials (with completely elastic behavior), but many materials do experience some plastic deformation during fracture. Orowan [28] suggested that the Griffith equation can be made more compatible with brittle fracture of metals by considering specific plastic deformation energy associated with crack extension (γ_p):

$$\sigma = \left[\frac{2E(\gamma_s+\gamma_p)}{\pi a}\right]^{1/2} \qquad (2.25)$$

In general, the Griffith equation can be modified by replacing $2\gamma_S$ with the fracture energy term, G_c such that [26]:

$$\sigma = \left(\frac{EG_c}{\pi a}\right)^{1/2} \qquad \text{(Plane stress)} \qquad (2.26)$$

$$\sigma = \left(\frac{EG_c}{\pi(1-\vartheta^2)a}\right)^{1/2} \qquad \text{(Plane strain)} \qquad (2.27)$$

The fracture energy is then the total dissipated energy during crack growth. It is defined as the critical required energy for crack propagation per unit area and expressed in J m^{-2}.

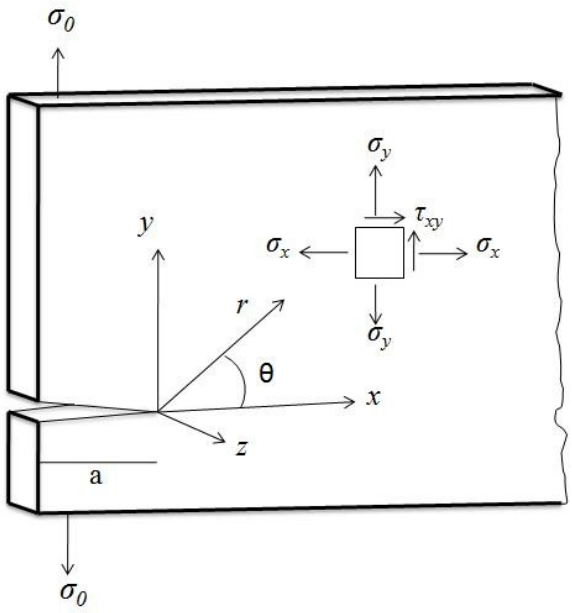

Fig. 2.7. The stress distribution in the vicinity of an edge crack in a thin sample loaded in tensile mode.

Another criterion for fracture was proposed by Irwin [24], who studied stress in the vicinity of a crack tip. When a thin plate is loaded in one direction, the geometry of the notch (as an edge crack) changes the stress distribution, developing a transverse elastic stress in the other direction as well as shear stress. For the tensile mode, the stress distribution in the vicinity of the crack tip in a thin plate (plane stress state) for an elastic solid in terms of the coordinates shown in Figure 2.7 is given by following equations [24]:

$$\sigma_{ij} = \sigma_0 \left(\frac{a}{2r}\right)^{\frac{1}{2}} f_{ij}(\theta) \tag{2.28}$$

$$f_{xx}(\theta) = cos\frac{\theta}{2}\left(1 - sin\frac{\theta}{2}sin\frac{3\theta}{2}\right) \tag{2.29}$$

$$f_{yy}(\theta) = cos\frac{\theta}{2}\left(1 + sin\frac{\theta}{2}sin\frac{3\theta}{2}\right) \tag{2.30}$$

$$f_{xy}(\theta) = sin\frac{\theta}{2}cos\frac{\theta}{2}cos\frac{3\theta}{2} \quad (2.31)$$

where σ_{ij} (σ_{xx}, σ_{yy}, and τ_{xy}) are the components of the stress tensor on an element at distance r and angle θ from the crack trip. σ_0 and a are the applied tensile stress and the length of the edge crack. The other extreme state is plane strain, where the stress state is triaxial since the thickness is sufficient to meet the elastic constraint. This state causes the most complex stress field. In the plain strain condition ($\varepsilon_{zz} = 0$ for a relatively thick plate), $\sigma_{zz} = \vartheta(\sigma_{xx} + \sigma_{yy})$, where ϑ is Poisson's ratio.

Irwin modified these equations to [24]:

$$\sigma_{ij} = \frac{K}{\sqrt{2\pi r}} f_{ij}(\theta) \quad (2.32)$$

where the parameter K is the stress intensity factor indicating the magnitude of the stress field based on linear elasticity theory. The crack would propagate in the material if K (K_I in mode I) reaches a critical value K_c (K_{Ic} in mode I). Irwin set K as [28]:

$$K = Y\sigma_0\sqrt{\pi a} \quad (2.33)$$

where Y is a dimensionless parameter depending on both the crack and specimen sizes and geometries, as well as the manner of load application. Fracture occurs when the applied stress exceeds the critical stress σ_c (Eq. 2.25). Thus, the critical value of the fracture toughness K_c (with units MPa $m^{1/2}$) is defined by:

$$K_c = Y\sigma_c\sqrt{\pi a} \quad (2.34)$$

There are two extreme cases for mode I loading, the plane stress and the plane strain conditions. The plane strain condition is the more severe stress state, resulting in a lower value of K_c for a thick sample compared to that of a thin sample in the plane stress condition. When a thin plate is loaded in the y direction, the geometry of the edge crack develops a transverse elastic stress in the x direction. A stress distribution of σ_y is formed due to the stress concentration effect of the crack tip, which results in an elastic strain gradient in front of the notch. Consequently, a different transverse strain occurs for

adjacent elements in the crack tip vicinity, leading to their separation. These elements can be considered tiny tensile samples connected to each other. In order to maintain continuity, a transverse stress σ_{xx} must exist across each interface [24]. For the plane

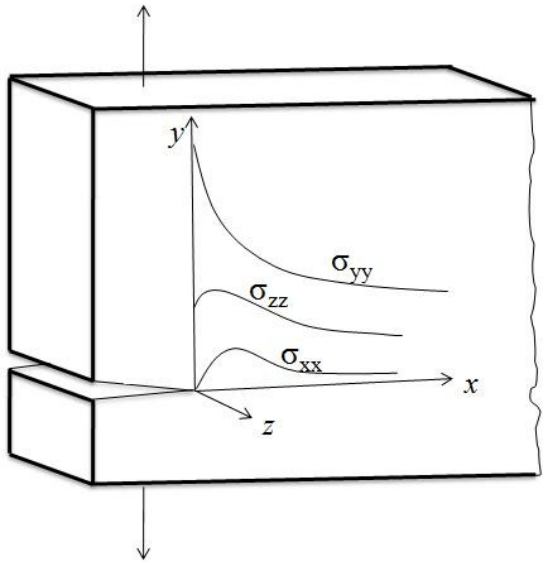

Fig. 2.8 Typical elastic stress field in front of the crack tip (adapted from Ref: 29).

stress condition, the stress in the thickness is too small and can be ignored. However, in the plane strain condition, an elastic stress in the z direction is also developed, where $\sigma_{zz} = \vartheta(\sigma_{xx} + \sigma_{yy})$. A typical plot of the elastic stress field in the vicinity of crack tip is shown in Figure 2.8. The following conditions must be met for Eq. 2.28 to hold: (i) linear elasticity of the matrix, (ii) infinitely sharp radius of the crack tip, and (iii) no damage zone around the crack tip. According to Figure 2.8, σ_{yy} becomes infinitely large when r approaches zero [29].

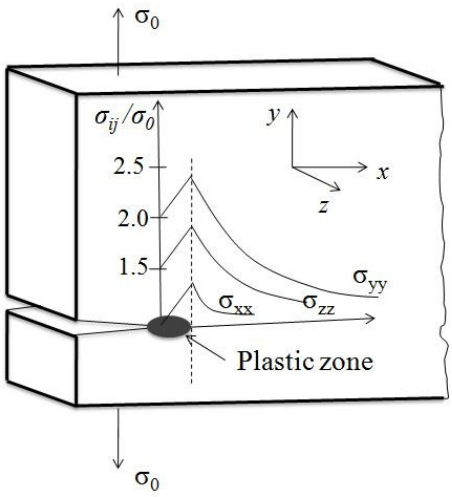

Fig. 2.9. Distribution of stresses during local plastic deformation (adapted from Ref:29).

However, in reality, plastic deformation begins at the crack tip when the local stress reaches the yield strength of the material. Therefore, a finite plastic zone is formed ahead of the crack tip and changes the stress distribution (Figure 2.9)

If the plastic zone is small (in the case of thermosets), it will not greatly disturb the elastic stress field where the extent of the plastic zone may be determined based on linear elastic fracture mechanics [26]. Figure 2.10 shows the radius of a circular plastic zone at the tip of a crack r_y.

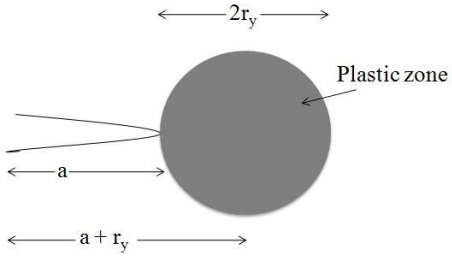

Fig. 2.10. Irwin model of the plastic zone at a crack tip (adapted from Ref:26).

For $r_y \ll a$, Eq. 2.33 is still valid, but the length of the crack must be $(r_y + a)$ instead of a. The size of the plastic zone radius is given by [26]:

$$r_y = \frac{1}{2\pi}\left(\frac{K_I}{m_p \sigma_y}\right)^2 \qquad (2.35)$$

where σ_y and m_p are the tensile yield strength and the plastic constraint factor respectively. m_p reflects the constraint on the developing plastic zone, which is caused by the surrounding elastic material. For two extreme states (plane stress and plane strain), the plastic zone radius in each state are given by following equations [26]:

$$r_y = \frac{1}{2\pi}\left(\frac{K_I}{\sigma_y}\right)^2 \qquad \text{(Plane stress)} \qquad (2.36)$$

$$r_y = \frac{1}{6\pi}\left(\frac{K_I}{\sigma_y}\right)^2 \qquad \text{(Plane strain)} \qquad (2.37)$$

In a thick plate (plain strain condition), the greater volume of elastic material leads to higher stress in the plastic zone, resulting in a smaller value of the plastic zone radius.

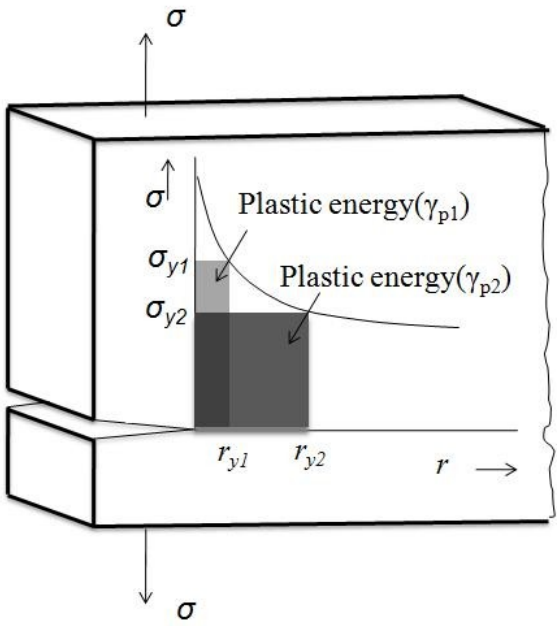

Fig. 2.11. Schematic of tensile stress as a function of distance from the crack tip in a state of plane stress, The relation between the yield stress and the plastic zone radius and plastic energy.

This localized plastic deformation in front of the crack tip plays an important role in fracture toughness. In a polymer with high yield strength, the concentrated stress in the crack tip provides a small plastic zone around the crack and a little plastic energy is dissipated during the crack growth. In contrast, in a polymer with low yield strength, a

larger plastic zone is formed, resulting in higher toughness due to higher dissipated plastic energy [30]. The effect of the yield stress of the material on the plastic zone size and plastic energy is illustrated in Figure 2.11.

K_c (K_{Ic} in mode I) and G_c (G_{Ic} in mode I) are intrinsic parameters that are independent of crack length and sample size. For polymers, they depend on temperature and displacement rate. The value of K_{Ic} at room temperature varies from 0.5 MPa.m$^{1/2}$ for very brittle materials up to 2 MPa m$^{1/2}$ for toughened thermosets. The value of G_{Ic}, depending on Young's modulus, varies from 100 J m^{-2} to 2000 J m^{-2}. For a valid determination of K_{Ic} and G_{Ic}, the samples must be thick enough to be in plane strain conditions. The edge notch (length a) has to be neither too short nor too long. In plane strain conditions, the relationship between these two parameters is as follows [27]:

$$G_{Ic} = \frac{K_{Ic}^2}{E}(1 - \vartheta^2) \qquad (2.38)$$

where E and ϑ are Young's modulus and Poisson's ratio, respectively.

In general, different modes of crack propagation have been detected [26,31] for which the relative load-deflection curves are shown in Figure 2.12. Mode I (Figure 2.12a) is stable or continuous crack propagation, which leads to a relatively smooth fracture surface. This type of propagation occurs at low temperatures and in fully cured polymers. At the maximum value of the load, the stable crack slowly initiates growth, and the displacement rate controls the rate of crack growth. The second mode is stick/slip propagation [26], also called unstable brittle mode (Figure 2.12b). The crack propagates at a peak load (P_i), corresponding to the critical stress intensity factor for initiation (K_{Ici}), and it is arrested at the minimum load (P_a), corresponding to the factor for arrest (K_{Ica}). The difference between initiation and arrest values is known as instability. In this mode, crack arrest lines can be seen on the fracture surface, where each line is related to a jump/arrest event. The crack arrest regions can vary from fine lines to broad bands, depending on material composition and testing conditions. The regions between arrest lines are relatively smooth and featureless. Finally, the third mode is stable ductile propagation [31], which can be observed at high temperatures in under-cured samples and thin sheets. The load-deflection curve corresponding to this propagation mode is

shown in Figure 2.12c. Firstly, the load rises linearly and then becomes non-linear by increasing deflection before the maximum load is reached. In this mode, there is a gradual transition from unstable brittle mode by raising the test temperature. The arrest lines first start to broaden and eventually cover the whole fracture surface. Note that K_{Ic} values for all modes of crack propagations are the same, since only the critical stress (σ_c) is necessary for K_{Ic} calculation.

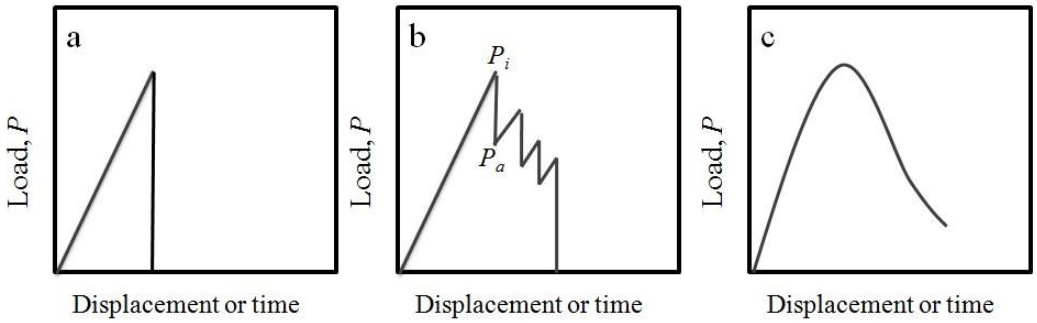

Fig. 2.12. Different types of crack propagation: a) Stable, b) Unstable, c) Ductile (adapted from Refs: 27, 31).

Different variables affecting the stability of crack propagation and corresponding stress levels in thermosetting polymers such as temperature and the rate of deformation (testing). An increase in the rate of deformation decreases K_{Ici} while K_{Ica} approximately remains constant. Eventually, there is a transition to continuous crack propagation at high rates. This stabilization of crack propagation at high speeds has been observed for a variety of thermosetting polymers. Investigations show that, at low temperature, crack propagation is continuous type; however, it becomes unstable at higher temperatures. Therefore, in viscoelastic thermosets, increasing the temperature would be similar to reducing the rate of testing, since both factors promote stick/slip propagation.

2.2.3.Failure mechanism

Thermosetting polymers have a relatively featureless fracture surface compared to other brittle polymers such as polystyrene. However, if stable test-pieces (sample pieces without a notch) are used, features can be observed on the fracture surface that are closely related to the mode of crack propagation [26]. Investigation into crack propagation in thermosets showed that cracks can propagate in an unstable stick/slip manner, although sometimes continuous propagation can be obtained in thermosets similar to glassy

thermoplastics. Some explanations have been proposed to explain unstable behavior in thermosets, the most convincing one of which is introduced by Gledhill et al. [26] They pointed out that in resins with low yield strength, crack propagation is unstable, whereas propagation is continuous in high yield strength resins. In other words, low yield strength might promote crack tip blunting, resulting in stick/slip propagation.

In general, crack propagation in polymers usually involves processes in which plastic and viscoelastic energy dissipation happen close to the crack tip. Two of these major energy absorption phenomena are shear yielding and crazing [26].

Shear yielding is a localized or inhomogeneous plastic deformation of a polymer, which cannot be completely recovered without increasing temperature. Shear yielding happens at constant volume, but it is obviously accompanied by a change in shape. In general, cooperative chain motion and local mobility are needed for yielding. In polymer glasses, cooperative chain motion occurs at T_g, which is considered α transition. In addition, there are segmental mobilities below T_g that are responsible for secondary transitions, such as β transition [27]. There are different types of localized motion (involving a smaller number of atoms) such as rotation of large lateral groups, oscillation of aromatic rings, and crankshaft-like motions on short-chain segments.

In polymer networks, the yielding process often requires the motion to occur in the β transition, which is mostly due to crankshaft-like motions [27]. In this transition, local motions of the polymer chain backbone occur where cooperative motion of surrounding chains is not required [32]. A network with a highly active β transition has more capability for dissipating energy. If the β transition temperature of a polymer network is above the ambient temperature (where most of the mechanical tests are done at ambient temperature) such as unsaturated polyesters (T(1 Hz) $\approx$ Hz K with activation energy H_β $\approx$ 100-180 KJ·mol^{-1}), the corresponding β relaxation is inactive [27]. In contrast, amine-crosslinked epoxies have β transition temperatures below the ambient temperature (T(1 Hz) $\approx 190 - 240$ K with activation energy $H_\beta \approx 70 \pm 30$ KJ·mol^{-1}), so the corresponding β relaxation is active, resulting in a more localized yielding compared to unsaturated polyesters.

Local shear stresses cause conformation changes in polymer chains. In thermosets, the chains between crosslinks can be aligned in the stretch direction, where more flexible chains undergo greater alignment [27]. In this case, shear bands are formed in which plastic strain is localized.

Glassy thermoplastics undergo deformation by crazing. When a tensile stress is applied to the polymer, microvoids are nucleated at points of high stress concentration in the material, created by cracks, flaws, scratches or molecular heterogeneities. During the development of microvoids, which happens in the plane perpendicular to the maximum principal stress, fibrils of plastically deformed material are formed, but microvoids do not coalesce to form a crack. As a result, an interpenetrating system of voids and polymer fibrils is formed, which creates a localized yielded region known as a craze. Crazing involves localized plastic deformation of the material resulting from strain softening. It occurs with an increase in volume, since it is a cavitation process. Crazing is increased by applying triaxial tensile stresses and may be inhibited by hydrostatic pressure. Crazes may grow and break down to make cracks at a level of stress much lower than that required for shear yielding, consequently leading to brittle fracture with low values of K_{Ic} and G_{Ic}.

In thermosetting polymers, there is little evidence for the occurrence of crazing, where craze-like structures are reported in toughened [33] or low crosslinked thermosets. The probability of crazing is reduced by increasing crosslink density. This is similar to the relationship between crazing formation and physical entanglements in thermoplastics [31] reported by Donald and Kramer. They showed that in thermoplastics, when the length of polymer chains between physical entanglements (l_c) decreases below ~20 nm, a transition from crazing to shear yielding happens. Similarly, this transition in thermosetting polymers might occur as crosslink density increases and the length of polymer chains between crosslink spots decreases. Crosslink sites prevent craze fibril formation. Therefore, crazing in thermosets is almost nonexistent, and shear yielding in these polymers is the major mechanism of plastic deformation.

Energy absorbing processes operate in highly localized regions around the crack tip. Since these mechanisms are confined to a very small volume relative to the whole

specimen, the total amount of plastic energy absorbed is low. Consequently, these materials are strongly susceptible to brittle fracture. A solution to improve the toughness of thermosetting polymers is to increase the proportion of these plastically deformed regions. A successful technique has been incorporating a second phase into the polymer matrix.

2.3.Toughening techniques

A polymer is strong when it has a high yield strength, and it is tough if it can experience bulk homogenous yielding. As mentioned, in polymer networks with high crosslink density, only localized plastic deformation can occur, resulting in their brittleness. Many studies on toughening of thermosetting polymers showed that an increase in thermal resistance, T_g or HDT (heat deflection temperature), and yield strength results in a decrease in toughness (K_{Ic}). Therefore, the objective is to improve toughness without sacrificing thermal properties and stiffness. In general, two methods of improving toughness can be considered: (I) plasticization and (II) promoting plastic deformation mechanisms via the creation of a heterogeneous structure, by such methods as incorporating a second phase into the polymer matrix [27]. With the plasticization method, a miscible low-T_g compound is added to the polymer, resulting in a reduction in the T_g and yield strength of the thermoset. Consequently, toughness is increased at the cost of thermal properties and stiffness and strength. Therefore, this technique is not suitable for toughening purposes. Alternatively, incorporation of a second phase in the system can increase the intensity of energy dissipation, since it causes a distribution of stress concentration in the whole system. Consequently, higher resistance against crack initiation is obtained. However, at a certain point, a crack is formed and starts to grow. In this case, several mechanisms for energy absorption become active during crack propagation, involving different energy dissipating processes. In the presence of these particles, energy dissipating processes can be classified into two major groups: (i) localized plastic deformation of the matrix, such as shear band formation of the matrix, which is a localized shear yielding; and (ii) damage processes, including particle-matrix debonding and material rupture, which may result in void formation (cavitation) or breakage of rigid particles. In addition, there are processes affecting crack front

propagation. Different factors determine the controlling mechanism and energy dissipating processes, including characteristics of the particles and matrix, and the interface between phases. In the following sections, different toughening agents will be introduced and the corresponding mechanisms and energy dissipating processes will be discussed.

The most frequently applied techniques for generating heterogeneous structure involve the addition of mineral fillers, rubbery, and thermoplastic particles to the matrix. The approach is to increase the number of sites experiencing localized energy absorbing deformation. In this case, a much greater volume of polymer is involved, resulting in an increase in toughness. Since the morphology of these systems plays an important role in the toughness of the final product, we briefly introduce possible morphologies first, and then different toughening techniques will be discussed.

2.3.1.Morphology of binary systems

A successful technique for toughening thermosets has been the incorporation of a second phase into the polymer matrix. The incorporating additive can be in the form of particles, which would be dispersed throughout the thermosetting matrix, leading to particulate morphology. Alternately, the toughening agent, such as liquid rubber or thermoplastic, can be miscible in the liquid thermosetting resin where phase separation happens during curing process, which determines the final morphology of the system. Phase separation during the curing process is essential, since the particulate morphology results in a greater improvement in toughness compared to homogeneous structure [34].

The shape, size, and size distribution of the second phase depend on the kinetics of the curing process and the mechanism of phase separation. In general, two types of phase separation can occur, binodal and spinodal decomposition [35].

Binodal decomposition, also called nucleation and growth, results in a particulate morphology (Figure 2.13a) in which spherical domains of the second phase are dispersed in a continuous matrix. In this morphology, very sharp interfaces are formed. Binodal decomposition is associated with metastability, meaning that there are large composition

fluctuations and an energy barrier. Firstly, domains of a minimum size are formed, which are called critical nuclei, and their size increases with time.

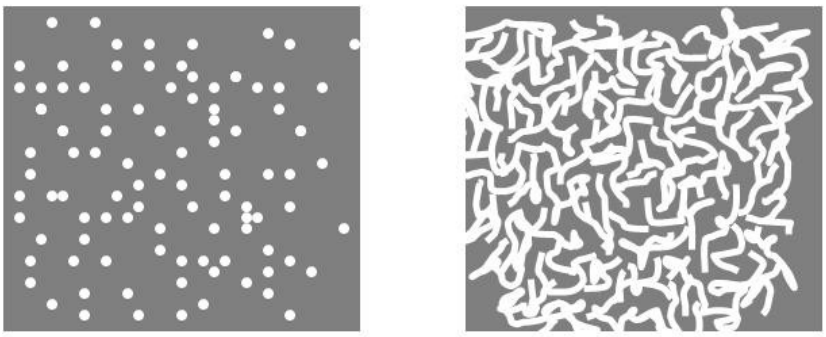

Fig. 2.13. Schematic diagrams of a) particulate morphology, b) co-continuous morphology.

Spinodal decomposition often leads to a co-continuous morphology (Figure 2.13b) with more diffuse interfaces. In spinodal decomposition, since the solution is initially uniform in composition, separation occurs by a diffusional flux against the concentration gradient (i.e., the diffusion coefficient is negative)[36]. In this mechanism, the energy barrier is negligible even where small fluctuations in composition can grow. In the initial stages, interconnected cylinders are formed, and with time the purification of phases occurs by mass transfer across the boundary.

2.3.2. Stress Analysis

The presence of an inclusion having a different modulus compared to the matrix can change the stress distribution in a system that is under an external load. The stress state around the inclusion can influence the energy dissipation processes, such as shear yielding and crazing (in the case of thermoplastics), and it also affects the post-yield behavior, such as debonding and tearing of soft particles [37].

For the first time, Goodier [38] solved the equation of elasticity to investigate the disturbing effect of small inclusions (with two spherical and cylindrical geometries) on a uniform stress distribution. In his solution, he assumed that an infinite solid surrounds the inclusion, where the matrix is subjected to a uniformly applied stress at infinity. In addition, the matrix has ideal properties of elasticity, isotropy, and homogeneity. The

analysis of the stress distribution inside and outside a spherical inclusion has been done based on the coordinate system presented in Figure 2.14. In this model, a single particle is considered, which is embedded in a uniform matrix subjected to uniaxial tension. The presence of the inclusion leads to a change of the initial stress from a uniaxial state to a triaxial state. Different stresses, including $\sigma^{rr}, \sigma^{\theta\theta}$, and $\tau^{r\theta}$, which are radial, hoop, and shear stress respectively, for the matrix and inclusion can be calculated based on Goodier's model. All stresses are strongly dependent on the ratio of the matrix shear modulus to that of the inclusion.

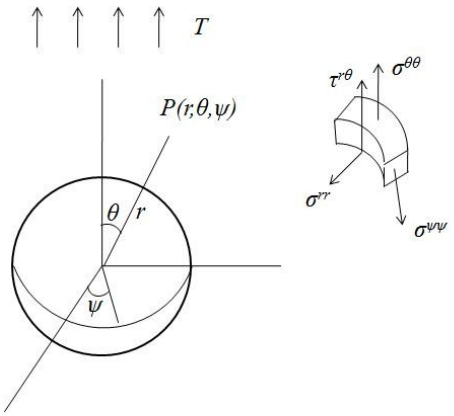

Fig. 2.14. Stress distribution in an element of a spherical particle.

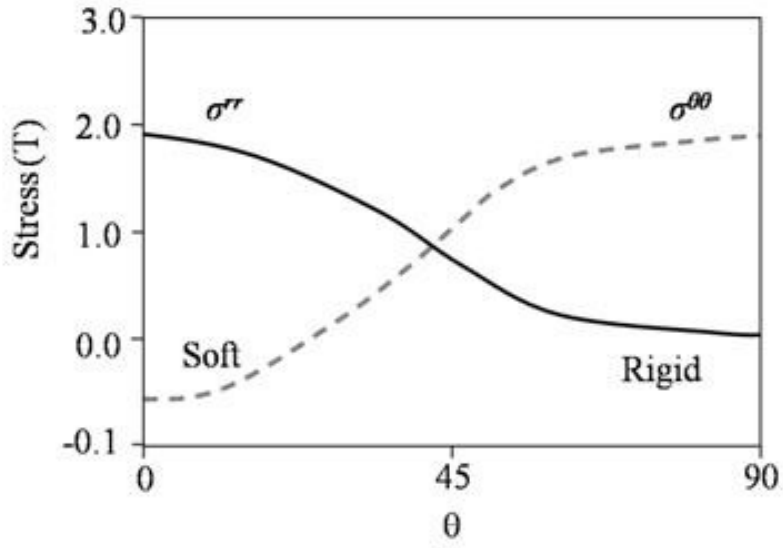

Fig. 2.15. Stress concentration outside the inclusion of different materials (adapted from Ref:37)

(Soft inclusion : G_1/G_2=1000, rigid inclusion:G_1/G_2=0.01, where G_1 and G_2 are shear modulus of the matrix and inclusion respectively).

Figure 2.15 shows a typical stress concentration profile in the region outside the spherical boundary, where the second phase is a rigid particle (glass bead) or a soft inclusion (rubber) [37]. For a single soft rubber particle, the stress concentration occurs at the particle equator with a factor around 2. In contrast, in the case of a glass bead, there is a stress concentration effect at the particle poles.

Figure 2.16 presents a typical stress distribution inside the inclusion. All stresses are normalized to the applied stress (T) where their intensities strongly depend upon the shear modulus ratio.

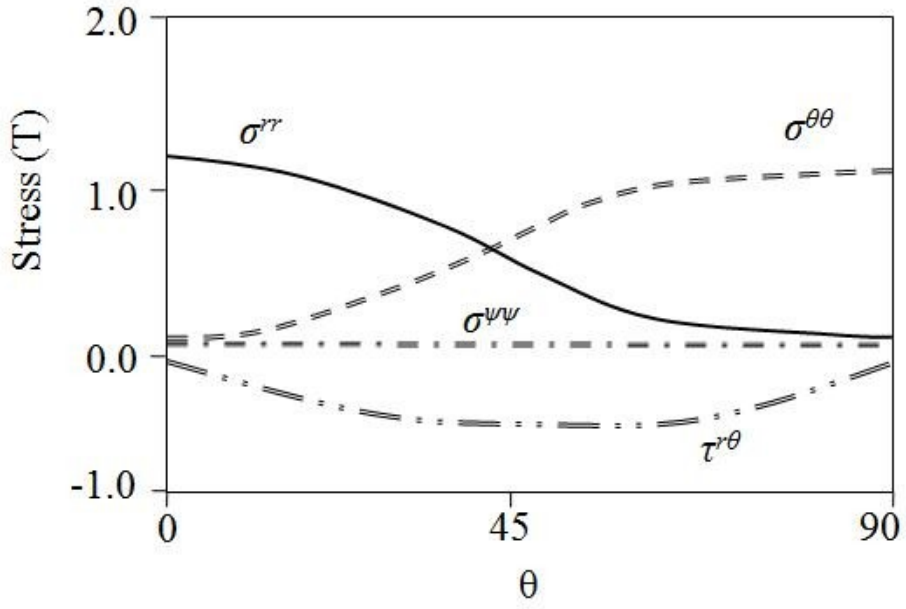

Fig. 2.16. Stress distribution inside an inclusion, shear modulus ratio of 1.0 (adapted from Ref:37).

Figure 2.17 presents the stress concentration around a single rubber particle in the matrix. As mentioned, for particles with a modulus lower than the matrix, the stress concentration occurs at the particle equator; otherwise, it happens at the particle pole.

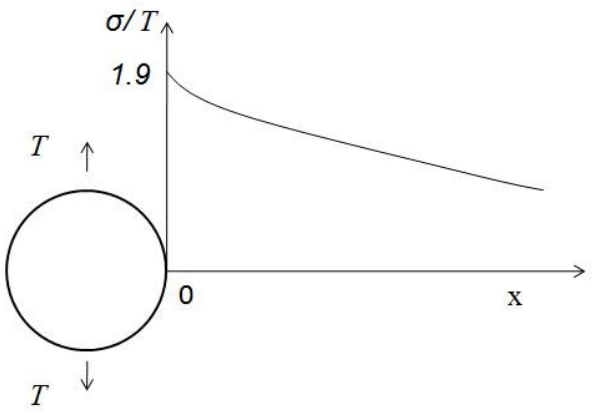

Fig. 2.17. Stress concentration around a single rubber particle (adapted from Ref:27).

If the concentration of the particles is increased, an overlap of the stress concentration effects of neighboring particles occurs (Figure 2.18). In this case, a larger volume fraction of the matrix is under an average load higher than the applied external load.

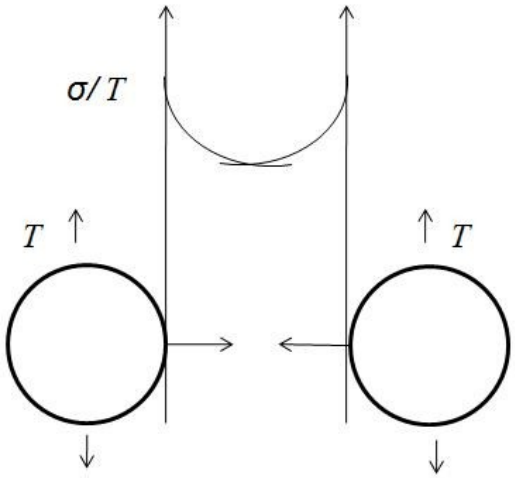

Fig. 2.18. Stress field overlap between rubber particles (adapted from Ref: 27).

2.3.3.Rubber toughening of thermosets

Rubber can be incorporated to thermosets in two forms, liquid and solid. Among solid additives, preformed core-shell rubber (CSR) particles are the most common additive, and will be discussed later. In the case of the liquid additive, the rubber is added to the thermoset precursor (before curing), then affects the polymerization reactions, leading to phase separation. Consequently, the rubber-modified thermoset will exhibit a two-phase

microstructure after curing of both phases, resulting in toughening of the matrix. In general, the following characteristics are required for rubbers as toughening agents [39]:

a) Thermodynamically, a major part of the rubber must be incompatible with the matrix for phase separation to occur.
b) There is an optimum value for the size of rubbery particles in each system to achieve the maximum improvement in toughness.
c) The rubber molecules should have sufficient interaction with the resin molecules to have enough solubility within the liquid resin. Therefore, some polar groups in the chemical structure of the rubber are essential.
d) Strong interfacial adhesion between the rubber and thermosetting matrix is essential.
e) For fine distribution of rubber particles during cure, the rate of crosslinking of the rubber by peroxide must be lower than that of thermoset.
f) The rubber must have a relatively high molecular weight to have lower solubility in the thermoset precursor, resulting in more separation during curing. Dissolved rubber molecules in the matrix can cause a reduction in the T_g and modulus of the system.

2.3.3.1.Toughening mechanisms

Incorporation of rubbery particles improves the toughness of thermosets via various mechanisms, including shear yielding, crack-bridging, craze-like damages [33], rubber particle cavitation, and rubber-matrix debonding [26,27,31].

In rubber-modified thermosets, the toughness is mainly improved by the energy dissipation mechanisms of the matrix, primarily localized shear yielding, due to the presence of the rubbery phase. The dispersed rubber phase initiates micro-shear bands. There is some controversy in micromechanics over explanations for how rubber particles promote shear yielding deformation. Newman and Strella [26] suggested that rubber particles can produce triaxial tension in the matrix, resulting in extensive shear yielding due to a rise in the local free volume. An additional interpretation can be given based on cavitation formation in the rubber particles. In the vicinity of the crack tip, a plastic zone is formed where the plastic deformation of the matrix provides the required conditions for

cavitation of the rubber particle, which is under maximum principal stress at its equatorial region, to occur. Sue et al. [40] proposed a micromechanical modeling of the cavitational process of the rubber particle at the crack tip. He calculated the hydrostatic tension components as well as the octahedral shear stress component (τ_{oct}), which is analogous to the stress deviator and responsible for plastic deformation around the rubber particle. In general, the presence of the particle in the vicinity of the crack tip caused an increase in both dilatation and deviator shear stress components. If cavitation of the rubber particle occurs, τ_{oct} is increased, whereas hydrostatic tension in the matrix is not fully dissipated. When the cavitational process of the rubber particle occurs, the stress state changes from triaxial to biaxial. As a result, τ_{oct} is significantly increased, which is favorable for yielding of the matrix. Cavitation occurs due to the rupture of the rubber phase. Therefore, the cavitational strength of the rubber particle becomes important. If this strength is low, the particle acts like a hole and τ_{oct} is moderately increased. In this case, the other stress components (hydrostatic tension) are increased to the point where they may control the fracture mode and the system undergoes brittle failure. At the other extreme, if the cavitational strength of the particles is too high, the hydrostatic tension components build up faster than τ_{oct}, resulting in brittle failure.

In some rubber-modified thermoset systems (especially in the case of epoxies) stress whitening has been reported. Some researchers [33] claimed that crazing is a controlling mechanism, where the presence of crazes can justify observed stress whitening, since shear yielding is essentially a constant-volume process. However, this does not seem correct, since crazing does not occur in highly crosslinked thermosets. It is generally believed that crazing can only take place in either under-cured thermosets or networks having low crosslink densities [27,33]. Sue et al. [33] proposed a craze-like structure justifying the stress whitening in rubber-modified epoxies. He called this structure "croid", which is derived from "crack" and "void". Croids are line arrays of cavitated rubber particles. These cavitation line arrays do not have any craze fibrils. Coalescence of the cavitated particles can occur, resulting in the formation of microcracks in the damage zone around the crack tip. The formation of massive croids can promote shear yielding of the matrix.

It is important to note that rubber particle cavitation happens only when the particles and matrix are well adhered. Otherwise, debonding at the rubber particle-matrix interface can occur instead. In this case, the degree of triaxial stress is reduced due to the formation of voids, but the increase in the octahedral shear stress component is not enough to significantly promote yielding of the matrix.

Crack-bridging is usually a secondary mechanism to improve toughness in multiphase polymers. The crack propagates around the rubber particles. When a crack begins to open, the particles are stretched between the crack surfaces until they tear. The particles play two roles: (1) they have a sort of bridging effect by applying compressive force on the crack wake, and (2) tearing of rubber particles occurs, leading to energy dissipation. In addition, this mechanism cannot explain stress whitening, the high fracture energy and toughness values at higher temperatures, or the transition in crack growth behavior [31].

Although shear-bands formation is the major mechanism controlling toughness in many thermosets, especially in epoxy resins, the intensity depends on the ductility of the matrix. An increase in crosslink density of the matrix decreases shear band formation [41] (e.g., in a rubber toughened epoxy with a very high degree of crosslink density). In the case of unsaturated polyester resin, there is controversy concerning the formation of shear bands. Kim et al. [41] claimed that, in rubber toughened unsaturated polyester, shear bands do not form due to the high crosslink density of UP and the very short chain length between crosslinks. Thus, toughness enhancement in rubber toughened UPR is very limited compared to other thermosets, especially epoxy resins. In contrast, in some studies [42-45], shear yielding in an unsaturated polyester matrix is introduced as the major source of energy dissipation during fracture.

2.3.3.2. Influence of morphology and network structure

According to the mechanisms controlling fracture behavior of rubber modified thermosets, the toughness depends both on the matrix, where the shear band forms, and the rubbery phase, which causes cavitation and crack-bridging. As mentioned, crosslink density and the T_g of the matrix can affect toughness by influencing shear yielding mechanisms. The presence of a low-T_g rubbery phase can reduce the T_g of the matrix, resulting in an increase in toughness by reducing shear yield strength of the matrix.

Clearly, a greater quantity of dissolved liquid rubber in the matrix causes a greater reduction in the T_g of the matrix.

The morphology of the system is key to controlling cavitation and crack-bridging mechanisms. Particulate morphology in rubber-thermosetting polymer systems leads to a greater improvement in toughness compared to homogenous blends. Even in the case of liquid rubber, which must be miscible in the uncured resin, phase separation during the cure is essential to achieve a significant improvement in toughness [34,39].

The degree of miscibility of liquid rubber with the thermoset resin plays an important role in the final size of rubber particles. When liquid rubbers can be completely dissolved in liquid thermosetting resin, phase separation occurs during curing leading to the formation of a fine dispersion of particles with diameters of a few microns or less [43]. In contrast, less soluble liquid rubber would be precipitated from the rubber-matrix mixture before curing. This inhomogeneity in the starting system leads to a coarse dispersion of rubber particles in the final cured product.

2.3.3.3. Influence of rubbery phase characteristics

There is a limit on the rubber volume fraction, since with too high rubber content, phase inversion happens, resulting in very poor mechanical properties [45]. In addition, controlling the phase separation of rubbery particles during the curing process becomes difficult at high rubber concentration [46]. Martuscelli et al. [43] found that there is an optimum rubber content in unsaturated polyester to achieve maximum toughness because too higher rubber content resulted in a relatively coarse dispersion of rubbery particles.

As mentioned, the size of rubber particles affects the type of fracture mechanism. In many studies [27], the effective range of rubber particle size for toughening has been found to be 0.1-10 μm in diameter. For a given volume fraction of the rubbery phase in a system, there is a critical particle size below which the toughness could be significantly improved. This critical size depends on the interparticle distance, which determines the intensity of stress-field overlap between neighboring particles. Stress overlap is favorable for shear band formation. In contrast, large rubber particles result in a modest increase in toughness by crack-bridging and crack deflection [41] because large rubber particles cannot be cavitated due to lower stress concentration.

2.3.3.4. Influence of interfacial adhesion

An adequately strong interfacial adhesion between phases is required to promote cavitation and crack-bridging mechanisms [27,41]; otherwise, particle-matrix debonding occurs. A method to improve adhesion is to use functionalized rubbers, which can be chemically bonded to the matrix. In this case, higher toughness values can be achieved. In the case of UPR, it is challenging to achieve high toughness because the solubility of most rubbers in the liquid resin is low, and there is usually a poor chemical reactivity of the rubber toward the polyester functionalities [44]. Various reactive liquid rubbers [39,41,42] have been used in attempts to overcome these drawbacks. Kim et al. [41] studied the effect of adhesion between polyurethane rubbers (reactive and non-reactive) and UPR on toughness. In the case of non-reactive rubber, lack of good adhesion between the two phases led to a moderate improvement in fracture toughness via debonding. In contrast, a chemical connection between the reactive rubber and matrix caused a significant improvement in toughness, since the controlling mechanism changed from rubber-matrix debonding to rubber cavitation. Similar results in the toughening of UPR by different rubbers have been reported [42,43,47]. The other approach to improving adhesion between the rubbery additive and UPR is applying a compatibilizer. Ragosta [44] synthesized a suitable block copolymer of the type A-B-A (Unsaturated polyester-rubber-unsaturated polyester) as a compatibilizing agent in UP/rubber blends. They reported a significant improvement in toughness by adding the copolymer to the UP/rubber blend. The block copolymer is located preferentially at the interface of the rubbery phase and UP. The presence of the compatibilizer resulted in a reduction in the size of the rubber particles, finer dispersion of the particles, and a stronger interface adhesion.

2.3.3.5. Other properties

There are limitations to use of rubbers because they cause reductions in elastic modulus [42,43], yield strength, and thermal properties [26,41]. Rubber particles cause a decrease in the stiffness of the system because the modulus of rubber particles is much lower than that of the matrix [45]. The presence of the rubbery phase reduces the compressive yield strength due to the lower shear modulus of this phase. This prevents the rubbery phase from supporting a considerable portion of the applied stress [42].

Cherian et al. [47] worked on different properties of rubber-modified isophthalic unsaturated polyester resins. He found that the addition of nitrile, styrene butadiene, natural, and chloroprene rubbers decreased surface hardness due to the lower surface hardness values of all types of elastomers. The presence of these additives caused an increase in abrasion loss, since the rubber particles behaved as fillers, which can be easily removed during abrasion.

2.3.3.6. Preformed rubber particles

Rubber additives can also be introduced in the form of previously cured particles. The most common preformed particles are core shell rubber (CSR) particles, which are prepared by emulsion polymerization. They consist of a rubbery core and an outer shell of glassy polymer. The rubber core must be well-grafted to the inner shell for good stress transfer and cavitation of the core. This is possible by adjusting the chemical structure of the rubbery core and shells [48]. CSR particles are typically synthesized by emulsion polymerization since this technique enables control of the size distribution of particles [27].

Dispersion of neat rubber particles in the thermoset precursors is almost impossible. CSR particles are stabilized by block-copolymers and surfactants. Consequently, the chemical structure of the shell plays an important role in this issue [48-50]. A good dispersion increases the interfacial area between the particles and matrix, resulting in a considerable increase in viscosity. The high viscosity is the main drawback for the use of core-shell particles. Another disadvantage is agglomeration of particles during storage or processing [27]. In the case of a good dispersion of CSR particles in thermosets, significant improvement in toughness can be achieved. In the presence of CSR particles, the major mechanism controlling fracture is croiding [33]. In addition, cavitation of CSR particles in croiding can also induce shear yielding of the matrix. In studies of the effect of CSR particles on mechanical properties of UPRs, the addition of these additives improved fracture toughness [48-50], but reduced tensile strength [48,49] and glass transition temperature [48] without significant change in modulus [49].

2.3.4. Thermoplastic toughening of thermosets

As mentioned, rubber toughening of thermosets has some drawbacks. The toughness improvement often comes at the expense of high temperature performance or modulus

and yield strength. In addition, the major mechanism controlling fracture toughness in rubber-modified thermosets is localized shear yielding of the matrix, which is promoted by cavitation of rubber particles. If the matrix has low yielding, like unsaturated polyesters with high β transition temperature, the efficiency of these toughening agents is reduced. For the same reason, rubbers are not significantly capable to improve toughness of high-T_g networks [27,36].

Being able to improve toughness while keeping T_g high for special applications is desirable, especially in the aerospace industry, where high-T_g thermoplastic could be a good alternative to rubber. The thermoplastic rich phase can be formed during curing from a homogenous thermoplastic-thermoset mixture, where the thermoplastic is initially miscible with the resin, or can be incorporated as a dispersed powder in the initial formulation.

The chemical nature of the thermoplastic controls its miscibility with the thermoset resin and consequently the phase-separation process. At a constant thermoplastic volume fraction, an increase in its molar mass can cause a higher degree of phase separation resulting in a more improvement in fracture toughness. However, the higher molar mass of the thermoplastic results in an increase in viscosity, causing processing difficulties.

When the thermoplastic additive is added in the form of powder, the final morphology can be controlled better compared to the in situ phase separation process. High T_g thermosets such as epoxy can be toughened by nonmiscible high T_g amorphous or semicrystalline thermoplastic powders, such as Polyamide, polyimides, and Poly(butylene terephthalate) [27]. In this case, curing must be done below the melting temperature of the thermoplastic to avoid partial miscibility between the phases. A size range of 10-30 μm has been reported in the literature as suitable size for thermoplastic powders [27].

2.3.4.1. Toughening mechanisms

In general, the presence of a rigid inclusion develops triaxial stress in the matrix, which is not favorable for shear yielding mechanisms. In this case, the major dilatational phenomenon is thermoplastic/matrix debonding, which is not as effective as cavitation

formation in rubber particles. Consequently, the degree of triaxial stress (the intensity of the dilatation stress component) is not substantially reduced, which is favorable for a continuous and stable crack propagation mode. As a result, shear yielding of the matrix does not play an important role in energy dissipation during crack propagation. Therefore, other mechanisms control fracture in thermoplastic-modified thermosets. Many studies on toughening of thermosets by thermoplastic additives have been done to understand these mechanisms, most of which involved epoxy systems due to their vast application in aerospace industries. Toughening mechanisms such as crack pinning, crack tip blunting , particle bridging, and crack path deflection have been proposed. Each mechanism will be briefly discussed below:

Crack pinning. The concept of crack pinning is based on a change in the length of the crack front as the crack interacts with inhomogeneous particles [36]. A simple example to understand this mechanism is the way that a line of trees provides good protection against the wind. Similarly, a line of particles acts as obstacles for the crack front during propagation [27]. Figure 2.19 shows a schematic of the crack pinning mechanism. During crack propagation, the growing crack is pinned by the particles, causing the crack front to bow out between the particles and resulting in a reduction in the rate of propagation. After bowing, the crack keeps propagating and after a distance of about one particle diameter, the crack front breaks free and again has a linear shape [51].

This mechanism has been modeled by Lange [52] and Evans [53]. Lange [52] derived an equation to give a quantitative estimation of the critical energy release rate (G_{Ic}) due to this mechanism:

$$G_{Ic} = G_{Ic_{matrix}} + \frac{T_L}{D_s} \tag{2.39}$$

where T_L is a constant, called the line tension, which refers to the additional length of the crack front due to bowing. D_s is the interparticle distance (surface to surface) and a function of the particle diameter, d_p, and the volume fraction of the particles, V_p, given by:

$$D_s = \frac{2d_p(1-V_p)}{3V_p} \tag{2.40}$$

When the diameter of all particles is the same, an increase in their volume fraction causes a decrease in D_s resulting in an increase in G_{Ic}. One problem related to Lange's theory comes from T_L [54]. Experimental data showed that T_L is not a constant but rather a function of particle size. This problem was resolved by Evans [53], who calculated T_L and demonstrated that the increase in fracture energy required to bow the crack depends upon the particle size and the particle spacing. Lange and Radford [55] reported a maximum in the relationship between toughness and volume fraction of inclusions that is not predicted by Evans's model. Rose [56] suggested an alternative analysis that is in better agreement with the experimental observations.

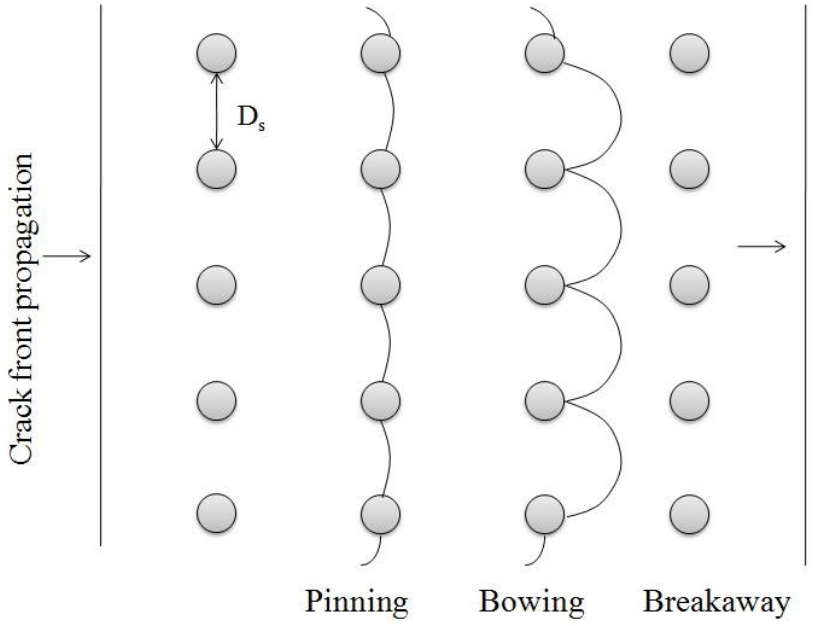

Fig. 2.19. A schematic diagram of the crack pinning mechanism (adapted from Ref:27).

One essential condition for pinning particles is impenetrability, which means that they should have sufficient stiffness. Therefore, this mechanism is not efficient with soft rubber particles, whereas with stiff particles such as rigid inorganic fillers, the crack pinning mechanism makes an important contribution. Evans [53] proposed using a parameter ε □ (impenetrability factor). More recently, Green et al. [57] have extended the analysis of Evans. They suggested that various factors affect the impenetrability of the particles. These factors are size, volume fraction, fracture toughness, and interfacial strength.

Crack tip blunting. The mechanism of crack tip blunting can take place due to localized shear yielding or damage, such as particle/matrix debonding and fracture of particles. The particles act as stress concentrators, resulting in the development of a triaxial stress state around the particles. In this case, the local stress may exceed the yield stress of the matrix or the adhesion strength of the particle/matrix interface, resulting in dissipation of energy by localized shear yielding or interface debonding respectively [27,36].

Particle bridging. Figure 2.20 shows a schematic diagram of the particle bridging mechanism. Sig et al. [36] modeled the toughening of a brittle resin by rigid and ductile particles. According to his model, the particles play two roles: (1) they have a sort of bridging effect by applying compressive force on the crack wake, and (2) these ductile particles can plastically deform in the crack tip region.

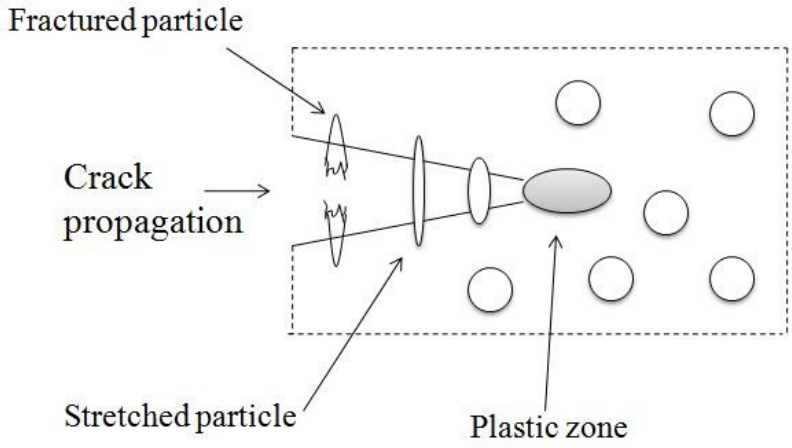

Fig. 2.20. A schematic diagram of the particle bridging mechanism (adapted from Ref:27).

Crack-path deflection. When a crack propagates in a particle-modified polymer, the particles can force the propagating crack to tilt out of the plane normal to the applied stress. Therefore, crack deflection causes a non-planar crack front, resulting in an increase in fracture surface area. The initial tilt angle of the crack, θ, depends on the location of the particle with respect to the propagating crack. Sometimes, the orientation of adjacent particles forces the crack to tilt in the opposite direction, resulting in a twist of crack front [58]. Figure 2.21 shows a schematic diagram of this mechanism illustrating tilting and twisting of the crack front.

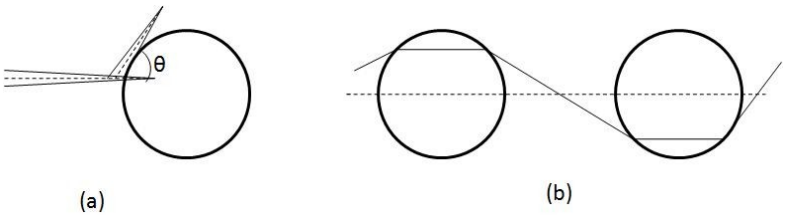

Fig. 2.21. A schematic of the crack-deflection mechanism, a) tilting, b) twisting of the crack (adapted from Ref:58).

If the adhesion strength of a matrix-particle interface is assumed to be close to the strength of polymer matrix, the increase in fracture energy due to deflection of crack by particles can be estimated by [59]:

$$\Delta G \approx \vartheta G_m V_p \qquad (2.41)$$

where G_m and V_p are the fracture energy of the matrix and the volume fraction of the particles respectively. ϑ $(\approx 0.3 - 0.5)$ is a factor indicating the fraction of particles deflecting the crack.

2.3.4.2. Influence of morphology and thermoplastic content

Typically, the particulate morphology results in a greater improvement in toughness compared to the homogeneous structure. Bucknall et al. [60] found the relationship between the morphology and fracture toughness of a thermoplastic-modified unsaturated polyester resin. The thermoplastic additive used was a reactive poly(vinyl acetate). They claimed that the particulate structure of the thermoplastic/thermoset system resulted in a greater improvement in fracture toughness compared to the co-continuous structure.

A contrary relationship between toughness and the morphology of a thermoplastic/unsaturated polyester system was reported [61]. In this case, impact strength was measured. A blend of compatible thermoplastics, such as poly(vinyl acetate) and polyurethane, with unsaturated polyester has co-continuous morphology due to strong interfacial adhesion. Since microvoids are formed at the interface of phases and inside thermoplastic-rich phases due to shrinkage of UPR, generally dispersed microvoids are formed in the co-continuous morphology. As a result, this morphology

leads to an increase in the toughness (impact strength) due to the crack blunting effect of microvoids. In contrast, the particulate structure leads to localized formation of microvoids, resulting in lower toughness of the system. There is an optimum content of microvoids because an excessively high volume fraction of microvoids can cause an adverse effect due to crack propagation through the voids.

2.3.4.3. Influence of interfacial adhesion

A critical level of adhesion between the thermoplastic and thermoset phase is required to ensure stress and strain transfers. One approach to improve the adhesion between two phases is to make some reactive end functional groups in thermoplastic molecules to form chemical bonds between two phases. Also, a block copolymer can be used as a compatibilizer, where each part of it is miscible with a specific phase [36].

2.3.4.4.Other properties

In the case of unsaturated polyester resins, thermoplastic additives have been widely applied to control high volume shrinkage of these resins, whereas few studies have investigated their effects on other properties.

I-Mechanical and thermal properties

Tensile properties depend on the morphology of the cured system, interfacial adhesion between the two phases, and degree of crosslink density of the continuous phase. These three factors all depend on compatibility between phases. The chemical structure and molecular weight of the thermoplastic control its compatibility with UPR. During the curing process, phase separation occurs, where for the less compatible system, the degree of phase separation is greater. Therefore, in an incompatible thermoplastic/unsaturated polyester system, a particulate morphology is formed consisting of a continuous UP-rich phase and a dispersed thermoplastic-rich phase. Since the small styrene monomers can diffuse into the thermoplastic-rich particles much faster than larger UP chains, the concentration of styrene monomers in the continuous phase is reduced. Consequently, a reduction in crosslink density occurs due to the lack of curing agent monomers. In contrast, in compatible thermoplastic/unsaturated polyester systems, better dispersion of different constituents resulted, due to a lower degree of phase separation. Consequently,

in these systems, the reduction in crosslink density is either much smaller or negligible, and a less reduction in tensile strength would be achieved.

The particulate morphology is suitable for improving fracture toughness. The lower compatibility of the system results in greater reduction in crosslink density and poorer interfacial adhesion. In most cases, the addition of the thermoplastic results in a reduction in tensile strength. In the best scenario, tensile strength may not significantly change for compatible thermoplastic/unsaturated polyester systems [61-63].

The Young's modulus of the whole system depends on the modulus of both the thermoplastic and thermoset components. In addition, Young's modulus is mainly connected to the degree of tightness of the network rather than crosslink density [61]. The addition of incompatible thermoplastics leads to a reduction in the concentration of styrene in the continuous phase. A smaller amount of the curing agent leads to shorter crosslinking bridges, meaning a higher degree of network tightness. Young's modulus is not significantly changed for incompatible thermoplastic/unsaturated polyester systems, since the higher degree of network tightness compensates for the lower modulus of the thermoplastic additive. In contrast, a reduction in modulus for compatible systems has been reported [61,64], since compatible thermoplastics typically have low molecular weight and T_g (even lower than the ambient temperature). Consequently, they have a low modulus, resulting in a reduction in the modulus of the whole system.

The glass transition temperature (T_g) of the major continuous thermoset phase depends on two opposing effects, the plasticization effect of the thermoplastic phase and the degree of crosslink density of the continuous phase. An incompatible thermoplastic causes a smaller plasticization effect since it typically has high T_g and molecular weight. On the other hand, it reduces the degree of crosslink density by decreasing the concentration of styrene monomer in the continuous phase. Because of this opposing effect of thermoplastics on T_g, both an increase and a decrease in T_g in thermoplastic/unsaturated polyester systems have been reported [62,63].

All of these investigations applied thermoplastic additives to reduce volume shrinkage, since a thermoplastic that is more compatible with UPR is more effective for controlling

volume shrinkage. For instance, polyvinyl acetate and polyurethane, with low molecular weight and low T_g (27°C and -45°C respectively [61]), are suitable as low profile additives. However, for the purpose of toughening, a high T_g or semicrystalline thermoplastic with high molecular weight is favorable [27]. To sum up, a lack of understanding of the effect of thermoplastics as toughening agents on fracture toughness and other properties of unsaturated polyester systems still remains.

II-Shrinkage

Volumetric shrinkage occurs through network formation in thermoset resins. This causes several product problems, such as poor surface quality, lack of dimensional control, and residual stress. Therefore, much work has been done on shrinkage control of UPR, primarily by incorporating low profile additives (LPAs) [64-70]. As mentioned, LPAs are thermoplastic polymers that are typically non-reactive additives. Most are incompatible with unsaturated polyesters, but soluble in styrene. Incompatibility between the thermoplastic additive and the resin increases the rate of phase separation, when in systems such as polystyrene/UPR and poly(methyl methacryalte)/UPR phase separation starts before any polymerization [65]. Ultimately, a non-uniform microstructure (the particulate morphology) is formed. In contrast, a compatible low profile additive/UPR system has uniform microstructure (the co-continuous morphology). During curing reaction, microvoids are generated in the interface of the two phases as well as inside the LPA-rich phase, which compensate for volume shrinkage. In a non-uniform microstructure, the generation of microvoids is localized in the dispersed LPA phase, whereas in the compatible systems, with co-continuous morphology, micovoids are uniformly generated in the whole system, resulting in greater compensation for shrinkage [61]. Different characteristics of low profile additives play roles in controlling volume shrinkage. For instance, the difference in polarity of the LPA and unsaturated polyester determines their compatibility, where closer polarity results in more compatibility. Another characteristic is the coefficient of thermal expansion and specific volume of the low profile additive, where higher values of these parameters lead to better shrinkage control [65].

2.3.5.Inorganic toughening agents

Another approach to improve fracture toughness of thermosetting resins is to use inorganic (e.g., glass and ceramic) materials. This group of additives can be classified into two main classes based on the size of their particles: I) additives composed of micron-sized particles are used for the preparation of composites, and II) materials having sub-micrometer- and nanometer-sized particles. The latter group leads to nanocomposites, which can be classified into two subclasses based on the particle geometry: nano particulate reinforced composites and layered silicate nanocomposites. In the following, each class of inorganic reinforcements will be discussed.

2.3.5.1.Inorganic micron-sized particles (particulate fillers)

The toughness of particulate-filled thermosets is affected by the properties and characteristics of the constituent phases: filler, thermoset matrix, and interfacial region. The relevant parameters are the filler aspect ratio, the particle size, filler volume fraction, the modulus and strength of the filler, the filler-matrix adhesion, and the toughness of the matrix. For the processing and application of these materials, viscosity of the uncured mixture must be sufficiently low to allow for processing and removal of air bubbles from the system [71].

Fracture mechanisms

The mechanism controlling fracture toughness in the case of particulate-filled thermosets such as systems containing silica and alumina particles is crack pinning [71,72]. For the case of poorly bonded glass beads, when no surface treatment is done to the filler, crack propagation was highly unstable. Fractography showed that particle/matrix debonding happened, resulting in crack tip blunting. Therefore, in this case, a combination of crack pinning and blunting mechanisms controls the fracture toughness [73]. In addition, Lee et al. [57,74] suggested that the major portion of fracture energy could be dissipated by the formation of micro-shear bands at the interface of glass beads and the matrix.

Influence of filler characteristics

The relationship between fracture toughness and volume fraction of the filler depends on the size of filler particles [62,75]. Sing et al. [75] found that with larger aluminum particles (3.5 and 20 μm), K_{Ic} of filled unsaturated polyester monotonically increases with

the volume fraction of the particles. In this case, the viscosity of the resin restricts the volume fraction of the filler with respect to processability. In contrast, for smaller particles (100 nm), an optimum value for the filler volume fraction was observed with a maximum value of fracture toughness. Also, Lange et al.[76] reported a dependency of fracture toughness of filled epoxy on the size of alumina trihydrate particles. They used fillers with three different particle sizes (1, 8, 12 μm), with the largest particles leading to the most improvement in fracture toughness.

Stiffer fillers result in a greater increase in the modulus and fracture toughness of the whole composite. For instance, if weak filler such as hollow silica microsphere is used, no improvement in toughness will be achieved [71]. This sort of filler may act as a source of flaws.

Other properties

The effect of inorganic filler on modulus and tensile strength is known [71,75]. An increase in the volume fraction of filler results in a parabolic rise in modulus, but a reduction in tensile strength. In the best case scenario, tensile strength of the composite is equal to that of unfilled resin. Tensile strength is first reduced by the addition of filler and then starts increasing up to the strength of unfilled resin with a higher volume fraction of filler.

At constant volume fraction, the particle size of glass beads might not significantly change the modulus and strength of the epoxy matrix [77]. A similar result was also observed in the case of toughening UPR with aluminum fillers of different particle sizes [75]. However, there is an upper boundary in particle size due to the higher probability of flaws for large particles. These flaws can lead to a decrease in strength.

2.3.5.2.Inorganic nanoparticle-reinforced composites

The approach of introducing micron-sized inorganic particles into the resin has failed to significantly improve fracture toughness of thermosetting resins [75]. In addition, these relatively large particles reduce the processing feasibility of the composite by substantially increasing the viscosity of the resin [78]. In contrast, nanoscale reinforcement of thermosetting resins makes them potential materials for substantial enhancement of fracture toughness, modulus, yield strength, and heat resistance.

Fracture mechanisms

Nanoparticles, such as silica, improve fracture toughness by promoting dissipating energy processes of the thermosetting matrix. These processes dissipate energy in a region around the crack tip, resulting in crack blunting. Two types of dissipating processes are: (I) localized shear band initiated by stress concentration around the particles; and (II) debonding of the particles from the matrix, in some cases followed by void growth in the matrix [78]. Particle-matrix debonding and void formation can reduce the degree of triaxial stress, which is favorable for shear band formation.

In a study on the effect of silica nanoparticles on the toughening of epoxy, done by Ragosta et al.[79], another fracture mechanism was proposed. In this case, a reaction between epoxy groups and silanol groups on the surface of the particles was detected, leading to an improvement in interfacial adhesion. Consequently, these nanoparticles restricted segmental motion within the matrix, resulting in an increase in activation energy for the yielding process. Despite the reduction in the intensity of the yielding process, fracture toughness increased. The critical crack length for the onset of brittle fracture (which is the fast and continuous crack propagation mode) was increased. They proposed that the required energy for fracture became more reliant on the breakage of chemical bonds.

A rise in volume fraction of nanoparticles improved fracture toughness of the nanocomposite [78-80]. Interestingly, the volume fraction may affect the influence of the nanoparticle size on the toughening of thermosetting resin [80]. At low volume fraction, fracture toughness was slightly affected by the particle diameter, whereas toughness was strongly dependent on the particle size at high volume fraction [80].

2.3.5.3. Layered silicate nanocomposites

Toughening of thermosetting polymers via incorporation of an additional phase strongly depends on the morphology. Particularly, in the case of layered silicate nanocomposites, the large contact area between the nano-reinforcement and the polymeric matrix causes the significant difference between nanocomposites and conventional composites. This strongly depends upon the degree of dispersion and

distribution of the silicate layers. The possible structures must firstly be introduced, and then fracture mechanisms will be discussed.

Morphology

Based on the degree of delamination of the silicate layers, polymer/clay systems can be classified into nanocomposites and conventional composites. The nature and interaction of the components as well as the preparation techniques determine the morphology of polymer/layered silicate systems. Ultimately, three morphologies are possible: phase-separated, intercalated, and exfoliated. In phase-separated morphology, polymer chains do not penetrate into the clay layers and the clay material is simply dispersed through the resin like a typical filler. This morphology leads to a conventional composite. In intercalated nanocomposites, the diffusion of polymer molecules into the galleries (spaces between the layers) causes an expansion in the interlayer distance while the ordered structure of the silicate layers is retained. The exfoliated structure is achieved when individual silicate layers are separated and randomly distributed throughout the polymeric matrix. In this morphology, a large interfacial area with the matrix is achieved, providing maximum reinforcement. Figure 2.22 shows the different morphologies of these reinforced materials.

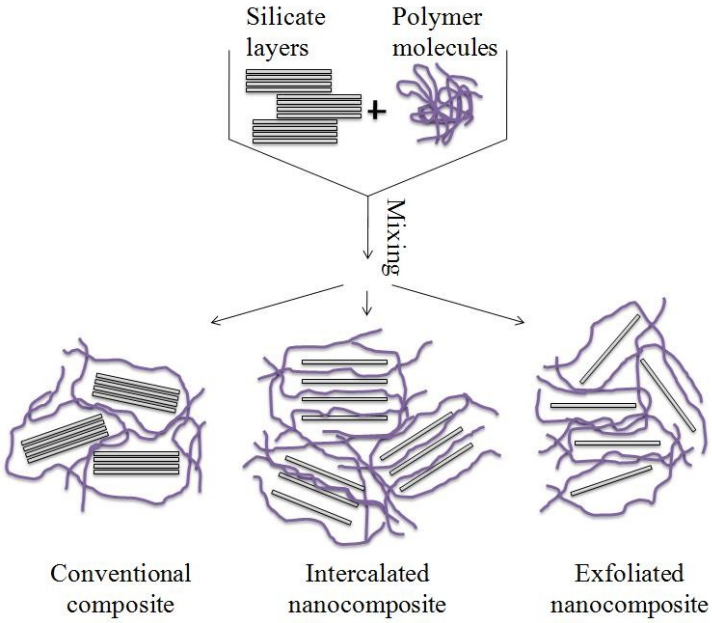

Fig. 2.22. Different morphologies of nanocomposites.

Fracture mechanisms

Specific size ranges of reinforcing filler can result in toughening of the polymer matrix [81]. Silicate layers in a fully exfoliated arrangement are too thin and small to change the direction of crack propagation, but can force a tortuous path. The tortuosity occurs locally around the clay platelets [82]. Therefore, a fully dispersed arrangement (exfoliated structure) of the layers cannot provide toughening of the polymer matrix. In contrast, a micron-sized structure of intercalated clay layers can lead to more improvement in toughness, likely via the crack deflection mechanism, resulting in an increase in the fracture surface area [83,84]. Zilg et al. [85] found that well dispersed intercalated layered silicates resulted in a greater improvement in the fracture toughness of epoxy compared to exfoliated layers. The exfoliation structure caused a greater improvement in the stiffness of the system.

Influence of interfacial adhesion

A specific characteristic of silicate layer reinforcements is the high aspect ratio of their layers (10-2000) [86]. If the silicate layers are dispersed and distributed finely, they have a large interfacial area with the matrix, resulting in a significant improvement in many properties. One factor facilitating exfoliation of the silicate layers is compatibility between the reinforcement and matrix. Since the chemical structure of the silicate layer makes them hydrophilic, a modification is required to make them compatible with organic polymers. For this purpose, ion exchange is a common technique in which the interlayer cations are exchanged with cationic organic surfactants. Poor compatibility results in aggregation of the silicate layers. Consequently, tensile strength, flexural strength, and fracture toughness are reduced due to the reduction in interfacial area. To understand the effect of interfacial adhesion, it is important to be familiar with the chemical structure and treatment of layered silicates.

I)Chemical structure

Montmorillonite is a common layered silicate which is composed of crystal layers. In each layer, one octahedral sheet of mainly aluminum hydroxide (with positive charges) is sandwiched between two silica tetrahedral sheets (with negative charges). This arrangement of the sheets results in electroneutrality. However, some isomorphic substitutions may occur within the layers; for instance, Al^{3+} is replaced by some cations

having less positive charges, such as Mg^{2+} or Fe^{2+}, resulting in a net negative charge in the structure. These negative charges can be counterbalanced by exchangeable alkali or alkaline earth cations [87]. This chemical structure is almost similar in layered silicates, which makes them hydrophilic.

II)Chemical treatment

The chemical structure of both the layered silicate and the organic surfactant are important for clay modification. The charge density of the clay determines the concentration of exchangeable ions in the galleries. The capacity of a layered silicate for ion exchanges is called the Cation Exchange Capacity (CEC). There is an optimum value for CEC of clays to achieve a fine dispersion [83]. High CEC values restrict the polymer diffusion into the galleries due to the lack of available spaces within the ion-populated silicate layers.

In addition, the structure of the organic surfactant determines the chemical affinity between the modified clay and organic polymers, as well as the d-spacing of the silicate layers. Greater compatibility between the modified clay and the matrix results in better diffusion of polymeric molecules into the galleries, improving the delamination and dispersion of the clay. For instance, a comparison between several commercial organoclays, including Cloisite Na^+, 10A, 15A, 25A, and 30B, [88] shows that different functional groups of surfactants alter the final morphology of clay/UPR nanocomposite. Better interaction between the functional group in the modifier and that of the polymer leads to enhanced exfoliation. Hydrogen bonding between hydroxyl groups of the clay modifier and the polymer can cause good interaction between the clay and thermoset, resulting in homogenous dispersion of the intercalated/exfoliated microstructure [89]. In contrast, poor chemical affinity between the clay and the polymer (e.g., in the case of Cloisite 10A/unsaturated polyester) causes a slight contraction of the silicate layers. In addition to the chemical nature of the surfactant, other parameters such as longer chains and/or bulky alkyl groups tend to improve the dispersion and delamination of the clay in nanocomposites by increasing the gallery spacing [89-91]

Based on the reactivity of the organic surfactants, they can be divided into non-reactive and reactive modifiers. In non-reactive organoclays, the layered silicate is treated with an inert cationic surfactant in which the main role of the modifier is to increase the

interlayer distance and the organophilicity of the clay. In addition to these effects, reactive modifiers allow for chemical bonding between the silicate layers and the matrix. Consequently, these modifiers result in higher interfacial adhesion between the clay and the thermoset polymeric matrix [90,92]. However, these covalent bonds between the modifier and polymer molecules theoretically hinder adjacent silicate layers from further separation during the curing reaction. As a result, the improvement in delamination may be restricted [89]. Therefore, both reactive and non-reactive organic modifiers could be used for clay modification to prepare a partially reactive organoclay [93,94]. The addition of this organoclay increases the degree of exfoliation in the nanocomposites.

Other properties

Clay affects the mechanical, flammability, barrier, and tribological properties of the thermosetting matrix. Concerning the mechanical properties, generally speaking, adding clay causes an increase in tensile modulus due to its high modulus compared to that of organic polymers. In most cases, an optimum clay loading was reported, since greater quantities of clay result in agglomeration and a lower quality of distribution [95,96]. Contrary observations are reported for tensile strength. In some cases, an optimum amount of clay was found to result in maximum tensile strength [95,97]. However, some studies found no significant change in tensile strength with the addition of clay [86,96], and Torre et al. [98] even reported a reduction of the tensile strength with the addition of clay. They claimed that interfacial debonding is the mechanism leading to the reduction in tensile strength. Adding organoclays improved the flexural modulus [98, 100-102] and storage modulus [92, 102] of UPR. It is worth noting that reactive-modified clays improve mechanical properties more significantly than the non-reactive-modified group.

Barrier properties of UPR/clay nanocomposites have also been examined [92,99]. The addition of an organoclay reduced the gas and liquid permeability of polyester due to the development of a tortuous path for small molecule diffusants. In fact, we often check the quality of the clay dispersion in nanocomposites by measuring their barrier properties.

Nazure et al. [88] evaluated the effect of different commercial organoclays on the flammability of UPR by cone calorimetry. The addition of clay caused a significant reduction of peak heat release rate, total heat release, and fire growth rate index. The

flame retardant properties of nanocomposites were found to depend on the chemistry of the organic modifier of the clay. The authors [88] found that nanoclay is less effective than conventional flame retardant; however, the combination of the two is the best alternative.

Tribological properties of the thermoset are strongly affected by clay. In the presence of nanoclay, a slight increase in hardness, a moderate decrease in the coefficient of friction, and a significant increase in wear resistance (by 85%) of UPR were observed [100].

Filler particles cause a decrease in shrinkage by restricting the polymer chain mobility during the curing reaction. Therefore, nanoclay can effectively control shrinkage independent of temperature even as a filler. Moreover, the expansion of the interlayer spaces of the silicate layers, resulting from the diffusion of polymer molecules into the galleries, can also reduce shrinkage [101]. However, contrary results have been also reported [102], indicating that nanoclay does not significantly reduce shrinkage.

2.3.6.Ternary systems

Incorporation of rubber additives to thermosets is a common technique to improve toughness. However, the addition of rubber typically results in a reduction in thermal stability and some mechanical properties, such as Young's modulus and compressive strength. On the other hand, the application of thermoplastic additives and nano-reinforcements, such as nanoclay, to improve toughness is not as effective as rubbers. Recently, it has been found that combinations of nanoclay and other additives have a synergistic effect to improve some properties, such as flame resistance, shrinkage control, and even toughness. Therefore, these ternary systems have attracted a lot of interest.

2.3.6.1.Ternary systems of rubber/clay/thermosets

As mentioned, rubber toughening occurs at the expense of thermal stability, stiffness, and the compressive strength. Recently, the approach of adding nano-reinforcement to rubber/thermoset systems for the purpose of improving the modulus has been proposed. Many studies have focused on ternary systems of rubber-modified epoxies with layered silicates, where different rubbers such as carboxyl-terminated butadiene-acrylonitrile copolymers (CTBN) [103], polyether rubbers [104], polyether polyols [105], acrylic

rubber [46] were examined. The stiffness of systems was determined by a balance of the ratio between soft and hard additives. The addition of organoclay to a rubber/epoxy system could offset the loss in modulus and strength. In acrylic rubber/clay/epoxy [46], a morphology study revealed the alignment of clay silicate layers along the interface of the rubber and epoxy. This adsorption of silicate layers to the rubber particles promoted rubber cavitation, resulting in an improvement in toughness. The other possible mechanism is multiple cracks controlling fracture in these ternary systems [72].

A few studies have been done on rubber/clay/UPR ternary systems. Ishak et al. [106] indicated that the mechanical properties of UP/rubber such as UP/liquid natural rubber can be improved by applying nano-reinforcements. The tensile strength, stiffness, and impact energy were slightly increased by incorporation of clay into the LNR/UP system. Another approach is to modify polyester molecules by forming a segmental copolymer with a rubber (e.g., polyurethane) attached to the end group of UP [107]. In this ternary system (rubber/UP/clay), a synergistic effect of clay and rubbery segment resulted in an improvement in toughness and flexural strength of the cured UPR; however, modulus was still reduced. Therefore, more investigation into rubber/clay/UPR systems is warranted.

2.3.6.2.Ternary systems of thermoplastic/clay/thermosets

Although, the combination of thermoplastic and clay has the potential to improve toughness, modulus, and gas barrier properties of thermosets [108], few studies have been done on thermoplastic/clay/thermoset ternary systems. In the case of epoxy resins, some thermoplastics such as poly ether polyols [109] and hydroxyl terminated poly ether ether ketone [108] have been used to prepare these ternary systems. The addition of nanoclay led to an increase in the tensile modulus and flexural modulus in the systems. The value of the fracture toughness in the thermoplastic/clay/epoxy system was greater than pure epoxy; this improvement was caused by crack path deflection and debonding mechanisms. However, an increase in clay loading resulted in a reduction in fracture toughness, suggesting that the thermoplastic plays the main role in improving toughness as compared to the nanoclay [108].

A few studies have been done into the morphology of these systems [72, 110]. For instance, Hernandez et al. [72] investigated thermoplastic-modified epoxy with clay, but the combined effect of clay and thermoplastic on the fracture toughness was not investigated. Only the effect of clay dispersion and distribution on the fracture toughness of the thermoplastic/epoxy was evaluated. They found that thermoplastic particles, poly(methyl methacrylate), and the silicate layers were dispersed throughout the continuous epoxy phase. A homogenous exfoliated structure resulted in less improvement in the fracture toughness compared to a heterogeneous intercalated/exfoliated structure. The presence of aggregates likely increased the crack propagation path in this ternary system, resulting in an improvement in toughness.

In the case of UPRs, thermoplastic additives have been widely used as LPAs to control volume shrinkage instead of toughening agents. To the author's knowledge, there is no study on the toughness of thermoplastic/clay/UPR ternary systems; most investigations have looked at the effect of thermoplastic/clay combination on volume shrinkage. Studies showed that a combination of a nanoclay and low profile additive (LPA) has a synergistic effect on the control of shrinkage [111,112]. Xu and Lee [111] claimed that almost all the silicate layers are distributed inside the LPA-rich phase, leading to faster reaction and earlier gelation of the LPA-rich phase, which is favorable for earlier stress cracking. A liquid LPA phase can release the stress arising from polymerization shrinkage of the system. Therefore, stress-induced cracks are not formed in the LPA-rich phase or in the LPA/UP interface until gelation happens in the LPA-rich phase. This local cracking leads to volume expansion, which can compensate for polymerization shrinkage. This explanation would be convincing if clay could increase the curing reaction rate. However, contrary observations have been reported indicating a reduction of the curing rate due to the addition of clay [99,113]. In addition, the presence of nanoclay compensates for the loss of some properties, caused by LPA, such as storage and flexural modulus.

Volume shrinkage in unsaturated polyester resins is approximately 7-10% [107], whereas for epoxy resins, it is 4-6% [114]. Thus, volume shrinkage in UPRs is a big issue, and low profile additives are usually used in commercial resins to overcome this serious problem.

2.4. Author's approach

Unsaturated polyester is an extremely brittle thermoset due to its high crosslink density. In these thermosets, when tensile stress is applied, crosslink sites constrain localized plastic deformation (elongation) of the material and consequently the formation of fibrils. Therefore, crazing as a dissipating energy process does not happen in these highly crosslinked thermosets and a localized yielding process strongly controls fracture toughness. Localized yielding of these networks is affected by secondary transition representing local mobility of the polymer chain segments. The secondary transition temperature and the intensity of these transitions are influenced by the chemical structure of the thermoset. In the case of unsaturated polyesters, β transition temperature is greater than room temperature resulting in low activity of these transition which likely leads to low fracture toughness; however, more investigation is required.

In general, the incorporation of a second phase to promote energy dissipating processes in the whole system is a successful technique to improve fracture toughness of thermosets. Between polymer toughening agents, rubbers are the most effective additive to improve fracture toughness, but they cause a reduction in thermal stability, elastic modulus, and compressive strength. Another group of polymer toughening agents are thermoplastics which are widely applied as low profile additives to control high volume shrinkage of unsaturated polyesters. The thermoplastic phase can not significantly improve fracture toughness, but it does not sacrifice other properties. Recently, it has been found that combinations of an inorganic nano-reinforcement (such as nanoclay) and polymer additives can have a synergistic effect to improve different properties and to compensate for the drawbacks of each additive. Since thermoplastics do not have any significant destructive effect on other properties of unsaturated polyesters and are widely used in commercial resins as low profile additives, if these additives can also play the role of toughening agent, two main drawbacks of these thermosets will be solved with the incorporation of one additive. Therefore, in this work, the effect of thermoplastic additives, on the toughening of UP in the presence of clay was investigated.

The morphology of multiphase systems controls different properties including fracture toughness. A thermoplastic/nanoclay/thermoset ternary system is a complex material

where the morphological study of each simpler binary system (clay/thermoset and thermoplastic/thermoset) is helpful to interpret behaviors of the complex ternary system. Two controlling microstructure characteristics of these systems are the size and distribution of the dispersed phase (additive). The effect of these microstructure characteristics on fracture toughness strongly depends on the mechanism controlling this property which is determined by the type of additive and its characteristics. Therefore, in each system the effect of microstructure must be evaluated. In addition, the presence of other additives may affect the characteristics of the matrix which significantly influence fracture toughness. Therefore, the effect of each additive on the thermoset characteristics must be explored. In this project, firstly we will evaluate the effect of each additive on the characteristics of the matrix, microstructure, and different properties of the system and then synthesize a novel hybrid ternary system to improve fracture toughness of unsaturated polyesters without sacrificing other properties such as glass transition temperature and elastic modulus.

Chapter 3

Layered silicate nanocomposites based on unsaturated polyesters

3.1. Introduction

Incorporation of rubber additives into thermosets is a common technique to improve toughness. However, the addition of rubber typically results in a reduction in thermal stability, Young's modulus, and compressive strength. On the other hand, thermoplastic additives and nano-reinforcements, such as nanoclay, are not as effective as rubbers at improving fracture toughness. Recently, it has been found that combinations of nanoclay and different additives can have a synergistic effect to improve fracture toughness. Therefore, these ternary systems have attracted a lot of interest.

The main objective of this project is to improve the fracture toughness of unsaturated polyester resins (UPRs) without compromising other properties. Since thermoplastics as low profile additives are typically added to commercial UPRs to control shrinkage, in this work, we followed the approach of applying both thermoplastic and nanoclay to improve fracture toughness. Firstly, the effect of nanoclay on curing characteristics and different properties, especially fracture toughness, must be understood, which is helpful for interpreting the behavior of complex ternary systems. In addition, mechanisms controlling fracture toughness in clay nanocomposites based on unsaturated polyesters must be explored.

3.2. Literature review

Unsaturated polyester resins have various applications in industry due to certain outstanding advantages. However, their poor chemical and flame resistance, as well as their brittleness call for the use of reinforcements in a wide range of their applications [115]. Since nano-reinforced matrix materials can result in improved composite products, the preparation of UPR-based nanocomposites has attracted a lot of interest. One of the most common nano-reinforcements is montmorillonite (MMT) with a layered structure. MMT is widely used due to the high aspect ratio of its crystal layers (10-2000) [116].

In general, polymer nanocomposites can be prepared via three methods: melt compounding, solvent casting, and in situ polymerization [117]. Thermoset nanocomposites, such as those based on phenol, epoxy, and unsaturated polyester resins, are synthesized by the in situ polymerization method. Based upon the degree of delamination of the silicate layers, intercalated and/or exfoliated microstructures can be achieved.

The fundamental principle for nanocomposite preparation is that the precursors (monomers and polymers) must be able to swell the silicate layers. Significant swelling and intercalation of organoclays can be achieved due to the low viscosity and polarity of thermoset resins [118]. For this to occur, chemical treatment of the nanoclay, a suitable mixing procedure, and appropriate swelling temperature are required. The clay modifier should be chosen by considering the chemical composition of the matrix. In the case of resins with high viscosity, mixing may be done at moderate or elevated temperatures (depending on the matrix) to reduce the viscosity of the mixture. A fine dispersion calls for a sufficient mixing time and/or a high shear rate [119].

In systems composed of two or more components with different molecular sizes, like unsaturated polyester resins, the order of mixing can be an important factor in clay dispersion and delamination. Generally, three mixing procedures can be used: (I) the nanoclay is directly mixed with the resin (simultaneous mixing), (II) a suspension of the clay in the reactive diluent (e.g., styrene) is prepared and then mixed with the thermoset resin or thermoset prepolymer (without reactive diluent), or (III) a mixture of the clay and the thermoset prepolymer is prepared and then mixed with the reactive diluent. Each mixing method has been examined in different studies. The first two mixing methods led to a higher concentration of styrene inside the clay galleries compared to extragallery regions because the diffusion of the small styrene monomers into the galleries is faster than that of the long-chain polyester molecules. This phenomenon leads to a decrease in the total crosslink density of the samples due to a lack of available curing agent for full conversion of the unsaturated bonds of UPR [120-122]. The third method, called the sequential method, led to an improvement in clay dispersion and distribution as well as in

the total crosslink density and glass transition temperature (T_g) of the nanocomposites [122,123]; however, fracture toughness was not reported.

Although the sequential mixing method can improve the degree of delamination and dispersion of clay, the high viscosity of the prepolymer causes many difficulties. In this case, the addition of a suitable solvent during the mixing procedure can be useful to reduce viscosity. For instance, Liu et al. [124,125] used a solvent to achieve a fine dispersion of clay in epoxy. First, they prepared a suspension of clay in acetone by using a high-pressure mixing machine (HPMM). The resulting paste was mixed with epoxy, first at room temperature and then at an elevated temperature (110-120°C). They found that the HPMM produced a stable high-viscosity suspension of delaminated clay, thereby promoting the diffusion of epoxy molecules into the silicate layers in the next step. Ultimately, a high degree of dispersion and delamination of clay in the matrix was achieved. They reported that the addition of clay caused an improvement in the fracture toughness of the epoxy.

According to the literature, more investigation into the effect of clay dispersion and distribution on fracture toughness of unsaturated polyester resins is required. In this work, we use different mixing methods for the preparation of clay/UPR nanocomposites with different nanostructures. Eventually, we evaluate the effect of clay on the fracture toughness of the system.

3.3. Experimental

3.3.1. Materials

The unsaturated polyester resin used was a general purpose orthophthalic resin (H596-CWA-12, Ashland Chemical), synthesized from maleic anhydride, phthalic anhydride, and propylene glycol. It contains styrene (45wt%) and the promoter cobalt octoate (0.1wt%). Styrene (Sigma Aldrich) used as the curing agent was distilled prior to use, using an IKA rotary evaporator under vacuum at 30°C to remove the inhibitors. The room temperature initiator employed for curing was methyl ethyl ketone peroxide (NOROX, MEKP-925H from NORAC Inc.). Cloisite 20A and 30B (Southern Clay Products Inc.) were used as the nanoclay.

3.3.2. Preparation procedures

Several mixing methods were examined to prepare the mixture of UPR and organoclay where just two important methods are presented here: (I) direct mixing method (DM) which is the most feasible method and (II) solvent-aided mixing method (SHM), which is a modified technique of the high-pressure mixing method (HPMM) used by Liu et al. [124]. The preparation of nanocomposites by these methods was conducted according to the following procedures:

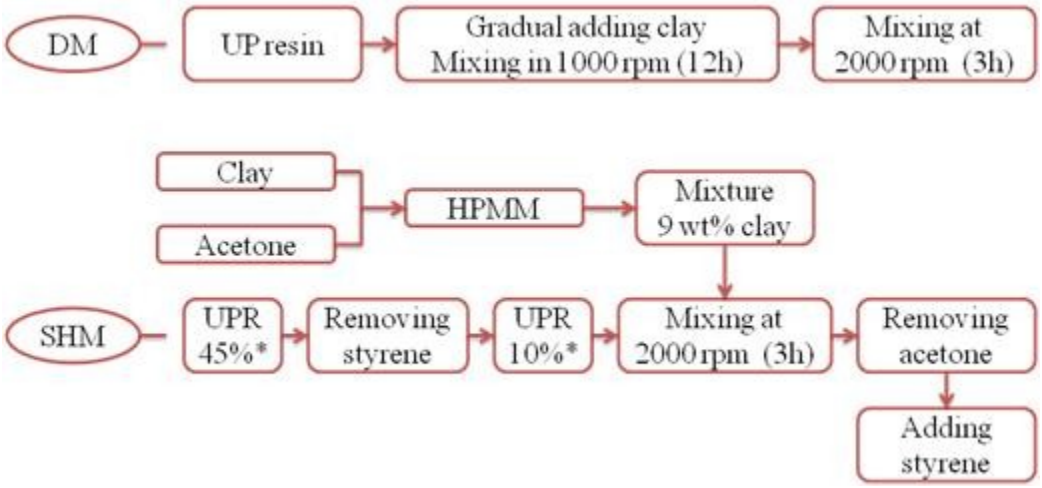

Fig. 3.1. Preparation procedures. DM: direct method; SHM: solvent-aided high-pressure method. *Weight percentage of styrene in the resin.

Other preparation procedures are presented in appendix A1, but only the results related to samples prepared by DM and SHM, as a reference method and the most successful method respectively, are presented in this chapter.

3.3.3. Characterization methods

Calorimetry was performed with a differential scanning calorimeter TA Q10 on 10 mg of uncured sample in a hermetic aluminum pan. The isothermal reaction rate profile was measured at 25°C, followed by a scan from 25°C to 300°C at a heating rate of 5°C/min to determine the total reaction heat.

Fourier transform infrared (FTIR) spectroscopy was used to monitor the conversion of the C=C bonds of unsaturated polyester and styrene. A FTIR spectroscope (Thermo

Nicolet, Nexus 670 FT-IR) with a resolution of 4 cm^{-1} in transmission mode was used. The liquid sample was sandwiched between two NaCl crystal windows.

Couette rheometry was conducted to measure the viscosity of different samples by using an Anton-Paar Physica MCR-500 stress controlled rheometer. X-ray diffraction analyses were performed using an X-ray diffractometer (Philips model X'PER) at the low angle range of 2θ with a scanning speed of 1°/min. The X-ray source was Cu-Ka radiation (λ = 1.540598 A°), using a 50 kV voltage generator and a 40 mA current.

Bar-shape specimens with rectangular cross section based on ASTM D790-07 were used to determine flexural properties on a MTS 312.21 (5 kN) testing machine at a constant crosshead speed of 1 mm/min. Fracture toughness tests were carried out according to ASTM D5045-99 using an MTS 312.21 (5 kN) on sharply notched three-point bend specimens. The samples with a single edge notch were cast from a rubber mold and the sharp crack was made by tapping a fresh razor blade frozen in liquid nitrogen into the notch. Dynamic mechanical measurements were made between 20°C and 180°C at 1 Hz, using a TA Instruments DMA 983 dynamic mechanical analyzer.

3.4. Results and discussion

3.4.1. Chemical reactions during curing

The curing of UPR proceeds via free radical polymerization between unsaturated polyester molecules and a vinyl monomer such as styrene. The important characteristic of the cured polyester is its crosslink density, which is dependent on the degree of cure and final conversion of the reactants. The addition of clay silicate layers intensifies the complexity of the curing process of UPRs, since the raw reactants diffuse into the clay galleries with different diffusion rates depending on their molecular sizes. It results in a change of the ratio of unsaturated polyester to styrene in extragallery regions, potentially changing crosslink density.

Conflicting observations regarding the curing reaction of nanoclay-reinforced UPRs have been reported. Some researchers reported that clay caused a reduction in the total curing rate and degree of conversion [126,127], as well as crosslink density [127]. In contrast, an increase in the curing rate with no significant change in the final degree of

cure due to the addition of clay has been also reported [128]. Consequently, more investigation into this issue is required. For this purpose, nanocomposites with varing clay loading (1, 3, and 5 phr) were prepared by the direct mixing method (DM).

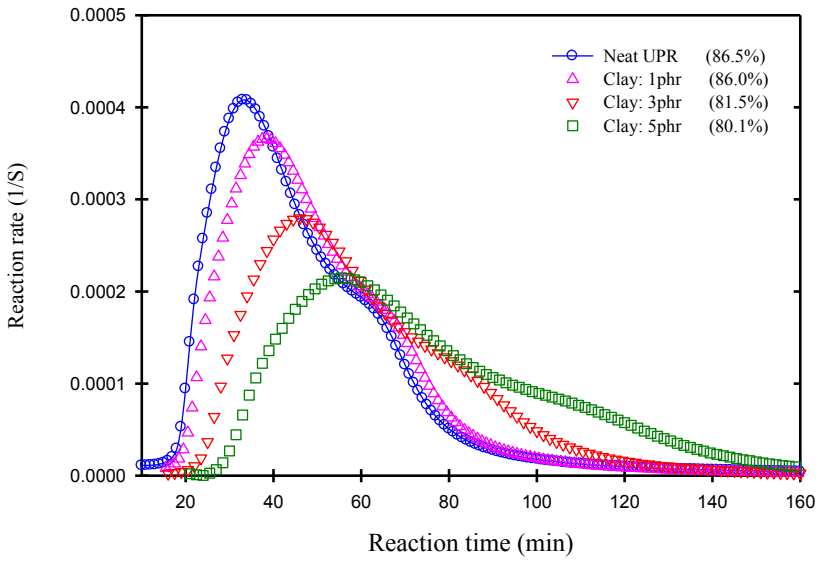

Fig. 3.2. Effect of clay loading on the total curing reaction rate. (Final degree of cure shown in parentheses).

Figure 3.2 shows the total reaction rate during the curing process. The addition of clay caused an increase in the induction time and a reduction in the reaction rate. This reduction is likely due to the restricting effect of clay on the mobility of the initiator and reactant molecules, as well as its neutralizing effect on the peroxide initiator [126]. Also, a reduction in the final degree of cure was observed (the values presented in parentheses and the figure is presented in appendix A2), which calls for more investigation. Therefore, we used FTIR spectroscopy to follow the conversion of each reactant during the curing process.

In order to do this, specific FTIR peaks related to each component (UP and styrene) were identified by following the work of Zhou and Yang [126]. Each chemical group in a molecule absorbs infrared radiation of some characteristic frequencies, where the absorbance can be measured by Beer's law:

$$A_i = \beta_i l C_i \qquad (3.1)$$

where A_i is the absorbance of the species determined from the peak height or peak area, β_i is the absorptivity (absorbing characteristic) of species i, l is the sample thickness, and C_i is the concentration of the species. Consumption of the C=C bonds of styrene can be followed by the change in the area of peaks at 912 or 992 cm^{-1} (CH_2=CH deformation), while a peak at 982 cm^{-1} is related to the C=C bonds of UP (trans CH=CH deformation) which are shown in Figure 3.3. Since the peak at 982 cm^{-1} overlaps with the peak at 992 cm^{-1}, they used a subtraction method. The absorbance of C=C bonds of styrene at 992 cm^{-1} can be calculated based on Beer's law:

$$A_{992} = (\beta_{992}/\beta_{912})\, A_{912} = KA_{912} \qquad (3.2)$$

From solutions with different styrene concentrations, they found a value of 0.48 for K. A_{982} can be calculated by subtracting A_{992} from the area of the overlapped peaks.

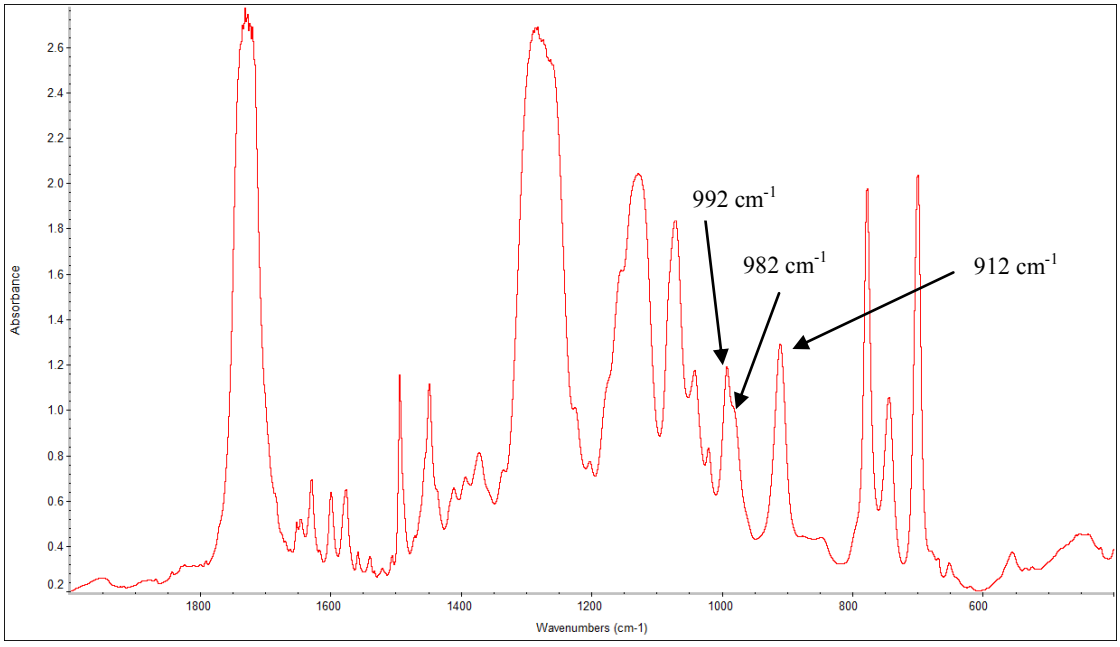

Fig. 3.3. FTIR spectrum of unsaturated polyester resin.

Firstly, we followed the conversion of each component for a pure UPR (Figure 3.4). FTIR data showed that the rate of styrene conversion is significantly lower than that of UP in the first period of curing, meaning that St/UP copolymerization is occurring. In the last stage of curing, when the final conversion of UP is almost done, styrene conversion

continues, indicating styrene homopolymerization at the end of curing. Therefore, the shoulder in DSC diagrams (Figure 3.2) is related to the homopolymerization of styrene.

We note that the addition of clay broadened the styrene homopolymerization shoulder in the DSC diagram. This indicates the trapping of styrene monomers inside the galleries, which then can be only reacted at higher temperatures in the last period of curing.

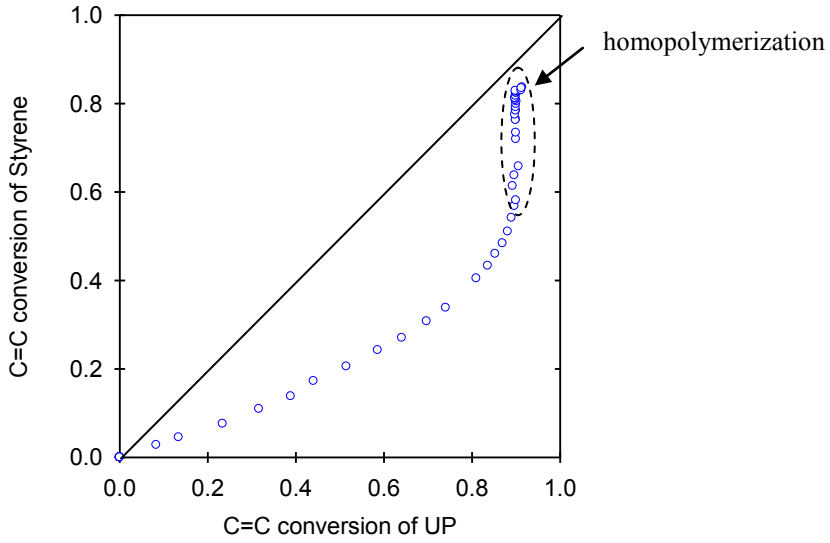

Fig. 3.4. FTIR data: relative conversion of styrene vs. UP.

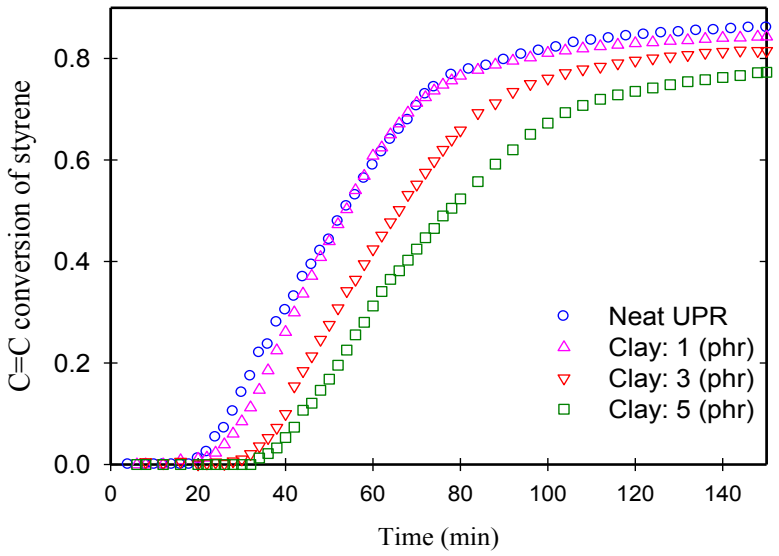

Fig. 3.5. FTIR data: styrene conversion vs. time for samples with different clay contents.

Figure 3.5 illustrates the effect of clay loading on styrene conversion. The addition of clay caused a reduction in styrene conversion due to the trapping of styrene monomers inside the galleries. Clearly, diffusion of styrene monomers into intragallery regions leads to a reduction in their concentration in extragallery regions. This results in a reduction in the degree of cure and likely crosslink density due to a lack of curing agent.

3.4.2. Nanostructure

We evaluated dispersion and distribution of clay silicate layers in both states of the material, liquid and solid. Viscosity of clay/UPR mixtures is a suitable criterion to evaluate the efficiency of each mixing method for dispersing clay. Figure 3.6 shows viscosity of the two mixtures prepared by DM and SHM.

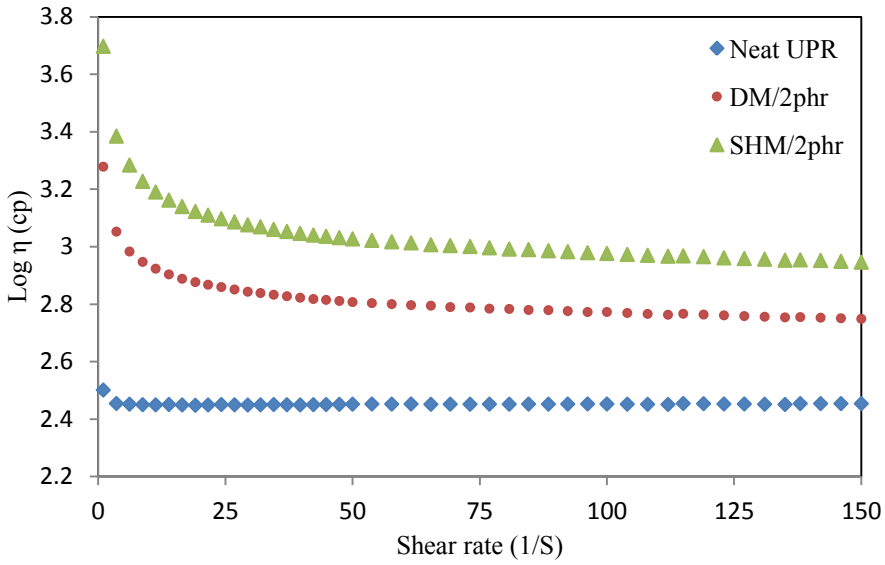

Fig. 3.6. Viscosity vs. shear rate of clay/UPR liquid mixture prepared via different mixing methods. DM: direct mixing method; SHM: solvent-aided high pressure mixing method.

Clearly, the addition of clay caused an increase in viscosity regardless of the mixing method. Moreover, the mixture prepared by SHM method has higher viscosity, indicating better dispersion and delamination of clay silicate layers. Therefore, different mixing techniques led to the different degree of clay dispersion and distribution in the liquid state.

In the cured samples, we used XRD to measure the d-spacing between the clay layers and to find out the degree of clay dispersion and distribution. Bragg's law defines a relation between the angle of incidence and d-spacing, given in Equation 3.3 [129]:

$$n\lambda = 2d\sin\theta \qquad (3.3)$$

where n is an integer that is considered to be 1, λ is the wavelength, θ is the angle of incidence, and d is the interplanar space between the clay layers.

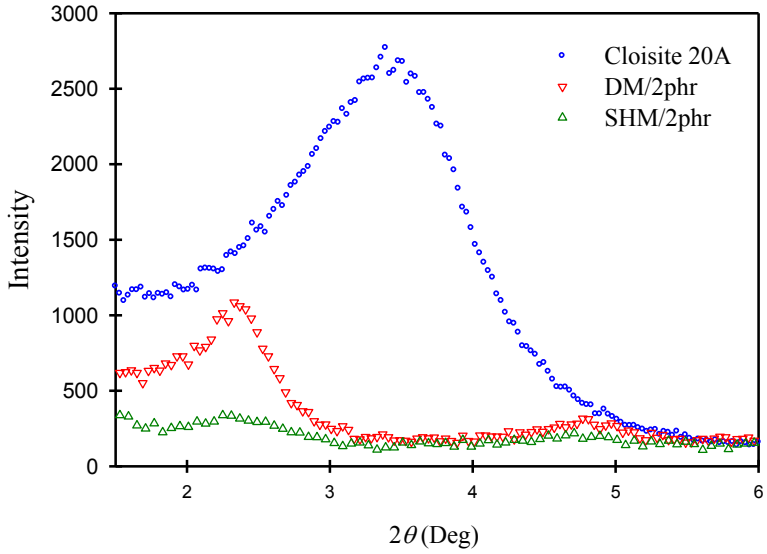

Fig. 3.7. XRD patterns of nanocomposites as compared to that of the original Cloisite 20A. All nanocomposites contain 2 phr clay.

Figure 3.7 presents X-ray diffraction patterns for two nanocomposite samples prepared by direct mixing and high-pressure mixing methods. None of the nanocomposites exhibit the d_{001} diffraction peak at 25.5°A, characteristic of the original Cloisite 20A clay, indicating good delamination and distribution of the silicate layers in the nanocomposites. In the case of the simple nanocomposite prepared by direct mechanical mixing method, the d-spacing is 37.9°A. For the sample prepared by SHM, a very low intensity peak is observed at a d-spacing of 39.1°A. DM method led to a fine intercalated/exfoliated structure, while SHM method was more effective for dispersion and distribution of clay silicate layers, leading to a higher degree of exfoliation according to the XRD patterns.

3.4.3. Glass transition temperature

DSC heat of reaction data indicated a slight reduction in the total degree of cure following the addition of clay. This indicates that the presence of clay silicate layers in the system may cause a reduction in the crosslink density of the matrix. Since crosslink density plays an important role in the fracture toughness of the matrix and consequently in the mechanism controlling fracture toughness to the reinforced system, the effect of clay on this characteristic of the matrix must be evaluated. A property reflecting crosslink density is glass transition temperature (T_g). Therefore, the T_g values of different samples with different clay loading and prepared by different methods were measured by DMA where the maximum in the loss modulus as a function of temperature was considered as T_g (appendix A3).

In general, clay can have two opposing effects on the T_g. On one hand, clay can increase the T_g of the thermosetting matrix by restricting the mobility of the polymer molecules. On the other hand, it can reduce the T_g by decreasing crosslink density of the matrix by trapping curing agent monomers.

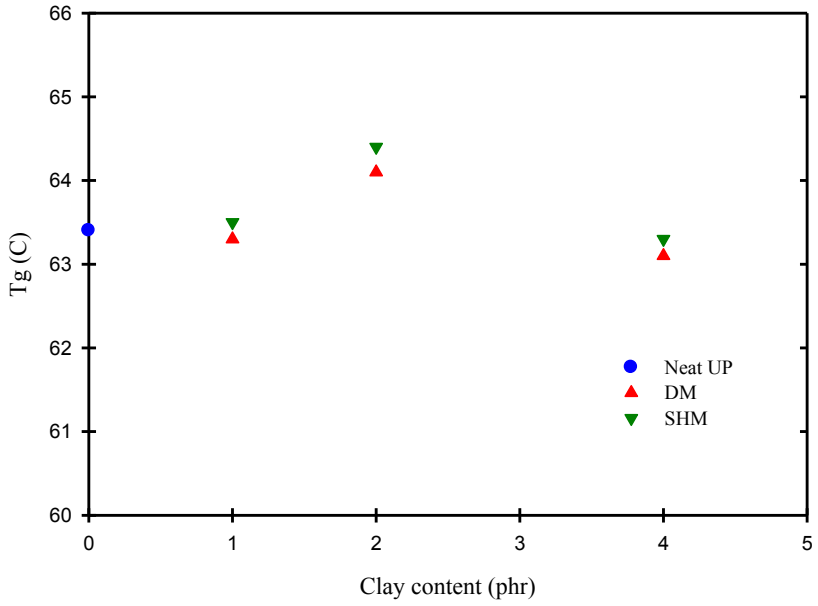

Fig. 3.8. Glass transition temperature as a function of clay content (phr) and mixing method. DM: direct mixing method; SHM: solvent-aided high pressure mixing method.

Figure 3.8 shows the addition of clay up to 2 phr slightly increased the glass transition temperature, likely due to the restricting effect of well-dispersed silicate layers. In addition, the T_g of all samples containing the same clay content is similar regardless of the mixing method, although the samples had different degrees of clay dispersion and distribution. This suggests that the level of difference in clay dispersion does not change the balance between the two opposing effects of clay.

In contrast, higher clay loading (4 phr) caused a slight reduction in the T_g, likely due to clay agglomeration. Agglomeration causes a reduction in crosslink density due to the increase in the concentration of trapped styrene inside the galleries, consequently resulting in a reduction in the T_g. In addition, the agglomeration of the silicate layers reduces interfacial surface areas, decreasing the restricting effect of clay. This reduction in the T_g is not large, indicating that this range of clay loading does not significantly change crosslink density.

3.4.4. Flexural properties

Figure 3.9 and 3.10 show flexural strength and flexural modulus of these nanocomposites prepared by two different methods. In the presence of a second phase, adhesive strength of the interface between the two phases plays important role in flexural strength. Figure 3.9 shows a reduction in the flexural strength by the addition of clay due to the imperfect adhesion at the interface between clay and unsaturated polyester. Different preparation techniques slightly affected flexural strength where an improved degree of dispersion and distribution, obtained by SHM, resulted in a slight increase in flexural strength via increasing the interfacial area between clay silicate layers and the thermosetting matrix. The addition of clay caused an increase in flexural modulus due to its high modulus compared to that of organic thermosetting matrix (Figure 3.10).

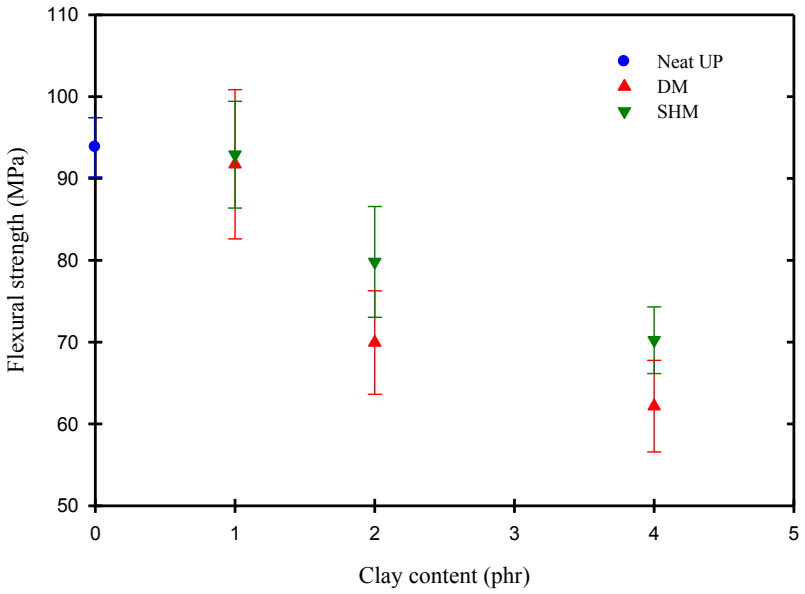

Fig. 3.9. Flexural strength as a function of clay content (phr) and mixing method. DM: direct mixing method; SHM: solvent-aided high pressure mixing method.

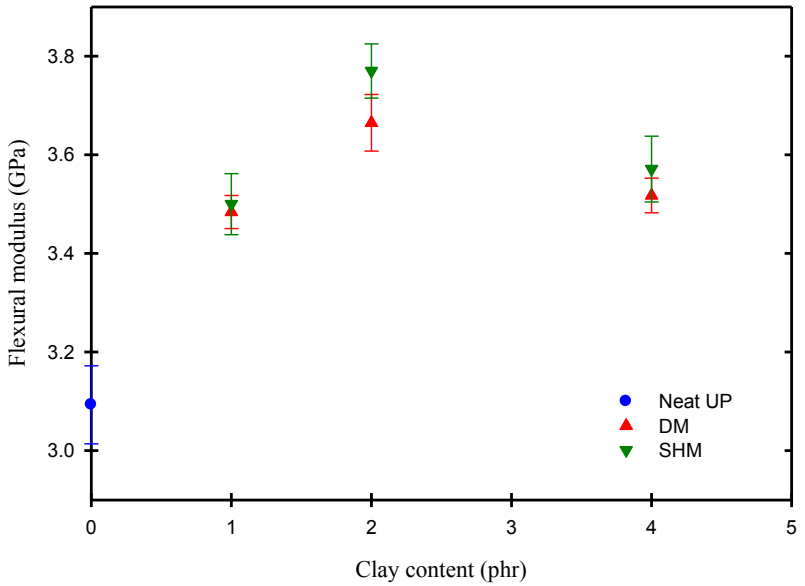

Fig. 3.10. Flexural modulus as a function of clay content (phr) and mixing method. DM: direct mixing method; SHM: solvent-aided high pressure mixing method.

2 phr clay content led to achieve a maximum value of modulus, since greater quantities of clay resulted in agglomeration and a lower quality of distribution. Therefore, a higher degree of exfoliation resulted in a more improvement in stiffness.

3.4.5. Fracture toughness and mechanisms

Figure 3.11 shows the effect of clay on the fracture toughness of unsaturated polyester. The addition of clay caused a slight increase in K_{Ic}, up to 2 phr clay, and further loading (4 phr) caused a reduction in fracture toughness. For constant clay content, the mixing method did not significantly influence fracture toughness, although it did change the degree of clay dispersion and distribution. It means an improved degree in exfoliation did not increase fracture toughness. For more investigation, the main preparation procedure (SHM) was followed by sonication. In the sonication technique, ultrasonic waves improve the dispersion and distribution of the silicate layers by inducing bubbles in the liquid mixture. Indeed, if these bubbles are formed in the interlayer spaces in the galleries, the layers can be separated [120]. However, no significant improvement in fracture toughness was observed by the application of sonication (appendix A4).

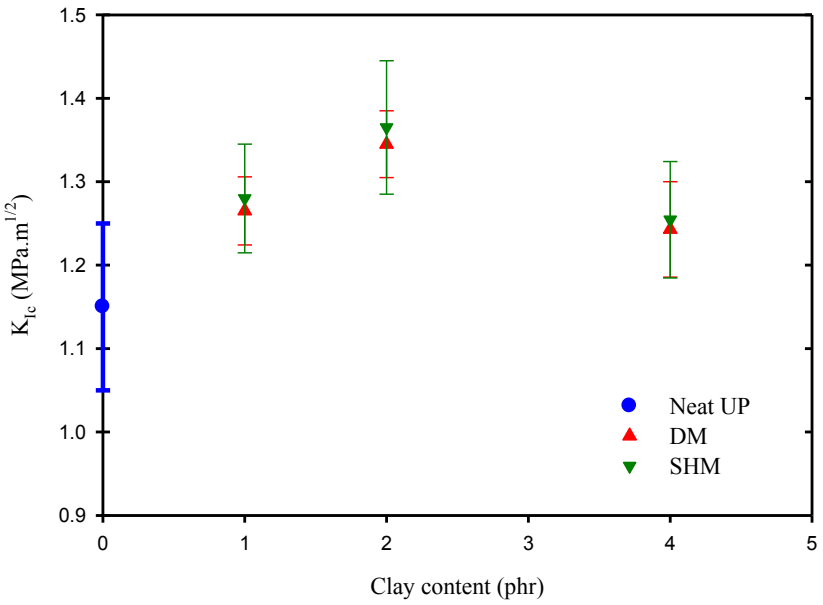

Fig. 3.11. Fracture toughness K_{Ic} as a function of clay content (phr) and mixing method. DM: direct mixing method; SHM: solvent-aided high pressure mixing method.

It is worth noting that Cloisite 30B, which is another commercial and common nano-reinforcement for unsaturated polyesters, was also examined. A comparison between two clays, cloisite 20A and 30B, indicated that cloisite 20A was slightly more efficient for improving fracture toughness of unsaturated polyester likely due to its larger d spacing

and its higher interaction with the thermosetting network (the results presented in appendix A5). Therefore, cloisite 20A was used for the preparation of all nanocomposite samples in this project.

Figures 3.12 shows SEM images of the fracture surface of neat polyester and a nanocomposite sample containing 2 phr clay prepared by DM, respectively. The presence of clay led to roughness on the fracture surface by causing a tortuous path for crack propagation and/or crack deflection.

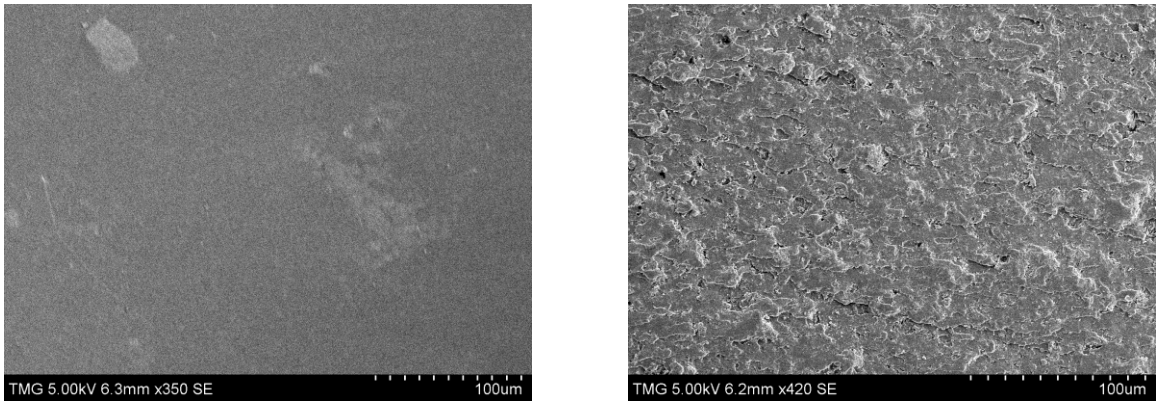

(a) (b)

Fig. 3.12. SEM images of the fracture surface of a) neat polyester, b) nanocomposite containing 2phr clay (Cloisite 20A) prepared by DM.

The nanostructure of nanocomposites plays a key role in fracture toughness. A fully exfoliated arrangement of silicate layers cannot significantly improve fracture toughness because the size of the platelets is too small to cause crack deflection during propagation [82]. These dispersed single layers can make a tortuous path for crack propagation, occurring locally around the clay platelets, which may result in an improvement in fracture toughness by slightly increasing the fracture surface area. In contrast, a micron-sized structure of intercalated tactoids of clay can intercept the crack front during propagation, leading to the occurrence of crack deflection, which can further increase the fracture surface areas [130-131]. Consequently, intercalated clay tactoids cause a greater improvement in fracture toughness compared to exfoliated layers.

The increase in fracture surface area caused by crack deflection is not the controlling mechanism for fracture toughness. Faber et al. [132] proposed a model to predict fracture toughness increments due to crack deflection around second phase particles. They calculated the fracture toughness improvement due to the crack deflection mechanism (based on stress intensity factors at the crack tip) and also the increment in fracture toughness caused by the increase in the fracture surface area. They found a significant difference in the two calculations and demonstrated that the surface area contribution can be considered a lower bound estimate of the toughening increment. This means that, during crack deflection, other energy dissipation processes are engaged to improve fracture toughness. During crack deflection, debonding between the particle and matrix occurs. Since the debonding phenomenon can cause a reduction in the degree of triaxial stress in the crack tip, similar to cavitation of rubber particles or void formation in the matrix, the conditions become more favorable for localized shear yielding of the matrix. Therefore, the other mechanism affecting fracture toughness during crack deflection is likely localized yielding of the matrix in the vicinity of the crack tip during propagation. Kinloch et al. [133] experimentally observed that the presence of intercalated clay tactoids caused crack deflection in the epoxy matrix, but the major contributing mechanism to toughening was localized plastic deformation of the matrix around the tactoids.

In highly crosslinked thermosets, secondary relaxations, such as β relaxation, related to localized motion of small segments of the molecules, strongly affects yielding in the glassy state [27]. Both unsaturated polyester and epoxy have β relaxation linked to local motions of ester groups and the CH_2-CH(OH)-CH_2 segments respectively. The β transition temperature is important for activation of relaxation. The β transition temperature of epoxy is much lower than ambient temperature, but it is much higher for unsaturated polyester. Therefore, β relaxation in epoxy is active at the testing temperature, which is typically room temperature, promoting a higher degree of plastic deformation. The high β transition temperature of unsaturated polyester renders it inactive at ambient temperature severely limiting severely the degree of localized plastic deformation in the vicinity of the crack tip. Glass transition and β transition temperature of epoxy and unsaturated polyester are presented in Table .3.1 [27].

Table 3.1. T_g, β transition temperature, T_β, and activation energy, H_β

Thermoset	Crosslinking agent	T_β (K)	T_g (K)	Activation energy (KJ.mol^{-1})
Epoxy	Amine	190-240	450	40-100
Unsaturated polyester	Styrene	350	400	100-180

Based on tanδ at 1 Hz frequency

The XRD data (Figure 3.7) indicated an intercalated/exfoliated structure for polyester samples prepared by different methods. Fracture toughness results suggest that the higher degree of exfoliation in the nanocomposite prepared by SHM method did not further improve fracture toughness due to the small increase in the fracture surface area caused by the exfoliated layers. Although in nanocomposite samples prepared by DM, the number of intercalated layers, which are favorable for crack deflection, is greater,. the value of fracture toughness is almost the same as that of samples prepared by SHM. The crack deflection mechanism can contribute a significant improvement in fracture toughness when energy dissipation processes such as localized yielding of the matrix occur. In the case of unsaturated polyester, intensity of the localized yielding around the crack tip is low due to its high β transition temperature. In conclusion, for toughening of unsaturated polyesters, all techniques involving localized yielding of the matrix, such as layered silicate toughening, are not as effective as in the case of epoxy, which has a low β transition temperature.

Higher clay loading (4 phr) resulted in a reduction in fracture toughness and T_g, likely due to the formation of aggregates of clay layers. Since in clay aggregates, adjacent tactoids are loosely bonded to each other by weak van der Waals forces [28], these aggregates are not stiff enough to force the crack to tilt out of the plane normal to the applied stress. Consequently, during propagation, the crack penetrates through the aggregates instead of being deflected. As a result, the degree of crack deflection is reduced, resulting in a reduction in fracture surface area, leading to the lower value of fracture toughness. In addition, the lower interfacial area between the layers and matrix also resulted in a reduction in dissipating energy due to clay/matrix debonding.

3.5. Conclusions

Different mixing methods were used for the preparation of clay nanocomposites based on UPRs. The solvent-aided high-pressure mixing method was a successful procedure to achieve a high degree of clay dispersion and delamination throughout the matrix. In general, the addition of clay causes a reduction in the total curing rate and an increase in the induction time. The silicate layers can trap styrene monomers, leading to a reduction in the concentration of styrene in extragallery regions and an increase in residual styrene after curing at room temperature. It can reduce the degree of cure and consequently crosslink density, especially in high clay loading. However, at lower clay loading, this reduction in the degree of cure and crosslink density is slight.

A fine intercalation/exfoliation of the silicate layers slightly improved fracture toughness, whereas an improved degree of exfoliation did not contribute significantly more improvement to fracture toughness. Intercalated silicate layers can cause crack deflection in thermosetting polymers which has the potential to contribute to fracture toughness. In this mechanism, other energy dissipating processes such as localized plastic deformation of the matrix in the vicinity of the growing crack tip contribute more improvement to fracture toughness compared to the contribution obtained by the increase in fracture surface area. The intensity of localized plastic deformation of unsaturated polyester during crack propagation is low since the β relaxation process of UP is inactive at room temperature. Consequently a lower improvement in fracture toughness is caused by crack deflection than might otherwise be expected. Therefore, for toughening of unsaturated polyesters, all techniques involving localized yielding of the matrix, such as layered silicate toughening, are not as effective as the case for toughening of epoxy which has a low β transition temperature meaning that its β-relaxation process is active at room temperature.

3.6. Author's approach

We are following the approach of incorporating both nanoclay and thermoplastic to improve fracture toughness of unsaturated polyester. Firstly, the effect of each toughening agent on different properties of unsaturated polyesters must be explored.

In this chapter, the effect of silicate layers on curing of UPR and fracture toughness of cured samples was evaluated. Investigation into the nanostructure of clay/UP nanocomposite and its fracture toughness revealed that for toughening of unsaturated polyesters with high β transition temperature, all toughening techniques involving localized yielding of the matrix, such as layered silicate toughening, are not as effective as in the case of epoxy, which has a low β transition temperature. Therefore, nanoclay is not a suitable additive to improve fracture toughness of UPs.

As the next step, we must evaluate the effect of thermoplastic additive on fracture toughness and then the effect of its combination with clay. Since the particulate morphology in binary systems results in a greater improvement in fracture toughness, we must use an incompatible thermoplastic which can lead to this morphology. Two common incompatible thermoplastics as low profile additives for UPRs are polystyrene and poly (methyl methacrylate).

We propose to use styrene and MMA as curing agents in the presence of a thermal initiator to compensate for the negative effect of clay on residual styrene and crosslink density of the thermoset. In addition, in situ polymerization of curing agents monomers in the presence of clay is a good approach to pursue two aims simultaneously: (i) improving dispersion and distribution of clay silicate layers, (ii) preparing the thermoplastic component as the toughening agent. Thus, we choose a homopolymer of styrene, polystyrene (PS), and a copolymer of MMA and St, P(MMA/S) as thermoplastic additives in our work.

In next chapter, the effect of these two thermoplastics on fracture toughness will be explored and we will choose the thermoplastic which results in more improvement in fracture toughness. Eventually, the influence of just the thermoplastic and then a combination of thermoplastic and clay on fracture toughness will be evaluated and likely mechanisms controlling fracture toughness will be proposed.

Chapter 4

In situ polymerization of polyester-based hybrid systems for the preparation of clay nanocomposites

S. Chaeichian, PM Wood-Adams*, SV Hoa

Center for Applied Research on Polymers and Composites (CREPEC), Department of Mechanical and Industrial Engineering, Concordia University, 1455 de Maisonneuve Boulevard West, EV004.251, Montreal, Quebec, Canada H3G 1M8

Abstract

Polystyrene and poly(methyl methacrylate/styrene) were prepared by in situ polymerization in the presence of Cloisite 20A, and were then used to synthesize unsaturated polyester-based thermoplastic/thermoset hybrids with improved properties. This approach allows for an increased degree of dispersion and delamination of the silicate layers as well as the presence of thermoplastic chains within the thermoset resin, which improve the physical properties of the system. During curing, methylemethacrylate promotes the conversion of styrene inside the clay galleries and also in the thermoplastic-rich phase. X-ray diffraction and transmission electron microscopy (TEM) revealed a fine intercalated/exfoliated structure in the nanocomposites. Fracture tests showed that a combination of clay and thermoplastic resulted in a synergistic improvement of the fracture toughness of the nanocomposite while stiffness was maintained at the level of the unmodified polyester. The hybrid systems exhibited spherical domains of thermoplastic-rich phase dispersed in the thermoset matrix. The clay was present only in the thermoplastic-rich phase with a portion congregated at the interface between the thermoset and thermoplastic domains. Interestingly, morphological studies showed that the clay layers surrounded microgels of thermoset contained within the thermoplastic domains. Such microgels of thermoset are thought to be fewer and smaller in the hybrid systems without clay, leading to smaller and more compliant dispersed phase domains at the same thermoplastic content and reduced fracture toughness.

Key words:

network forming polymers; multi-phase materials; fracture toughness

4.1. Introduction

Unsaturated polyester resin (UPR), containing unsaturated polyester molecules (Figure 4.1) and styrene which acts as a diluent and cross-linking agent, is a thermosetting polymer. These materials are cured via free radical polymerization between the unsaturated carbon-carbon bonds on the polyester chains and those on styrene, producing a cross-linked structure with styrene bridging the polyester chains. Due to the random nature of free radical polymerization, reactions other than the desired cross-linking also occur, including styrene homopolymerization producing linear chain segments and a polyester-polyester reaction producing broadly spaced cross-linkages. The degree of conversion in such a system includes all of the reactions and is therefore not necessarily directly related to the crosslinking density while the final properties are of course strongly dependent on the network structure.

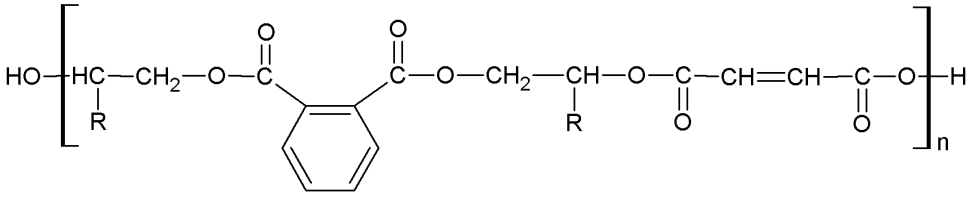

Fig. 4.1. Structure of general purpose, unsaturated orthophthalic polyester.

UPR is widely used in composite applications due to its low cost, versatility, excellent wetting, ease of curing, and a wide processing temperature range. However, its high volume shrinkage, as brittleness and poor chemical and flame resistance, require the use of reinforcements and additives in most applications [23]. Since nano-reinforced matrix materials can lead to improved composite products, the preparation of UPR-based nanocomposites is the focus of our work. Montmorillonite (MMT), a mica type silicate with a layered structure, has been commonly employed as a nano-reinforcement because of the high aspect ratio of its crystal layers [134]. The challenge in preparing useful UPR based nanocomposites is in achieving the fine degree of dispersion and delamination required for significant property improvement.

The preparation of clay nanocomposites based on thermosetting resins includes swelling and dispersing of organoclay in the matrix, followed by network formation during curing. In resin systems composed of two or more components with very different molecular sizes, such as UPR, the mixing order plays an important role in the homogeneity of the mixture and the final properties. Three mixing methods have previously been used: (I) direct mechanical mixing of clay with the resin which contains unsaturated polyester and styrene (St) [116,122,128,135] , (II) preparation of clay suspension in the styrene followed by mixing with the pure prepolymer (without diluents) [121,136] , and (III) preparation of a mixture of the clay and the thermoset prepolymer, either by mechanical mixing (sequential mixing) [128]. or in situ polymerization of the prepolymer in the presence of clay [137] followed by mixing with the reactive diluent.

The first two mixing methods lead to a high concentration of styrene inside the clay galleries as a result of the high diffusion rate of styrene as compared to that of the long polyester molecules. This causes a reduced styrene concentration in the extragallery regions ultimately lowering by a few percent the degree of cure and total crosslinking density [92]. Due to the lack of polyester chains, homopolymerization of styrene is the main reaction that occurs inside the galleries. Styrene homopolymerization under UPR room temperature curing conditions is slow, in part because clay can reduce the efficiency of peroxide initiators by neutralizing them and restricting their mobility [126]. Therefore, during the curing process, the rate of intragallery reactions is much lower than that of extragallery reactions (primarily cross-linking between styrene and polyester). Free radical copolymerization between unsaturated polyester and styrene (St) causes significant volume shrinkage even at moderate conversion [128]. The shrinkage imposes compressive forces on the surface of the silicate layers before the intragallery reactions have had time to produce molecules of significant size. This restricts the clay spacing and the final degree of clay delamination [98].

To avoid the accumulation of styrene monomers inside the galleries, Suh et al.[122], proposed the sequential mixing method (method III). They claimed that this mixing method led to homogenous dispersion of styrene monomers and polyester molecules throughout the system based on data showing higher crosslinking density. Katoch et al.

[137] prepared nanocomposites by in situ polymerization of unsaturated polyester followed by incorporation of styrene, resulting in a fine dispersion and distribution of clay silicate layers in the nanocomposites. In studies in which the third mixing method described above was employed, none of the poor properties of UPR such as brittleness, flame resistance, and shrinkage were evaluated for the nanocomopsites. In a few studies employing methods I and II, properties including impact strength [122], fracture toughness [116,128] , and flame resistance [88] were partially improved by the addition of clay. However, contradictory observations related to the effect of clay on volume shrinkage were reported [102,135]. In summary, nanoclay has been shown to improve mechanical properties to a certain extent while shrinkage control and fracture toughness have not been significantly improved. In our work, we address the improvement of fracture toughness by combining well-dispersed clay with a hybrid thermoplastic/thermoset system.

Low profile additives (LPAs), typically thermoplastic polymers, are often added to control shrinkage of thermosetting polymers [113,140-142]. In unsaturated polyester systems that are cured at low temperature, shrinkage is reduced by the formation of reaction-induced microvoids at the interface between the two phases. This occurs at a very late stage in the curing process because of the lower reaction rate in the thermoplastic-rich phase compared to the polyester-rich phase [142] leading to the formation of microvoids only after the thermoset-rich phase has already shrunk. In an attempt to improve the efficiency of LPAs at low temperatures, Cao et al. [142] used divinylbenzene (DVB) and trimethylopropane trimethacrylate as second comonomers and 2,4-pentandione as a co-promoter. They found that the addition of a second comonomer and co-promoter can reduce shrinkage by increasing the reaction rate in the LPA-rich phase. Another approach to reducing shrinkage is adding nanoclay to unsaturated polyester systems with LPAs [111]. In such systems, the clay platelets residing in the LPA-rich phase increase the stiffness of this phase resulting in an earlier onset of microcracking.

Rubbery polymers are often added to thermosetting matrices to improve fracture toughness at the cost of thermal stability and stiffness [60]. Alternatively, thermoplastic-polymeric toughenes allow for better thermal stability with a smaller reduction in

stiffness. Therefore, the potential of these materials as toughenners has been investigated to some extent, but many aspects of their effects on morphology and properties of thermosetting polymers remain unclear [36,60,143].

In the present work, our goal is to produce toughened polyester-based nanocomposites that exhibit equal or higher modulus and glass transition temperature as the unmodified polyester. In situ copolymerization of methyl methacrylate (MMA) and styrene (St) in the presence of clay is used to improve the dispersion and delamination of the silicate layers and also to synthesize a thermoplastic additive, which can improve the fracture properties of the nanocomposite. MMA also acts during final curing to promote styrene conversion throughout the system allowing the stiffness of the network polymer to be maintained.

4.2.Experimental

4.2.1.Materials

Cloisite 20A (Southern Clay Products Inc.) was used as the nanoclay. Methyl methacrylate (Sigma Aldrich) and styrene (Sigma Aldrich) were used as both copolymerization reactants and crosslinking agents for curing. The styrene and MMA were distilled prior to use using an IKA rotary evaporator under vacuum at 30°C to remove the inhibitors. The thermal initiator was benzoyl peroxide (Sigma Aldrich) and the room temperature initiator employed for curing the whole system was methyl ethyl ketone peroxide (NOROX, MEKP-925H from NORAC Inc.). The unsaturated polyester resin (H596-CWA-12, Ashland Chemical), is a general purpose orthophthalic resin synthesized from maleic anhydride, phthalic anhydride, and propylene glycol. It contains styrene (45wt%) and the promoter cobalt octoate (0.1wt%).

In this work we consider four different classes of materials: (1) simple polyesters which contain unsaturated polyester and one or two crosslinking agents along with a promotor and one or more initiators; (2) simple nancomposites which contain Cloisite 20A in addition to the components of class 1; (3) hybrid polyesters which contain a thermoplastic additive (either polystyrene or poly(methyl methacrylate-co-stryene) in addition to the components of class 1; and (4) hybrid nanocomposites which contain

Cloisite 20A in addition to the components in class 3. We use SP (simple polyester), SN (simple nanocomposite), HP (hybrid polyester), HN (hybrid nanocomposite) as the first two letters in the names of our samples. The term simple is chosen to describe classes 1 and 2 because these systems contain only one polymeric phase. In comparison, the hybrid systems contain two polymeric phases that are likely connected to some degree with covalent bonds. In the name of each sample, the number refers to the molar ratio of curing agents, MMA/St_{CA}, and the polymer abbreviation at the end of the name specifies the type of thermoplastic present, either the copolymer of MMA and styrene, P(MMA/S), or polystyrene (PS). For example, the sample called *HN/0.2/P(MMA/S)* is a hybrid nanocomposite formed with a curing agent mixture of molar ratio of 0.2 methyl methacrylate to styrene and containing the copolymer of MMA and styrene as a secondary polymeric phase.

4.2.2.In situ polymerization of thermoplastic component

The mixture of clay and comonomers (MMA and St) was prepared as follows. First, dried clay (6.3 phr based on the weight of comonomers) was mixed with the raw reactants at 1000 rpm for 1hour at room temperature, followed by high shear mixing at 7500 rpm for 15 minutes, slow mixing at 500 rpm for 30 minutes, and then another 15 minutes at 7500 rpm.

The polymerization, either MMA/St copolymerization or St homopolymerization, was initiated by adding 0.2 mol% BPO, and carried out at approximately 65°C under reflux in a nitrogen atmosphere while mixing at 300 rpm. The conversions of the monomers were determined by ^{1}H NMR and used to determine the overall composition of the reaction product mixture. In the case of hybrid polyester preparation, the polymerization of MMA and/or St is completed as above but in the absence of clay. When the desired conversion was achieved (after about 6 hours) the reaction was slowed by dropping the temperature to ~ −20°C. After about 24 hours of low temperature storage, the reaction mixture was heated to room temperature prior to its incorporation into the unsaturated polyester resin. We note that at the low conversions used here, the concentration of free radical initiator does not change significantly. Therefore BPO, at approximately the initial content, will be present in the hybrid systems where it acts as a secondary initiator. Also, because we

have not stopped the reaction chemically it is likely that we have some living thermoplastic chains that continue to react during the final curing of the hybrid system.

4.2.3.Hybrid polyester and nanocomposite preparation

For curing, the final ratio of curing agent to unsaturated polyester must be kept constant (equivalent to 45wt% styrene) for all samples. Therefore, a portion of the styrene was removed from the original unsaturated polyester resin by distillation using an IKA rotary evaporator under vacuum conditions at 50 °C, producing a resin containing 20wt% styrene. The resulting concentrated resin was mechanically mixed with the reaction products from in situ polymerization and additional comonomer (styrene and/or MMA) as required to give the desired ratio of the two curing agents with overall moles of curing agents equivalent to 45wt% styrene at 1000 rpm for 3hours. Methyl ethyl ketone peroxide (MEKP) (1wt % based on the weight of the unsaturated polyester and the curing agents) was added and the mixture was mixed for further 2 minutes under vacuum to remove air bubbles. The mixture was poured into molds, cured at room temperature for 12 h and post-cured at 110°C for 4hour. In order to represent the relative amount of MMA and St available to take part in the curing reaction, we use the molar ratio, MMA/St_{CA}. A ratio of 0 indicates that only styrene is present for curing.

4.2.4.Simple nanocomposite preparation

For comparison purposes, simple nanocomposites were prepared by the direct mixing process. The clay (2 phr) was gradually added to the resin and mixed for 8hour at 2000 rpm. The mixture was cast and cured following the same procedure as above.

4.2.5.Characterization Methods

^{1}H NMR of the in situ polymerization products were dissolved in chloroform and submitted to ^{1}H NMR analysis using a 500 MHz Varian spectrometer. Molecular weight and molecular weight distribution were determined by gel permeation chromatography (GPC) with a Viscotek VE1122 pump and a refractive index (RI) detector. Three PolyAnalytik columns (PAS-103L, -105L, and -106L) were used with THF as an eluent at 30°C and a flow rate of 1 mL/min. Linear polystyrene (PS) standards were used for calibration.

Calorimetry was performed with a differential scanning calorimeter (TA Q10) on 10 mg of uncured sample in a hermetic aluminum pan. The isothermal reaction rate profile was measured at 25°C, followed by a scan from 25-300°C at a heating rate of 5°C/min to determine the total reaction heat.

X-ray diffraction analyses were performed using an X-ray diffractometer (Philips X'PER) at low 2θ with a scanning speed of 1°/min. The X-ray source was Cu-Ka radiation (λ= 1.540598 A ˚), using a 50 kV voltage generator and a 40 mA current.

Dumb-bell specimens (ASTM D638-82a type V) were used to determine tensile properties on an Instron 3365 (5 kN) testing machine at a constant crosshead speed of 1mm/min. Fracture toughness tests were carried out according to ASTM D5045-99 using an MTS 312.21 (100 kN) on sharply notched three-point bend specimens. Dynamic mechanical measurements were made between 20-180°C at 1 Hz, using a TA Instruments DMA 983 dynamic mechanical analyzer.

The fracture surface of broken samples was coated by a thin layer of Pd for the microscopic characterization. A Hitachi S-4700 FE-SEM 2 kV scanning electron microscope and an optical microscope (Variscope) were used to observe the fracture surface. The nanostructure of nanocomposite samples were also examined with transmission electron microscopy (TEM) using a JEOL JEM-2100F microscope operating at a 200kV accelerating voltage. The samples were cut into thin sections (50-80 nm thickness) using an ultramicrotome with a diamond knife.

4.3.Results and discussion

4.3.1.In situ polymerization of thermoplastic component

Methyl methacrylate and/or styrene were (co)-polymerized via free radical polymerization in the presence of nanoclay in order to improve the dispersion and delamination of the clay layers as well as to synthesize a thermoplastic additive, either P(MMA/S) or PS, for the hybrid system. A relatively low conversion is sufficient to produce the desired small amount of thermoplastic. The total monomeric conversion was kept constant (around 20%) for all molar ratios of MMA to styrene. This corresponds to a thermoplastic content of 7wt% in the final cured hybrid system. It is known that at low

conversions in this type of copolymerization [144,145] the molecular weight and molecular weight distribution are relatively insensitive to monomer molar ratios and that only the chemical composition of the copolymer is affected by the molar ratio of the monomers.

The composition of the thermoplastic copolymer affects the compatibility between the thermosetting and thermoplastic-rich phases. The compatibility between the two phases can be estimated from Flory-Huggins interaction parameters (χ_{ij}) calculated from solubility parameters according to the following equation (Eq. 1) [146]

$$\chi_{ij} = \frac{V_r}{RT}\left(\delta_i - \delta_j\right)^2 \qquad (1)$$

where V_r is the reference molar volume (styrene was taken as a reference), δ_i is the solubility parameter for species *i,* R is the gas constant, and *T* is the absolute temperature. The group contribution method can be used to calculate the solubility parameter of the species [35].

$$\delta = \frac{\rho \sum G}{M} \qquad (2)$$

where ρ represents the density, *M* is the molecular weight of the repeat unit and *G* is the group molar attraction coefficient. The solubility parameters of unsaturated polyester, St, MMA, polystyrene (PS), poly(methyl methacrylate) (PMMA), and MMA/St copolymer P(MMA/S) are summarized in Table 4.1 along with the relevant Flory-Huggins interaction parameters. PS and PMMA are known to be incompatible with UPR whereas poly(vinyl acetate) (PVAc) is compatible with UPR [65]. The Flory-Huggins interaction parameter between unsaturated polyester and PVAc is around 3.2 x 10^{-2} which is about half that between unsaturated polyester and PS (6.7 x 10^{-2}) or PMMA (5.44 x 10^{-2}). Thus, the composition of our copolymer does not have a significant effect on the compatibility between it and the pure unsaturated polyester. However, since the MMA can be incorporated into the network as a second crosslinking agent, we can expect an improved compatibility between the network and the thermoplastic component.

Using gel permeation chromatography (GPC) we determined that the number average molecular weight (M_n) of the thermoplastic copolymer synthesized in the absence of clay was approximately 87000. It was not possible to submit the systems containing clay to GPC analysis and it is possible that the M_n of the polymers synthesized by in situ (co-)polymerization may be slightly different due to the effect of clay on the radical initiation. However, Nikolaidis et al. [147] reported that Closite 20A did not significantly affect the reaction rate of in situ polymerization of MMA at low conversions and we therefore expect that our in situ polymerized copolymers have approximately the same M_n as above.

Table4.1. The Flory-Huggins interaction parameters of MMA, St, unsaturated polyester, and the thermoplastic copolymer

	PS (9.03)†	**P(MMA/S)* (9.1)**	**PMMA (9.18)**
St (9.04)	2.5×10^{-6}	1.07×10^{-4}	6.04×10^{-4}
MMA (8.89)	6.4×10^{-4}	1.41×10^{-3}	2.66×10^{-3}
unsaturated polyester (10.48)	6.7×10^{-2}	6.10×10^{-2}	5.44×10^{-2}

†The values in parentheses indicate the solubility parameters $(Cal/cm^3)^{1/2}$

*The copolymer is 18 mol% MMA

4.3.2.Chemical reactions during solidification

During curing, UPR and styrene undergo free radical copolymerization to form a three-dimensional network via microgel formation, gelation, and finally vitrification. The presence of a comonomer (MMA) makes curing more complex due to the number of different possible reactions including copolymerization of unsaturated polyester and St or MMA, copolymerization of MMA and St, as well as homopolymerization of each component. The probability of each reaction, during curing, can be estimated based on the monomer reactivity ratios of unsaturated polyester, St, and MMA (Table 4.2). The reactivity ratio, r_{ij}, of component *i* reacting with component *j* is related to the reaction kinetic constants according to the following equation [13].

$$r_{ij} = \frac{k_{ii}}{k_{ij}} \qquad (3)$$

Here, k_{ii} is the kinetic constant for homopolymerization of component i and k_{ij} is the kinetic constant for copolymerization of components i and j. If the reactivity ratio is less than 1, then copolymerization is more likely than homopolymerization. According to Table 4.2, all copolymerization reactions dominate over homopolymerization with the exception of copolymerization of MMA and unsaturated polyester which is less likely than the homopolymerization of MMA. Also, the copolymerization of MMA and styrene is more likely than either styrene or MMA homopolymerization. This means that under curing conditions, MMA is most likely to copolymerize with St rather than to take part in any other reaction, while St is expected to copolymerize with unsaturated polyester and MMA rather than homopolymerize. The copolymerization of unsaturated polyester and St, which determines the degree of crosslinking, is clearly in competition with the copolymerization of MMA and St, which determines the length of the crosslinking bridges or the compactness of the network. Therefore, the amount of MMA monomer in the system plays an important role in these two characteristics of the network.

Table 4.2. Monomer reactivity ratios [13]

Monomer 1	Monomer 2	r_{12}	r_{21}
DEF*	St	0.02 - 0.11	0.29 - 0.63
DEF*	MMA	0.04 - 0.05	2.10 - 40.3
St	MMA	0.28 - 0.59	0.31 - 0.54

*The reactivity of unsaturated polyester is assumed to be similar to that of diethyl fumarate (DEF)

In order to evaluate the effect of MMA on the reactions during curing of simple polyesters, a series of isothermal DSC experiments were carried out at 25°C. The DSC results are plotted in Figure 4.2 in terms of the total reaction rate as a function of time. In the neat UPR, SP/0.0 where the number in the name refers to the molar ratio of curing agents MMA/St_{CA}, reaction rate curve we find two peaks; the shorter time peak is related to the crosslinking reaction between St and unsaturated polyester and the longer time peak is due to St homopolymerization. When MMA is present, the long-time peak is eliminated indicating a significant reduction in styrene homopolymerization. The reaction rate is decreased in the initial stage likely reflecting a slower unsaturated polyester conversion as compared to SP/0.0, which contains only St as a crosslinking agent. This can be understood by considering the reactivity ratios. We recall that MMA prefers homopolymerization compared to copolymeriztion with unsaturated polyester (r_{21} = 2.10-

40.3 > 1) whereas St prefers copolymerization with unsaturated polyester over homopolymerization (r_{21} = 0.29-0.63 < 1). In addition, the monomer reactivity ratios indicate that St/unsaturated polyester copolymerization (r_{21} = 0.29-0.63) is similar in reaction rate constant to St/MMA copolymerization (r_{12} = 0.28-0.59). The total reaction rate was increased at the intermediate times due to the copolymerization between St and MMA, which is much faster than St homopolymerization (r_{12} = 0.28-0.59 < 1). The final total conversion was not significantly affected by the presence of MMA.

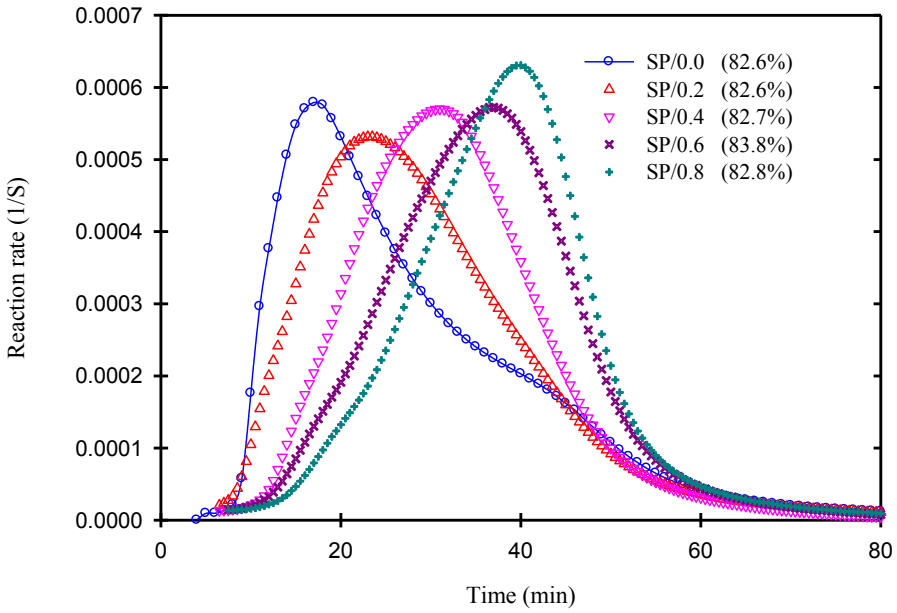

Fig. 4.2. Effect of MMA content on the curing reaction rate of simple polyester systems.The MMA/St_{CA} ratios are given by the numerals in the sample names. The values given within parentheses in the legend are the final conversions of the systems.

Next, the effect of MMA on the isothermal curing reactions of simple nanocomposites (2 phr clay) at 25°C was studied (Figure 4.3). Clay caused a reduction in the curing rate and an increase in the induction time, as expected [92]. The effect of MMA on the curing of simple nanocomposites is similar to that in the curing of simple polyesters, but with broader peaks, indicating longer curing periods. These results confirm the observation of Zhou et al. [92] who found that clay causes a reduction in St conversion during curing of UPR. The presence of MMA increased the total conversion as compared to that of the

UPR-clay system (SN/0.0), which contains only St as a curing agent, due to the St/MMA copolymerization, which can occur in both the intra- and extra-gallery spaces. Finally we note that the simple systems do in fact contain some P(MMA/S) and/or PS chain segments which may be connected to the network covalently or simply linear chains. In optical micrographs, we do not observe any phase separation in these systems indicating that the content of purely thermoplastic linear chains is likely very low.

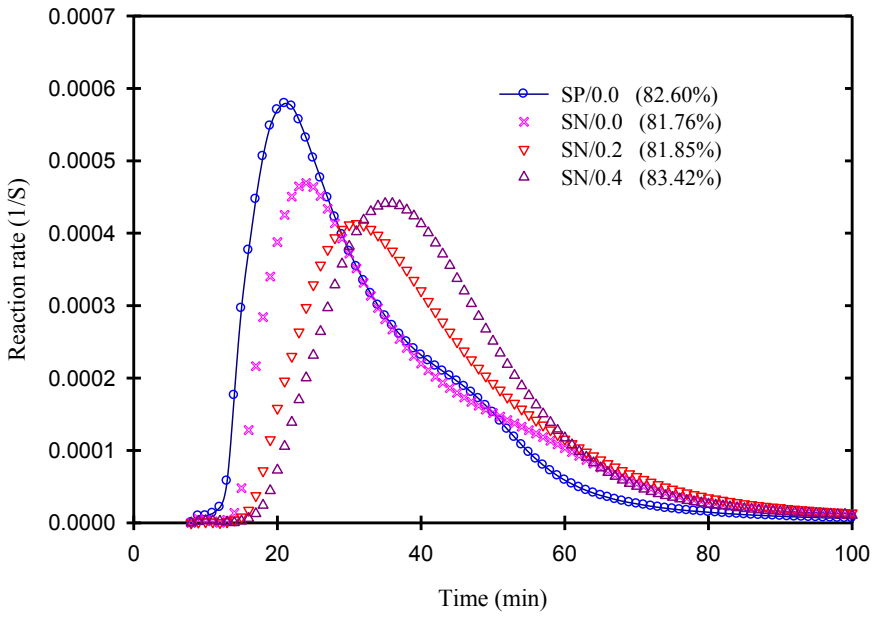

Fig.4.3. Effect of MMA content on the curing reaction rate of simple nanocomposites. For comparison, the data for simple polyester (SP/0.0) are repeated from Figure 1. The MMA/St_{CA} ratios are given by the numerals in the sample names. All simple nanocomposite samples contain 2 phr clay. The final conversion of each system is given in parentheses in the legend.

The curing behavior of hybrid systems is more complex due to phase separation of the system into thermoset-rich and thermoplastic-rich phases. Hsu et al. [65] investigated the effect of different thermoplastic additives on the curing behavior of unsaturated polyester. They noted that the incompatible thermoplastic additives (PS and PMMA) resulted in a phase-separated morphology with spherical particles dispersed throughout the thermoset matrix. No such phase separation was observed in the system with a compatible thermoplastic (PVAc) which has a uniform structure through the entire sample.

In an incompatible unsaturated polyester/styrene/thermoplastic system there are two major phases, unsaturated polyester-rich and thermoplastic-rich. Styrene easily diffuses into the thermoplastic-rich phase as compared to the larger molecules of unsaturated polyester. Therefore, within this phase there is a high concentration of styrene but a low concentration of unsaturated polyester. Additionally, the concentration of the promoter is low in the thermoplastic-rich phase, and high in the unsaturated polyester-rich phase due to the complexation between of the cobalt atom of the promoter and the carboxyl groups of the unsaturated polyester [142]. As a result, the reaction rate in the thermoplastic-rich phase is lower than in the unsaturated polyester-rich phase. The system becomes even more complex when a second curing agent, such as MMA in our case, is present.

Note that in the hybrid systems studied here, the majority of the thermoplastic is produced during the preliminary (co-)polymerization step where MMA and/or styrene are reacted to produce linear copolymer or homopolymer chains dissolved in excess monomer(s). The reaction mixture may contain a fraction of living polymer chains that can continue to react under the curing conditions of the hybrid system along with the monomers (MMA and/or styrene) and the unsaturated polyester. A small amount of new P(MMA/S) and/or PS chain segments are also produced during the curing reaction.

The effects of MMA content and thermoplastic component (TP) on the isothermal curing of hybrid nanocomposites (those containing unsaturated polyester, St, MMA, clay, and TP) are shown in Figure 4.4 As in the case of simple nanocomposites (Figure 4.3), hybrid nanocomposite systems containing both MMA and St as curing agents exhibit only one exotherm peak while those containing only St as a curing agent exhibit a broad peak with a shoulder. In comparison to the simple nanocomposites, the curing process is slower in the hybrid nanocomposite systems, especially in the case when only St is present as a curing agent. Hsu et al. [65] found that in UPR systems containing thermoplastic additives, the compatible UPR-PVAc system exhibited fast curing with a single exotherm peak. Here we have managed to achieve the same result but by introducing the second curing agent MMA rather than introducing a more compatible TP. Since MMA is small it can also diffuse quickly into the TP-rich phase, resulting in a high concentration of both St and MMA in this phase. As MMA/St copolymerization is faster

than St homopolymerization, the reaction rate inside the thermoplastic-rich phase increased as compared to those systems containing only St as a curing agent leading to a higher overall reaction rate. However, there is an optimum MMA content because excess MMA can result in a decrease in unsaturated polyester conversion by consuming too much of the St. From the results in Figure 4.4, we can conclude that for these hybrid nanocomposite systems the optimum MMA/St_{CA} is something less than 0.3.

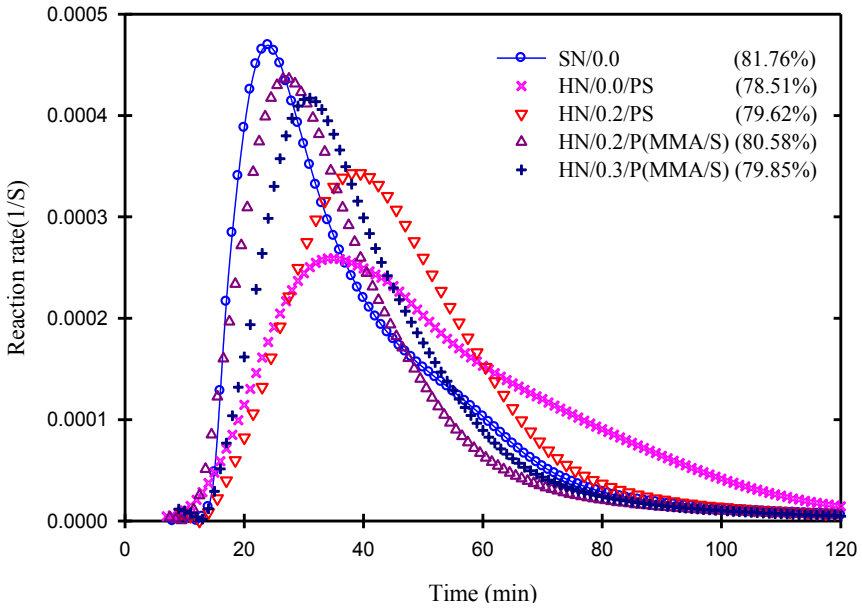

Fig. 4.4. Effects of MMA content on the curing reaction rate of hybrid nanocomposites. For comparison the data for simple nanocomposite (SN/0.0) are repeated from Figure 2. The MMA/St_{CA} ratios are given by the numerals in the sample names. All nanocomposite samples contain 2 phr clay. All hybrid systems contain 7 wt% thermoplastic. The final conversion of each system is given in parentheses in the legend.

4.3.3.Micro- and nanostructure of polyester-based systems

Figure 4.5 presents X-ray diffraction patterns for simple and hybrid nanocomposites. None of the nanocomposites exhibit the d_{001} diffraction peak at 25.5Å characteristic of the original Cloisite 20A clay, indicating good delamination and dispersion of the silicate layers. In the case of the simple nanocomposite prepared by direct mechanical mixing, SN/0.0, the d-spacing was found to be 36.7 Å. For the hybrid system containing the thermoplastic copolymer, HN/0.2/P(MMA/S), a low intensity peak occurs at a d-spacing of 38.5 A°. Note that the number in the sample name refers to the molar ratio of the

curing agents MMA/St_{CA} and the polymer abbreviation refers to the thermoplastic in the system. This indicates that the in situ polymerization method produces a finer intercalated/exfoliated structure than the direct mechanical mixing method. Additionally, in situ copolymerization is more effective in this regard as compared to in situ styrene homopolymerization (compare with results for HN/0.2/PS). This is because the polarity of MMA renders it is more compatible than styrene with the silicate layers.

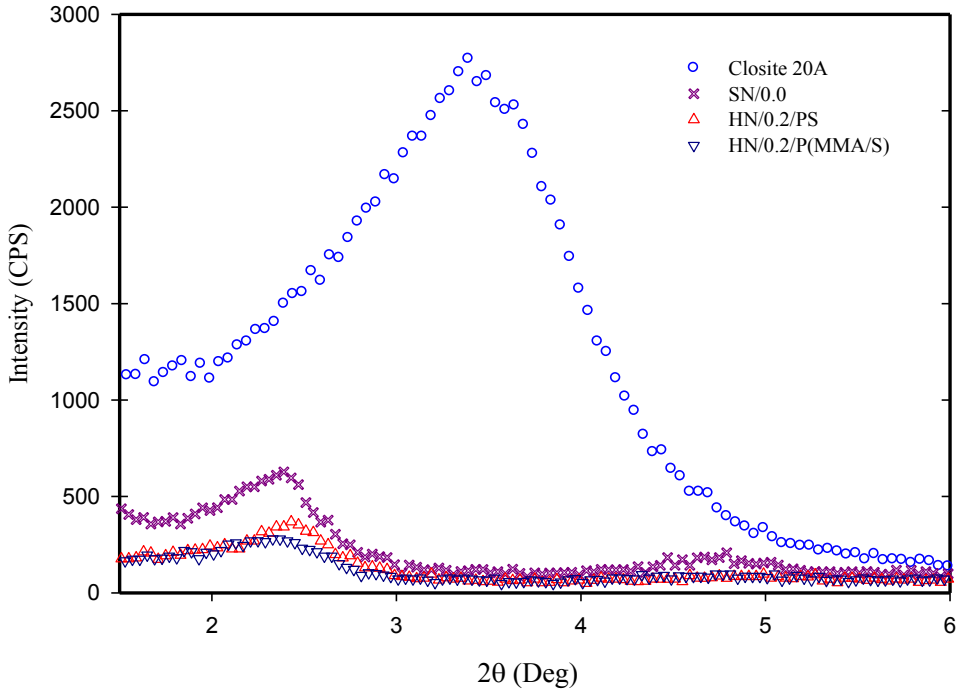

Fig.4.5. XRD patterns of nanocomposites as compared to that of the original Cloisite 20A. All nanocomposites contain 2 phr clay and hybrid systems contain 7 wt% thermoplastic.

The hybrid systems exhibit a phase-separated morphology with spherical thermoplastic-rich domains dispersed homogeneously throughout the continuous thermoset-rich phase (Figure 4.6). The state of dispersion of clay within the hybrid nanocomposite, HN/0.2/P(MMA/S), was observed via transmission electron microscopy (Figure 4.7). The clay is finely dispersed and a high degree of exfoliation is achieved with only a few small tactoids of 3 or 4 layers remaining. The micrograph in Figure 4.7a indicates that the clay layers are segregated within the thermoplastic-rich phase. Silicate layers are also arranged parallel to the interface between the thermoplastic and thermoset phases. This structure is similar to Pickering emulsions in which nanoparticles stabilize

droplets of one liquid within another by reducing the interfacial tension. Such a structure can only form with clay when a high degree of delamination is achieved.

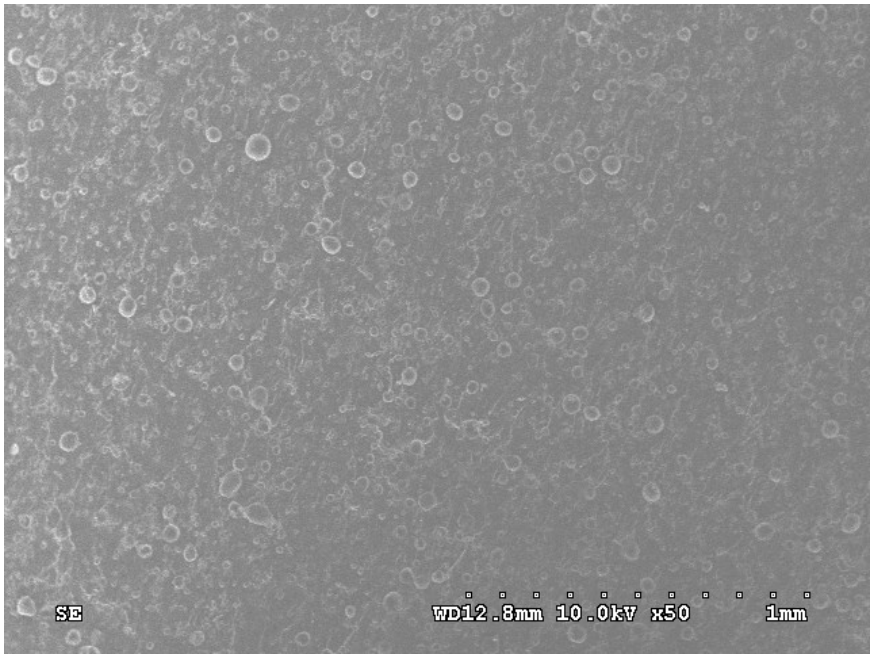

Fig.4.6. Low magnification SEM image showing dispersed phase microstructure typical of all hybrid systems studied (HP/0.2/P(MMA/S)).

We also observe small spherical domains (~250 nm diameter) within the thermoplastic rich particles, which are bordered by clay layers. It is likely that these small particles are thermoset-rich microgels that were stabilized by the presence of clay layers at their interfaces and then trapped within the thermoplastic-rich domain by gelation. Hybrid systems such as considered here, consist of two liquid phases prior to curing. Under quiescent conditions, the minor phase (thermoplastic-rich) in this two-phase liquid system will form spherical droplets. Although the minor phase is rich in thermoplastic it also contains sufficient unsaturated polyester and cross-linking agents (styrene and/or methyl methacrylate) for some curing to take place. When adjacent polyester chains in the thermoplastic-rich phase are linked together they begin to form a polyester-rich sub-domain in the form of microgels. At this time, the thermoplastic molecules are expelled

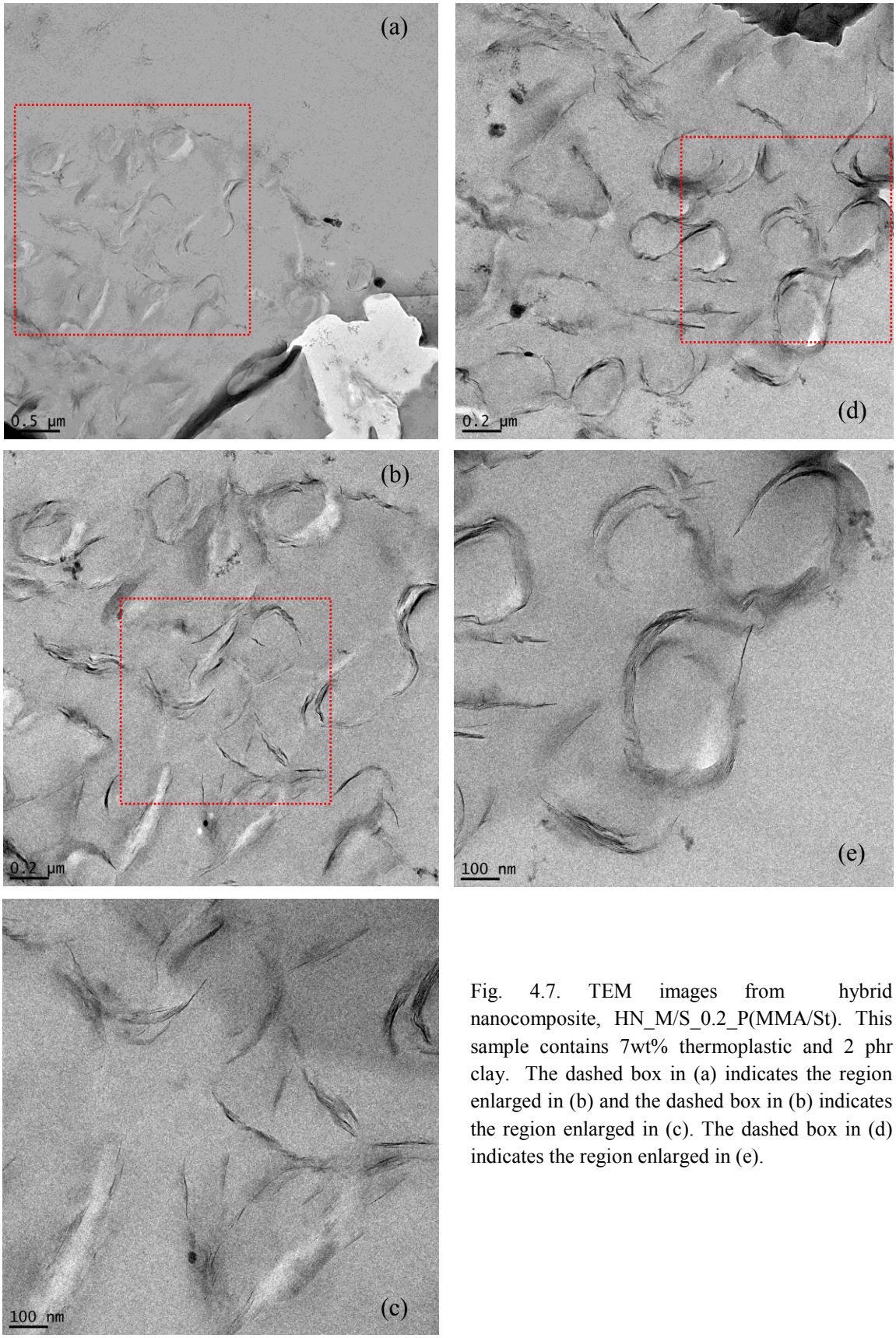

Fig. 4.7. TEM images from hybrid nanocomposite, HN_M/S_0.2_P(MMA/St). This sample contains 7wt% thermoplastic and 2 phr clay. The dashed box in (a) indicates the region enlarged in (b) and the dashed box in (b) indicates the region enlarged in (c). The dashed box in (d) indicates the region enlarged in (e).

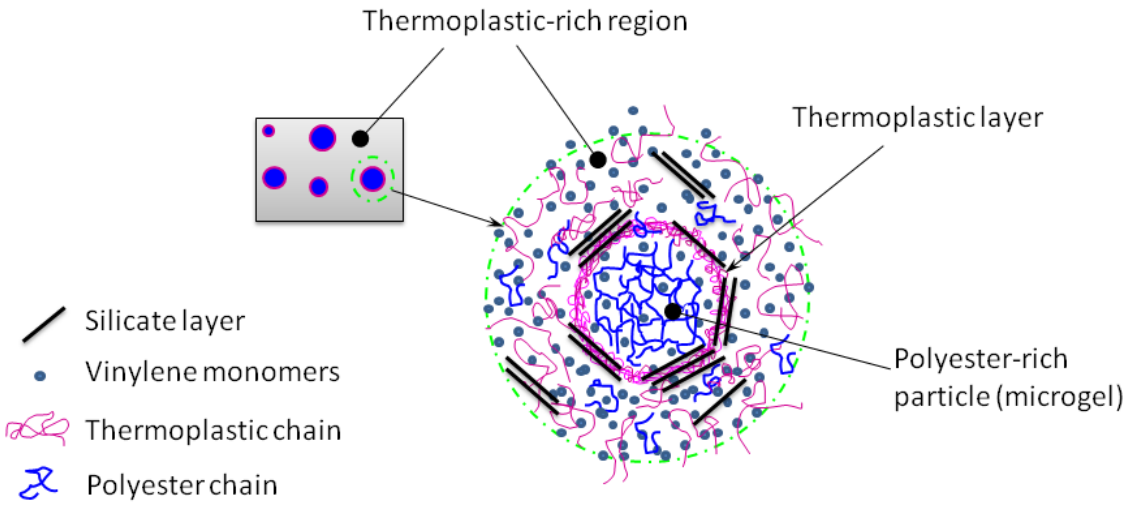

Fig. 4 8. Schematic of polyester-rich microgel surrounded by a thermoplastic layer during the curing process.

from and eventually surround the microgels [65] (Figure 4.8). The thermoplastic layer acts as a barrier and prevents the migration of polyester chains in and out of the microgels. Since well-dispersed silicate layers tend to preferentially locate at the interface of thermoplastic and thermoset phases, they surround the microgels and stabilize the structure until curing is complete.

The above hypothesis is supported by a study of the larger scale morphology of hybrid polyester and two nanocomposites with optical microscopy (Figure 4.9). The simple nanocomposite (Fig. 4.9a) has a featureless morphology at this scale as expected. Fig. 4.9b and Fig. 4.9c, show that the thermoplastic particles in the system without clay, HP/0.2/P(MMA/S), are smaller than those in the equivalent clay containing system, HN/0.2/P(MMA/S), although the thermoplastic mass in these two systems is the same. This means that the clay affects the degree of phase separation and the size of thermoplastic-rich droplets before and during curing. Phase separation and the resulting morphology is controlled by the degree of compatibility between thermoplastic and thermoset components, and the mobility of the various molecules at various time during mixing and the subsequent quiescent curing process.

We propose that the microstructure develops in the following manner. In the first stage of mixing the unsaturated polyester resin with the thermoplastic/clay mixture, small

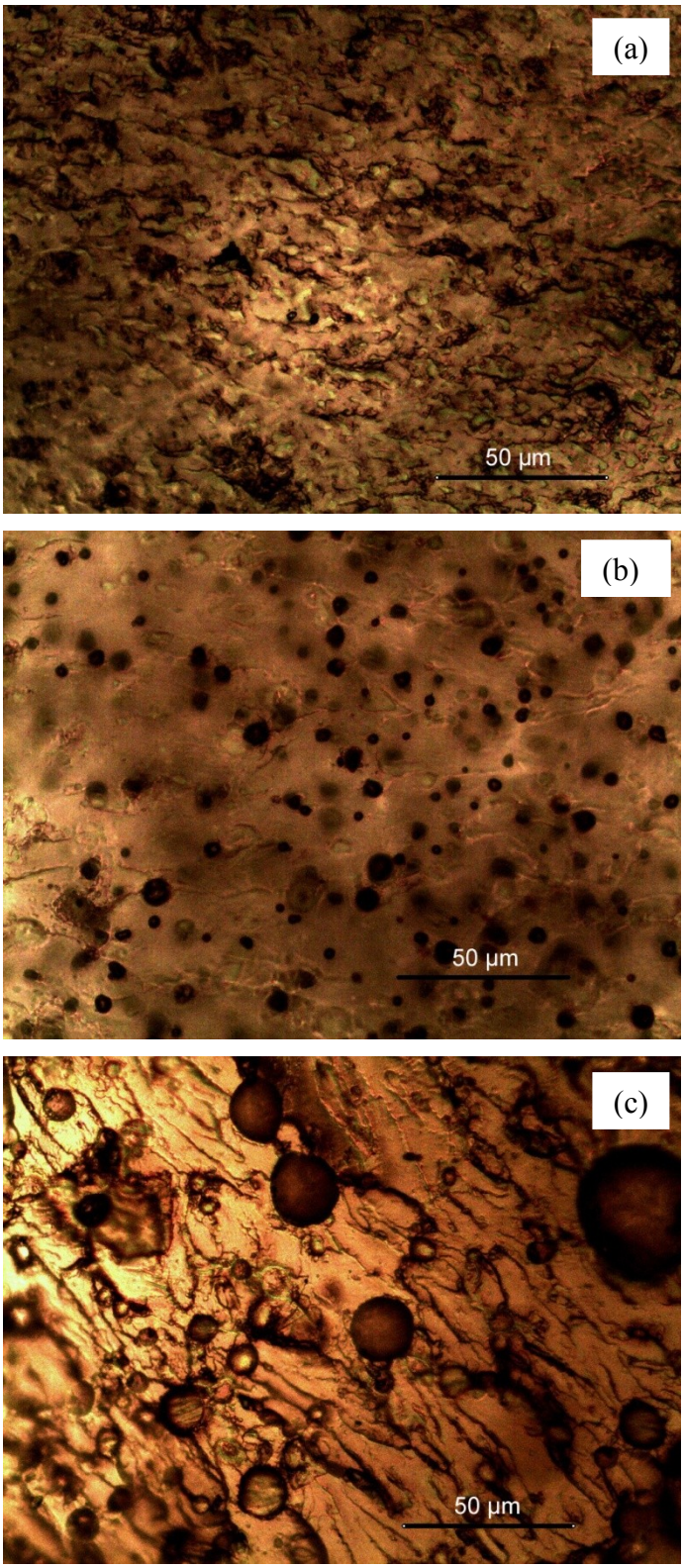

Fig. 4.9. Optical micrographs of polyester based systems. a) SN_M/A_0.0, b) HP_M/S_0.2_P(MMA/S), c) HN_M/S_0.2_P(MMA/S. Both nanocomposites contain 2 phr clay and 0.2 wt% BPO. Particles through the transparent samples are visible and appear lighter or darker depending on the focal length and their depth.

droplets of the thermoplastic mixture are dispersed through the polyester/curing agent phase. During the mixing, these droplets are swollen as the curing agent monomers (styrene and MMA) and polyester chains diffuse inwards. When exfoliated clay is present, the thermoplastic-rich droplets have a much larger viscosity than the continuous phase, even when swollen with monomers. This means that the size of the droplets attained during the mixing will be higher when clay is present because shear-induced droplet breakup will be less severe [148]. After 4 hours, the mechanical mixing is stopped and under quiescent conditions, coalescence of the droplets occurs, during curing, until the network gels. The final size of the droplets after curing will then depend on the size of the dispersed phase attained during mixing, the rates of diffusion of various materials in and out of the thermoplastic rich phase under quiescent conditions and the gel time. Exfoliated clay layers inside the thermoplastic-rich phase result in both a larger droplet size at the start of the curing process and also hinder the mobility of the long chain molecules, reducing the rate of diffusion of unsaturated polyester chains out of the TP-rich domains. Consequently, the concentration of unsaturated polyester inside the thermoplastic-rich phase is higher than it would be at equilibrium.

4.3.4.Properties

Glass transition temperature

The glass transition temperatures were determined from DMA via the maximum in the loss modulus as a function of temperature. The glass transition temperature (T_g) is primarily dependent on the crosslinking density in both single phase and hybrid network polymers. The glass transition temperatures of the various systems studied here are shown in Figure 4.10 as a function of the curing agent ratio, MMA/St_{CA}. The competition between unsaturated polyester crosslinking and MMA/St copolymerization during curing means that there is an optimum curing agent molar ratio that gives the maximum T_g for all systems. The optimum curing agent ratio depends on the nature and composition of the system as shown in Figure 4.10. In the case of simple polyesters, we observe the highest T_g at MMA/St_{CA} = 0.4. Clay causes a reduction in T_g of the simple nanocomposite, SN/0.0, as compared to that of the simple polyester, SP/0.0, implying a drop in the crosslinking density. The thermal initiator, BPO was incorporated in order to offset the reduction in crosslinking by decreasing the residual styrene [13] and enhancing

the rigidity of the system. The addition of 0.2 mol% BPO to the simple nanocomposite systems increased T_g, even above those of the simple polyesters. As before, we find a non-monotonic effect but with the maximum at MMA/St_{CA} = 0.2. Increasing the BPO level to 0.4 mol% resulted in a lower T_g at all curing agent ratios (data not shown). In the case of hybrid systems, the T_g depends primarily on the crosslinking density in the networked phase but in these systems the nature of the thermoplastic phase influences the diffusion of MMA and St between phases thereby affecting the degree of crosslinking. This results in a lower T_g as compared to the simple nanocomposites. All nanocomposite samples presented in the following section incorporate 0.2 mol% BPO.

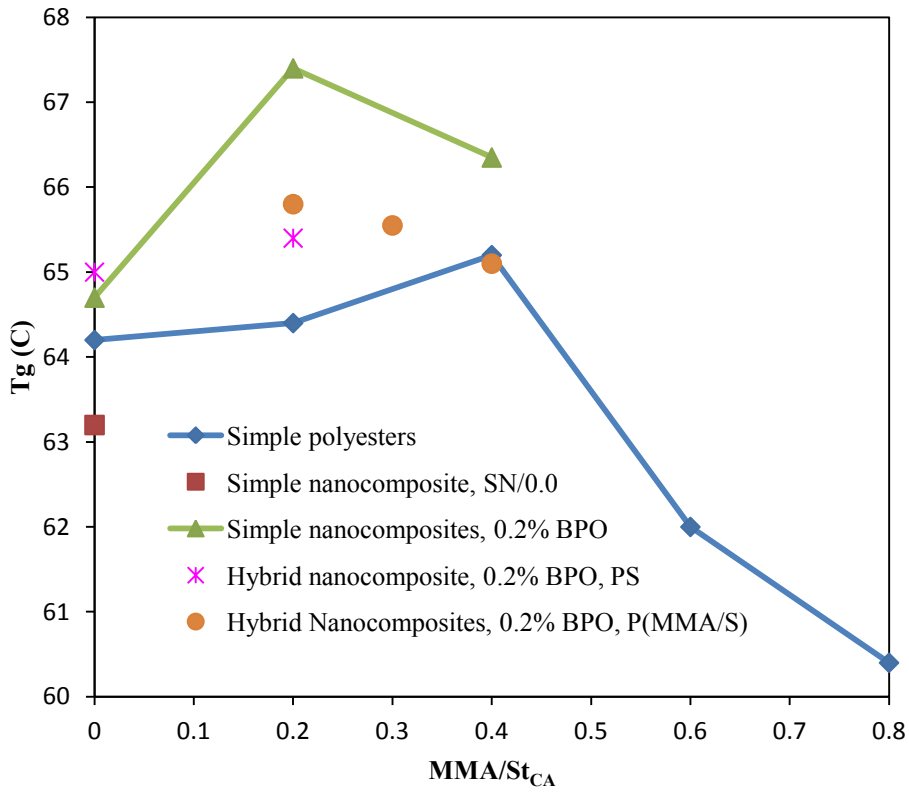

Fig. 4. 10. Glass Transition temperatures of polyesters and their nanocomposites (2 phr clay) as a function of curing agent ratio.

Tensile properties

The tensile properties of our samples are summarized in Table 4.3. In hybrid systems, the presence of the dispersed organic phase slightly decreases the tensile strength as compared to the simple systems due to a somewhat imperfect adhesion at the interface of

the unsaturated polyester-rich and thermoplastic-rich phases. Using the Takayanagi model, Huang et al [17]. demonstrated that the tensile strength of UPR systems containing a TP phase is predominately determined by that of the major continuous cross-linked polyester phase. This means that, amongst the group of hybrid systems studied here, tensile strength is mostly dependant on crosslinking density, which our T_g data indicate is highest when $MMA/St_{CA} \sim 0.2$. Our tensile test results corroborate the DSC curing studies and the T_g measurements in this regard.

According to the Flory-Huggins parameters (Table 4.1), MMA in the thermoplastic copolymer of the hybrid systems decreases the compatibility between St and the TP phase. Therefore, under curing conditions in hybrid systems containing P(MMA/S) we expect a reduced styrene content in the thermoplastic phase, as compared to hybrids containing PS, thus leading to increased styrene concentration in the continuous polyester phase. This allows for an increase in the degree of crosslinking, the T_g and the tensile strength (compare samples HN/0.2/PS with TS = 45.4 MPa and HN/0.2/P(MMA/S) with TS = 51.0 MPa). We also note that MMA in the TP copolymer slightly improves the compatibility of the TP phase with the polyester, which may result in an improved adhesion at the interface and therefore contribute to the increase in tensile strength.

Due to its high stiffness, clay slightly increases the modulus of the simple nanocomposite, relative to the simple polyester. The hybrid nanocomposites all had the same modulus as the neat resin SP/0.0, within experimental uncertainty. According to Huang et al.[17] the modulus is primarily determined by the degree of network compactness, which depends on the length of crosslinking bridges. Since our hybrid systems have the same modulus irrespective of MMA/St_{CA} we conclude that MMA content does not significantly affect the length of crosslinking bridges in our hybrid systems. This is an important result because according to the reactivity ratios (Table 4.2) the copolymerization of MMA and St is more likely than any other reaction involving MMA and is in competition with the copolymerization of unsaturated polyester and St. We recall that crosslinks are formed by copolymerization with unsaturated polyester and either St or MMA whereas linear chain segments are formed by the copolymerization of MMA and St. We note that the modulus of the hybrid nanocomposite is less than that of

the simple nanocomposite because the clay layers are located in the dispersed thermoplastic-rich particles in the hybrid systems and therefore do not contribute to the stiffness of the thermosetting matrix.

Table 4.3. Tensile properties and fracture toughness (K_{Ic})

Sample	[a] Average TP particle radius (μm)	20A (phr)	Tensile strength (MPa)	Tensile modulus (MPa)	K_{Ic} (MPa.m$^{1/2}$)
SP/0.0	NA	0	61.7 (2.7)[c]	3264 (66)	1.23 (0.01)
SN/0.0	NA	2	59.5 (1.3)	3409 (60)	1.36 (0.08)
HP/0.2/P(MMA/S)	4.5 (1.2) [b]	0	54.8 (3.2)	3442 (70)	1.48 (0.05)
HN/0.0/PS	7.0 (2.1)	2	45.7 (2.4)	3244 (66)	1.69 (0.03)
HN/0.2/PS	6.7 (2.2)	2	45.4 (2.5)	3227 (53)	1.78 (0.06)
HN/0.2/P(MMA/S)	9.6 (2.7)	2	51.0 (0.9)	3138 (53)	1.87 (0.07)
HN/0.3/P(MMA/S)	7.1 (2.2)	2	48.9 (1.2)	3231 (50)	1.69 (0.05)
HN/0.4/P(MMA/S)	6.9 (2.0)	2	47.4 (1.5)	3343 (73)	1.63 (0.02)

[a] The thermoplastic mass in the system is 7wt% in all hybrid systems.
[b] The average particle radii (standard deviations) were determined by image analysis of optical micrographs in Figure 8 and similar images for systems not included in that figure.
[c] The values in parentheses are standard deviations of mechanical properties from 7 samples.

Fracture toughness

The fracture toughness, K_{Ic}, which turns out to be the most interesting property of our hybrid systems, is also presented in Table 4.3. Note that the number in the sample names refers to the molar ratio of curing agents MMA/St_{CA} and the polymer abbreviation refers to the type of thermoplastic in the system. The addition of clay caused a slight improvement in toughness of the simple system (K_{Ic} of SN/0.0 is 11% higher than that of SP/0.0) as a result of the tortuous path for crack propagation induced by the silicate layers [128]. More significant is the increase in fracture toughness caused by the thermoplastic additive; K_{Ic} of HP/0.2/P(MMA/S), is 20% higher than that of SP/0.0. There is a synergistic effect when both clay and a thermoplastic additive are present, leading to an increase of 52% in the toughness of HN/0.2/P(MMA/S) as compared to that of SP/0.0.

We can understand the mechanism behind the increased toughness of our systems by considering other toughened UPR based materials. For example, Bucknall et al.[60] reported an increase in fracture toughness of UPR with the addition of poly (vinyl acetate) which they attributed to PVAc behaving like a conventional toughening rubber

although it is in its glassy state. In rubber-modified resins, the triaxial stress field at the crack tip causes cavitations within the rubber particles, reducing the yield stress and provoking extensive shear yielding. More recently [143], epoxy was toughened by the inclusion of another glassy, thermoplastic polymer, poly(ether sulfone). The authors suggested that the toughening mechanism was plastic deformation of the thermoplastic-rich phase, resulting in an increase in the overall toughness of the whole system.

We believe that a glassy particulate thermoplastic-rich phase can act as a rigid filler where the increase in toughness is governed by several mechanisms including crack pinning, debonding of the particulate phase from the continuous phase, and crack blunting[149]. In crack pinning, the energy required for crack growth increases with the ratio of the particle size to the particle spacing (r/c) up to an optimum value [149]; therefore a larger particle size with a smaller spacing in our hybrid system results in a higher value of K_{Ic}. In the hybrid systems, the presence of the particulate second phase of large size and fine spacing improves the fracture toughness. Importantly, regardless of the thermoplastic composition, the clay and the thermoplastic phase have a synergistic effect on the toughness. This can be explained by considering the morphology of these hybrid systems and micrographs of the details of the fracture surface.

SEM images of the fracture surface of a hybrid polyester (Figure 4.11a, b, and c) show that the thermoplastic-rich particles have been fractured with the matrix. This means that neither debonding nor crack pinning are controlling the fracture in this case. In these images, a few faint fracture tails can be observed behind the thermoplastic-rich particles. These tails are formed because the crack passes more slowly through the thermoplastic area compared to the thermoset matrix [143] causing small variations in the height of the crack front. In the regions far past the particles, the crack fronts meet up again at different heights leading to the formation of these tails. In this case, the plastic deformation of the TP-rich particles likely results in the small toughening effect.

In contrast, the SEM images of the fracture surface of a hybrid nanocomposite (Figure 4.12 a, b, and c) suggest a different mechanism because the particles are mostly intact. Therefore, plastic deformation of thermoplastic-rich phase is not the mechanism

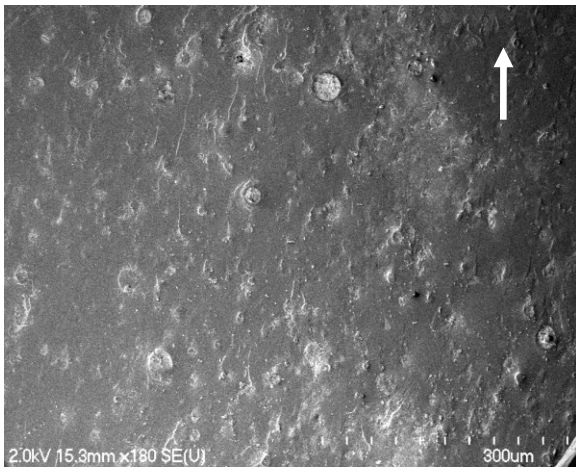

(a)

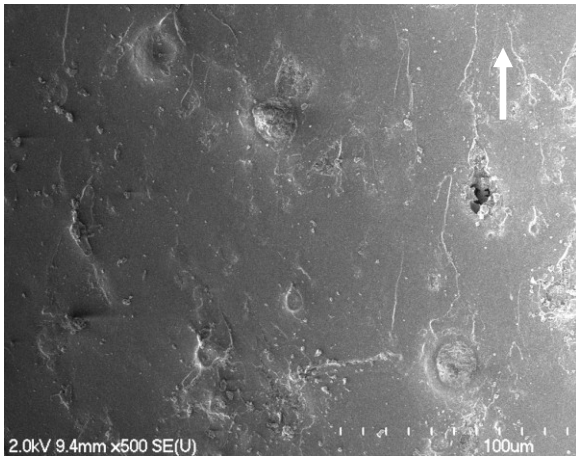

(b)

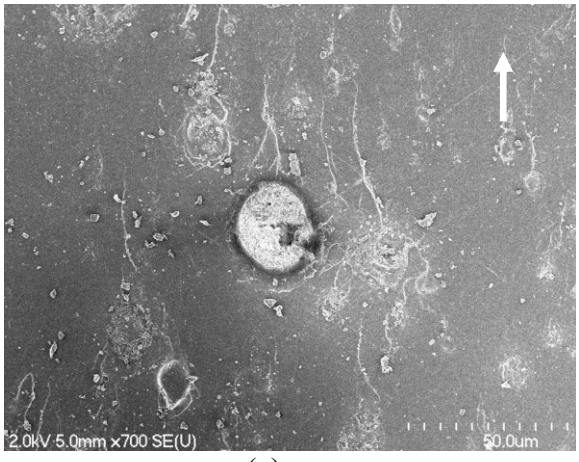

(c)

Fig. 4.11. SEM images of fracture surface of HP_M/S_0.2_P(MMA/St). The arrows indicate direction of fracture.

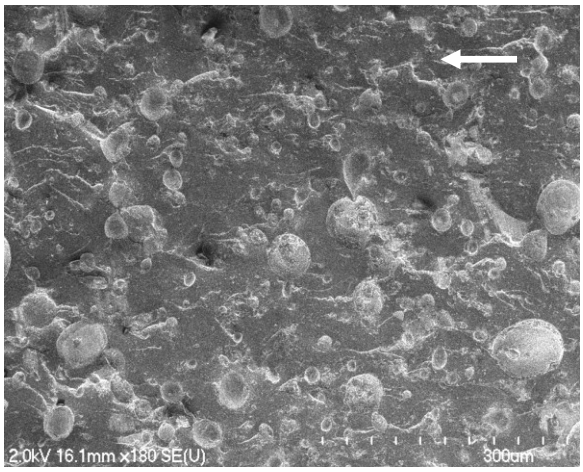

(a)

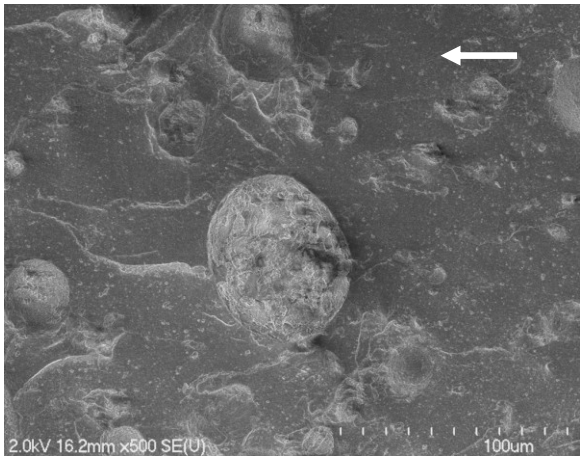

(b)

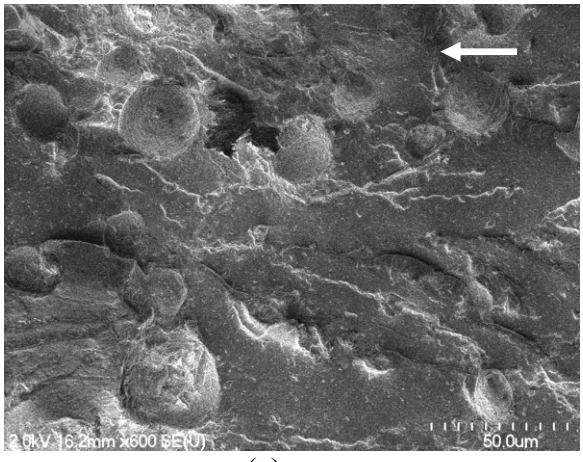

(c)

Fig. 4.12. SEM images of fracture surface of HN_M/S_0.2_P(MMA/St). The arrows indicate direction of fracture.

controlling fracture toughness in these systems. Many thick fracture tails are visible behind the particles in the SEM micrographs consistent with pinning of the crack front [54]. This is also reflected in the optical micrograph in Fig. 4.9c where the roughness of the fracture surface of HN/0.2/P(MMA/S), is clearly visible. This can be compared to the relatively smooth fracture surface of the hybrid polyester, HP/0.2/P(MMA/S), Fig 4.9b.

The relationship between fracture toughness and TP-rich particle radius for the hybrid systems containing P(MMA/S) is shown in Figure 4.13.

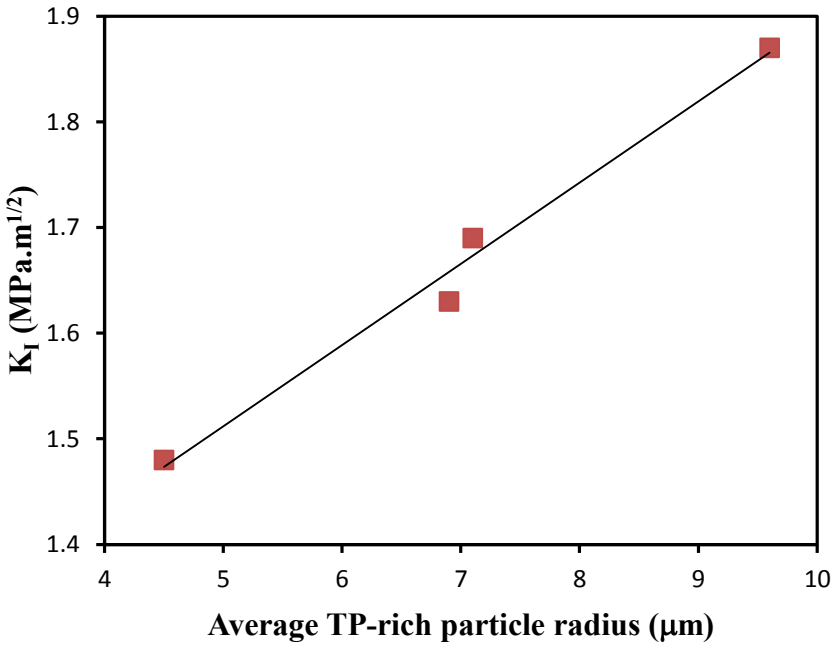

Fig. 4.13. Relationship between fracture toughness and size of the thermoplastic-rich domains for hybrid systems containing P(MMA/S).

Although the major mechanism controlling the fracture in hybrid nanocomposite systems is crack pinning, debonding of the particles from the matrix (breakdown of the particle/matrix interface) is also likely. This leads to a reduction in the effectiveness of crack pinning, but results in crack tip blunting and unstable propagation which can increase the fracture toughness [149]. Therefore, in the hybrid nanocomposite systems, the mechanism controlling fracture is complex with both blunting and pinning occurring simultaneously.

These results are important because unsaturated polyesters could find additional commercial applicability if their toughness were improved via a method that does not simultaneously sacrifice other properties such as stiffness and thermal stability. For instance, a common technique to improve toughness is the addition of rubber [43,45] , but in most cases these tougheners reduce the modulus by up to 35% [42,43,45], the compressive yield strength by up to 45% [42], and the glass transition temperature (T_g) [150]. In contrast, our technique significantly improves fracture toughness and not only preserves stiffness but also increases the glass transition temperature of the polyester. In addition, due to the high volume shrinkage of UPRs, a thermoplastic additive is almost always added to commercial formulations to control shrinkage. Interestingly, the technique described here produces the required thermoplastic additive via a simple procedure as a consequence of forming the hybrid system. Also, our hybrid nanocomposites have the potential to exhibit improvements in other properties such as flame resistance, thermal stability, and water absorption resistance with the presence of well-dispersed silicate layers and thermoplastic particles.

4.5.Conclusions

A new class of unsaturated polyester-based thermoplastic/thermoset hybrids and their layered silicate nanocomposites were developed. Relationships between precursor material composition, solid-state structure and physical properties were explored, demonstrating the potential of these new materials. The hybrid nanocomposites exhibit complex micro- and nanostructures that are controlled by the composition of the system prior to curing. The addition of methyl methacrylate (MMA) as a secondary curing agent for the unsaturated polyester allows for increased styrene conversion in the presence of clay. This occurs because the polyester chains are essentially excluded from the clay galleries and without MMA the styrene in the galleries remains unreacted after curing is complete. Exfoliation of the clay can be achieved by the copolymerization of MMA and styrene in the absence of unsaturated polyester, producing a suspension of finely dispersed clays layers in a solution of copolymer chains and the remaining comonomers. The hybrid is formed by combining the suspension with unsaturated polyester and curing to produce the final phase separated microstructure.

A synergistic effect of clay and thermoplastic on fracture toughness was observed and attributed to the size of the spherical minor phase domains which are rich in thermoplastic and contain the delaminated silicate layers. The combination of thermoplastic and delaminated clay produces minor phase particles that appear to act as rigid fillers and the major mechanism of energy dissipation during fracture is crack pinning. This results in significantly increased fracture toughness; we observed an increase of 52% while maintaining the stiffness and slightly increasing the glass transition temperature. It is possible that with more refinement of the composition and curing conditions, even higher values of fracture toughness can be achieved.

4.6. Author's approach

In this chapter, the most effective thermoplastic causing a greater improvement in fracture toughness was chosen. The results indicated that the size of thermoplastic-rich domains has a significant influence on fracture toughness. However, particle distribution is another microstructure characteristic affecting fracture toughness. Thus, more morphological studies of the ternary hybrid systems are required.

In addition to microstructure, other factors including the characteristics of each phase such as crosslink density of the matrix as well as the toughness and stiffness of the dispersed particles can have a key role in fracture toughness and mechanisms controlling fracture toughness. Therefore, more experiments must be conducted to explore the effect of these factors and prioritize their importance in influencing fracture toughness. For this purpose, a suitable range of synthesis process variables including clay, MMA, and the thermoplastic content must be chosen to vary these factors and evaluate their effect.

In this chapter, based on preliminary evidences, crack pinning as a likely mechanism controlling fracture toughness was proposed where it causes an improvement in fracture toughness by perturbing the crack front during propagation. It is worth noting that normally, a combination of different mechanisms control fracture toughness. For instance, other perturbations such as crack deflection may also occurs which can affect the efficiency of crack pinning. Therefore, more investigation must be done to investigate

the effect of other likely mechanisms on fracture toughness. In addition, the contribution of all mechanisms to fracture toughness of the system must be compared.

Chapter 5

Morphological characterization of clay/thermoplastic/unsaturated polyester hybrid nanocomposites by atomic force microscopy

Abstract

Development of nanocomposite materials has created a growing need for micro- and nanostructure studies. Atomic force microscopy (AFM) is a powerful tool for morphology studies due to its versatile capabilities. Tapping mode AFM can yield information about the topography and local mechanical properties of materials on the nanoscale. In this work, the capability of AFM for the morphological characterization of thermoplastic/clay/unsaturated polyester ternary systems was assessed. AFM sample preparation was performed by ultramicrotome to precisely preserve the nanostructure of the specimen. Interpretation of tapping mode AFM images confirmed information obtained from optical microscopy and transmission electron microscopy (TEM) and allowed a qualitative assessment of the local mechanical properties of the different phases and components.

5.1 Introduction

Tapping mode atomic force microscopy (TM-AFM) has become an important tool that allows an assessment of the surface topography and local properties of materials in a single scan, without causing extensive damage to the sample surface [151]. AFM can work on different materials in various environmental conditions, including vacuum, gaseous, and liquid environments [152]. In addition, it has the capability to characterize the mechanical properties of materials on the nanometer scale. Local mechanical properties of materials can be measured by monitoring the phase shift in the phase imaging mode [153,154]. Phase image analysis based on phase shift magnitude provides a way to observe spatial variations in the composition, friction, adhesion, and viscoelasticity of the surface.

Since the morphology of materials, especially multiphase systems, plays a determining role in final properties such as shrinkage, tensile properties, and toughness, different

techniques have been developed for the study of morphology, including electron microscopy (scanning electron microscopy or SEM, and transmission electron microscopy or TEM) and atomic force microscopy (AFM). AFM is a good alternative to electron microscopy, since it has lower limitations with regard to contrast and resolution [155]. In addition, AFM samples do not need a conductive coating, like SEM samples do, or staining, as for TEM samples [156]. However, the surface quality of an AFM sample is very important, since AFM follows the topography of the specimen surface. This means the sample preparation technique must be carefully designed as to avoid any extensive damage to the sample surface and preserve the original structure.

A convenient preparation technique for AFM samples is to polish the cross section surface of the specimen [157], but this is not accurate. In contrast, microtomy is more controllable and can be used for AFM sample preparation of multiphase materials, such as polymer blends and polymer nanocomposites. The morphology of a complex ternary polymer blend of three thermoplastics [158] was studied via AFM with a specimen prepared by cryomicrotome. AFM was able to characterize all possible morphologies of the ternary polymer blend: a) matrix/core-shell dispersed phase, b) tri-continuous, c) matrix/two separate dispersed phases, and d) bi-continuous/dispersed phase morphologies. The capability of AFM for the morphological studies of other polymer blends such as thermoplastic/thermoset [143,159] and interpenetrated systems of two thermosets [160] has also been demonstrated.

The development of nanocomposite materials has caused a growing need for nanostructure studies. Since AFM has the ability to work in nanoscale, its efficiency has been evaluated in various studies, especially for the case of layered silicate nanocomposites [161-167]. In all cases, the quality of the cross section surface was the key. A few studies included high quality AFM images of the structure of silicate layered nanocomposites whose matrix was a rubber [155,163,164]. General speaking, a greater difference in elastic and/or viscoelastic properties of the matrix and the dispersed phase leads to a higher phase contrast. This means that similar mechanical properties for two phases make it difficult to distinguish between them in the AFM image.

In this work, we used AFM for a more accurate micro- and nanostructure study of our complex ternary nanocomposite specimen on ultramicrotome prepared samples. The material is a thermoplastic/clay/unsaturated polyester hybrid nanocomposite that we introduced previously as a stiff unsaturated polyester with improved fracture toughness [168]. Here, we presented a qualitative analysis of local mechanical properties of the different components in the system based on phase contrast.

5.2 Experimental

5.2.1 Materials

The unsaturated polyester resin was provided from Ashland Chemical (H596-CWA-12), containing 45wt% styrene and 0.1wt% cobalt octoate promoter. Methyl methacrylate (MMA) and styrene (St) were used as both copolymerization reactants and crosslinking agents for curing. Cloisite 20A (Southern Clay Products Inc.) was used as the nanoclay. Benzoyl peroxide (BPO) was used as a thermal initiator, and methyl ethyl ketone peroxide (MEKP) as the room temperature initiator for curing.

In this work, we consider two different classes of materials: (i) hybrid polyester (HP), containing unsaturated polyester resin and 7wt% of the thermoplastic additive (the copolymer of methyl methacrylate and styrene, P(MMA/S)), with a molar ratio between curing agents (MMA/St_{CA}) around 0.2; and (ii) hybrid nanocomposite (HN), containing 2-phr Cloisite 20A in addition to the components of Class (i) with the same molar ratio of curing agents.

5.2.2 Hybrid polyester and nanocomposite preparation

The mixture of clay and vinylene monomers (MMA and styrene) was prepared and then in situ copolymerization of styrene and MMA was carried out to produce a MMA/styrene copolymer as the thermoplastic component of the hybrid system, P(MMA/S). After mixing the resin with the copolymerization product, the prepared mixture was poured into the mold and cured at room temperature. We have previously described these procedures in detail [168].

5.2.3. Characterization methods

The nanostructures of nanocomposite samples were examined with transmission electron microscopy (TEM) using a JEOL JEM-2100F microscope, operating at a 200kV accelerating voltage. The sample was cut into thin sections (50-80 nm thickness) using an ultramicrotome (LEICA EM FC7) with a diamond knife.

For AFM, samples were sectioned at room temperature using the ultramicrotome, equipped with glass and diamond knives. Initially, a glass knife was used to obtain a smooth surface parallel to the knife edge. The microtome was operated at a cutting speed of 1 mm/s and a feed step of 500 nm. This was followed by microtoming the sample with a diamond knife (Cryo 35° representing the angle of knife). The cutting speed and feed step were 1 mm/s and 100 nm, respectively. Experiments were carried out with a MultiMode SPM, of the Veeco Metrology Group, operating in tapping mode at room temperature under atmospheric conditions. Topographic (height) and phase images were recorded simultaneously. Commercial silicon cantilever probes (App Nano, ACT Series) were used. Manufacturer nominal values for the length, spring constant, and resonance frequency of the cantilever are 125 μm, 37 N/m, and 300 kHz, respectively.

5.3 Results and Discussion

5.3.1 Microstructure characterization

Although the scanning area via AFM is small, tapping mode AFM images clearly represent the matrix-dispersed structure, where thermoplastic-rich particles are dispersed throughout the thermoset-rich continuous phase. The geometric shape of the dispersed phase is mostly spherical, as shown in Figure 5.1. Figure 5.1a shows the microstructure of the HP sample, which is a binary system without clay, and Figure 5.1b illustrates the morphology of the HN sample which is a ternary system containing 2-phr clay. Height AFM images show the topological map of the cross section surface, and the phase images represent a shift of the cantilever phase from its free oscillation while the tip is in contact with the surface. This means that the latter represents the heterogeneity of the local mechanical properties of the materials, allowing the AFM to distinguish between the thermoplastic-rich phase and the continuous thermoset-rich phase. In contrast, TEM

cannot differentiate between these phases, since staining is required in order to observe each phase. In addition, since the presence of stiff silicate layers makes the local properties of the thermoplastic-rich domains heterogeneous, AFM can differentiate between thermoplastic-rich particles containing silicate layers (Fig. 5.1b) and those without clay (Fig. 5.1a).

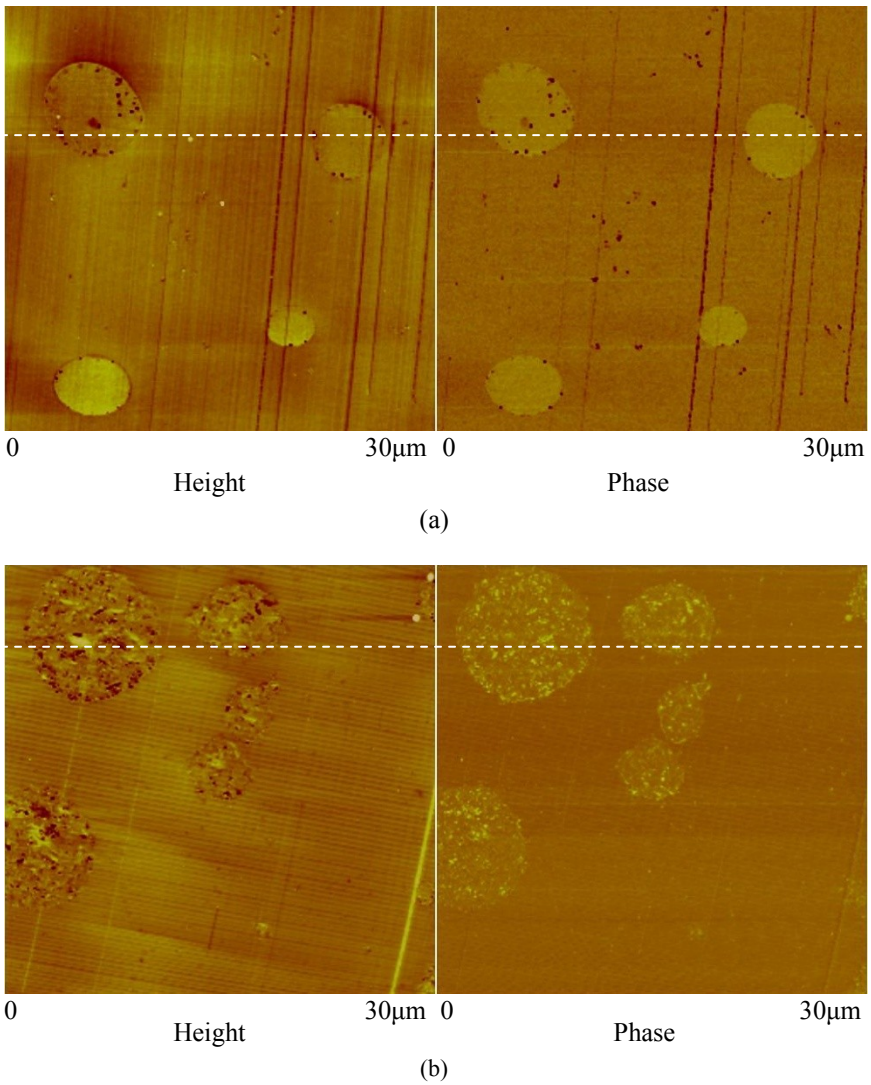

Fig. 5.1. AFM images of a) HP binary system (set point ratio: 0.88) and b) HN ternary system containing 2-phr clay (set point ratio: 0.95). Both samples contain 7wt% thermoplastic, P(MMA/S).

The other capability of AFM is to provide 3D images (height and phase) of the cross section of the samples, giving greater detail. The phase image of the HP sample (Figures 5.2a) shows greater phase shifts for the thermoplastics compared to the thermoset, where section analysis is required for more exploration. In the phase image of the HN sample

(Figure 5.2b), the presence of clay silicate layers in the thermoplastic-rich domains causes heterogeneity in the phase shift, where in some spots the phase shift of the cantilever is significantly increased, requiring a closer look.

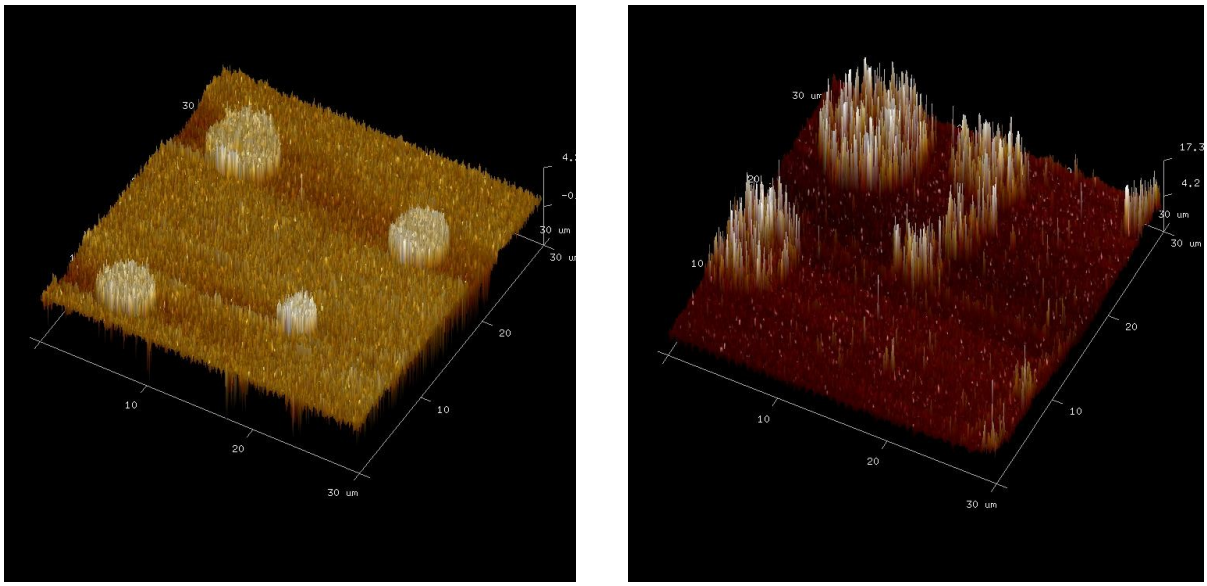

(a) (b)

Fig. 5.2. 3D phase images of: a) HP binary system, b) HN ternary system. Both samples contain 7wt% thermoplastic, P(MMA/S).

5.3.2 Nanostructure study

Figure 5.3 shows tapping mode AFM images of a thermoplastic-rich domain in a sample without clay. Interestingly, at higher magnification, the phase image apparently shows globule-type structures—small compact particles—inside the thermoplastic-rich domain. This sort of nanostructure has been observed by SEM in the literature [65].

In our previous work [168], we claimed a fine degree of dispersion and delamination of clay silicate layers in the hybrid nanocomposite sample according to X-ray diffraction patterns and TEM results. Transmission electron microscopy (Figure 5.4) shows a fine dispersion and distribution of clay within the hybrid nanocomposite where a high degree of exfoliation is achieved. TEM micrographs indicate that the majority of the clay layers are located inside the thermoplastic-rich phase, indicating that clay silicate layers have greater interaction with the thermoplastic compared to unsaturated polyester. In addition,

the TEM images illustrated that clay layers are preferably arranged parallel to the interface between the thermoplastic and thermoset phases [168].

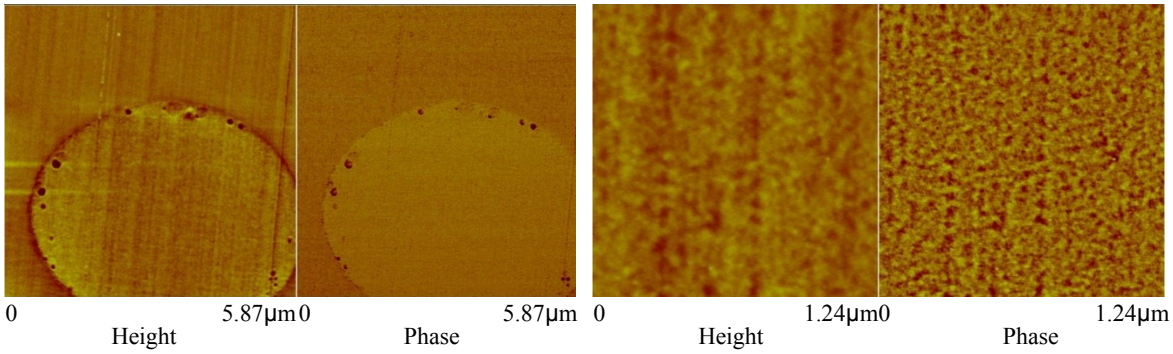

Fig. 5.3. Tapping mode AFM images of the HP sample: a) a thermoplastic domain without clay (set point ratio: 0.88), b) higher magnification of an internal part of the thermoplastic-rich domain (set point ratio: 0.68).

Figure 5.5 shows tapping mode AFM images (height and phase images) of thermoplastic-rich domains. Both TEM (Figure 5.4) and AFM (Figure 5.5) images show small spherical domains (~250 nm diameter) within the thermoplastic-rich particles, which are surrounded by clay layers. These small subdomains are likely unsaturated polyester microgels, which are surrounded by clay silicate layers [168]. The TEM images can reveal these microgels only because of the presence of silicate layers in the interface between the microgels and thermoplastic; otherwise, this instrument does not have the capability to distinguish between the thermoplastic and thermoset components inside the thermoplastic-rich domains.

A comparison between Figure 5.3b and Figure 5.5 suggests that the presence of silicate layers changed the nanostructure inside the thermoplastic-rich domains. After mixing the thermoplastic component with thermoset resin, thermoplastic-rich droplets are formed, wherein phase separation occurs during curing process [168]. In the absence of clay, phase separation inside the thermoplastic-rich domains led to the formation of a globule-type structure lacking distinct continuous and dispersed phases. In contrast, in the hybrid nanocomposite sample, separate pure unsaturated polyester microgels were formed, which are dispersed within all of the thermoplastic particles. The clay silicate layers inside the thermoplastic-rich droplets hindered the diffusion of unsaturated polyester molecules out of the thermoplastic-rich droplets, resulting in an increase in the concentration of unsaturated polyester inside this phase. In addition, the particulate

structure within the thermoplastic-rich domains suggests that the presence of clay silicate layers in the droplets likely promoted a submicro-phase separation during curing process, leading to the formation of submicron-sized thermoset microgels dispersed throughout the thermoplastic continuous phase.

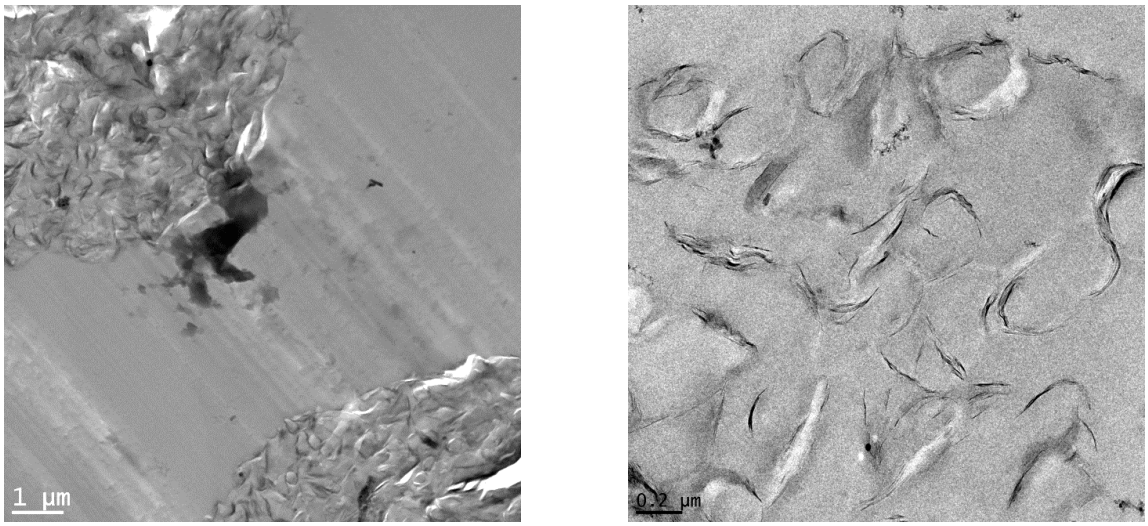

(a) (b)

Fig. 5.4. TEM images from the hybrid nanocomposite, Clay/P(MMA/S)/UPR, containing 7wt% thermoplastic and 2-phr clay. A) Sections of two thermoplastic-rich domains, b) nanostructure of a domain in higher magnification.

In tapping mode AFM, phase images distinguish various components based on their different mechanical properties. In general, three factors influence the phase image: the topography of the surface, material properties (stiffness and damping), and instrumental parameters (e.g., free oscillation amplitude, set point ratio) [154]. The observation of scratches in the phase image (Figure 5.1a) is an example of the effect of the topography on the phase image. The presence of the silicate layers in the thermoplastic-rich phase causes heterogeneity in local mechanical properties, also influencing the phase image. The amplitude set point ratio, which is the ratio of the engaged amplitude to the free vibration amplitude, influences the interaction force (repulsive/attraction) between the tip and the specimen, resulting in a change in the phase shift.

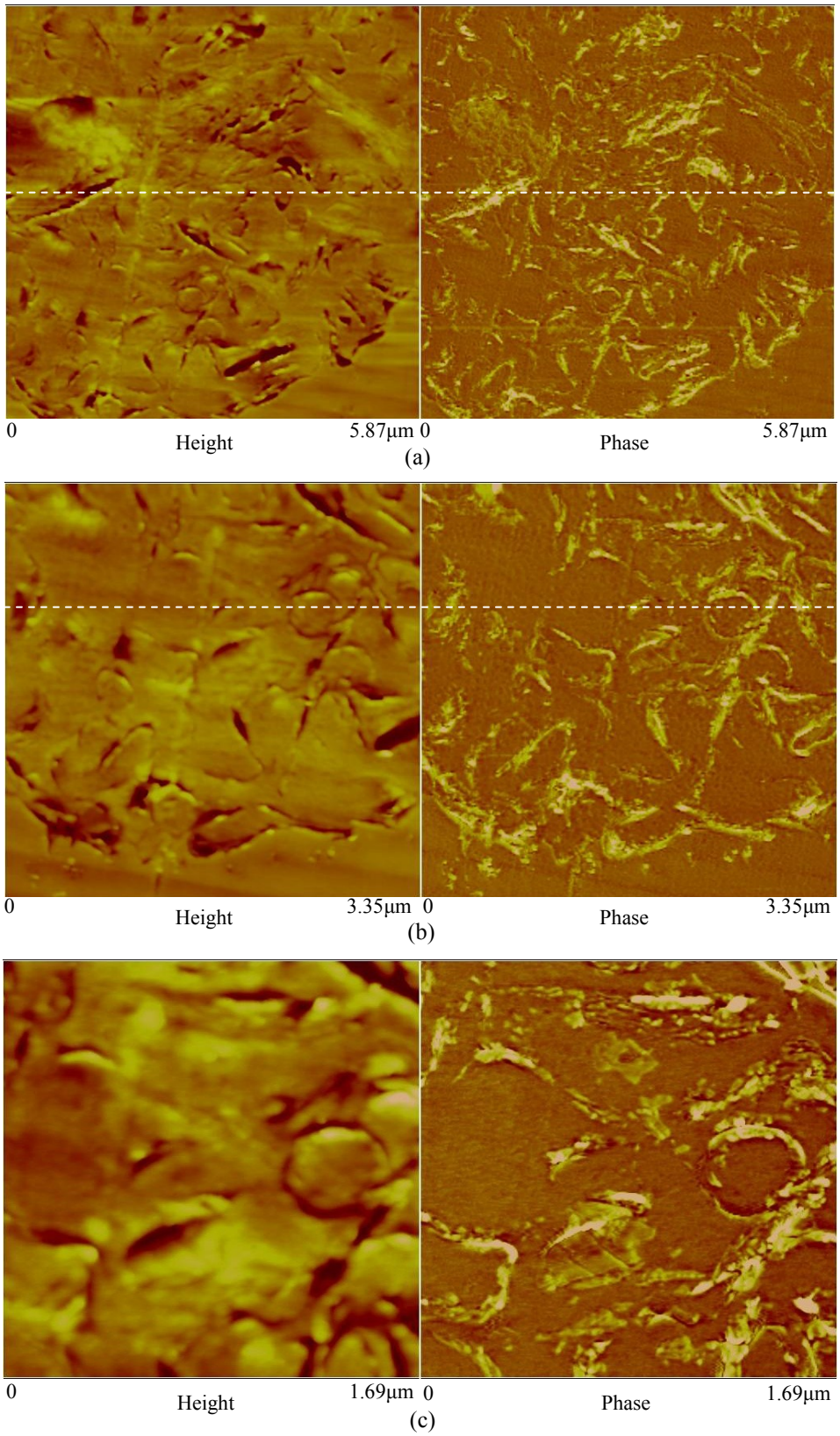

Fig. 5.5. Tapping mode AFM images of a thermoplastic-rich domain in the hybrid nanocomposite with different magnification (set point ratio: 0.71).

Achalla et al. [169] found a relationship between the force applied on the surface of the specimen and the phase image contrast. Two-phase contrast reversals in the phase image were observed by increasing the tapping force (reducing the set point ratio). As the set point decreases from 1 to 0, an increase in the phase shift occurs, followed by a decrease, and eventually it again increases [154]. The change of the average tip-sample interaction force from attractive to repulsive causes the first reversal. Trapping of the tip in the sample likely causes the second reversal. In all AFM images of our samples, according to the set point value applied during scanning, the clay as a stiff material is brighter than the two polymeric components and has a higher value of phase shift.

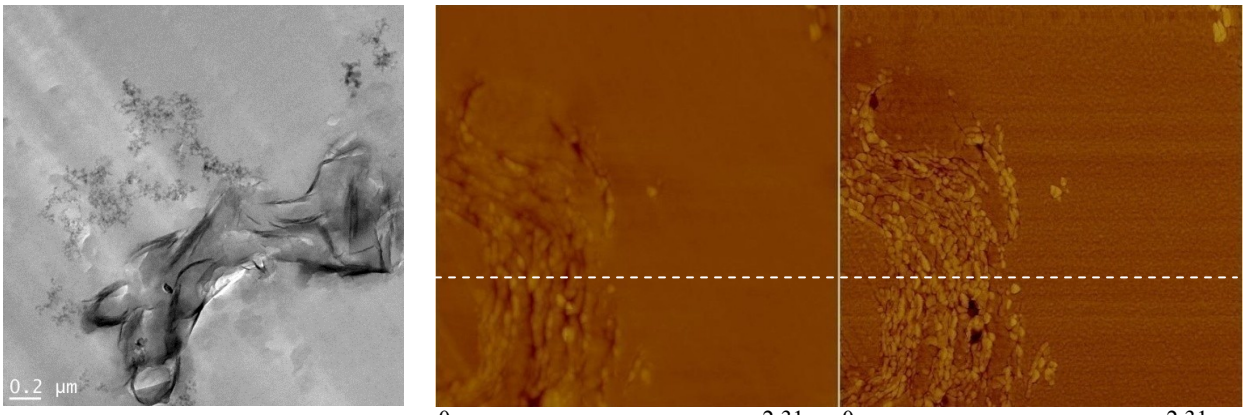

Fig. 5.6. a) TEM image, b) AFM images of intercalated silicate layers dispersed throughout the thermoset-rich phase (set point ratio: 1.2).

In our AFM image we can also observe partially intercalated silicate layers dispersed throughout the thermoset-rich phase. Typically, the phase shift can lead to clear phase images when the mechanical properties of constituents are significantly different, like in clay/rubber systems [163,164]. In our system, although the stiffness of the thermosetting matrix is high compared to rubber and very similar to that of the other components in our material, an ultramicrotome could make a clean cut while maintaining very sharp interfaces between the clay and the polymer matrix, leading to high quality phase images where intercalated silicate layers can be clearly observed (Figure 5.6). Section analysis of

phase images is required to get more information about the local mechanical properties from phase contrast.

5.3.3 Local mechanical properties

In tapping mode, the phase shift (i.e., the difference between the phase angle of the free oscillating and interacting cantilever) is used to monitor variations in the local properties, such as stiffness, hardness, and viscoelasticity [155]. Different mathematical models have been developed to find a correlation between local mechanical properties and phase shift [151,154,170]. In our hybrid systems, the glassy thermoplastic and unsaturated polyester mainly experienced elastic deformation associated with the tip-sample interaction force. Therefore, the variation in the phase shift can be related to the sample modulus as follows [170]:

$$\Delta\varphi = \epsilon \langle\alpha\rangle E^* \left(\frac{Q}{K}\right) \tag{5.1}$$

where ϵ is a number between 1.9 and 2.4 which is a coefficient in a relation between the surface stiffness and E^* as well as the radius of the contact area , α. Q and K are the quality factor, representing viscous damping, and the spring constant of the oscillating cantilever, respectively. During scanning, the spherical tip touches the sample surface, making a circular contact area with a radius of α. In tapping mode, the tip makes intermittent and momentary contact during each cycle of oscillation, where the contact area varies with time during each contact. Therefore, the time-averaged values of contact area and contact radius, $\langle\alpha\rangle$, are used. E^* is the effective modulus:

$$\frac{1}{E^*} = \frac{\left(1-\vartheta_1^2\right)}{E_1} + \frac{\left(1-\vartheta_2^2\right)}{E_2} \tag{5.2}$$

E_1 and E_2 are the Young's moduli and ϑ_1 and ϑ_2 are the Poisson's ratios of the tip and sample respectively. Eq. 5.1 shows that $\langle\alpha\rangle$ and E^* have the opposite effect on the change of the phase shift in response to the applied force on the sample by the tip. In a softer material, the tip can make a larger contact area, hence a greater $\langle\alpha\rangle$, leading to an increase in the phase shift. In contrast, a stiffer material with a high Young's modulus

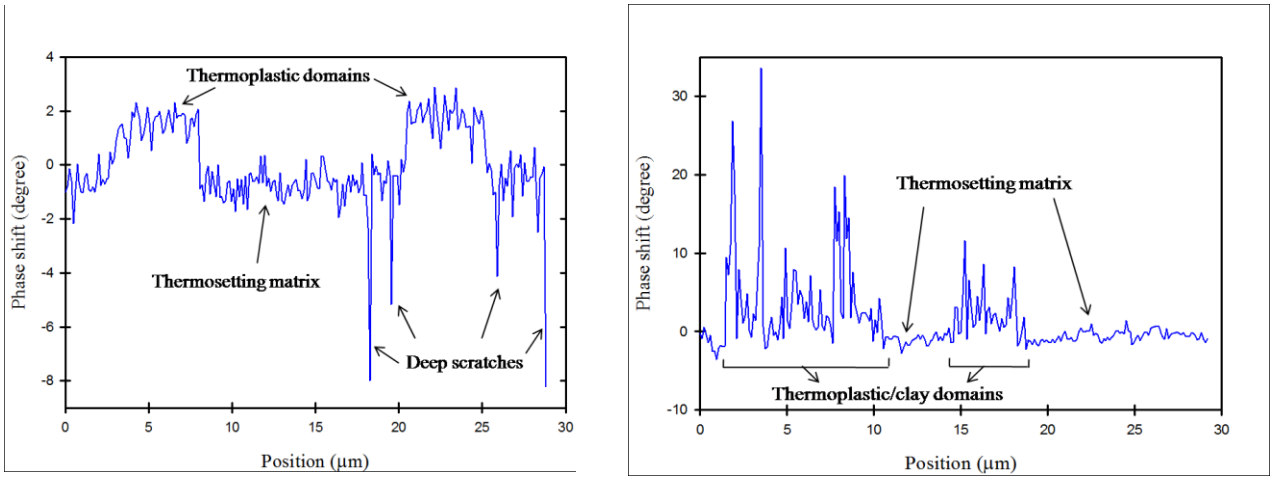

(a) (b)

Fig. 5.7. Section analysis of images in Figure 5.1a and b at the locations indicated in the figures. Phase shifts of different components are presented: a) HP sample, b) HN sample. (All samples contain 7wt% the thermoplastic).

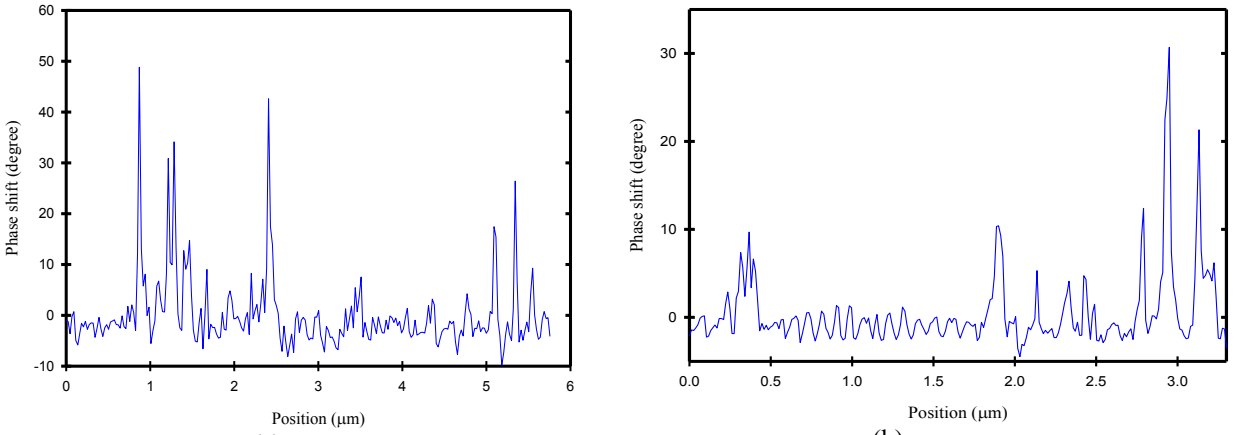

(a) (b)

Fig. 5.8. Section analysis of images in Figure 5.5a and b at the locations indicated in the figures. Phase shifts of the silicate layers are presented.

results in an increase in the phase shift. The effect of these parameters is enhanced by increasing the set point ratio. In multiphase systems, one of these parameters is dominant in controlling the phase shift, depending on the magnitude of the difference between mechanical properties of the phases.

In our systems, since both polymeric components, thermoplastic (P(MMA/S)) and thermoset (UPR), are glassy (hard) with comparable elastic properties, their parameters $\langle\alpha\rangle$ and E^* must also be similar. Therefore, the phase contrast between the thermoplastic-rich particles and the thermoset matrix is expected to be small. Figures 5.7-9 show section analyses of different samples (hybrid polyester, HP, and hybrid nanocomposite, HN). In these figures, phase shift versus position for the lines shown in the related 2D phase images are plotted. Figure 5.8a confirms that the phase contrast between the thermoplastic-rich domains and the matrix is low. However, the phase shift in the thermoplastic-rich phase is slightly greater than that of the thermoset region, suggesting that the glassy thermoplastic is a bit stiffer than the thermoset. There are also some negative values of the phase shift, which are caused by deep scratches, likely because the overall force acting on the tip is attractive since the tip does not touch the sample in these regions.

In the hybrid nanocomposite (Figure 5.7b), the presence of clay silicate layers in the thermoplastic-rich particles causes peaks in phase shift. Section analysis of phase images captured at higher magnification (Figure 5.8) shows that these peaks are due to the clay silicate layers. The high modulus of the clay compared to the organic polymers increases the effect of effective modulus (E^*), leading to a significant increase in phase shift.

Figure 5.9 shows the section analysis of a phase image of intercalated silicate layers dispersed throughout the thermosetting matrix. There are some negative values representing deep channels in the interface, likely caused by debonding between the silicate layers and the matrix during microtomy. In contrast, the large negative phase shift were not observed in the section analysis of thermoplastic-rich particles (Figure 5.8) suggesting that deep channels in the interface of clay and thermoplastic do not exist. This means that the interfacial adhesive strength between clay and the thermoplastic is stronger than that of clay and the thermoset.

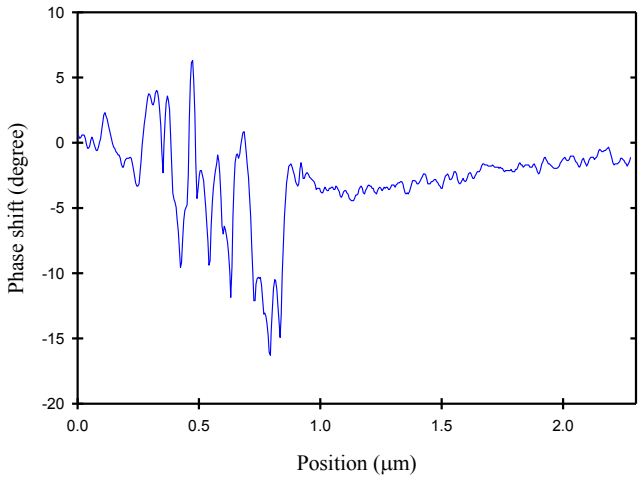

Fig. 5.9. Section analysis of images in Figure 5.6b at the locations indicated in the figure. Phase shifts of the silicate layers dispersed throughout the matrix are presented.

Interestingly, section analysis of phase images related to HP and HN samples (Figures 5.7.a and b respectively) does not show any deep channel in the interface between the thermoplastic-rich domains and the thermoset-rich matrix indicating a good interfacial adhesive strength between these phases. Suitable strong interfacial adhesive strength is favourable for toughening by increasing the efficiency of crack pinning mechanism [58]. (More investigation and discussion will be done in the following chapter.)

5.4 Conclusions

The sample preparation procedure has a very important effect on the quality of AFM images. The ultramicrotome is a powerful instrument for specimen preparation to maximize the capability of AFM, since microtomy preserves the original nanostructure of the sample. In the morphology study of the thermoplastic/clay/unsaturated polyester hybrid nanocomposite, AFM could distinguish between different polymeric phases (thermoplastic and thermoset), whereas TEM cannot. AFM allowed us to see the different nanostructures for the thermoplastic-rich domains with and without clay. This suggests that the presence of silicate layers changes the nanostructure of the thermoplastic-rich domains, likely by affecting sub-micro-phase separation. The silicate layers caused a change in nanostructure within the thermoplastic-domains from co-continuous to particulate structure indicating more complete phase separation inside the thermoplastic-

rich domains in the presence of the silicate layers. AFM had the capability to detect the silicate layers dispersed throughout different phases and regions including the thermoplastic-rich phase, continuous thermoset-rich phase, and the interface between thermoplastic and thermoset. In addition, local mechanical properties of different phases and components were qualitatively assessed based on phase contrast. AFM showed that the thermoplastic component is a little bit stiffer than the thermoset matrix, and the presence of silicate layers significantly increases the stiffness of the domains. Section analysis showed negative values of phase shifts in the interface between clay and thermoset indicating debonding between these components during microtomy whereas interfacial debonding between clay and thermoplastic inside the particles did not occur. This suggests that the interaction between clay and the thermoplastic is stronger than that of between clay and the thermoset. Also, section analysis of phase images indicated that there is fine interfacial adhesive strength between two phases which is essential for toughening based on crack pinning mechanism.

Chapter 6

Effect of morphology on fracture toughness of thermoplastic/unsaturated polyester hybrid nanocomposites

6.1.Introduction

Unsaturated polyester resins (UPRs) are thermosetting polymers with a high crosslink density, which leads to superior properties. A glassy polymer can be tough if it can experience bulk homogenous yielding. In polymer networks with high crosslink density, the only energy dissipating process that may occur is localized plastic deformation (micro-shear band formation) resulting in brittleness [31]. To improve fracture toughness, incorporation of a second phase in the system can increase the intensity of energy dissipation by distributing stress concentration in the whole system resulting in the occurrence of localized plastic deformation in a larger volume of the sample. Consequently, higher resistance against crack initiation is obtained. However, at a certain stress, a crack is formed and starts to grow. In this case, several mechanisms for energy absorption become active during crack propagation involving different energy dissipating processes such as localized plastic deformation of the matrix, matrix void formation, cavitation of soft inclusions (e.g., rubbers), particle/matrix debonding, and plastic deformation of the inclusion. In addition, the inclusion located in front of the crack tip may perturb the crack front during propagation. Perturbation of the crack front leads to crack deflection and/or crack pinning.

The most frequently applied additives for improving fracture toughness are mineral fillers or rubbery/thermoplastic particles, where each toughening agent has its own drawbacks. The rubbery dispersed phase can result in a significant improvement in fracture toughness but at the cost of elastic modulus [42,43,45] , compressive yield strength [42], and thermal stability [36,150]. Thermoplastics [36,143] and inorganic additives including particulate fillers [36,71] and nano-reinforcements [84-86] can also be used for this purpose without adversely affecting other properties, but they are not as effective as rubber additives. Therefore, a combination of different additives is often used not only to compensate for and modify the drawback of each additive, but also to take advantage of any synergistic effects. Therefore, ternary systems, which typically consist

of a polymeric additive (e.g., thermoplastic or rubber), inorganic nano-reinforcement such as layered silicates, and thermosetting resins, have attracted a lot of interest [60,108,171]. Recently, we introduced novel thermoplastic/thermosetting hybrid nanocomposites as ternary systems to improve the fracture toughness of unsaturated polyester [168]. The technique led to a substantial improvement in toughness without sacrificing other properties.

In the presence of a secondary phase, the morphology of the system strongly influences fracture toughness [60, 168]. In the case of polymeric additives, typically, the dispersed phase or particulate morphology results in a greater improvement in toughness compared to a homogeneous structure [34,39,60]. Bucknall et al. [60] investigated the effect of morphology on fracture toughness in a thermoplastic-modified unsaturated polyester resin. They claimed that the particulate structure resulted in a greater improvement in fracture toughness of the system compared to the co-continuous structure. The nanostructure of layered silicate nanocomposites also plays a key role in fracture toughness and its controlling mechanisms. An exfoliated arrangement of the silicate layers cannot significantly improve fracture toughness because the size of the platelets is too small to cause crack deflection during propagation. These dispersed single layers can make a tortuous path for crack propagation occurring locally around the clay platelets. In contrast, a micron-sized structure of intercalated tactoids of clay can intercept the crack front during propagation, leading to the occurrence of crack deflection, which further increases fracture surface areas [84,85]. A few studies have looked at the microstructure of ternary systems [108,171,172]. In the case of UPRs, the effect of clay and thermoplastics, used as low profile additives, on controlling volume shrinkage has been investigated [111,112]. To the author's knowledge, there is no study on the toughness of thermoplastic/clay/unsaturated polyester ternary systems and the effect of their microstructure on fracture toughness.

In our previous work [168], we found that the dispersed second phase acted as a rigid filler, where the major mechanism controlling fracture toughness may be crack pinning. The crack pinning mechanism involves two processes including crack trapping and crack face bridging. Crack trapping refers to the perturbing effect of the inclusion on the crack

front, where the front is forced to bow out between the obstacles. In addition, non-deformed elastic materials make a bridged zone ahead of the crack tip that restrains the crack opening displacement, a phenomenon called crack bridging. The crack pinning mechanism was firstly modeled by Lange [52], who only considered crack trapping, and then modified by Evans [53], who demonstrated that the increase in fracture energy required to bow the crack depends upon the particle size and spacing. Later, Lange and Radford [55] reported a maximum in the relationship between toughness and the volume fraction of inclusions, which is reflecting the particle size and interparticle spaces. However, Evans's model cannot predict the optimum volume fraction. Rose [56] suggested an alternative analysis that was in better agreement with experimental observations. He assumed that non-deformed elastic materials act as springs, applying pressure on the crack faces, where this pressure is a linear function of the crack opening displacement. His model agrees with experimental data when particle concentrations are modest. Later, Bower and Ortiz modified Rose's models to predict the maximum toughening likely generated by crack trapping [174].

In all models, the microstructure characteristics (particle size and interparticle distance) play a key role in the crack pinning mechanism. The main objective of this work is to evaluate the effect of the microstructure on fracture toughness in our hybrid nanocomposite ternary systems. For this purpose, firstly the effects of synthesis process variables (such as the amount of different components and the ratio of curing agents) on the characteristics of the different phases, including matrix crosslink density and its localized yielding, as well as impenetrability of second phase particles, were evaluated. Suitable variable amounts were found to achieve more improvement in fracture toughness. Finally, a correlation between fracture toughness and microstructure characteristics was explored.

6.2.Experimental

6.2.1. Materials

Cloisite 20A (Southern Clay Products Inc.) was used as the nanoclay. Methyl methacrylate and styrene (Sigma Aldrich) were distilled prior, using an IKA rotary

evaporator under vacuum at 30°C to remove the inhibitors. Benzoyl peroxide (Sigma Aldrich) was used as a thermal initiator for the thermoplastic synthesis, and the room temperature initiator employed for curing the whole system was methyl ethyl ketone peroxide (NOROX, MEKP-925H from NORAC Inc.). The unsaturated polyester resin (H596-CWA-12, Ashland Chemical) is a general purpose orthophthalic resin synthesized from maleic anhydride, phthalic anhydride, and propylene glycol. It contains 45wt% styrene and 0.1wt% cobalt octoate promoter.

In this work, we consider three different classes of materials: (1) simple polyesters (SP) that contain unsaturated polyester and one or two crosslinking agents; (2) simple nanocomposites (SN) that contain Cloisite 20A in addition to the components of class 1; (3) hybrid nanocomposites (HN) that contain the thermoplastic additive (copolymer of methyl methacrylate and styrene, P(MMA/S)) in addition to the components of class 2. In the sample names, the first number refers to the molar ratio of MMA/St_{CA} as curing agents and the second number refers to clay loading in phr units.

6.2.2. Hybrid polyester and nanocomposite preparation

The mixture of clay and vinylene monomers (MMA and styrene) was prepared, and then in situ copolymerization of styrene and MMA was carried out. After mixing the resin with the copolymerization product, the prepared mixture was poured into the mould and cured at room temperature. More information about the procedures is mentioned in our previous work [168].

6.2.3. Characterization methods

Calorimetry was performed with a differential scanning calorimeter TA Q10 on 10 mg of uncured sample in a hermetic aluminum pan. The isothermal reaction rate profile was measured at 25°C, followed by a scan from 25 to 300°C at a heating rate of 5°C/min to determine the total reaction heat. Dynamic mechanical measurements were made between 20 and 180°C at 1 Hz, using a TA Instruments DMA 983 dynamic mechanical analyzer.

Dumbbell-shaped specimens based on ASTM D638-82a (type V) were used to determine tensile properties on an Instron 3365 (5 kN) testing machine at a constant crosshead speed of 1 mm/min. Fracture mechanic tests were carried out by MTS 312.21

(100 kN) according to ASTM D5045-99 on sharply notched three-point bend specimens at a constant crosshead speed of 10 mm/min.

A Hitachi S-4700 FE-SEM 2-kV scanning electron microscope was used to observe the fracture surface. The microstructure study was done using an optical microscope (Variscope).

6.3. Results and discussion

In our hybrid nanocomposite systems, four material characteristics can influence fracture toughness: (I) matrix characteristics, (II) dispersed phase characteristics, (III) adhesion strength of the interface between phases, and (IV) microstructure characteristics of the system. In this work, we evaluated parameters controlling the microstructure. Their ranges were chosen in order to minimize their effects on other material characteristics affecting fracture toughness. We found an interesting correlation between fracture toughness, K_{Ic}, and a microstructure characteristic the ratio of the particle size, radius r, to the interparticle distance, c. This is the most important contribution of this work (Figure 6.1).

There are three original variables affecting these characteristics: (I) molar ratio of curing agents (MMA/St_{CA}), (II) clay loading, and (III) thermoplastic content. In addition, we used two more preparation methods for a proper evaluation of the effect of process variables on the microstructure and fracture toughness of the system. In the following, we discuss how the synthesis process parameters control the microstructure and affect the characteristics of different phases (the dispersed and continuous phase).

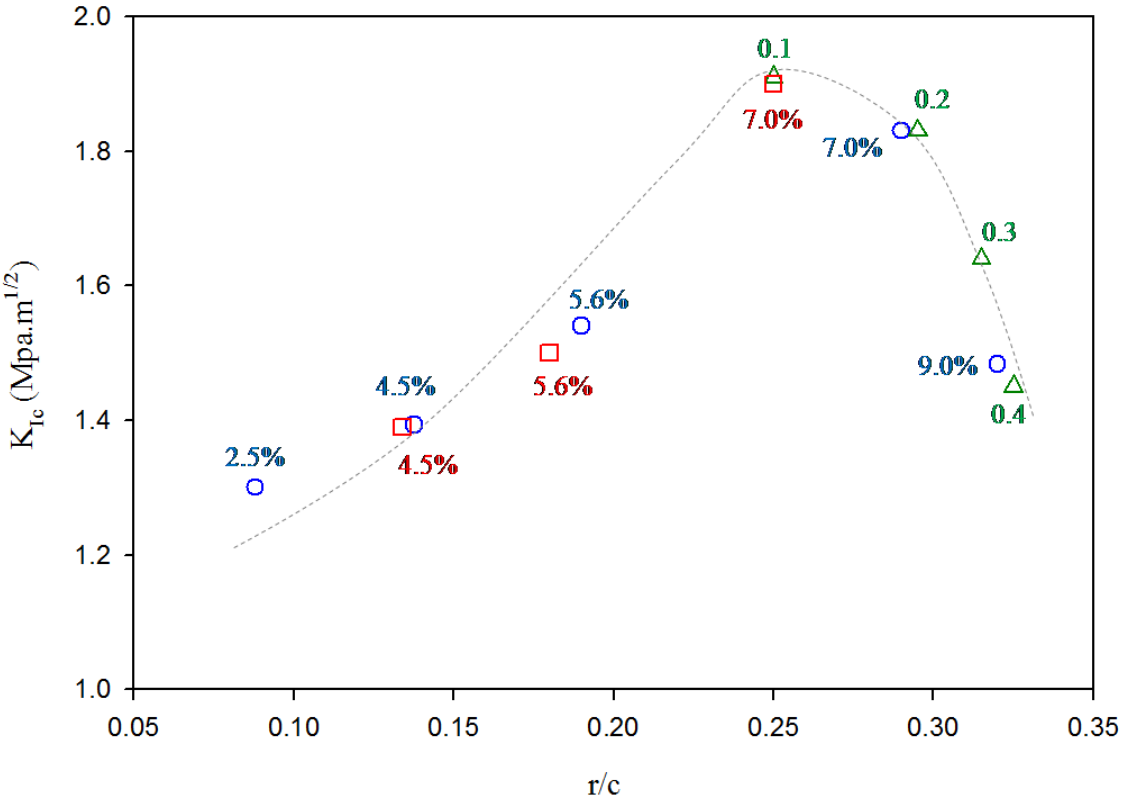

Fig. 6.1. Correlation between K_{Ic} and *r/c*(○) hybrid nanocomposite samples containing 2phr clay with MMA/St_{CA}: 0.2 and different P(MMA/S) contents, the numbers indicate the weight percentage of P(MMA/S), (□) hybrid nanocomposite samples containing 2 phr clay with MMA/St_{CA}: 0.1 and different P(MMA/S) contents, the numbers indicate the weight percentage of P(MMA/S), (△) hybrid nanocomposite samples containing 2phr clay and 7wt% P(MMA/S) with different MMA/St_{CA}, the numbers indicate the molar ratio of MMA/St. (Dashed line is drawn to aid the eye only).

6.3.1.Characteristics of the continuous thermoset-rich phase

The crosslink density of the thermosetting matrix strongly influences fracture toughness and its controlling mechanisms. High crosslink density prevents crazing by restricting fibril formation [31]. In addition, it decreases micro-shear band formation (localized shear yielding) by limiting the conformation changes of the polymer chains. The key synthesis process parameter affecting crosslink density is the molar ratio of curing agents. Other process variables, including the clay and thermoplastic content, may affect crosslink density by changing the concentration of the curing agents in the continuous thermosetting phase. In general, different diffusion rates of the reactants, including curing agents and unsaturated polyester, into the clay or thermoplastic phase

decrease the homogeneity of the system. For instance, clay galleries dispersed throughout the matrix can reduce the concentration of the curing agents in the continuous phase by trapping them resulting in a reduction in crosslink density.

For different toughening techniques, the improvement in fracture toughness of the thermoset strongly depends on localized yielding in the vicinity of the growing crack tip, which requires cooperative chain motion and local mobility. In polymer networks, the yielding process often needs the motion to occur following the β relaxation mechanism, which is mostly due to crankshaft-like motions. The β transition temperature, controlling localized plasticity, strongly depends on the chemical structure of the network. Since the second curing agent, methyl methacrylate (MMA), participates in the network formation, it is expected to affect the β transition.

Since the molar ratio of the curing agents is the variable directly affecting the characteristics of the matrix, we first evaluate its effect in simple polyester systems (systems without clay and thermoplastic). Then the effect of all synthesis process variables on the matrix characteristics in the complex hybrid systems will be evaluated.

In the previous work [168], we described the effect of different molar ratios of curing agents, MMA/St_{CA} (0.2, 0.4, 0.6, and 0.8), on the degree of cure and glass transition temperature, T_g. Clearly, a high degree of cure is prerequisite for reaching high crosslink density. DSC data indicated that the final degree of cure at room temperature for all samples with different MMA contents is almost the same at around 83%. The glass transition temperature is a suitable criterion that directly depends upon crosslink density of the thermosetting matrix. The data showed that a low amount of MMA, up to a molar ratio of 0.4, slightly increased T_g, indicating a minor increase in crosslink density. In contrast, a higher molar ratio resulted in a significant reduction in T_g, illustrating a decrease in crosslink density. Therefore, we chose a variation range of 0.1 to 0.4 for the molar ratio of the curing agents to minimize the effect of changes in crosslink density for the hybrid systems and eventually in fracture toughness.

Tensile strength also reflects the crosslink density of a thermoset. Table 6.1 presents mechanical properties of these simple polyesters. The presence of even a small amount of

MMA resulted in a slight increase in tensile strength compared to neat UPR (SP/0.0), indicating a slight increase in crosslink density, consistent with the T_g results. The tensile strength of all simple polyesters containing MMA but with varying contents is the same, suggesting this range of comonomer ratio does not change crosslink density (Figure 6.2).

The modulus of all samples containing MMA is almost the same, suggesting that the compactness of the network is not affected by MMA content in this range of variation. The presence of MMA did cause a slight increase in modulus compared to neat polyester (SP/0.0).

Table 6.1. Tensile properties of simple polyester samples containing different MMA contents.

Sample	Tensile Strength (MPa)	Tensile modulus (GPa)	Inelastic strength (MPa)	K_{Ic} (MPa. $m^{1/2}$)	r_y (μm)
SP/0.0	61.5 (3.0)[a]	3.34 (0.06)	36.8 (0.6)	1.15 (0.09)	51.7
SP/0.1	70.5 (1.8)	3.53 (0.03)	32.3 (0.6)	1.33 (0.07)	90.6
SP/0.2	70.6 (2.3)	3.56 (0.04)	31.9 (0.2)	1.32 (0.06)	90.7
SP/0.3	71.8 (2.6)	3.57 (0.06)	32.3 (0.7)	1.31 (0.08)	87.3
SP/0.4	71.2 (2.2)	3.50 (0.05)	31.5 (0.5)	1.28 (0.05)	87.7

[a] The values in parentheses are standard deviations of mechanical properties from seven samples.

The data in Table 6.1 indicate that the presence of MMA in the network results in a slight improvement in fracture toughness (K_{Ic}). In a brittle thermoset, the major mechanism controlling fracture toughness is localized shear yielding (micro-shear band formation) in the vicinity of the growing crack tip [31]. The observed improvement in fracture toughness is likely due to the effect of MMA on localized yielding of the thermoset where the inelastic strength σ_i, the stress when a material does not elastically deform, can represent this aspect of mechanical behavior. The inelastic strength was calculated by using a 0.2% offset strain criterion. The presence of MMA in the network caused a slight reduction of inelastic strength compared to neat UPR (SP/0.0), but different MMA contents resulted in the same value of σ_i (Figure 6.2).

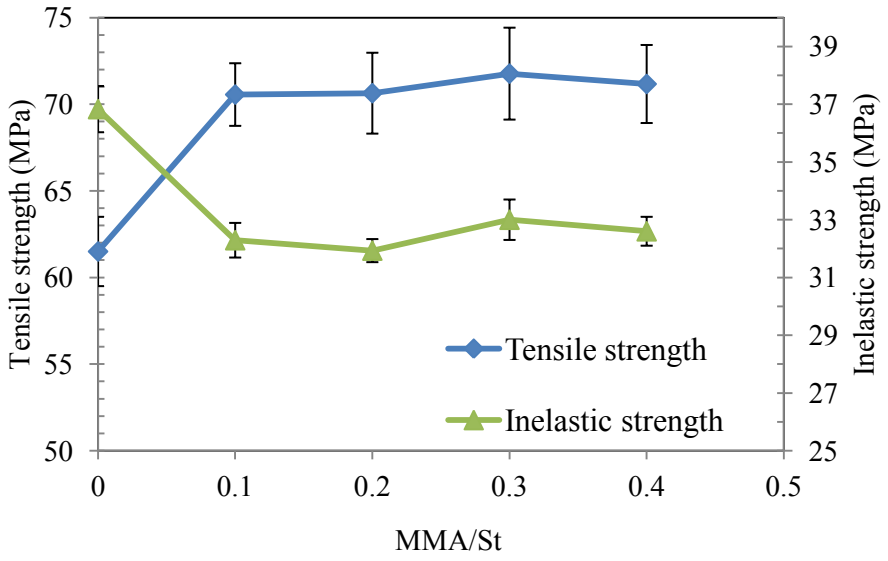

Fig. 6.2. Effect of MMA content on tensile strength and inelastic strength of simple polyesters.

There is a concentrated stress field in the vicinity of the crack tip that can exceed the yield strength of the polymer, leading to localized yielding. In this case, we can estimate the plastic zone size in the crack tip based on the Irwin model, where the equation for the plane strain condition is [24]:

$$r_y = \frac{1}{6\pi}\left(\frac{K_{Ic}}{\sigma_y}\right)^2 \qquad (6.1)$$

where r_y, K_{Ic}, and σ_y are the radius of the plastic zone around the crack tip, critical stress intensity factor, and tensile yield strength, respectively where inelastic strength can be used instead of σ_y in brittle materials. The values of r_y for different simple polyester samples are presented in Table 6.1. The presence of MMA in the network structure resulted in an increase in the size of the plastic zone (r_y) around the crack tip, indicating higher energy dissipation during crack propagation, which results in the improvement in fracture toughness. This effect of MMA on localized yielding of the matrix is likely due to its effect on the β transition temperature of the matrix. The unsaturated polyester network has a β relaxation because of the ester group, which is inactive at ambient temperature (a typical testing temperature) since the β transition temperature of UP when cured with styrene is high (80-100°C for a frequency of 1 Hz) [27]. The ester group in methyl methacrylate causes the β relaxation for poly (methyl methacrylate) with a low

transition temperature ($0<T_{\beta}<30$°C) [175]. Since the inelastic strength of the system is reduced by the addition of MMA, it is likely that the presence of MMA in the network, replacing some styrene units, promotes localized yielding of the network. As a result, a slight increase in fracture toughness was achieved.

Therefore, the addition of MMA as the second curing agent causes a slight increase in crosslink density and localized yielding of the thermoset, but different ratios of MMA/St_{CA} led to the same results. Therefore, the matrix characteristics do not play an important role in controlling fracture toughness in this range of MMA/St_{CA}.

In the hybrid nanocomposite systems, different experiments were designed to evaluate the effect of the synthesis process parameters, including MMA/St_{CA} (0.1, 0.2, 0.3, and 0.4), clay loading (1, 2, and 3 phr), and P(MMA/S) content (2.5, 4.5, 5.6, 7, and 9wt%), on the degree of cure and T_g of the matrix. These variables did not significantly change the final degree of cure (data are presented in Appendix A6). In hybrid nanocomposites, the presence of clay and the thermoset-rich phase can affect crosslink density by changing the concentration of curing agent monomers in the continuous thermoset-rich phase.

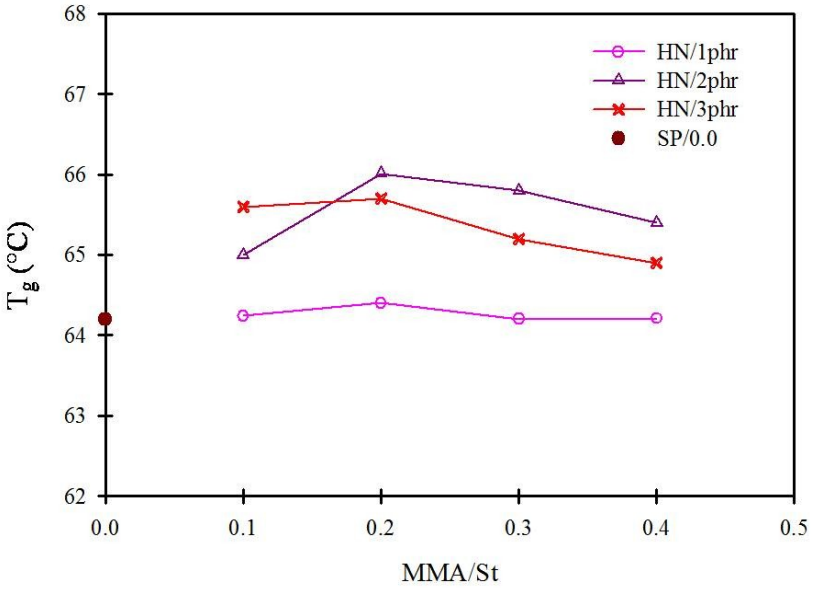

Fig. 6.3. Effect of MMA content on the T_g of hybrid nanocomposite samples with different clay loading (all samples contain 7wt% P(MMA/S)).

Since, in the determined range of MMA/St_{CA} ratio (0.1-0.4), different MMA contents in simple polyesters did not significantly affect T_g, we do not expect substantial changes in the T_g of hybrid systems containing different amounts of clay and MMA.

Figure 6.3 shows the effect of MMA and clay content on the T_g of the hybrid nanocomposites containing 7wt% P(MMA/S). As reported in the previous work [168], the hybrid nanocomposite system has a slightly higher glass transition temperature compared to neat polyester. The addition of clay caused a slight increase in T_g, likely due to its restricting effect on the mobility of the polymer segments in both phases.

In addition to crosslink density, localized yielding of the matrix may be affected by the synthesis process variables. For simple polyesters, we used Irwin's theory to estimate the plastic zone size at the crack tip, since the major energy dissipating process is localized plastic deformation of the matrix. In hybrid nanocomposites, this estimation is not valid, as different mechanisms contribute to the toughening of the thermoset via various energy dissipating processes. However, inelastic strength can represent localized yielding of the matrix. Table 6.2 presents tensile properties of hybrid nanocomposite samples with different clay, MMA, and P(MMA/S) contents. The data show that the inelastic strength of hybrid nanocomposites is not significantly affected by different synthesis process variables.

In the presence of a second phase, adhesive strength of the interface between the two phases plays an important role in tensile strength. The data in Table 6.2 indicate that the incorporation of a second phase either thermoplastic (HP/0.1 and HP/0.2) or clay (SN/0.0/2phr, SN/0.0/3phr) causes a reduction in tensile strength due to the imperfect adhesion at the interface between two phases. Figure 6.4 shows the effect of clay and MMA content on the tensile strength of hybrid nanocomposite samples. Clay loading up to 2 phr causes a slight decrease in tensile strength, while higher loading (3 phr) leads to a significant reduction in tensile strength (Figure 6.5). In particulate composites, interfacial adhesion strength strongly depends on the size of spherical particles, where it is decreased by an increase in the size of the particles [176]. Table 6.3 presents the size

(average diameter) of the thermoplastic-rich particles in different hybrid nanocomposites. The addition of clay up to 2 phr slightly increased the size of the thermoplastic-rich domains, resulting in a small reduction in tensile strength. In contrast, 3-phr clay loading led to a significant increase in the particle size and resulted in a substantial reduction in tensile strength. For each clay loading, the tensile strength of hybrid nanocomposites containing MMA is the same (Figure 6.4), suggesting that crosslink density did not change with MMA content .

Higher P(MMA/S) content resulted in a reduction in tensile strength due to the increase in the volume fraction of the dispersed phase. The presence of clay silicate layers slightly increased the modulus of the nanocomposites due to the high stiffness of clay relative to polymers. This is an advantage of this toughening technique compared to rubber toughening techniques.

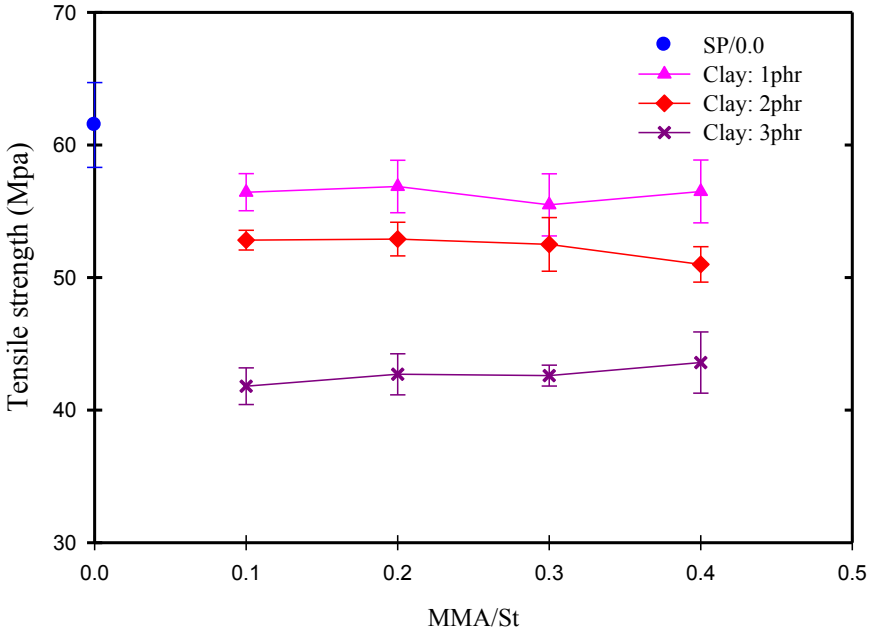

Fig. 6.4. Effect of MMA content on tensile strength of hybrid nanocomposite samples with different clay loading (all samples contain 7wt% P(MMA/S)).

These results show that in our hybrid nanocomposite systems, the system composition did not affect the crosslink density and localized yielding in a manner sufficient to change fracture toughness. In fact, we used a range of values for the synthesis process parameters

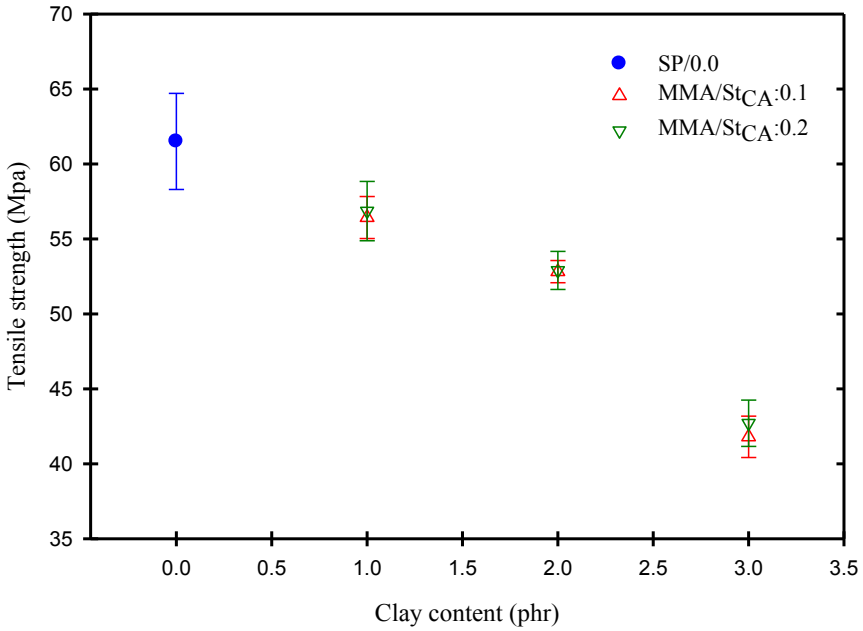

Fig. 6.5. Effect of clay content on tensile strength of hybrid nanocomposite samples with different MMA content (all samples contain 7wt% P(MMA/S)).

Table 6.2. Tensile properties of simple and hybrid nanocomposites.

Sample	Tensile Strength (MPa)	Inelastic Strength (MPa)	Tensile Modulus (GPa)
SP/0.0	61.5 (3.0)[c]	36.8 (0.6)	3.35 (0.06)
SN/0.0/2phr	57.7 (1.3)	32.6 (0.5)	3.42 (0.06)
SN/0.0/3phr	51.0 (2.9)	32.0 (0.3)	3.41 (0.08)
HP/0.1	56.5 (3.1)	31.2 (0.4)	3.51(0.05)
HP/0.2	57.3 (3.2)	31.0 (0.5)	3.52 (0.06)
HN/0.1/1phr[a]	56.4 (1.4)	29.5 (0.4)	3.35 (0.05)
HN/0.2/1phr[a]	56.9 (1.9)	28.3 (0.3)	3.35 (0.04)
HN/0.3/1phr[a]	55.5 (2.3)	28.7 (0.7)	3.37 (0.04)
HN/0.4/1phr[a]	56.5 (2.4)	30.1 (0.6)	3.38 (0.05)
HN/0.1/2phr[a]	52.8 (0.7)	28.8 (0.2)	3.40 (0.04)
HN/0.2/2phr[a]	52.9 (1.3)	29.1 (0.5)	3.41 (0.04)
HN/0.3/2phr[a]	52.5 (2.0)	29.9 (0.4)	3.45 (0.05)
HN/0.4/2phr[a]	50.9 (1.3)	29.6 (0.3)	3.43 (0.06)
HN/0.1/3phr[a]	41.1 (1.4)	28.1 (0.7)	3.42 (0.04)
HN/0.2/3phr[a]	42.7 (1.5)	27.5 (0.4)	3.40 (0.06)
HN/0.3/3phr[a]	42.6 (0.8)	27.7 (0.3)	3.44 (0.05)
HN/0.4/3phr[a]	43.6 (2.3)	28.5 (0.6)	3.39 (0.07)
HN/0.2/2phr/2.5wt%[b]	56.1 (2.1)	28.9 (0.7)	3.39 (0.04)
HN/0.2/2phr/4.5wt%	55.6 (2.1)	29.1 (0.9)	3.41 (0.03)
HN/0.2/2phr/5.6wt%	54.7 (1.1)	29.2 (0.4)	3.42 (0.05)
HN/0.2/2phr/7.0wt%	52.5 (1.3)	29.1 (0.5)	3.41 (0.04)
HN/0.2/2phr/9.0wt%	47.4 (3.2)	29.0 (0.4)	3.44 (0.06)

[a] These hybrid nanocomposite samples contain 7wt% P(MMA/S).
[b] The last number represents the mass fraction of P(MMA/S).
[c] The values in parentheses are standard deviations of the property from seven samples.

to keep the matrix characteristics constant for different samples and minimize its effects on the fracture toughness of the hybrid nanocomposites.

6.3.2 Microstructure

Table 6.3 presents the particle size and interparticle distance in the different samples, indicating that changes in composition and synthesis process variables caused significant change in the microstructure characteristics. To interpret the effect of each variable, the microstructure development in these systems must be understood. During mixing of the unsaturated polyester resin with the thermoplastic/clay mixture, small droplets of thermoplastic-rich phase are formed. Small molecules of curing agents (MMA and styrene) can diffuse into the droplets faster than unsaturated polyester (UP) molecules. Consequently, these droplets are first swollen by curing agent monomers. This swelling makes it easier for UP molecules to diffuse into the droplets. Therefore, these thermoplastic-rich droplets are expanded to contain all constituents. The presence of exfoliated clay inside the droplets causes an increase in their viscosity. The much larger viscosity of the droplets compared to that of the continuous phase leads to an increase in the resistance of the droplets against shear stress during mixing. As a result, the size of the droplets attained during the mixing and will be higher when clay is present [168]. The final size of the droplets after curing will then depend on the size of the dispersed phase before solidification, the rates of diffusion of constituents in and out of the thermoplastic-rich phase under quiescent conditions, and likely the gel time. We explored the effect of the gel time on the final size of the thermoplastic-rich domains as well as fracture toughness of the hybrid samples. The results showed that the gel time does not affect fracture toughness of the hybrid nanocomposite systems (Appendix A8).

Table 6.3 indicates that the addition of clay causes an increase in the final size of the thermoplastic-rich domains. The effect of MMA content on the size of the thermoplastic-rich domains depends on clay loading. The Florry Huggins interaction parameter between the MMA monomer and P(MMA/S) is approximately 1.41×10^{-3}, which is greater than that between styrene and the copolymer [168] (1.07×10^{-4}). This means there is more compatibility between the copolymer, P(MMA/S), and styrene compared to the copolymer and MMA, leading to faster diffusion of styrene into the thermoplastic-rich phase. Therefore, styrene monomers are expected to have the highest concentration inside

the droplets. On the other hand, an increase in MMA/St_{CA} ratio, meaning a reduction in the total concentration of styrene in the whole system, results in a reduction in the concentration of styrene in the thermoplastic-rich phase and likely a higher polyester concentration.

Table 6.3. Average particle size, interparticle distance, and K_{Ic} of different samples.

Samples	Particle Diameter (d=2r) (μm)	Interparticle distance-C (μm)	r/c	K_{Ic} MPa·m$^{1/2}$
SP/0.0	---	---	---	1.15 (0.09)
SN/0.0/2phr	---	---	---	1.33 (0.06)
SN/0.0/3phr	---	---	---	1.29 (0.08)
HP/0.1	3.50 (1.2)[d]	8.76 (3.1)	0.20	1.44 (0.1)
HP/0.2	3.40 (1.4)	9.02 (2.7)	0.19	1.42 (0.05)
HN/0.1/1phr[a]	3.91 (0.8)	8.31 (3.9)	0.24	1.54 (0.07)
HN/0.2/1phr[a]	4.10 (0.9)	8.23 (4.2)	0.25	1.52 (0.08)
HN/0.3/1phr[a]	3.94 (1.1)	7.98 (4.1)	0.25	1.49 (0.06)
HN/0.4/1phr[a]	3.85 (0.9)	8.71 (4.3)	0.22	1.47 (0.05)
HN/0.1/2phr[a]	4.55 (0.6)	8.94 (4.2)	0.25	1.91 (0.05)
HN/0.2/2phr[a]	5.35 (0.7)	9.09 (4.6)	0.29	1.83 (0.06)
HN/0.3/2phr[a]	5.69 (1.0)	9.01 (4.8)	0.32	1.64 (0.04)
HN/0.4/2phr[a]	5.87 (0.9)	9.00 (5.0)	0.33	1.57 (0.06)
HN/0.1/3phr[a]	9.24 (2.5)	13.70 (11.2)	0.34	1.56 (0.09)
HN/0.2/3phr[a]	10.48 (3.5)	14.27 (10.3)	0.37	1.59 (0.07)
HN/0.3/3phr[a]	11.15 (3.1)	13.68 (11.8)	0.41	1.53 (0.08)
HN/0.4/3phr[a]	11.10 (3.3)	14.45 (12.4)	0.38	1.50 (0.09)
HN/0.1/2phr/4.5%[b]	2.00 (0.7)	7.70 (2.7)	0.13	1.39 (0.04)
HN/0.1/2phr/5.6%[b]	2.95 (0.9)	8.2 (2.9)	0.18	1.52 (0.05)
HN/0.1/2phr/7.0%[b]	4.55 (0.6)	8.94 (4.2)	0.25	1.91 (0.05)
HN/0.2/2phr/2.5%[b]	1.37 (0.5)	7.27 (2.6)	0.09	1.34 (0.04)
HN/0.2/2phr/4.5%[b]	2.09 (0.9)	7.60 (3.1)	0.14	1.44 (0.05)
HN/0.2/2phr/5.6%[b]	3.07 (1.1)	8.05 (3.4)	0.19	1.58 (0.03)
HN/0.2/2phr/7.0%[b]	5.35 (0.9)	9.09 (4.6)	0.29	1.83 (0.06)
HN/0.2/2phr/9.0%[b]	6.40 (1.2)	9.71 (5.6)	0.33	1.55 (0.05)
1NUP+1NTP[c]	---	---	---	1.54 (0.07)
2NUP+TP[c]	---	---	---	1.45 (0.06)

[a] These hybrid nanocomposite samples contain 7wt% P(MMA/S).
[b] The last number represents the mass fraction of P(MMA/S).
[c] These samples contain 2-phr clay and 7wt% P(MMA/S) with MMA/St=0.2.
[d] The values in parentheses are standard deviations of the property.

This results in an increase in the concentration of UP microgels. Eventually larger thermoplastic-rich particles are formed [168]. For 1-phr clay loading, MMA content does not have a significant effect on the final particle size, suggesting that the content of clay

silicate layers is not enough to hinder diffusion of UP chains. In contrast, for higher clay loading, the addition of MMA caused an increase in the particle size (Figure 6.6).

The other microstructure parameter is related to the distribution of the thermoplastic-rich domains. Table 6.3 presents the interparticle distance in different samples, where the standard deviation values represent non-uniformity of particle distribution. The data show that interparticle distance is not significantly affected by MMA and P(MMA/S) content.

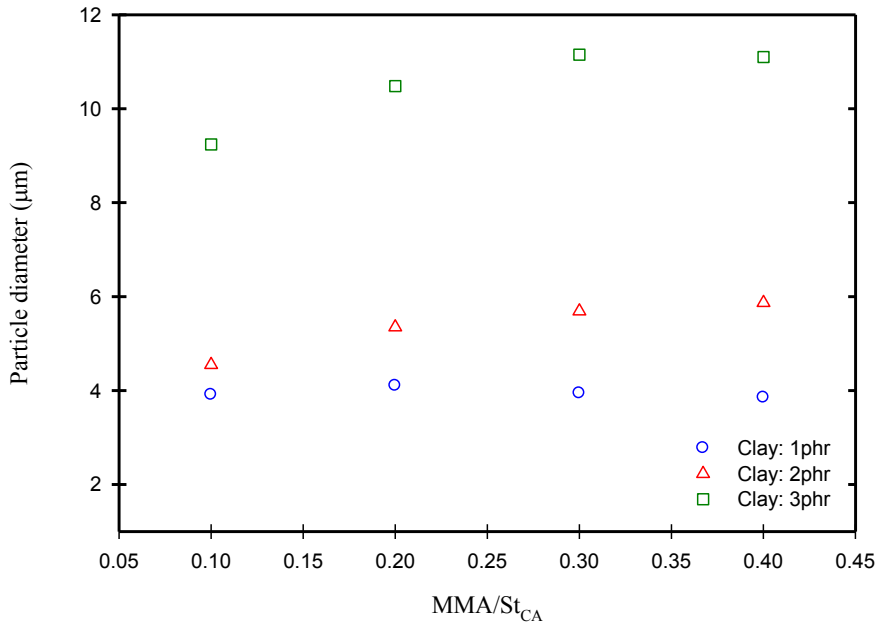

Fig. 6.6. Effect of MMA content on particle diameter in hybrid nanocomposite samples with different clay loading (all samples contain 7wt% P(MMA/S)).

Only a clay loading of 3 phr resulted in a significant increase in the interparticle distance and standard deviation. A high content of clay in the thermoplastic-rich phase causes a significant increase in viscosity and density of the thermoplastic-rich droplets in the liquid state (before curing). High viscosity results in an increase in the resistance of the droplets against shear stress during mixing, leading to a significant increase in the final size of the thermoplastic-rich domain and the non-uniformity of particle spacing distribution.

6.3.3.Fracture toughness and controlling mechanisms

In hybrid polyester samples (HP/0.1 and HP/0.2), the thermoplastic additive forms a second phase dispersed throughout the matrix, as shown in SEM micrographs of the fracture surface (Figure 6.7). The SEM images show that the majority of the thermoplastic-rich particles are fractured due to their low stiffness and fracture toughness [173]. This means the thermoplastic-rich domains cannot perturb the crack front during crack propagation. In the images, a few faint fracture tails can be observed behind the thermoplastic-rich particles. The propagation of the crack through the thermoplastic area is slower compared to the thermoset matrix, causing small variations in the height of the crack front. These tails are formed because the crack front segments meet up again at different heights after passing the thermoplastic domains [168]. In this case, the major energy dissipating process is likely the plastic deformation of the thermoplastic-rich particles, leading to a small improvement in fracture toughness (Table 6.3). In addition, SEM images show some cavities and intact particles, illustrating the occurrence of the particle/matrix debonding, which can make a small contribution to toughening via crack blunting.

In hybrid nanocomposites, the presence of clay silicate layers in the thermoplastic-rich domains results in an increase in their stiffness and fracture toughness, increasing their impenetrability. In general, rigid second phase inclusions, located in front of the crack tip, can perturb the crack front during propagation, causing a reduction in the stress intensity [132]. Two dominant perturbations are crack deflection and crack pinning. In most cases, they occur simultaneously, but the dominant perturbing process is determined by the adhesion strength of the interface between the inclusion and matrix. When the crack approaches or intercepts the inclusion, if the interfacial adhesion strength is less than the stress at the crack tip, then the crack is forced by the impenetrable inclusion to tilt out of the plane normal to the applied stress and propagate through the interface, causing a non-planar crack front. Consequently, crack deflection causes a high roughness on the fracture surface and increases the fracture surface area, resulting in an improvement in fracture toughness. However, this increment in fracture toughness can be considered a lower bound estimate of the total increase in fracture toughness via crack deflection [58]. This means, during crack deflection, other energy dissipating processes

are engaged to improve fracture toughness, such as localized plastic deformation of the matrix in the vicinity of the growing crack tip. These energy dissipating processes strongly depend upon the characteristics of the matrix, including its crosslink density and localized yielding, which depend on the chemical structure. On the other hand, if the interfacial adhesion strength is high enough, the inclusion resists against the propagating crack. The crack front is forced to bow between the particles, causing a reduction in the stress intensity along the bowed segments of the crack front, but an increase in the stress intensity at the particles. Therefore, crack bowing results in a non-linear crack front, increasing the fracture toughness. Crack pinning leads to a lower degree of roughness on the fracture surface compared to crack deflection.

Table 6.3 presents the K_{Ic} of hybrid nanocomposites with different clay loading. The addition of 1 phr clay caused a slight improvement in fracture toughness compared to hybrid polyesters, whereas 2 phr of clay resulted in a significant improvement in fracture toughness (Figures are presented in appendices A9-A11). SEM images (Figure 6.8) of the fracture surface related to the hybrid nanocomposite sample containing 1 phr of clay (HN/0.1/1phr) show a high degree of roughness, indicating that the dominant mechanism controlling fracture toughness is crack deflection instead of crack pinning. The clay content in the thermoplastic-rich particles is not enough to increase impenetrability of all domains. In other words, the concentration of the impenetrable particles is not enough to reduce the stress intensity at the crack tip by inducing a large number of bowed segments of the crack front. Therefore, this high stress field at the crack tip overcomes the interfacial adhesion strength, resulting in crack deflection instead of crack pinning. Since the β transition temperature of unsaturated polyester, which is responsible for local mobility of the polymer segments and consequently localized yielding, is much higher than the testing temperature (room temperature), the intensity of localized yielding of the matrix in the vicinity of the crack tip is expected to be low. Consequently, crack deflection can only lead to a slight improvement in fracture toughness, mainly by increasing the fracture surface area.

Figure 6.9 shows SEM images of the fracture surface of a hybrid nanocomposite with 2-phr clay loading, HN/0.1/2phr. The images suggest a different mechanism because the particles are mostly intact and the roughness of the fracture surface is very low. In

addition, many thick fracture tails are visible behind the particles in the micrograph plane which is located on the plane normal to the applied stress. All of these features are consistent with pinning of the crack front. Therefore, we conclude that crack pinning is the dominant perturbing process and controlling mechanism which results in a significant improvement in fracture toughness.

In contrast, a higher clay loading (3 phr) resulted in a smaller improvement in fracture toughness. SEM images of HN/0.1/3phr samples (Figure 6.10) show all signs of crack pinning, including low roughness of the fracture surface, intact particles, and thick fracture tails behind the particles. The number of intact domains in these samples is greater compared to the samples containing 2 phr. The fracture of the perturbing particles in the wake of the crack depends on the ratio of the fracture toughness of the particles ($K^P{}_c$) to the fracture toughness of the matrix ($K^m{}_c$). A higher ratio (K_c^p/K_c^m) results in an increase in the number of intact particles [173]. Since clay content in the thermoplastic-rich domains determines their fracture toughness and consequently their resistance against fracture, higher clay loading increased the number of intact particles.

Bower and Ortiz [173] evaluated the effect of particle bridging on the fracture toughness of a brittle matrix where particles make bridges between two sides of the crack and resist against crack opening. They claimed that if $K^P{}_c$ is comparable to $K^m{}_c$, the particles are penetrated by the crack and particle bridging does not contribute to toughening. If the fracture toughness of the particles exceeds a critical value, the obstacles will be intact in the wake of the crack and particle bridging occurs. When $K^P{}_c$ is lower than this critical value, crack bowing occurs, but particles are fractured in the wake of the crack. They believed that particle bridging is a very effective toughening mechanism due to its contribution to energy dissipation. However, this mechanism can only contribute a significant improvement to the fracture toughness of a brittle matrix when the particles are tough and the interfacial adhesion between the particles and matrix is strong. In our systems, the number of intact particles in the samples containing 3-phr clay is much higher than other samples with lower clay loading (2 phr), but the overall values of fracture toughness are lower. In addition, the thermoplastic-rich domains are not particularly tough. Although the presence of clay inside the domains increases somewhat their fracture toughness, these particles are still fundamentally brittle.

Therefore, particle bridging likely does not contribute a significant improvement to fracture toughness in our systems, and the major controlling mechanism must be crack pinning.

According to the crack pinning mechanism, the growing crack is pinned by impenetrable particles, causing the crack front to bow out between them. After bowing, the crack keeps propagating and after a distance of about one particle diameter, the crack front breaks free and resumes its linear shape [51]. In this case, two distances become important to controlling toughening, namely: (i) the interparticle distance and (ii) the distance that the crack propagates along the particles before breaking free, referred to as the critical propagation distance. The former is linked to the particle concentration and diameter. Fracture toughness is increased when the interparticle distance decreases and the critical propagation distance increases. Therefore, the spatial distribution of particles plays an important role in fracture toughness. Table 6.3 presents the interparticle distance and its standard deviation, which represents the degree of non-uniformity of the particle distribution in space. Higher clay loading (3 phr) leads to a sudden increase in the interparticle distance and its standard deviation. This means some areas are free of the thermoplastic-rich particles while dense aggregations of particles exist in other regions. Heterogeneity of distribution of the impenetrable particles resulted in a reduction in the efficiency of the crack pinning mechanism, likely by reducing the number of the bowed segments of the crack front. Consequently, hybrid nanocomposite samples with higher clay loading (3 phr) have lower fracture toughness compared to those samples with better particle distribution (2 phr clay loading).

Both perturbations, crack deflection and crack pinning, strongly depend on the characteristics of the second phase (the dispersed inclusion), including stiffness and fracture toughness, where the inclusion must be able to resist against the crack front during its propagation. In our systems, the clay content inside the thermoplastic-rich domains controls these characteristics. In order to investigate further, we used two more preparation procedures to have better control of the location of the clay silicate layers with a constant clay loading (2 phr). In the first procedure, a mixture of clay (2 phr) and thermoset was prepared and then mixed with the neat thermoplastic. In this case the majority of clay silicate layers are located in the continuous thermoset matrix, and the

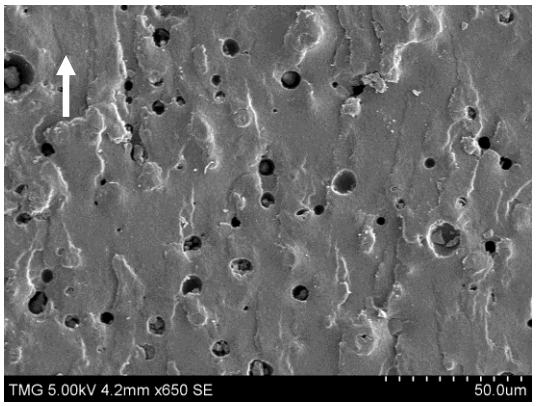

(a)

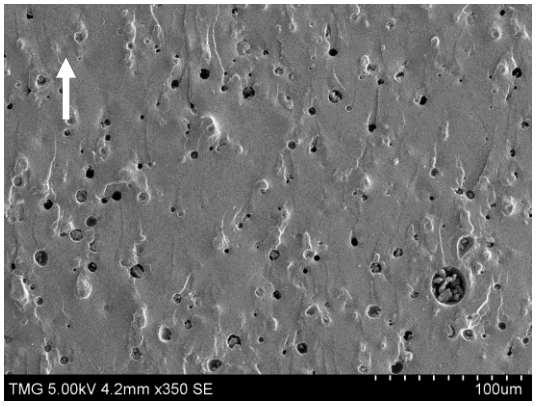

(b)

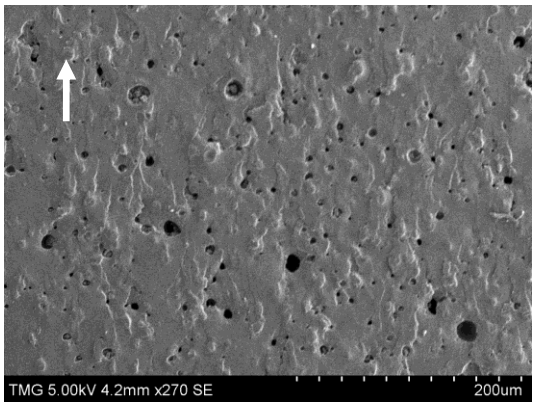

(c)

Fig. 6.7. SEM images of fracture surface of HP/0.1 containing 7wt% P(MMA/S). The arrows indicate direction of fracture.

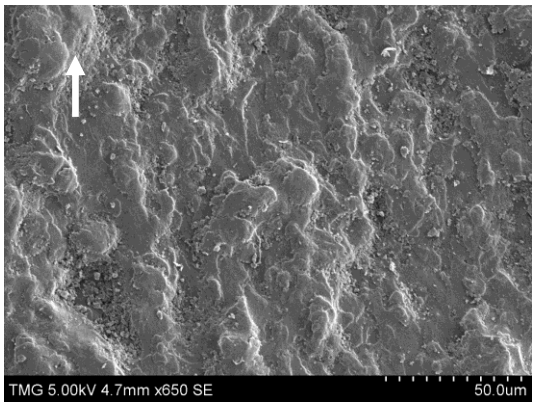

(a)

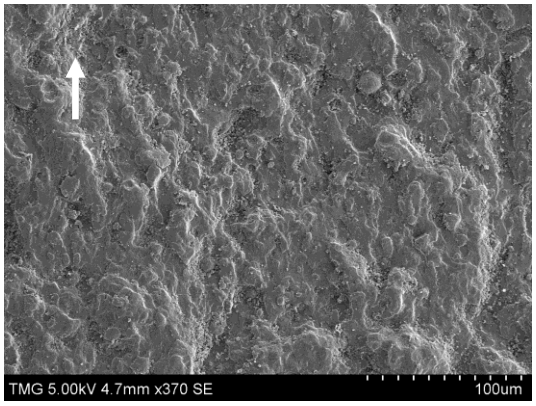

(b)

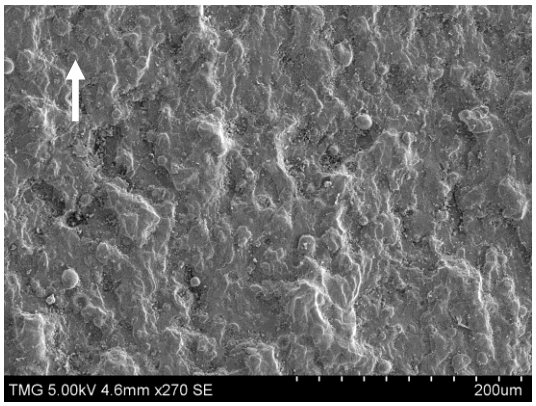

(c)

Fig. 6.8. SEM images of fracture surface of HN/0.1/1phr containing 7wt% P(MMA/S). The arrows indicate direction of fracture.

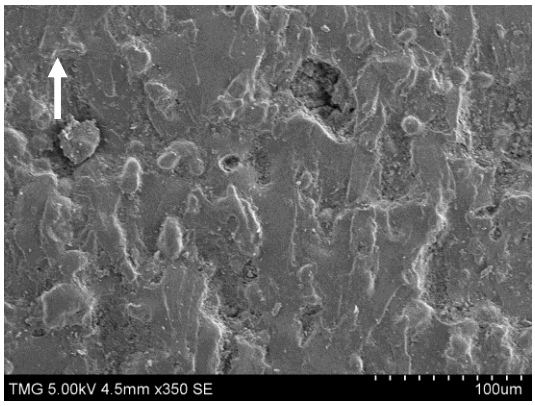

(a)

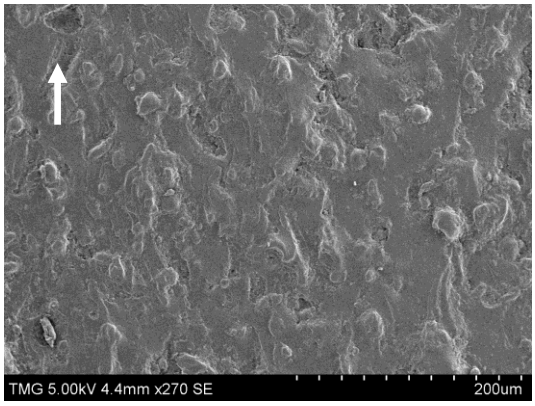

(b)

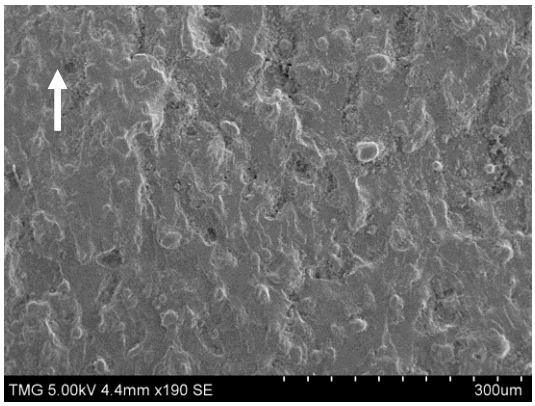

(c)

Fig. 6.9. SEM images of fracture surface of HN/0.1/2phr containing 7wt% P(MMA/S). The arrows indicate direction of fracture.

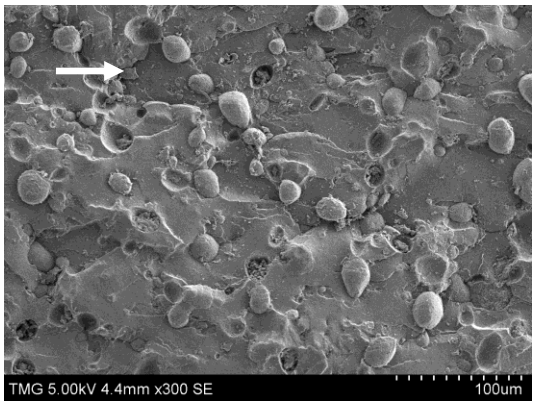

(a)

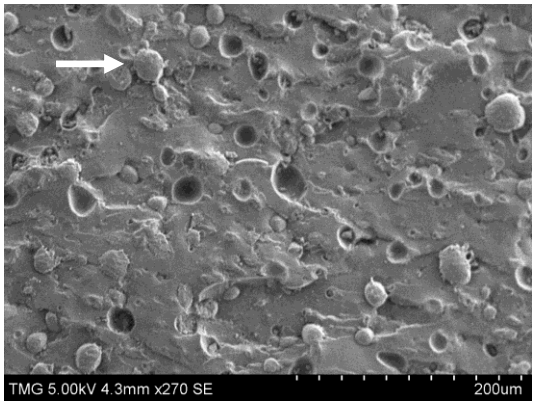

(b)

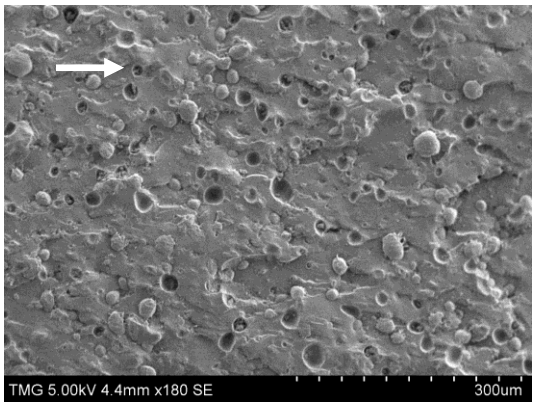

(c)

Fig. 6.10. SEM images of fracture surface of HN/0.1/3phr containing 7wt% P(MMA/S). The arrows indicate direction of fracture.

sample is called (2NUP+TP). In the second procedure, a half-part of clay (1 phr) was mixed with the thermoset and the other part was added to the whole system as a mixture with the thermoplastic, and this sample is called (1NUP+1TP). In this case, there is a more uniform dispersion of the silicate layers in both phases. The third sample was prepared via the major procedure (used for the preparation of all HN samples), where the entire clay content was introduced to the system with the thermoplastic component. The value of fracture toughness of each sample is presented in Table 6.3. In the former two samples, the improvement in fracture toughness is not significant since the clay content inside the thermoplastic-rich domains is not enough to increase the impenetrability of the domains to resist against the crack front propagation. This suggests that crack trapping was not the controlling mechanism of fracture in the samples containing low clay (less than 2phr).

The stiffness of the inclusion can affect the contribution of each mechanism (crack deflection and crack pinning) to fracture toughness by impacting interfacial adhesion strength. The ratio of the particle modulus (E_p) to the matrix modulus (E_m) strongly affects the interfacial debonding strength, where a higher ratio (E_p/E_m) leads to a lower interfacial adhesion strength [37,176]. For soft particles like rubber, lower interfacial adhesion is appropriate for the integrity of the rubber and the matrix, whereas for stiff particles like glass-beads interfacial bonding is essential. A very stiff particle creates a high stress state across the interfacial region, increasing the occurrence of interfacial debonding [37]. Weak interfacial adhesion strength resulted in an increase in the occurrence of crack deflection because the stiff particles force the crack front to tilt out the plane and propagate through the interface. Since the efficiency of crack deflection for toughening strongly depends on the matrix characteristics such as localized yielding and unsaturated polyester is not able to undergo significant localized yielding, a promotion of crack deflection compared to crack pinning processes in our system is to the detriment of toughening. Therefore, the addition of very stiff ceramic inclusions like glass beads is likely not as effective as our thermoplastic-rich domains with moderate stiffness. Incorporation of glass beads requires strong interfacial bonding between the two phases, the ceramic particles and UP matrix; otherwise, debonding occurs, resulting in a reduction in the efficiency of crack pinning. In contrast, for our system, the stiffness ratio

of the thermoplastic-rich domains and UP-rich matrix is suitable for the occurrence of crack pinning. In addition, in our system the interaction between the two organic and partially polar polymeric phases is much higher than the interaction between a ceramic particle (like glass beads) and the organic thermoset polymer (UP), resulting in a better interfacial adhesion.

6.3.4.Effect of microstructure on fracture toughness

In order to evaluate the effect of the microstructure on fracture toughness, we designed experiments where clay loading was kept constant (2 phr) to reach adequate impenetrability for thermoplastic-rich particles and suitable particle distribution. We changed MMA content ($0.1<MMA/St_{CA}<0.4$) and P(MMA/S) content (2.5, 4.5, 5.6, 7.0, 9.0wt%).

In the previous work [168], we found that the size of the thermoplastic-rich particles play important role in fracture toughness and we observed an increase in this property when the particle diameter increased. In crack pinning mechanism, an increase in the particle size promotes perturbation of the crack front resulting in an increase in fracture toughness, but the particle size is not the only influencing factor where the interparticle distance and spatial particle distribution also have controlling effect on the efficiency of crack pinning mechanism. Table 6.3 shows the effect of the particle size on fracture toughness of HN samples (figures are presented in appendices A10 and A11). Although a larger size is favourable for toughening, a best size was observed due to the important effect of the interparticle distance on the number of bowed segments of the crack front during propagation. Therefore, a ratio of particle radius to interparticle distance must be considered to correctly evaluate the effect of the microstructure on fracture toughness.

Figure 6.1 shows the correlation between fracture toughness and r/c for hybrid nanocomposite samples with different contents of MMA and P(MMA/S). The diagram shows a range of r/c values to achieve maximum fracture toughness. It does not matter which variable caused the change in the particle size and interparticle distance. Lange and Radford [55] also reported a maximum in the relationship between toughness and volume fraction of inclusions affecting the particle size and interparticle distance. For a high concentration of particles, interparticle distances are reduced. Lange and Radford [55]

pointed out that for each particular size of particles, there is an optimum interparticle distance resulting in maximum crack trapping. Although more bowed segments of the crack front are favourable for maximum toughening, there is also a minimum interparticle distance where the bowed segments of crack front can be formed and crack bridging, caused by the non-deformed matrix, occurs. Otherwise, very low interparticle distance leads to significant overlapping of stress fields caused by adjacent particles, increasing stress intensity in the region between particles. Consequently, this high stress intensity can cause fracturing of the interface, reducing the efficiency of crack pinning. Therefore, in our systems, a range of r/c values was observed to achieve maximum fracture toughness.

Figure 6.11 shows the effect of r/c on fracture toughness of different HP and HN samples which are classified based on the controlling mechanisms. Although a combination of mechanisms normally control fracture toughness, but in this figure only the dominant mechanisms are considered. Figure 6.11 shows crack pinning is the most effective mechanism to improve fracture toughness where r/c has a significant role in the efficiency of this mechanism.

Table 6.3 shows that a significant increase in the size of particles in HN samples containing 3-phr clay caused a substantial increment in the heterogeneity of spatial particle distribution. Although the major mechanism controlling fracture toughness in these samples is crack pinning, a sharp reduction in fracture toughness can be seen due to polydispersity of the interparticle distance in these samples. This means that the degree of uniformity of the particle distribution also plays an important role in the efficiency of crack pinning mechanism. This polydispersity indicates the aggregation of the particles which results in a reduction in the efficiency of crack trapping by the particles and crack bridging by the matrix.

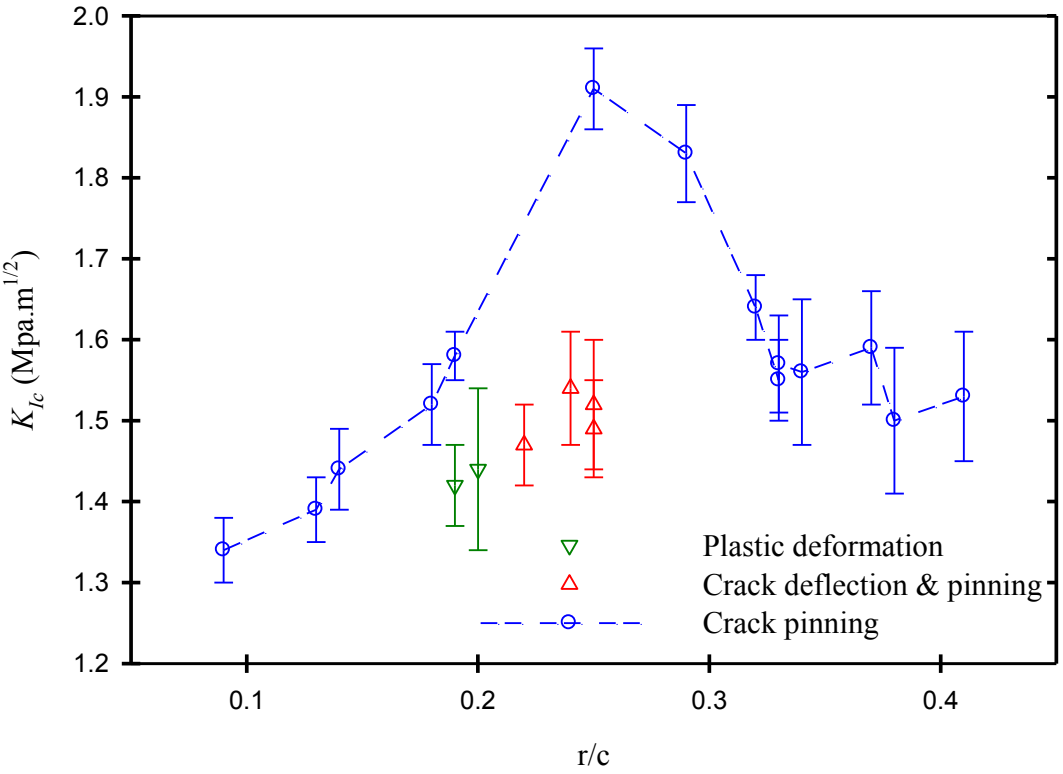

Fig. 6.11. K_{Ic} vs. r/c where the controlling mechanism is a parameter (Only major mechanisms are considered here).

6.4. Conclusions

The effect of synthesis process variables, including the contents of clay, MMA, and P(MMA/S), on the characteristics of the continuous phase and dispersed phase was evaluated. The major variable affecting the matrix characteristics, crosslink density and localized yielding, is the ratio of curing agents (MMA content) where a specific range of MMA/St_{CA} was selected for study to minimize the change of these characteristics.

The most important characteristic of the dispersed phase is its impenetrability. The presence of clay silicate layers in the thermoplastic-rich domains increases their stiffness and fracture toughness, enhancing their impenetrability. Impenetrable particles can perturb the crack front during propagation, leading to the simultaneous occurrence of crack deflection and crack pinning. Contribution of each mechanism to fracture toughness is controlled by the impenetrability of the particles. Lower impenetrability caused the occurrence of crack deflection, resulting in a lower improvement in fracture

toughness due to low localized yielding of unsaturated polyesters. Higher clay loading (more than 1 phr) sufficiently increased impenetrability of the thermoplastic-rich domains, leading to an increase in the contribution of the crack pinning mechanism.

In addition to impenetrability of obstacles, the particle size and interparticle distance are important in the efficiency of crack pinning. For each specific particle size, there is an optimum interparticle distance, resulting in the maximum improvement in fracture toughness. Between all variables, clay content had the greatest effect on the microstructure of the system, where the addition of clay resulted in an increase in size and interparticle distance. However, a large particle size causes a less homogeneous spatial particle distribution, resulting in a reduction in the efficiency of crack pinning. Therefore, the most suitable clay loading (2 phr) was identified relating to the maximum value of fracture toughness corresponding to a suitable particle size and interparticle distance.

To explore the effect of microstructure on fracture toughness, hybrid nanocomposite samples containing 2-phr clay with different contents of MMA and P(MMA/S) were prepared. The addition of MMA and P(MMA/S) resulted in an increase in the size of particles without significant change in the interparticle distance. Therefore, an interesting correlation between the microstructure and fracture toughness was found, where a best ratio of particle size to interparticle distance (r/c), in a range between 0.2 and 0.3, was found to achieve the maximum value of fracture toughness (about 65%).

Chapter 7

Conclusions, Contributions, and Recommendations for Future Work

7.1. Conclusions

Firstly, organoclay nanocomposites based on unsaturated polyesters were investigated to evaluate the effect of the silicate layers on curing reactions and the final properties of the thermoset, since there is some controversy surrounding these issues. The addition of clay causes a reduction in the total curing rate and an increase in induction time. The silicate layers can trap styrene monomers (as the curing agent), leading to a reduction in the concentration of styrene in extragallery regions and an increase in the residual styrene after curing at room temperature. This resulted in a decrease in the degree of cure and consequently crosslink density of the network, especially in high clay loading. However, in lower clay loading, this reduction in the degree of cure and crosslink density is slight.

To evaluate the effect of nanostructure on fracture toughness of the system, different mixing methods were used for the preparation of clay nanocomposites based on UPs, leading to the different degree of clay dispersion and distribution. The solvent-aided high pressure mixing method was successful to achieve a high degree of clay dispersion and delamination throughout the matrix. For comparison, a simple mechanical mixing method was also used. The results indicated that an almost identical improvement in fracture toughness for all nanocomposite samples prepared by different methods was achieved. A fine intercalation/exfoliation of the silicate layers slightly improved fracture toughness, while a higher degree of exfoliation did not contribute greater improvement. Intercalated silicate layers can have the potential to cause crack deflection in unsaturated polyester, contributing an improvement in fracture toughness. In this mechanism, other energy dissipation processes such as localized plastic deformation of the matrix in the vicinity of the growing crack tip contribute greater improvement to fracture toughness compared to the contribution obtained by the increase in fracture surface area. On the other hand, the intensity of localized plastic deformation of unsaturated polyester during crack propagation is low, since the β transition temperature of UP, which is responsible for local mobility of the polymer chains, is higher than room temperature, resulting in

inactivation of the β relaxation, causing a reduction in the efficiency of the crack deflection mechanism. A slight improvement in the fracture toughness of the nanocomposite systems was caused by the increase in fracture surface area. Therefore, for toughening of unsaturated polyesters, all techniques involving localized yielding of the matrix, such as layered silicate toughening, are not as effective as the case for toughening of thermosets such as epoxy, which have β transition temperature lower than room temperature.

We introduced a second dispersed phase with suitable impenetrability to the thermoset to perturb crack front propagation. For this purpose, a new class of ternary systems (thermoplastic/organoclay/unsaturated polyester hybrid nanocomposites) was developed. Relationships between precursor material composition, micro- and nano-structure, and mechanical properties were explored, demonstrating the potential of this new ternary hybrid system.

To compensate for the negative effect of clay on the final degree of cure and crosslink density of the thermoset matrix, a second curing agent, methyl methacrylate (MMA), and a thermal initiator were used. The addition of MMA allowed for increased styrene conversion, resulting in an improvement in glass transition temperature and higher crosslink density. In situ polymerization between two curing agents (MMA and styrene) in the presence of clay silicate layers was carried out to improve clay dispersion and distribution and to prepare the second dispersed phase for toughening. Complex micro- and nano-structures for hybrid nanocomposites were observed, which can be controlled by the composition of the system prior to curing. A synergistic effect of clay and thermoplastic on fracture toughness was observed, resulting in a significant improvement in fracture toughness. Two different thermoplastics, polystyrene (PS) and a copolymer of MMA and styrene (P(MMA/S)) with a composition of 18 mol% MMA, were examined, where the copolymer resulted in greater improvement in fracture toughness due to stronger adhesion strength between the copolymer and unsaturated polyester.

The morphology study showed that a combination of clay and thermoplastic led to the formation of spherical minor phase domains, which are rich in thermoplastic and contain the delaminated silicate layers surrounding tiny microgels of pure unsaturated polyester.

The presence of silicate layers increased the stiffness and impenetrability of the thermoplastic-rich domains that appeared to act as rigid fillers, where the major mechanism of energy dissipation during fracture is crack pinning. The potential of this new ternary hybrid system to improve fracture toughness by perturbing crack front propagation was demonstrated, where more refinement of the composition further improved fracture toughness. In addition, the initial morphological study illustrated that microstructure plays an important role in fracture toughness, calling for more investigation. Therefore, we used atomic force microscopy (AFM) to gather more information about the morphology and local mechanical properties of the system.

The preparation procedure of samples has a very important effect on the quality of AFM images. The ultramicrotome is a powerful instrument for specimen preparation to maximize the characterization capability of AFM, since microtomy preserves the original nanostructure of the sample. In the morphological study of the thermoplastic/clay/unsaturated polyester hybrid nanocomposite, AFM could distinguish between different polymeric phases (thermoplastic and thermoset), whereas TEM does not have this capability without staining. AFM showed different nanostructures for the thermoplastic-rich domains with and without clay. This suggests that the presence of silicate layers changes the nanostructure of the thermoplastic-rich domains, likely by affecting phase separation. The silicate layers caused a change in nanostructure from co-continuous to particulate, representing more complete phase separation inside the thermoplastic-rich domains. AFM had the capability to detect the silicate layers dispersed throughout different phases and regions, including the thermoplastic-rich phase, continuous thermoset-rich phase, and the interface between thermoplastic and thermoset. In addition, local mechanical properties of different phases and components were qualitatively assessed based on phase contrast. AFM showed that the thermoplastic component is a little bit stiffer than the thermoset matrix, and the presence of silicate layers significantly increased the stiffness of the domains, where higher stiffness of the particles is favourable for the crack pinning mechanism. Section analysis showed negative values of phase shifts in the interface between clay and thermoset, representing the occurrence of debonding between these components. In contrast, interfacial debonding between clay and thermoplastic inside the particles did not occur. This

suggests that the interaction between clay and thermoplastic is stronger than between clay and thermoset. Interestingly, no deep channel at the interface of the thermoplastic-rich and continuous phases was detected. This means that the adhesive strength in the interface between the two phases is strong enough to increase the occurrence of crack trapping.

For more refinement of the composition of the system, the effect of synthesis process variables, including the content of clay, MMA, and P(MMA/S), on the characteristics of the continuous and dispersed phases was evaluated. The major variable affecting the matrix characteristics, crosslink density and localized yielding, is the ratio of curing agents (MMA content), where a specific variation range of MMA/St_{CA} (0.1 to 0.4) was selected to minimize the change of these characteristics. However, the presence of MMA in the system, in the mentioned range, slightly increased crosslink density and localized yielding of the thermoset matrix. Other variables did not significantly change these characteristics of the thermoset-rich phase, indicating that these characteristics do not play important roles in the achieved improvement of fracture toughness in the hybrid systems.

The most important characteristic of the dispersed phase is its impenetrability. The presence of clay silicate layers in the thermoplastic-rich domains increased their stiffness and fracture toughness, enhancing their impenetrability. Impenetrable particles can perturb the crack front during propagation, leading to the simultaneous occurrence of crack deflection and crack pinning. Contribution of each mechanism to fracture toughness is controlled by impenetrability of the particles. Lower impenetrability causes fracture in the domains and a lower reduction in stress intensity in the crack tip, leading to the propagation of the crack front through the interface between two phases and consequently the occurrence of crack deflection. It results in a lower improvement in fracture toughness, since low localized yielding of unsaturated polyesters caused a reduction in the efficiency of crack deflection mechanism. Higher clay loading (2 phr and above) sufficiently increased impenetrability of the thermoplastic-rich domains, leading to an increase in the resistance of the domains against the crack front. As a result, the

stress intensity of the crack tip is decreased and the efficiency of the crack pinning mechanism is increased.

In addition to impenetrability of obstacles, the particle size and interparticle distance are important in the efficiency of crack pinning. For each specific particle size, there is an optimum interparticle distance, resulting in the maximum improvement in fracture toughness. Between all variables, clay content had the most effect on the microstructure of the system, where the addition of clay resulted in an increase in size and interparticle distance. However, the large particle size disturbed particle distribution, resulting in a reduction in the efficiency of crack pinning. Therefore, the best clay loading (2 phr) was observed to achieve the maximum value of fracture toughness, corresponding to suitable particle size, interparticle distance, and particle impenetrability.

To find out the effect of microstructure on fracture toughness, hybrid nanocomposite samples containing 2-phr clay with different MMA and P(MMA/S) contents were prepared. The addition of MMA and P(MMA/S) resulted in an increase in the size of particles without significant change in interparticle distance. Therefore, an interesting correlation between the microstructure and fracture toughness was observed, where the best ratio of the particle size to interparticle distance (r/c), in a range between 0.2 and 0.3, was found to achieve the maximum improvement in fracture toughness (about 65%). In addition to this outstanding improvement in fracture toughness, a slight improvement in the T_g and elastic modulus were achieved.

In the case of unsaturated polyesters, mechanisms in which localized yielding of the matrix do not play any important role in energy dissipation and consequently in the efficiency of the mechanism, like crack pinning, are more effective for improving fracture toughness.

7.2. Contributions

During this research, various aspects of unsaturated polyester toughening were studied. Most findings and results could be useful for different toughening techniques of thermosets.

For the first time, the effect of the nanostructure of organoclay nanocomposites based on UPs on fracture toughness was explored. In the literature, mainly chemical treatments were applied to improve the degree of clay dispersion and distribution, normally without reporting the final fracture toughness property. We applied different mechanical mixing methods to achieve different nanostructures. We found out that the characteristic and chemical structure of the thermoset matrix determine the efficiency of toughening techniques based on nano-reinforcements.

For improving the fracture toughness of unsaturated polyesters, we proposed that toughening techniques in which localized yielding of the matrix has a smaller role in the efficiency of the mechanism controlling fracture toughness are more successful. Therefore, we introduced a novel ternary hybrid system, containing a polymeric dispersed phase with suitable mechanical properties (fracture toughness and stiffness) and appropriate interfacial adhesion with the matrix. The obtained thermoplastic-rich domains have properties between brittle organic thermoplastics and rigid inorganic particulate fillers, which is favourable for the crack pinning mechanism. In addition, our technique involves feasible preparation procedures, where all raw reactants are typically used in commercial general purpose UPRs.

In the case of UPRs, thermoplastics have been widely applied as low profile additives (LPAs) to control volume shrinkage of these resins. While there has been a significant lack of information about the effect of thermoplastics on other properties of UPRs, especially fracture toughness, this study contributes useful information about these aspects of a common thermoplastic that is typically used as an LPA for unsaturated polyester resins.

Recently, ternary systems composed of polymeric additives, inorganic nano-reinforcements, and thermosets have attracted a lot of attention. These systems have synergistic effects to improve different physical and mechanical properties, while the micro- and nano-structures of these systems have very important roles to control final properties. In general, few studies have been done on the morphology of these new systems, and more investigations are required. In this work, precise morphological studies were done on a sample of these ternary systems.

Atomic force microscopy is a powerful instrument for nanostructure and microstructure studies. AFM can give information about local mechanical properties of materials, but is typically used for those materials composed of phases with significantly different viscoelastic properties, like soft rubbers, and rigid materials, like inorganic fillers. In this study, we modified the preparation technique and were able to capture high quality phase images. Section analysis of these images gave valuable information about the local mechanical properties of the ternary system composed of hard materials.

The morphological studies in this work enabled the determination of the role of microstructure characteristics (size and distribution of particles) on the fracture toughness of a ternary system in which crack pinning is the dominant controlling mechanism. In addition, an interesting correlation between microstructure characteristics and fracture toughness was found.

7.3. Recommendations for future work

The following recommendations are proposed based on the present research:

I. In this work, we found that the characteristics of the thermosetting matrix, which are directly dependent upon chemical structure, play an important role in the efficiency of toughening techniques and mechanisms controlling fracture toughness. It would be interesting to further investigate this area by preparing hybrid thermosets, such as a combination of unsaturated polyester and vinylester, which have a similar mechanism of network formation but different localized yielding. Another option is to use a different curing agent change the chemical structure of the network (increasing flexibility) in order to achieve better properties of the matrix.

II. In these new hybrid systems, crack deflection and crack pinning are two mechanisms controlling fracture toughness that can occur simultaneously. Interfacial adhesion strength plays an important role in determining which mechanism has the greater contribution to toughening. Hence, while crack pinning is a more effective mechanism for controlling fracture toughness of unsaturated polyesters, improving interfacial adhesion strength between two phases would be

favorable. For this purpose, living free radical copolymerization of the thermoplastic or chemical treatment of the thermoplastic to make reactive functional groups (like unsaturated double bonds) may be interesting approaches. It would be helpful to estimate interfacial interactions between phases based on surface energies of the components.

III. In unsaturated polyester resins, thermoplastics are typically applied as low profile additives to control fracture toughness. In this research, we introduced these ternary systems to improve fracture toughness. It would be interesting to explore the effect of this toughening additive on volume shrinkage of UPRs.

IV. This technique has a limitation on incorporation of higher clay content due to polydispersity of particle distribution. Therefore, it is strongly recommended that the technique be further developed and modified to improve the distribution of the thermoplastic-rich domains throughout the matrix to achieve greater improvement in fracture toughness.

V. In the literature, few studies reported optimum values for microstructure parameters to achieve the maximum fracture toughness of systems in which crack pinning is the controlling mechanism. Our experimental data are useful to develop theoretical models of the crack pinning mechanism for these polymeric ternary systems.

VI. This technique caused a significant improvement in fracture toughness, even with slight improvement in elastic modulus and T_g. It is interesting to investigate the application of this ternary hybrid system as matrix for fiber-reinforced composites in structural applications. For this purpose, the effect of the toughening agents on the viscosity of the ternary system, as the matrix, must be explored.

7.4. List of publications

- ***Sina Chaeichian****, Paula Wood-Adams, Suong Van Hoa*, "In situ polymerization of polyester-based hybrid systems for the preparation of clay nanocomposites" *Polymer*, Vol. 54, No. 5, pp.1512-1523 (2013).

- ***Sina Chaeichian**, Paula Wood-Adams, Suong Van Hoa*, "Effect of morphology on fracture toughness of thermoplastic/thermoset/clay hybrid nanocomposite", Conference paper at the 19th International Conference on Composite Materials, August 2013, Montreal, Canada.
- ***Sina Chaeichian**, Paula Wood-Adams, Suong Van Hoa*, "Synthesis of a thermoplastic/thermoset hybrid system for the preparation of clay nanocomposite based on unsaturated polyester resins", Conference paper at the 15th European Conference on Composite Materials, May 2012, Venice, Italy.
- The submission of three more journal papers is planned.

Appendix

A1. Other mixing methods

Two other mixing methods are (i) mixing by a high speed mixer machine, (ii) alternative SHM where the order of mixing steps is changes compared to SHM.

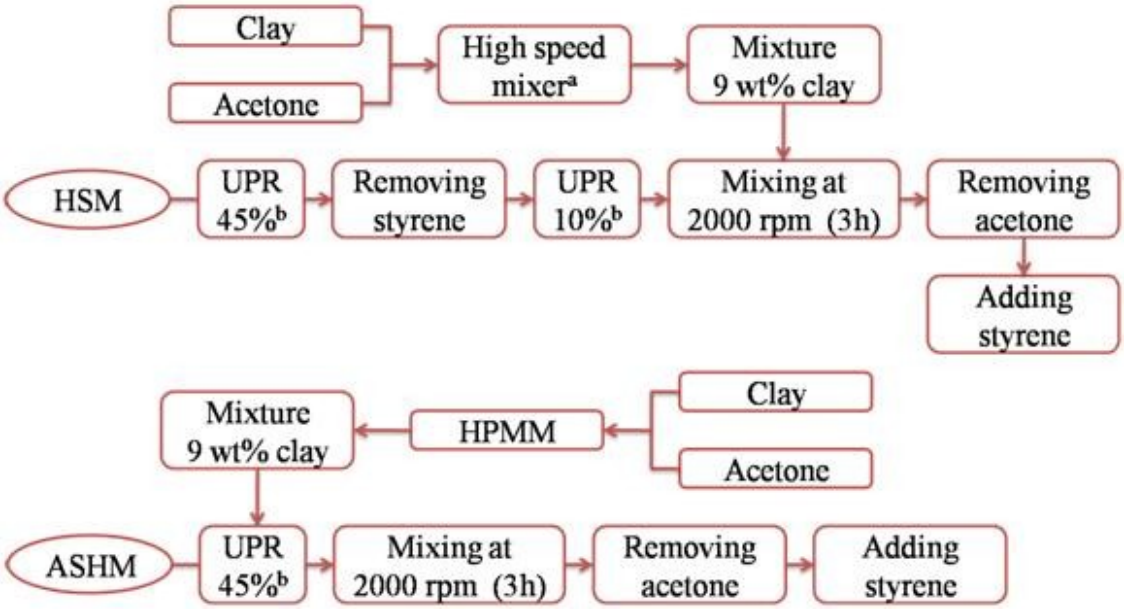

Fig.A1.1. Preparation procedures. HSM: high speed mixer method; ASHM: alternative solvent-aided high-pressure method.

[a] shear rate was increased step by step (5000, 10000, 15000, 20000), where each step was about 15 min with a rest time for 20 min between each step

[b] Weight percentage of styrene in the resin.

A2. Effect of clay on the total degree of cure

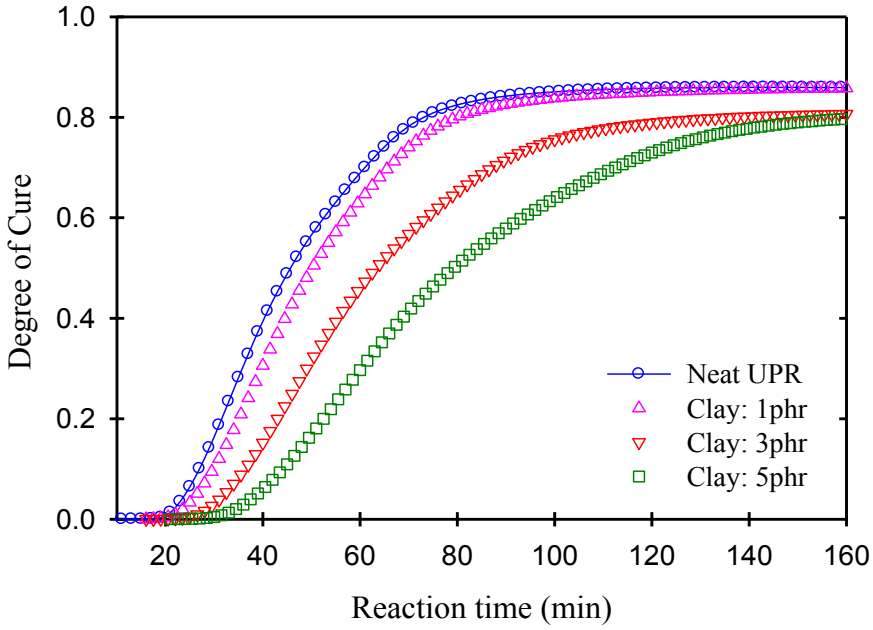

Fig. A2.1. Effect of clay loading on the total degree of cure.

A3. DMA results, loss modulus

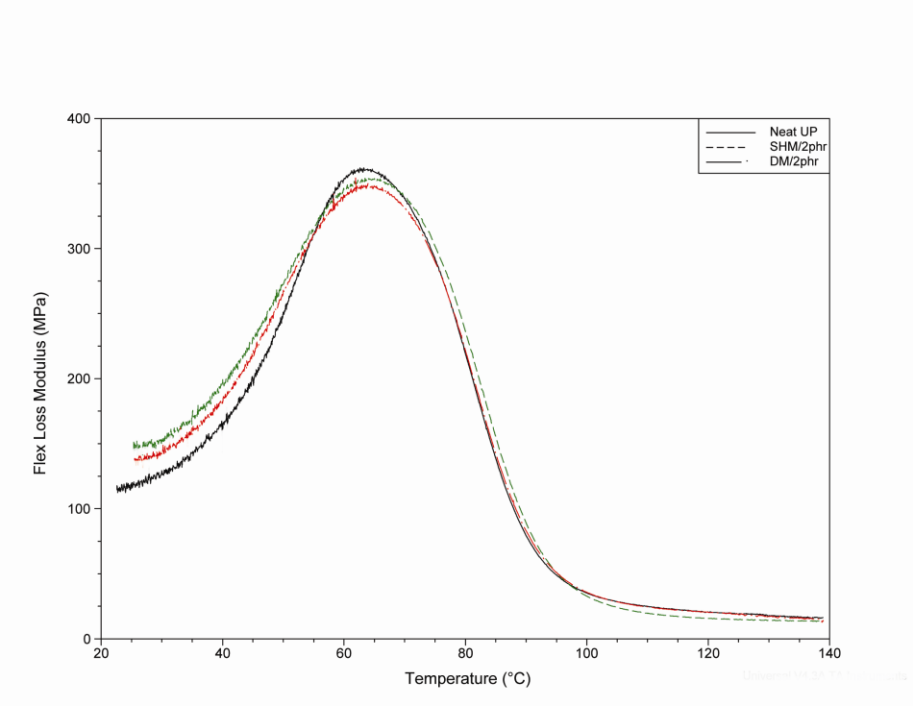

Fig. A3.1. Effect of clay loading on loss modulus (glass transition temperature)

A4. Fracture toughness of samples prepared by HSM and ASHM

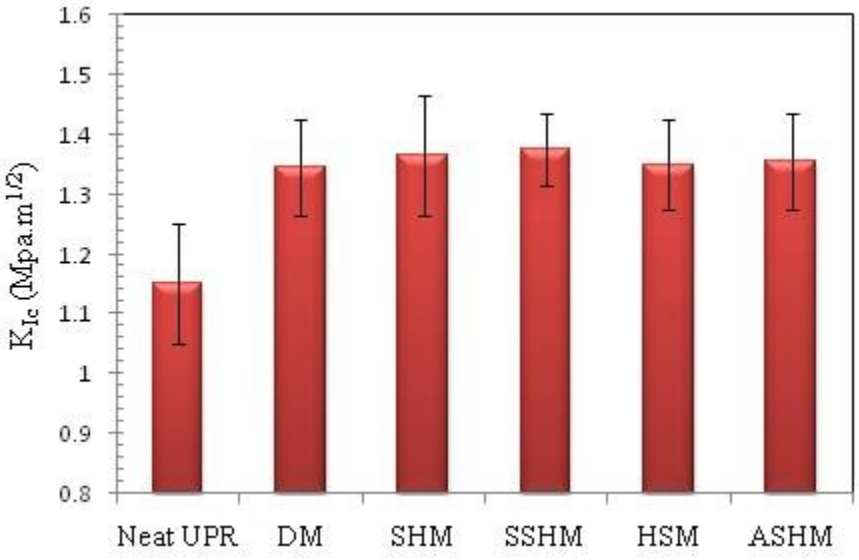

Fig. A4.1. Fracture toughness K_{Ic} as a function of mixing method. Nanocomposite samples contain 2phr cloisite 20A, DM: direct method, SHM: solvent-aided high pressure mixing method, SSHM: SHM followed by sonication, HSM: high speed mixer machine method, ASHM: alternative SHM.

A5. Comparison between Cloisite 20A and 30B

Table. A5.1. Properties of organically modified clay

Commercial name	Organic modifier	Density (g/cc)	d spacing (nm)
Cloisite 20A	$CH_3 - N^+(CH_3)(HT)(HT)$	1.77	2.42
Cloisite 30B	$CH_3 - N^+(CH_2CH_2OH)(CH_2CH_2OH)(T)$	1.98	1.85

HT: Hydrogenated Tallow (~65% C18; ~30% C16; ~5% C14)

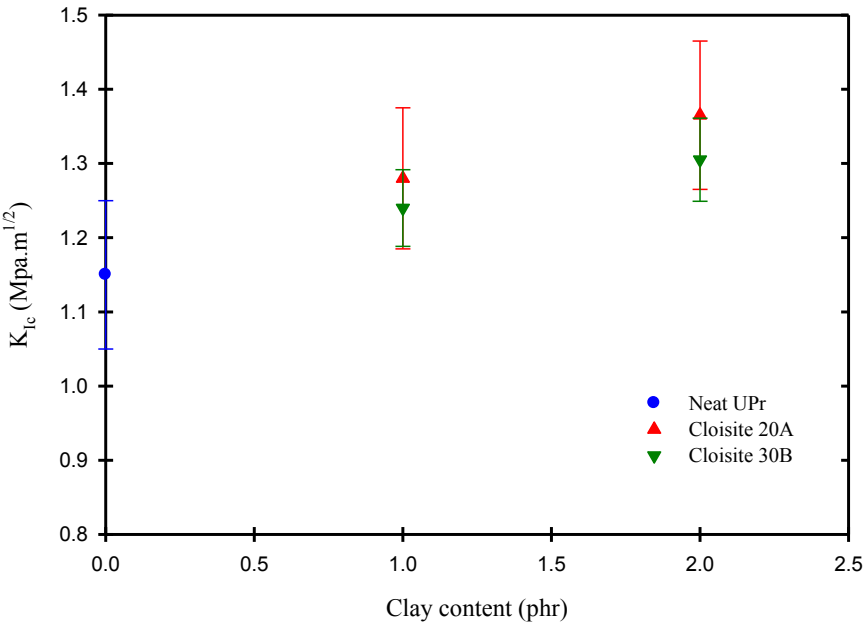

Fig. A5.1. Fracture toughness K_{Ic} as a function of clay content (phr) and clay type. All samples were prepared by SHM: solvent-aided high pressure mixing method.

A6)Chemical reactions during curing

To evaluate the effect of MMA content on the curing process in a hybrid system, for each clay content (1, 2, 3 phr), four MMA/St ratios (0.1, 0.2, 0.3, and 0.4) were used. Figures A4.1-3 show the effect of MMA content on the total reaction rate and degree of cure (presented in parentheses) for hybrid nanocomposites with different clay loading. The addition of MMA slightly increased the induction time, where in higher clay loading the increase is more substantial. The change in the total reaction rate due to different MMA contents is negligible, and the final degree of cure is also independent of MMA content.

Figure A4.4-7 shows the effect of clay loading on the total reaction rate and degree of cure. The addition of clay caused a slight reduction in both characteristics regardless of MMA content. The change in the degree of cure is not significant, indicating that crosslink density likely was not changed by varying these parameters.

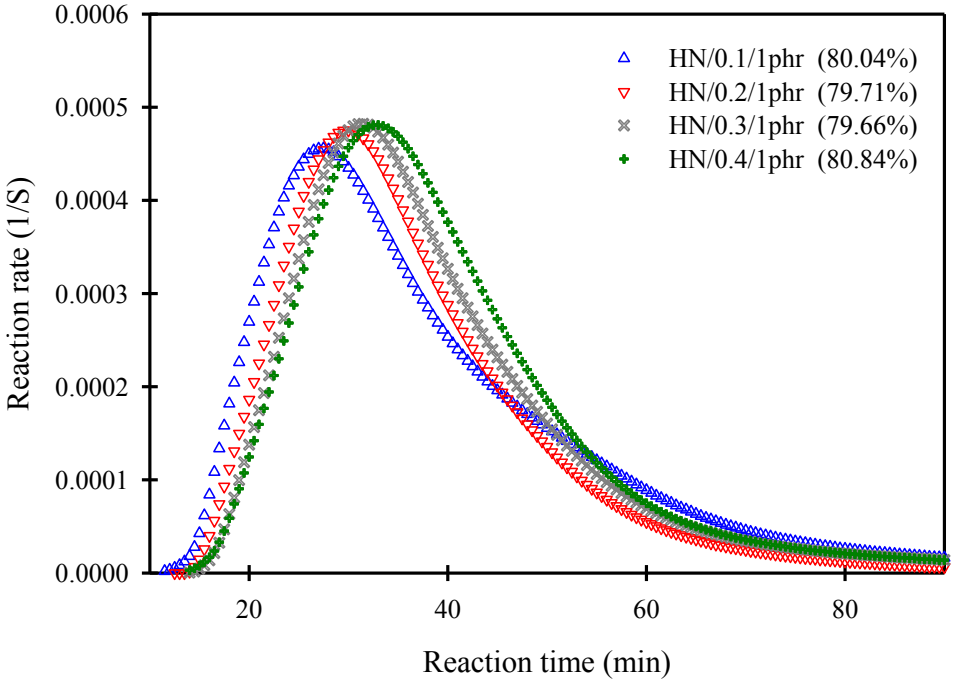

Fig.A6.1. Effect of MMA on curing rate of hybrid nanocomposites containing 1phr clay.

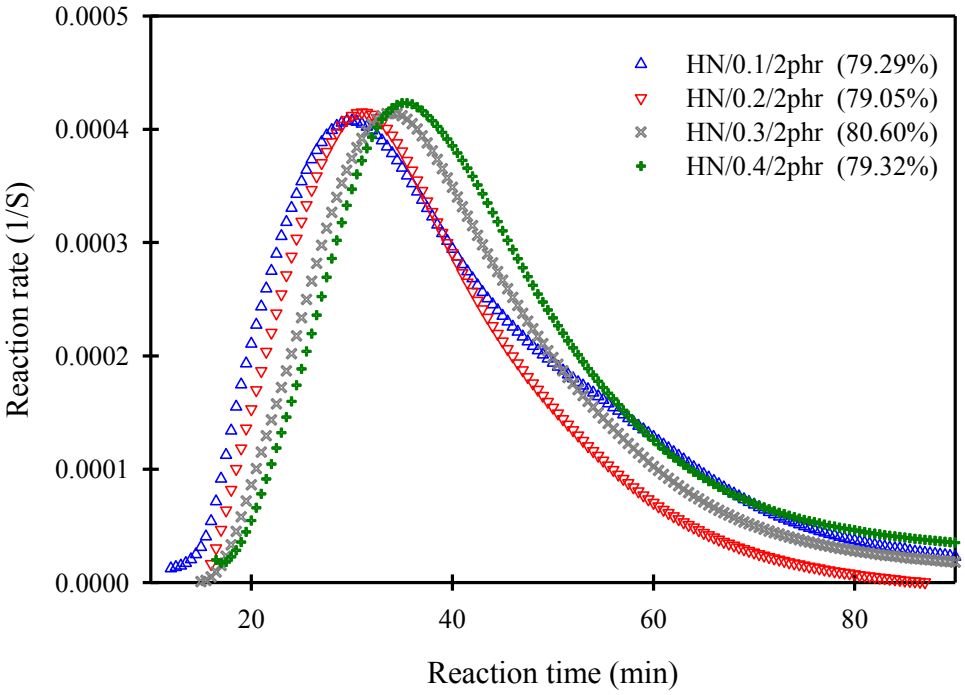

Fig.A6.2. Effect of MMA on curing rate of hybrid nanocomposites containing 2phr clay.

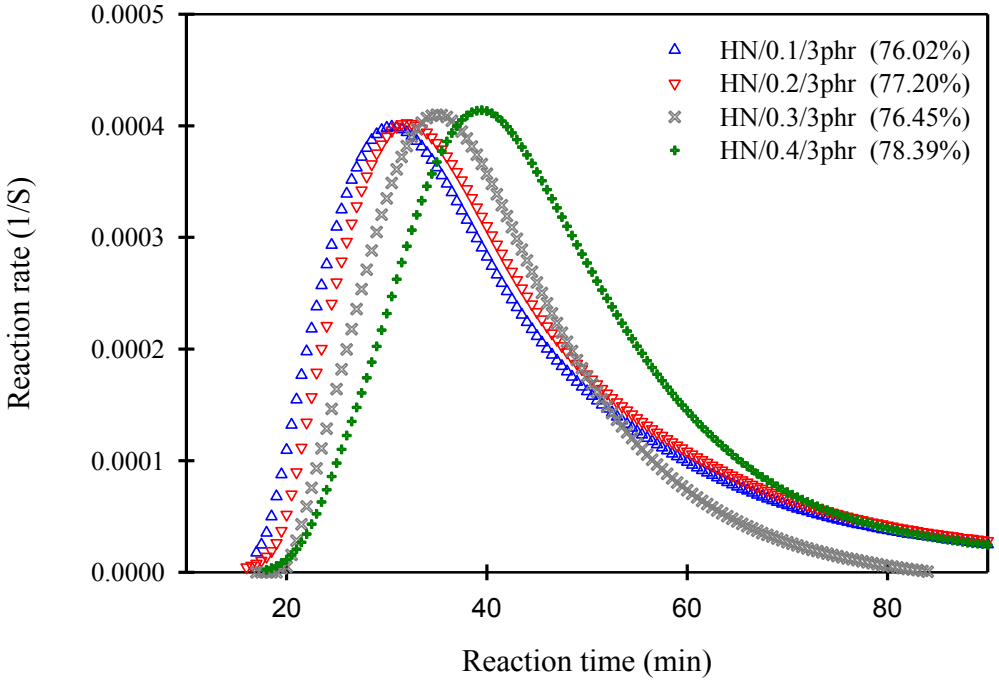

Fig. A6.3. Effect of MMA on curing rate of hybrid nanocomposites containing 3phr clay.

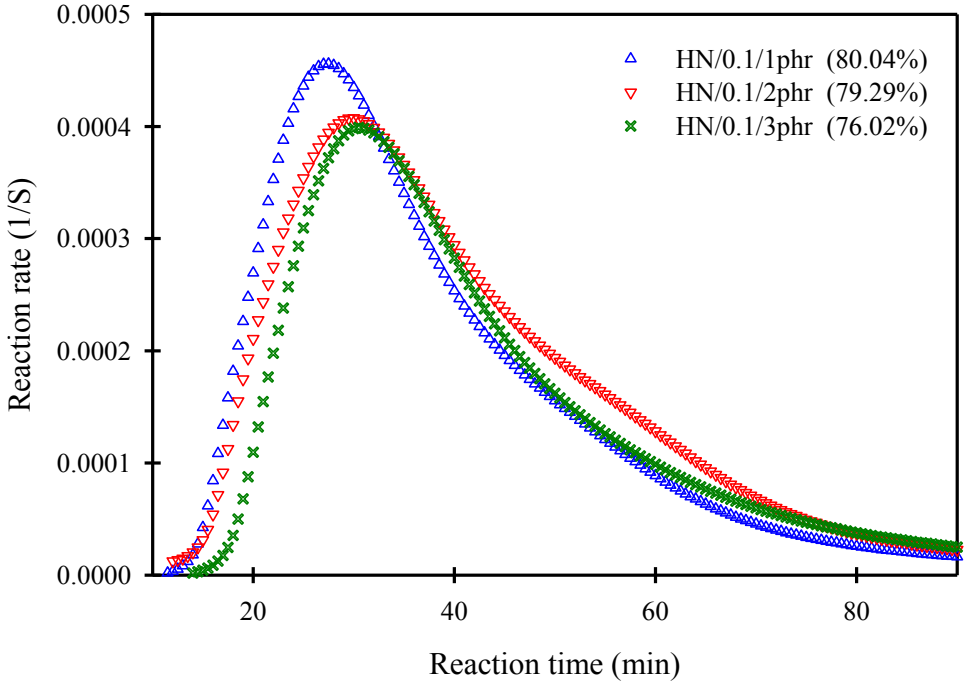

Fig. A6.4. Effect of clay on curing rate of hybrid nanocomposites with MMA/st:0.1, 7wt% P(MMA/S)).

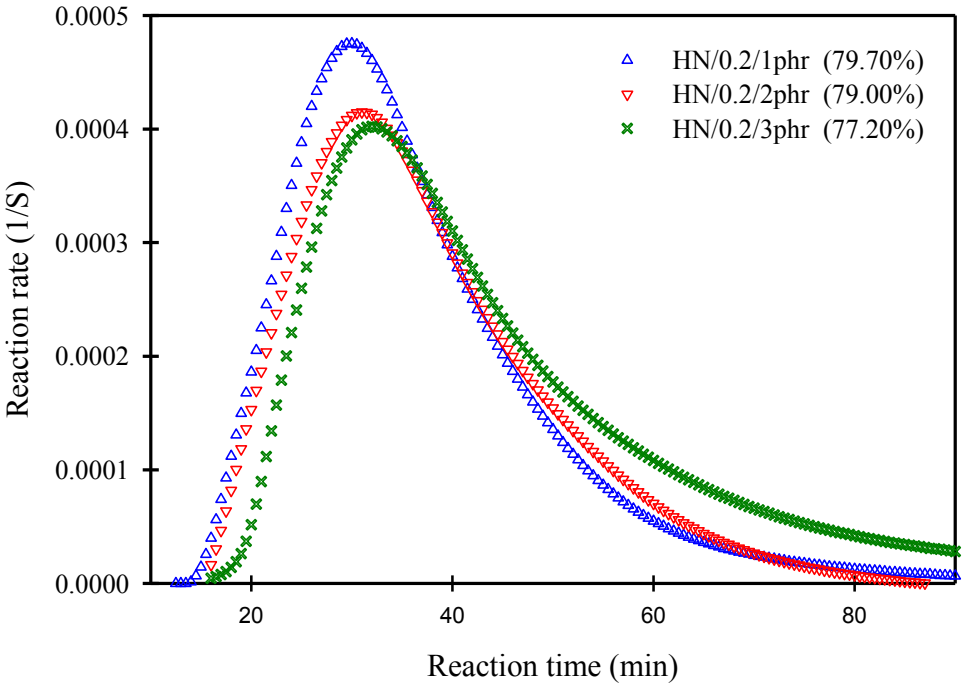

Fig. A6.5. Effect of clay on curing rate of hybrid nanocomposites with MMA/st:0.2, 7wt% P(MMA/S)).

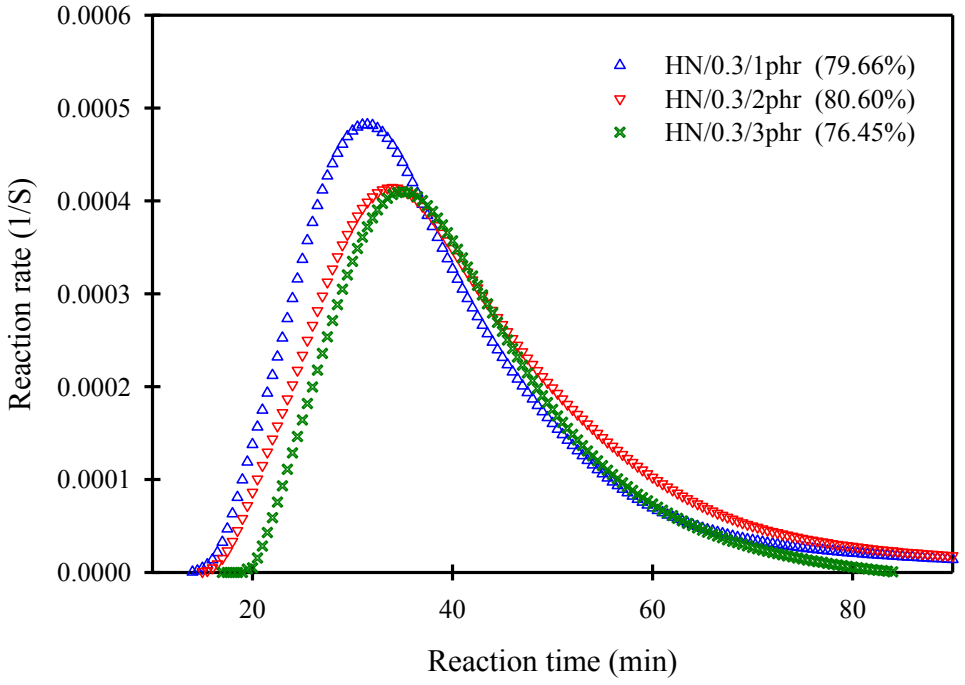

Fig. A6.6. Effect of clay on curing rate of hybrid nanocomposites with MMA/st:0.3, 7wt% P(MMA/S)).

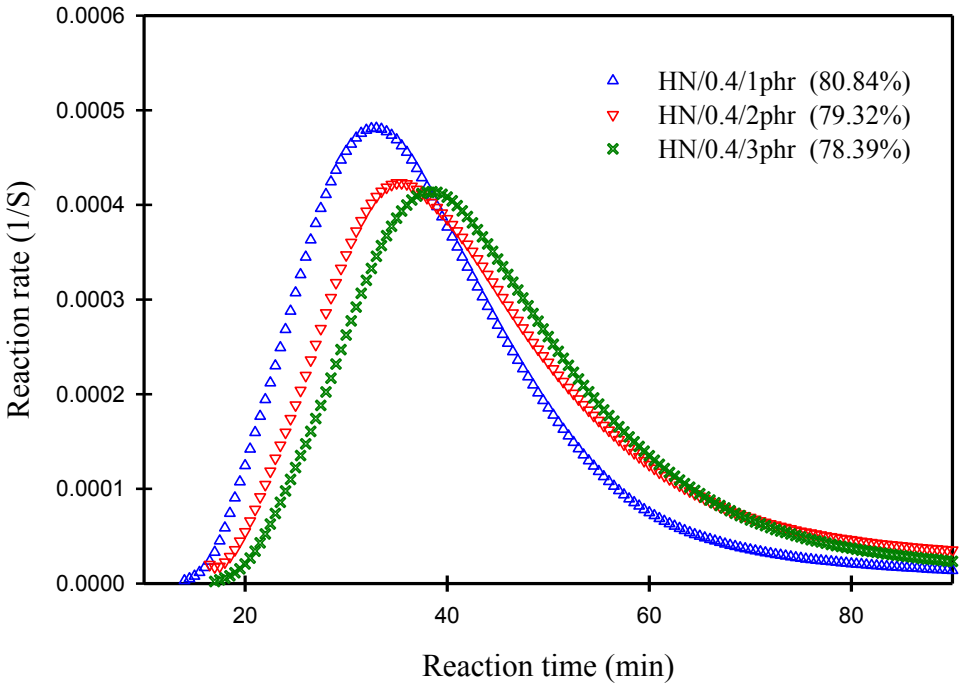

Fig. A6.7. Effect of clay on curing rate of hybrid nanocomposites with MMA/st:0.4, 7wt% P(MMA/S)).

A7)Tensile properties of hybrid nanocomposites

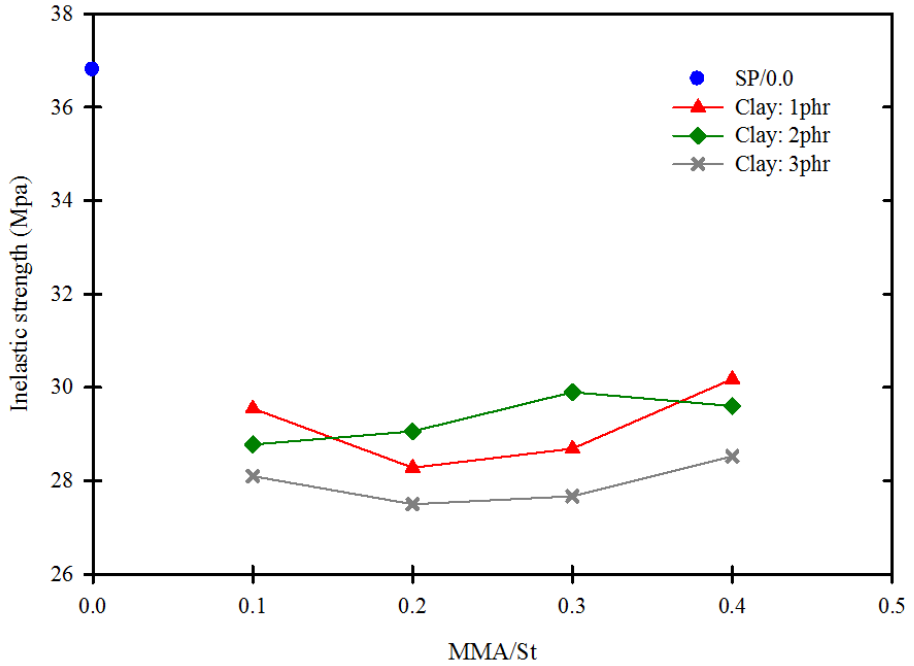

Fig. A7.1. Effect of MMA content on inelastic strength of hybrid nanocomposites with different clay contents (all samples contain 7wt% P(MMA/S)).

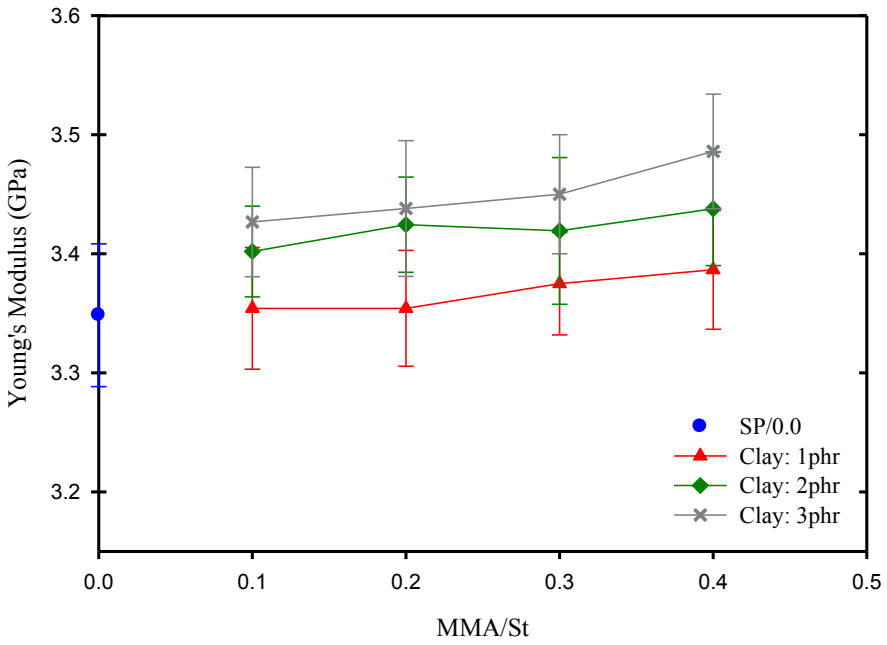

Fig. A7.2. Effect of MMA on elastic modulus of hybrid nanocomposites with different clay contents (all samples contain 7wt% P(MMA/S)).

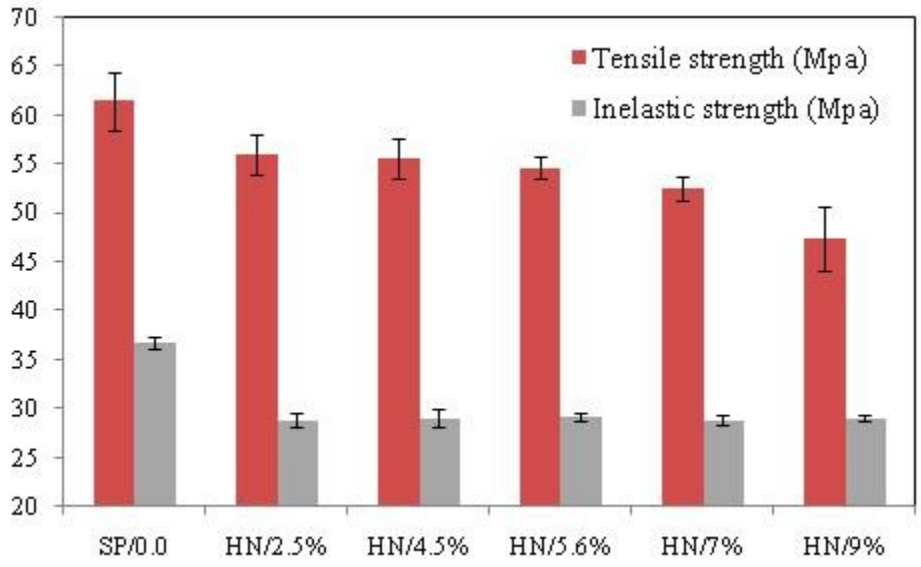

Fig. A7.3. Effect of thermoplastic mass on tensile strength and inelastic strength (hybrid nanocomposites, HN, contain 2-phr clay with MMA/St_{CA}=0.2).

A8) Effect of gel time on fracture toughness

The synthesis process variables can change the gel time which may affect fracture toughness by changing the size of the final thermoplastic-rich particles. For this purpose, we added hydroquinone as an inhibitor (1000 ppm) to increase the gel time. The inhibitor was added to the mixtures of UPR and the copolymerization product, containing different MMA, clay, and P(MMA/S) content, before curing.

Figures A6.1 and A6.2 show the reaction rate during room temperature curing of two hybrid nanocomposite samples, (HN/0.1/2phr/4.5wt%) and (HN/0.2/2phr/5.6wt%), respectively. The addition of 1000 ppm hydroquinone significantly increased the induction time and the gel time via reducing the reaction rate. Although a large amount of the inhibitor is used, the final degree of cure was not significantly changed to affect fracture toughness.

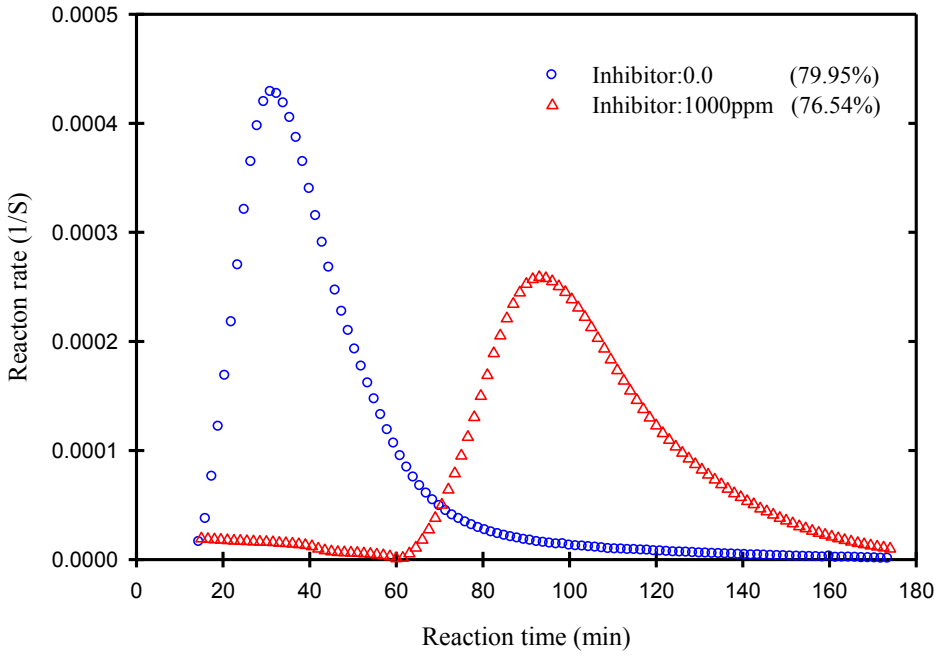

Fig.A8.1. Effect of hydroquinone on the reaction rate of a hybrid nanocomposite sample containing 2phr clay and 4.5wt% P(MMA/S) with MMA/St_{CA}:0.2.

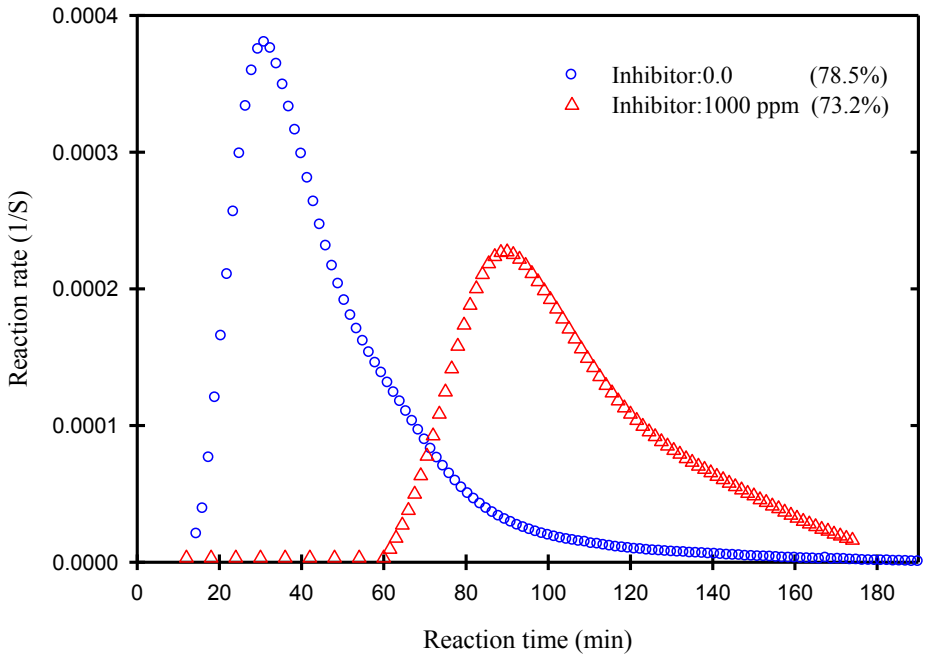

Fig.A8.2. Effect of hydroquinone on the reaction rate of a hybrid nanocomposite sample containing 2phr clay and 5.6wt% P(MMA/S) with MMA/St_{CA}:0.1.

Table A8.1. Effect of inhibitor on K_{Ic} and particle diameter

Sample	Hydroquinone (ppm)	Particle diameter (μm)	K_{Ic} (Mpa.m$^{1/2}$)
HN/0.1/2phr/4.5wt%	0.0	2.0 (0.7)	1.39 (0.04)
HN/0.1/2phr/4.5wt%	1000	2.11 (0.6)	1.40 (0.05)
HN/0.1/2phr/5.6wt%	0.0	2.95 (0.9)	1.52 (0.05)
HN/0.1/2phr/5.6wt%	1000	3.05 (0.8)	1.55 (0.06)
HN/0.1/3phr/7wt%	0.0	9.24 (2.5)	1.56 (0.09)
HN/0.1/3phr/7wt%	1000	9.10 (2.1)	1.51 (0.08)
HN/0.2/2phr/5.6wt%	0.0	3.07 (1.1)	1.58 (0.03)
HN/0.2/2phr/5.6wt%	1000	2.94 (1.0)	1.54 (0.05)
HN/0.2/3phr/7wt%	0.0	10.48 (3.5)	1.59 (0.07)
HN/0.2/3phr/7wt%	1000	10.60 (3.8)	1.54 (0.06)

[a] The last number represents the mass fraction of P(MMA/S).
[b] The values in parentheses are standard deviations of the property.

The gel time can influence the particle size by affecting the available time for the diffusion of different constituents (especially unsaturated polyester) out of the dispersed phase during quiescent conditions. Since the presence of clay silicate layers in the thermoplastic-rich phase restricts the diffusion of the constituents out of the thermoplastic-rich phase during quiescent conditions and curing process, the gel time did not significantly affect the final size of the particles and consequently fracture toughness (Table A6.1).

A9) Effect of the synthesis process variables on fracture toughness

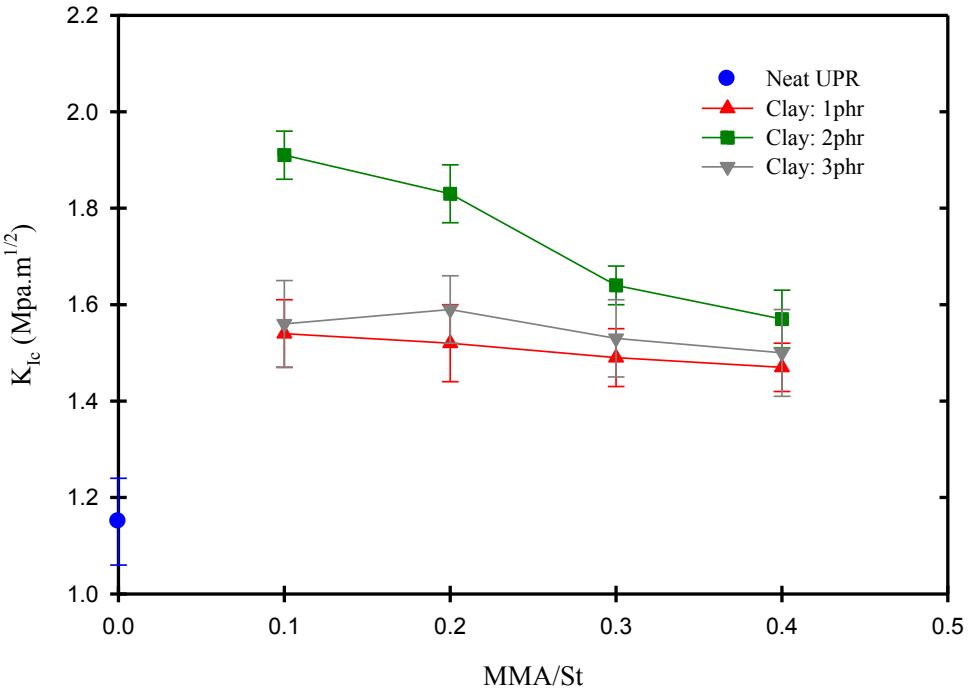

Fig. A9.1. Effect of clay and MMA content on fracture toughness
(All hybrid nanocomposite samples contain 7wt% P(MMA/S)).

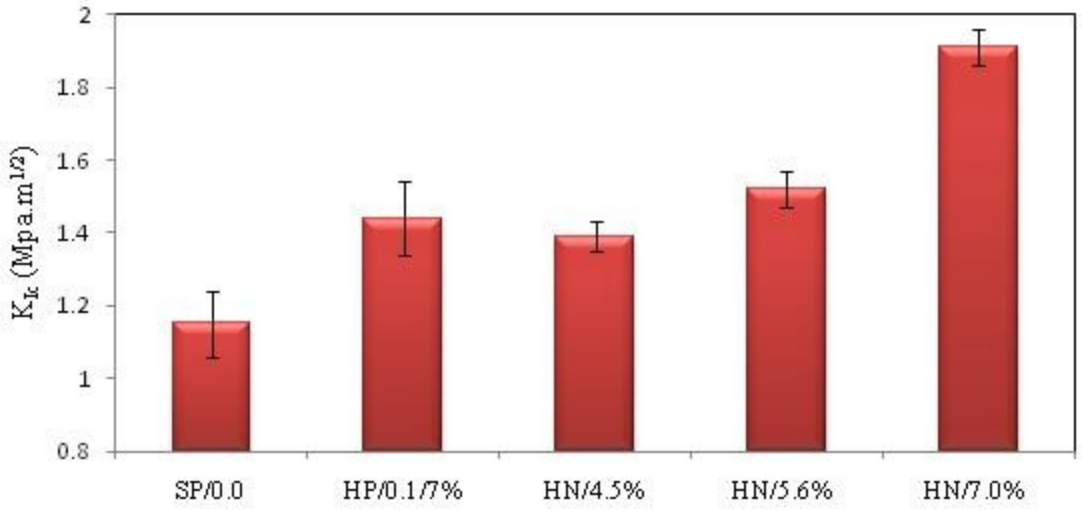

Fig. A9.2. Effect of the thermoplastic content on fracture toughness (All hybrid nanocomposite samples contain 2-phr clay with MMA/St_{CA}:0.1).

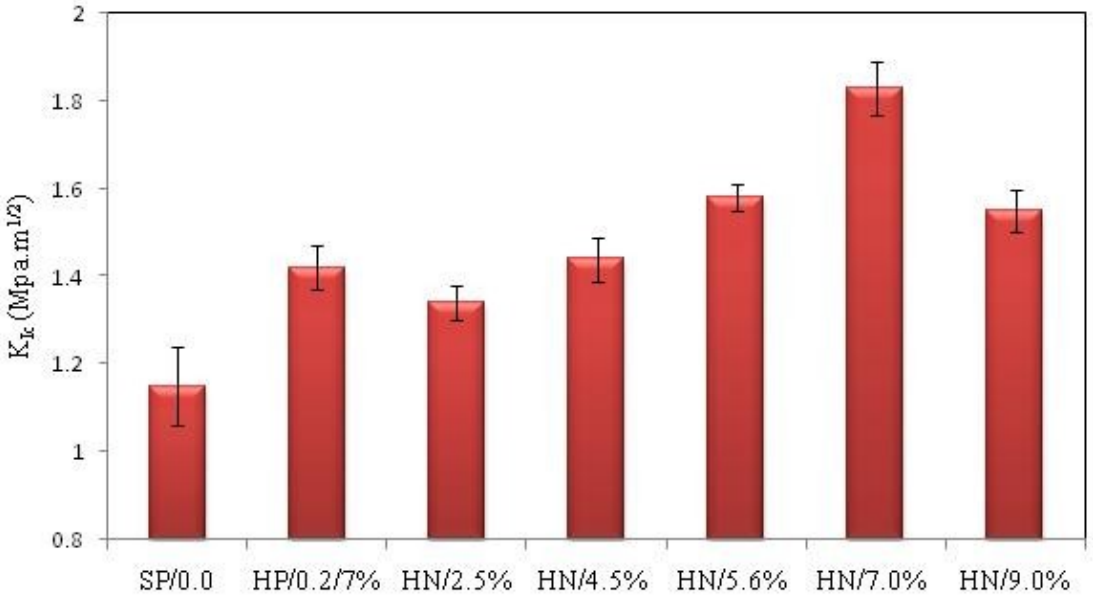

Fig. A9.3. Effect of the thermoplastic content on fracture toughness (All hybrid nanocomposite samples contain 2-phr clay with MMA/St_{CA}:0.2).

A10) Relationship between the particle size and K_{Ic}

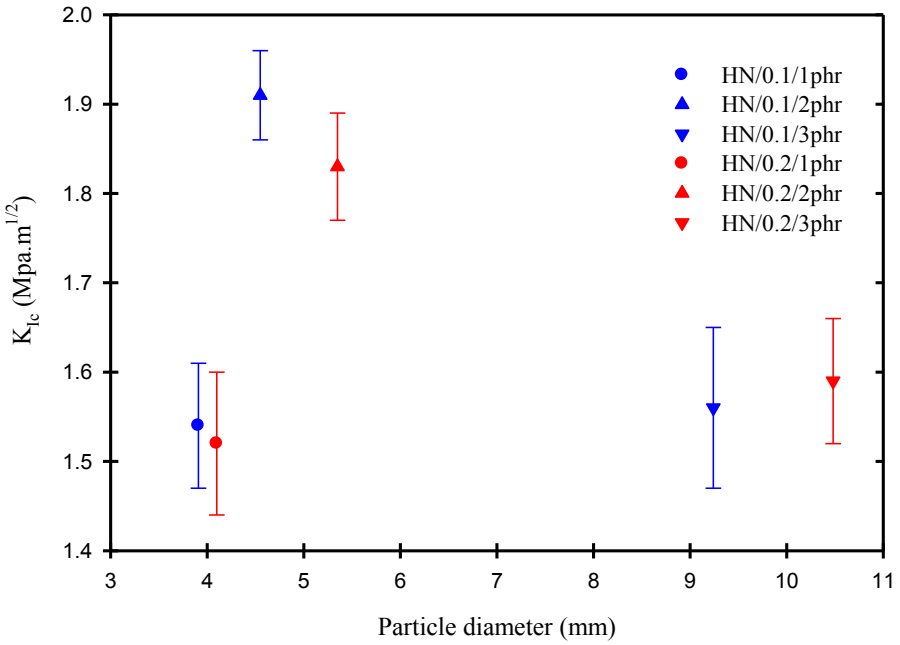

Fig. A10.1. K_{Ic} vs. the particle diameter. The size of particles is a function of clay and MMA content (wt%). (all samples contain 7wt% P(MMA/S)).

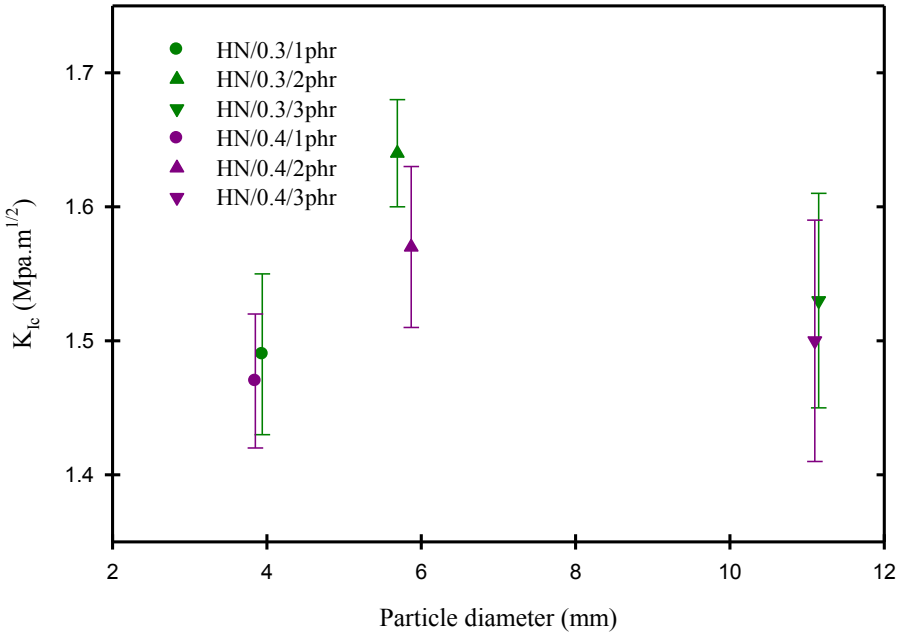

Fig. A10.2. K_{Ic} vs. the particle diameter. The size of particles is a function of clay and MMA content (wt%). (all samples contain 7wt% P(MMA/S)).

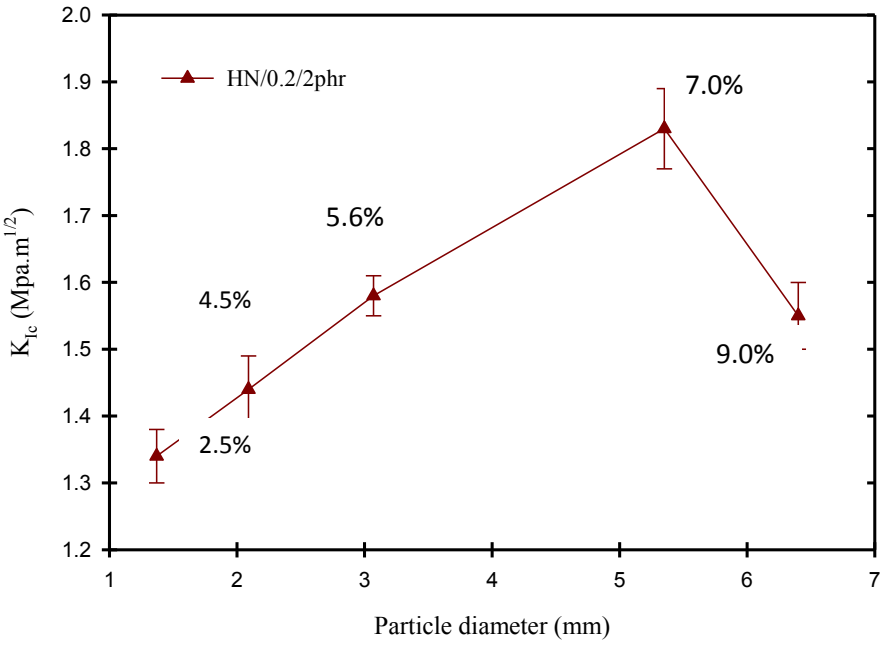

Fig. A10.3. K_{Ic} vs. particle diameter. The size of particles is changed by varying the thermoplastic mass (wt%).

A11) Relationship between the interparticle distance and K_{Ic}

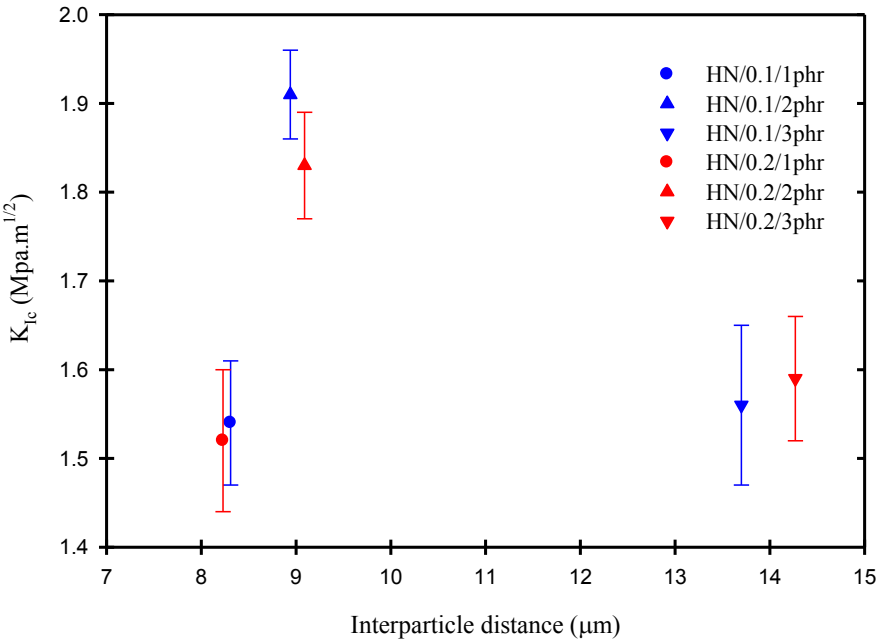

Fig. A11.1. K_{Ic} vs. the interparticle distance . The size of particles is a function of clay and MMA content (wt%). (all samples contain 7wt% P(MMA/S)).

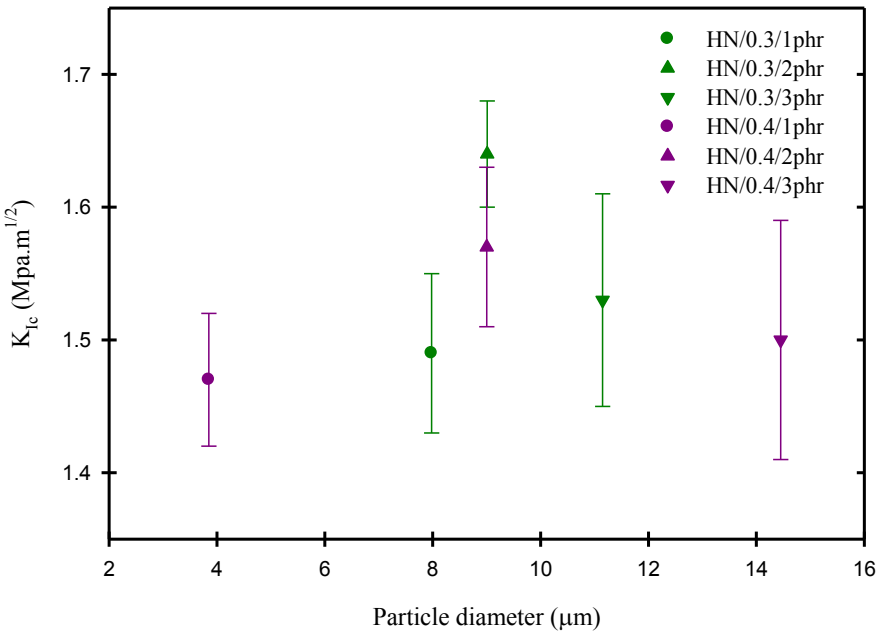

Fig. A11.2. K_{Ic} vs. the interparticle distance . The size of particles is a function of clay and MMA content (wt%). (all samples contain 7wt% P(MMA/S)).

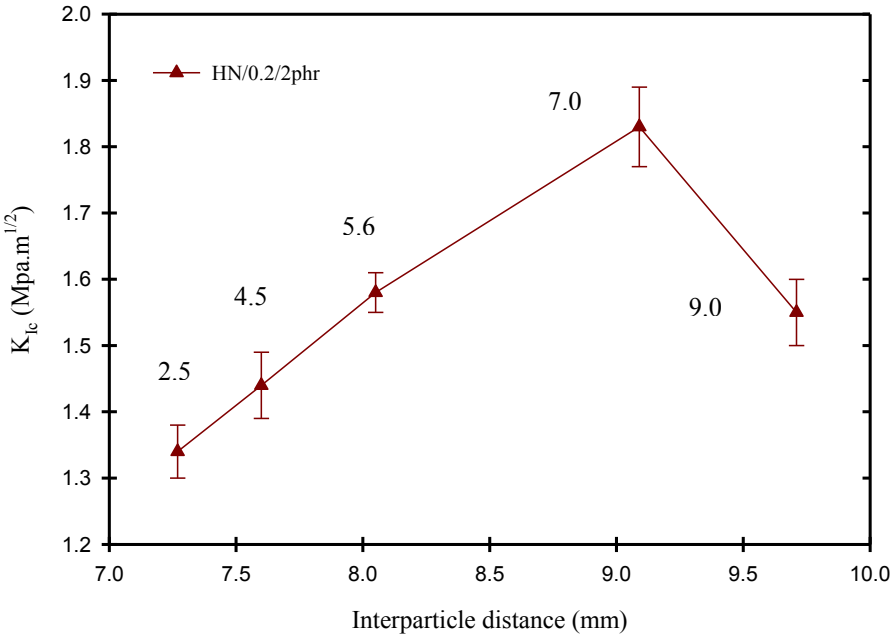

Fig. A11.3. A relationship between K_{Ic} and the interparticle distance.

References

[1] J. Scheirs, T.E. Long, , Modern Polyester: Chemistry and Technology of Polyesters and Copolymers, John Wiley and Sons, Ltd, (2003)

[2] Y. S. Yang, L. J. Lee, Polymer, Vol:22, No. 10, pp.1793-1800 (1988)

[3] J. C. Lucas, J. Borrajo. R. J. J. Williams, Polymer, 34, 15, pp. 3316-3319 (1993)

[4] P. Eisenberg, J.C. Lucas, R. J. J. Williams, Journal of Applied polymer Science, Vol. 65, pp. 755-760 (1997)

[5] X. Ramis, J. M. Salia, Journal of Polymer Science: Part B; Polymer Physics, Vol. 37, pp. 751-768 (1999)

[6] H. Yang, L. J. Lee, Journal of Applied Polymer Science, Vol. 84, pp. 211-227 (2002)

[7] L. Li, X. Cao, J. Lee, Polymer, Vol. 45, pp. 6601-6612 (2004)

[8] Y. J. Huang, C. J. Chen, Journal of Applied Polymer Science, Vol. 48, pp. 151-165 (1993)

[9] B. Mortaigne, B. Vivien, Polymers for Advanced Technologies, Vol. 7, pp. 813-821 (1996)

[10] I. M. Harpaz, M. Narkis, Macromolecule Symposium, Vol. 242, pp.201-207 (2006)

[11] X. Ramis, J. M. Salia, Polymer, Vol.36, No.18, pp.3511-3521 (1995)

[12] L. Li, J. J. Lee, Polymer Engineering and Science, Vol.41, No.1, pp. 53-65 (2001)

[13] X. Cao, L.J. Lee, Polymer, Vol.44, No. 5, pp.1507-1516 (2003)

[14] J. C. Lucas, J. Borrajo, R. J. J. Williams, Polymer, Vol. 24, No. 15, pp. 3216-3219 (1993)

[15] P. Eisenberg, J. C. L. Roberti, J. J. Williams, Journal of Applied Polymer Science, Vol. 65, No. 4, pp. 755-760 (1997)

[16] L. E. Nielsen, Journal of Macromolecular Science, Part C: Polymer Reviews, Vol. 3, No.1, pp. 69-103 (1969)

[17] Y. J. Huang, L. D. Chen, Polymer, Vol. 39, No.26, pp. 7049-7059 (1998)

[18] M. G. Lua, M .J. Shimb, S. W. Kim, Thermochimica Acta, Vol.323, No.1-2, pp.34-72 (1998)

[19] C. P. Hsu, L. J. Lee, Polymer, Vol. 34, No. 21, pp. 4496-4505 (1993)

[20] C. P. Hsu, L. J. Lee, Polymer, Vol. 34, No.21, pp. 4516-4523 (1993)

[21] H. Yu, S. G. Mhaisalkar, E. H.Wong, Macromolecular rapid communications, Vol. 26, pp. 1483-1487 (2005)

[22] R. P. Singh, M. Zhang,D. Chan, Journal of Materials Science, Vol. 37, No. 4, pp. 781-788 (2002)

[23] J. E. Mark, Polymer data handbook, Oxford university press, Inc. 1999

[24] G. E. Dieter, Mechanical Metallurgy, McGraw Hill Boston, 3rd edition(1986)

[25] J. G. Williams, Stress Analysis of polymers, John Wiley and Sons, 2nd edition (1980)

[26] A. J. Kinloch, R. J. Young, Fracture Behaviour of Polymers, Applied Science Publishers (1983)

[27] J. P. Pascault, H. Sautereau, J. Verdu, R.J. J. Williams, Thermosetting Polymers, Marcel Dekker Inc. (2002)

[28] D. Williams, Jr. Callister, Materials Science and Engineering: An Introduction, John Wiley and Sons, Inc. 6th edition (2003)

[29] H. J. Sue, Polymer Engineering and Science, Vol:36, No:18, page:2320(1996)

[30] A. E. Mayr, W. D. Cook, D. H. Edward, Polymer, Vol. 39, No.16, pp. 3719 (1998)

[31] A. J. Kinloch, S. J. Shaw, D. A. Tod, Polymer, Vol. 24, No. 10, pp. 1341-1354 (1993)

[32] G. D. Smith, D. Bedrov, Journal of polymer science: Part B: Polymer Physics, Vol. 45, pp. 627 (2007)

[33] H. J. Sue, Journal of materials science, Vol. 27, pp. 3098-3107 (1992)

[34] L. Suspene, Y. S. Yang, J. P. Pascault, Advances in Chemistry, Vol. 233, pp.163-188 (1993)

[35] L. H. Sperling, Introduction to Physical Polymer Science, John Wiley and Sons, Inc. 4th edition (2006)

[36] C. K. Riew, A. J. Kinloch, Toughened Plastic I: Science and Engineering, Advances in Chemistry Series233,American Chemical Society, Washengton, DC (1993)

[37] S. H. Liu, E. B. Nauman, Journal of Materials Science, Vol. 25, pp. 2071-2076(1990)

[38] J. N. Goodier, Journal of Apllied Mechanics, Vol. 55, No.1, pp. 39-44 (1933)

[39] A. B. Cherian, E. T. Thachil, Polymer-Plastics Technology and Engineering, Vol. 44, No. 3, pp. 391-405 (2005)

[40] H. J. Sue, Polymer engineering and science, Vol:36, No18, pp. 2320 (1996)

[41] D. S. Kim, K. Cho, J. H. An, C. E. Park, Journal of Materials Science, Vol. 29, No. 7, pp.1854-1866 (1994)

[42] M. Abbate, E. Martuscelli, P. Musto, G. Ragosta, M. Leonardi, Journal of Applied Polymer Science, Vol.62, No. 12, pp. 2107-2119 (1996)

[43] E. Martuscelli, P. Musto, C. Ragosta, C. Scarinzi, E. Bertotti, Journal of Polymer Science: Part B: Polymer Physics, Vol. 31, pp. 619-632 (1993)

[44] G. Ragosta, M. Bombace, E. Martuscelli, P. Musto, P. Russo, G. Scarinzi, Journal of Materials Sicence, Vol. 34, No. 5, pp. 1037-1044(1999)

[45] M. L. L. Maspoch, A. B. Martines, Polymer Engineering and Science, Vol. 38, No.2, pp. 290-298(1998)

[46] S. Balakrishnan, P. R. Start, D. Raghavan, S. D. Hudson, Polymer, Vol. 46, pp. 11255-11262 (2005)

[47] B. Cherian, A. Thachil, E. T. Thachil, Progress in Rubber and Plastics Technology, Vol. 17, No. 4, pp. 205-224 (2001)

[48] Y. J. Huang, J. H. Wu, J. G. Liang, M. W. Hsu, J. K. Ma, Journal of Applied Polymer Science, Vol. 107, pp. 939-950 (2008)

[49] M. Ahmadi, M. R. Moghbeli, M. M. Shokrieh, Polymer Engineering and Science, Vol. 52, No. 9, pp. 1928-1937 (2012)

[50] S. Guhanathan, M. S. Devi, Journal of Applied Polymer Science, Vol. 94, pp. 511-528 (2004)

[51] D. A. Norman, R. E. Robertson, Polymer, Vol. 44, pp. 2351-2362, (2003)

[52] F. F. Lange, Philosophical . Magazine. Vol. 22, pp. 983 (1970)

[53] A. G. Evans, Philosophical. Magazine. Vol. 26, pp. 1327 (1972)

[54] J. Spanoudakis, R. J. Young, Journal of Materials science, Vol. 19, pp. 473-486 (1984)

[55] F.F. Lange, K. C. Radford, Journal of Materials Science, Vol. 6, pp. 1197 (1971)

[56] L. R. F. Rose, Mechanics of Materials, Vol. 6, pp. 11-15 (1987)

[57] J. Lee, A. F. Yee, Polymer, Vol. 42, No. 2, pp. 589-597(2001)

[58] K. T. Faber, A. G. Evans, Acta metal, Vol. 31, No. 4, pp. 565-576 (1983)

[59] V. V. Kozii, B. A. Rozenberg, Advances in Polymer Science, Vol. 72, pp. 45-67 (1985)

[60] C. B. Bucknall, I. K. Partridge, M. J. Philips, Polymer, Vol. 32, No. 5, pp. 786-790 (1991)

[61] Y. J. Huang, J. C. Horng, Polymer, Vol. 39, No. 16, pp. 3683-3695 (1996)

[62] Y. J. Huang, S. C. Lee, J. P. Dong, Vol. 78, No. 3, pp. 558-568 (2000)

[63] J. P. Dong, J. H. Lee, D. H. Lai, Y. J. Huang, Journal of Applied Polymer Science, Vol. 100, pp. 867-878 (2006)

[64] W. Li, L. J. Lee, Polymer, Vol. 39, No. 23, pp. 5677-5687 (1998)

[65] C. P. Hsu, M. Kinkelaar, P. Hu, L. J. Lee, Polymer Engineering and Science, Vol. 31, No. 20, pp. 1450-1460 (1991)

[66] L. Suspene, D. Fourquier, Y. S. Yang, Polymer, Vol. 32, No. 9, pp. 1593-1604 (1991)

[67] W. Li, L. J. Lee, K. H. Hsu, Polymer, Vol. 41, No. 2, pp. 711-717 (2000)

[68] W. Li, L. J. Lee, Polymer, Vol. 41, No. 2, pp. 697-710 (2000)

[69] M. Haider, P. Hubert, L. Lessard, Composites: Part A: Applied Science and Manufacturing, Vol. 38, No. 3, pp. 994-1009 (2007)

[70] W. Li, L. J. Lee, Polymer, Vol. 41, No. 2, pp. 685-696 (2000)

[71] A. C. Moloney, H. H. Kausch, T. Kaiser, H. R. Beer, Journal of Materials Science, Vol. 22, No. 2, pp. 381-393 (1987)

[72] M. Hernandez, J. D. Rumeau, H. Sautereau, Journal of Applied Polymer Science, Vol. 118, pp. 3632-3642 (2010)

[73] K. B. Su, N. P. Suh, Society of Plastics Engineers, Vol. 27, pp. 46 (1981)

[74] J. Lee, A. F. Yee, Polymer, Vol. 42,No. 2, pp. 577-588(2001)

[75] R. P. Sing, M. Zhang, D. Chan, Journal of Materials and Science, Vol. 37, pp. 781-788 (2002)

[76] F. F. Lange, K. C. Radford, Journal of Material and Science, Vol. 6, No. 9, pp. 1197-1203 (1971)

[77] J. Spanoundakis, R. J. Young, Journal of Materials Science, Vol. 19, No.2, pp. 473-486 (1984)

[78] T. H. Hsieh, A. J. Kinloch, K. Masania, A. C. Taylor, S. Sprenger, Polymer, Vol. 51, No. 26, pp. 6284-6294 (2010)

[79] G. Ragosta, M. Abbate, P. Musto, G. Scarinzi, L. Mascia, Polymer, Vol. 46, No.23, pp. 10506-10516 (2005)

[80] T. Adachi, M. Osaki, W. Araki, S. C. Kwon, Acta Materialia, Vol. 56, No. 9, pp. 2101-2109 (2008)

[81] A. S. Zerda, A. J. Lesser, Journal of Polymer Science: Part B: Polymer Physics, Vol. 39, No. 11, pp. 1137-1146 (2001)

[82] W. P. Liu, PhD. Thesis in the Department of Mechanical and Industrial Engineering, Concordia University (2005)

[83] Y. W. Mai, Z. Z. Yu, Polymer Nanocomposites, CRC press (2006)

[84] K. Wang, L. Chen, J. Wu, M. L. Toh, C. He, A. F. Yee, Micromolecules, Vol. 38, pp. 788-800 (2005)

[85] C. Zilg, R. MuElhaupt, J. Finter, Macromolecular Chemistry and Physics, Vol. 200, No. 3, pp. 661- 670 (1999)

[86] X. Kornmann, L. A. Berglund, Polymer Engineering and Science, Vol. 38, No. 8, pp. 1351-1358(1998)

[87] S. J. Ahmadi, Y. D. Huamg, Journal of Material Science, Vol. 39, pp. 1919-1925 (2004)

[88] S. Nazure, B. K. Kandola, Polymers for Advanced Technologies, Vol. 17, pp. 294-303(2006)

[89] Y. Someya, M. Shibata, Polymer Engineering and Science, Vol. 44, No. 11, pp. 2041-2046 (2004)

[90] X. Fu, S. Qutubuddin, Polymer Engineering and Science, Vol. 44, No. 2, pp. 345-351(2004)

[91] D. Yebassa, S. Balakrishnan, Nanotech, Vol. 3, pp.246-249(2003)

[92] Y. Zhang, Q. Cai, Journal of Applied Polymer Science, Vol. 92, pp. 2038-2044 (2004)

[93] D. Yebassa, S. Balakrishnan, Journal of Polymer Science: Part A: Polymer Chemistry, Vol. 42, pp.1310-1321 (2004)

[94] S. Balakrishnan, D. Raghavan, Journal of Reinforced Plastic and Composites, Vol. 24, No.1, pp. 5-20, (2005)

[95] B.W. Jo, S.K. Park, Construction and Building Materials, Vol. 22, pp.14-20(2008)

[96] A. B. Inceoglu, U. Yilmazer, Polymer Engineering and Science, Vol. 43, No. 3, pp. 661-669(2003)

[97] T. Y. Tsai, C. H. Kuo, Applied Clay Science, Vol. 49, pp. 224-228(2010)

[98] L. Torre, M. Chieruzzi, J. M. Kenny, Journal of Applied Polymer Science,Vol.115, pp. 3659-3666(2010)

[99] R. K. Bharadwaj, A. R. Mehrabi, Polymer, Vol. 43, pp. 3699-3705(2002)

[100] D. Ray, S. Sengupta, Macromolecular Materials and Engineering, Vol. 291, pp. 1513-1520(2006)

[101] A. Al-Khanbashi, M. El- Gamal, Journal of Applied Polymer Science, Vol. 98, pp. 767-773(2005)

[102] M. H. Beheshti, M. Vafayan, Polymer Composites, Vol. 1, pp. 10(2008)

[103] W. Liu, S. V. Hoa, M. Pugh, Polymer Engineering and Science, Vol. 44, No. 6, pp. 1178-1186 (2004)

[104] J. Frolich, R. Thomann, R. Mulhaupt, Macromolecules, Vol. 36, No. 19, pp. 7205-7211 (2003)

[105] I. Isik, U. Yilmazer, G. Bayram, Polymer, Vol. 44, No. 20, pp. 6371-6377 (2003)

[106] A. Ishak, M. H. Farihan, Journal of Reinforced Plastics and Composites, Vol. 29, No. 18, pp.2834-2841 (2010)

[107] C. Wang, Z. Pan, L. Zhang, D. Yang, W. Li, Polymers for Advanced Technologies, Vol. 17, No. 7-8, pp. 528-533 (2006)

[108] A. Asif, V. L. Roa, K. N. Ninan, Polymers for Advanced Technologies, Vol. 22, pp. 437-447 (2011)

[109] I. Isik, U. Yilmazer, G. Bayram, Polymer, Vol. 44, No. 20, pp.6371-6377 (2003

[110] M. Herandez, B. Sixou, J. Duchet, H. Sautereau, Polymer, Vol. 48, No. 4, pp. 4075-4086 (2007)

[111] L. Xu, L. J. Lee, Polymer, Vol. 45, No. 21, pp.7325-7334(2004)

[112] M. H. Beheshty, M. Vafayan, M. Poorabdollah, Polymer Composites, Vol. 30, No. 5, pp. 629-638 (2009)

[113] Y. Zhou, X. Yang, Polymer International, Vol. 56, pp. 267-274(2007)

[114] S. V. Hoa, P. Ouellette and T. D. Ngo, Journal of composite materials, Vol. 43, No. 7, pp. 783-803 (2009)

[115] J. E. Mark, Polymer data handbook, Oxford University Press, Inc. 1999

[116] X. Kornmann, L. A. Berglund, Polymer Engineering and Science, Vol. 38, No. 8,pp. 1351-1358(1998)

[117] S. J. Ahmadi, Y. D. Huamg, Journal of Material Science, Vol. 39, pp.1919-1925 (2004)

[118] R. Kotsilkova, Thermoset Nanocomposite for Engineering Applications: Smithers Rapra Technology, (2007)

[119] X. Fu, S. Qutubuddin, Polymer Engineering and Science, Vol. 44, No. 2, pp. 345-351(2004)

[120] D. Yebassa, S. Balakrishman, Journal of Polymer Science: Part A: Polymer Chemistry, Vol. 42, pp. 1310-1331 (2004)

[121] S. Balakrishnan, D. Raghavan, Journal of Reinforced Plastic and Composites, Vol. 24, No. 1, pp. 5-20, (2005)

[122] D. J. Suh, Y. T. Lim, O. Park, Polymer, Vol. 41, pp. 8557-8563(2000)

[123] L. M. Harpaz, M. Narkis, M. Siegmann, Polymer Engineering and Science, Vol. 45, No.2, pp. 174-186 (2005)

[124] W. Liu, S. V. Hoa, M. Pugh, Composites Science and Technology, Vol. 65, No. 2, pp. 307-316 (2005)

[125] W. Liu, S. V. Hoa, M. Pugh, Composites Science and Technology, Vol. 65, No. 15-16, pp. 2364-2373 (2005)

[126] Y. Zhou, X. Yang, D. Jia, Polymer International, Vol. 56, No. 2, pp. 267-274 (2007)

[127] R. K. Bharadwaj, A. R. Mehrabo, C. Hamilton, C. Trajillo, M. Murga, R. Fan, A. Chavira, A. K. Thompson, Polymer, Vol. 43, No. 13, pp. 3699-3705 (2002)

[128] L. Xu, L. J. Lee, Polymer Engineering and Science, Vol .45, No. 4, pp. 496-509 (2005)

[129] D. Ray, S. Sengupta, S. P. Sengupta, A. K. Mohanty, M. Misra, Macromolecular Materials and Engineering, Vol. 291, pp. 1513-1520 (2006)

[130] C. Zilg, R. Mulhaupt, J. Finter, Macromolecular Chemistry and Physics, Vol. 200, pp. 661-670 (1999)

[131] K. Wang, L. Chen, J. Wu, M. L. Toh, C. He, A. F. Yee, Macromolecules, Vol. 38, No. 3, pp. 788-800 (2005)

[132] K. T. Faber, A. G. Evans, Acta Metall, Vol.31, No. 4, pp. 565-576(1983)

[133] A. J. Kinloch, A. C. Taylor, Journal of Materials and Science, Vol. 41,No. 11, pp.3271-3297(2006)

[134] X. Kornmann, L. A. Berglund, Polymer Engineering and Science, Vol. 38, No. 8, pp.1351-1358(1998)

[135] Y. Zhang, Q. Cai, Z. Jiang, K. Gong, Journal of Applied Polymer Science, Vol. 92, No.3, pp. 2038-2044(2004)

[136] D. Yebassa, S. Balakrishnan, E. Feresenbete, D. Raghavan, P. R. Start, S. D. Hudson, Journal of Polymer Science, Part A: Polymer Chemistry, Vol. 42, No. 6, pp.1310-1321(2004)

[137] S. Katoch, P. P. Kundu, Journal of Applied Polymer Science, Vol.122, No. 4, pp.2731-2740(2011)

[138] M. Haider, P. Hubert, L. Lessard, Composites , Part A : Applied Science and Manufacturing, Vol. 38, No. 3,pp.994-1009(2007)

[139] Y. J. Huang, C. M. Liang, Polymer, Vol. 37, No. 3, pp. 401-412(1996)

[140] W. Li, L. J. Lee, Polymer, Vol. 39, No. 23, pp.5677-5687(1998)

[141] W. Li, L. J. Lee, Polymer, Vol. 41, No. 2, pp.685-696(2000)

[142] X. Cao, L. J. Lee, Journal of Applied Polymer Science, Vol. 82, No. 3, pp.738-749(2001)

[143] R. D. Brooker, A. J. Kinloch, A. C. Taylor, The Journal of Adhesion Vol. 86, No. 7, pp.726-741(2010)

[144] H. U. Khan, B. M. L. Wadehra, Polymer, Vol. 22, No. 4, pp. 488-490(1981)

[145] K. F. O' Driscoll, J. Huang, European Polymer Journal, Vol. 25, No. 7-8, pp. 629-633(1989)

[146] Y. J. Huang, C. J. Chu, J. P. Dong, Journal of Applied Polymer Science, Vol. 78, No. 3, pp. 543-557(2000)

[147] A. K. Nikolaidis, G. P. Achilias, G. P. Karayannidis, European Polymer Journal, Vol. 48, No. 2, pp. 240-251(2012)

[148] H. P. Grace, Chemical Engineering Communications, Vol. 14, No. 4, pp. 225-277(1982)

[149] A. C. Moloney,H. H. Kausch, T. Kaiser, H. R. Beer, Journal of Materials Science, Vol. 22, No. 2, pp. 381-393(1987)

[150] B. A. Sjogren, L. A. Berglund, Polymer Composites, Vol. 20, No. 5, pp. 705-712(1999)

[151] Y. Zhao, Q. Cheng, M. Qian, J. H. Cantrell, Journal of Applied Physics, Vol. 108, No.094311, pp.1-7(2010)

[152] B. Tang, A. H. W. Ngan, J. B. Pethica, Nanotechnology, Vol. 19, No. 49, pp.7 (2008)

[153] J. Stawikowska, A. G. Livingston, Journal of Membrane Science, Vol.425-426, No. 1, pp. 58-70 (2013)

[154] W, Xu, P. M. Wood-Adams, C. G. Robertson, Polymer, Vol. 47, No. 13, pp. 4798-4810 (2006)

[155] M. Maiti, A. K. Bhowmick , Polymer, Vol. 47, No. 17, pp. 6156-6166 (2006)

[156] A. Chafidz, I. Ali, M. E. A. Mohsin, R. Elleithy, Journal of Polymer Research, Vol. 19, pp.9860 (2012)

[157] S.R. Lim, W. S. Chow, Journal of Applied Polymer Science, Vol. 123, No. 5, pp. 3173-3181 (2012)

[158] S. Ravati, B. D. Favis, Polymer, Vol. 51, No. 20, pp. 4547-4561 (2010)

[159] C. Serré, M. Vayer, R. Erre, N. Boyard, C. Ollive, Journal of materials science, Vol. 36, pp. 113-122 (2001)

[160] J Karger-Kocsis, O. Gryshchuk, J. Fröhlich, Composites Science and Technology, Vol. 63, No 14, pp. 2045-2054 (2003)

[161] A. K. Barick, D. K. Tripathy, Materials Science and Engineering, Vol. 527, No. 3, pp. 812-823 (2010)

[162] A. Ganguly, A. K. Bhowmick, Y. Li, Macromolecules, Vol. 41, No. 16, pp 6246-6253 (2008)

[163] S. Sadhu, A. K. Bhowmick, Journal of materials science, Vol. 40, pp. 1633-1642 (2005)

[164] M. Maiti, A. K. Bhowmick , Polymer, Vol. 47, No. 17, pp. 6156-6166 (2006)

[165] B. Yalcin, M. Cakmak, Polymer, Vol. 45, No. 19, pp. 6623-6638 (2004)

[166] A. Ganguly, A. K. Bhowmick, Y. Li, Macromolecules, Vol. 41, No. 16, pp. 6246-6253 (2008)

[167] A. Mirmohseni, S. Zavareh, Journal of Polymer Research, Vol. 17, pp. 191-201 (2010)

[168] S. Chaeichian, P. M. Wood-Adams, S. V. Hoa, Polymer, Vol. 54, No. 5, pp. 1512-1523(2012)

[169] P. Achalla, J. McCormick, T. Hodge, C. Moreland, P. Esnault, A. Karim, D. Raghavan, Journal of Polymer Science, Part B, Polymer Physics, Vol. 44, No. 3, pp.492-503(2006)

[170] S. N. Magonvo, V. Elings, M. H. Whangbo, Surface Science, Vol. 375, No. 2-3, pp. L385-391 (1997)

[171] L. Lsik, U. Yilmazer, G. Bayram, *Polymer*, Vol. 44, No. 20, pp 6371-6377, 2003

[172] I. Ahmad, F. M. Hassan, Reinforced Plastics and Composites, Vol. 29, No. 18, pp. 2834-2841 (2010)

[173] A. F. Bower, M. Ortiz, Journal of Mechanics and Physics of Solids, Vol. 39, No. 6, pp.815-858 (1991)

[174] T. M. Mower, A. S. Argon, Mechanics of Materials, Vol. 19 (1995), 343-364

[175] N. A. Fleck, W. J. Stronge, J. H. Liu, Proc. R. Soc. Lond,. A, 429 (1990), 459-479

[176] M. H. Zhang, J. K. Chen, Coputational materials Science, Vol. 61, No.1, pp. 6-11(2012)